Optical Remote Sensing of Water Quality Parameters

Interpretation of Reflectance Spectra

Optical Remote Sensing of Water Quality Parameters

Interpretation of Reflectance Spectra

PROEFSCHRIFT

ter verkrijging van de graad van doctor
aan de Technische Universiteit Delft,
op gezag van de Rector Magnificus,
prof.ir. K.F. Wakker,
in het openbaar te verdedigen ten overstaan van een commissie
aangewezen door het College van Dekanen
op dinsdag 11 januari 1994 te 16.00 uur

door
Johannes Krijgsman
geboren te Rotterdam,
civiel ingenieur

Dit proefschrift is goedgekeurd door de promotor: prof.dr. M. Donze

Published and distributed by:
Delft University Press
Stevinweg 1, 2628 CN Delft
The Netherlands
Telephone +31 15 783254
Telefax +31 15 781661

CIP-GEGEVENS KONINKLIJKE BIBLIOTHEEK, DEN HAAG

Krijgsman, Johannes

Optical Remote Sensing of Water Quality Parameters: Interpretation of Reflectance Spectra / Johannes Krijgsman. - Delft: Delft University Press. - Ill. Thesis Delft University of Technology. - With ref.
ISBN 90-6275-952-1
NUGI 841
Subject headings: optical remote sensing / water quality parameters / reflectance

Printed in The Netherlands
Cover Design: Graffito, Breda

Table of Contents

CHAPTER 1
INTRODUCTION AND SUMMARY

1.1 Introduction

1.1.1 Optical Remote Sensing

Suspended and dissolved substances in surface water change its colour. Clear water is blue, water rich in aquatic humus is yellow and the colour of turbid water depends on the mixture of the constituents. The water colour can vary from dark blue-green via bright green and brown to red. The colour is determined by the light scattered out of the water and that reflected at the water surface. Light that originates from below the water surface shows characteristic influences of the diverse colours of components in the water. Absorption diminishes light intensities and scattering changes its angular distribution. The intensity of reflected light increases with the amount of scattering and decreases by absorption.

Parameters related to water colour are used to study environmental processes like the primary production of biomass and the distribution of (polluted) suspended matter. Areal photography has been used for a long time in such studies. Quantitative photometric images are certainly better. Measurements of the spectral distribution of light intensity can be obtained by optical remote sensing, a technique to collect colour data by detection of upward radiance at a distance. Optical remote sensing of surface water is a cost effective way to obtain colour data of remote or extended areas. After interpretation the colour data is converted to spatial and temporal distribution patterns of parameters of water quality. These parameters can also play a role to calibrate and validate two- and three dimensional hydrodynamic and ecological models. Interactions between waterbodies like the in- and outflow of polluted water and their mixing processes can be visualised and in part quantified. Resuspension of bottom material in dependence on wind characteristics can be observed over whole lakes.

Optical remote sensing can be used to derive concentrations of aquatic humus, suspended algae and suspended silt from measurements of light scattered out of the water. Special applications include mapping and tracking of oil slicks, ice cover and floating layers of algae.

The remote sensing technique has limited value for stratified waters because the upper layer of about one irradiance attenuation length (Gordon 1975a) masks the deeper layers. Sathyendranath and Platt (1989a) reported that vertical stratification of biomass in the ocean

significantly influences the accuracy of biomass estimates obtained by remote sensing of the concentration in the surface layer, however, remote sensing is still the only method available to estimate primary production on a global scale.

To date quantitative observations are made by satellites in a small number of broad wavelength bands. Instruments with high spectral resolution are flown in aircraft. Line detectors have been available for some decades, imaging instruments for a few years (Dekker 1993). It is to be expected that these instruments will also be placed in satellites in the near future. These high spectral resolution sensors will require new calibration procedures using sea-truth data and new algorithms to interpret the spectral colour data.

For the interpretation of satellite observations field data can vary from nonexistent to a considerable amount. Sea-truth is always inadequate compared to the spatial resolution of the images, and it is not clear what kind and how much sea-truth data must be collected to obtain an overall picture with a desired accuracy. A strategy is needed to optimize the incorporation of field data in the calibration procedure. The amount and kind of field measurements that would form an optimal contribution at a reasonable price to enhance the value of satellite or airborne measurements is not obvious. In the absence of field data default values are needed for the optical properties of the constituents of water together with error estimates of these values for sensitivity analysis (Prieur and Satheyendranath 1981). Since the optical properties of dissolved and suspended matter vary in time and space the purpose of field measurements in a specific investigation is to improve on the default values and their error margins.

The logistic effort to collect sea-truth data simultaneously with remotely sensed data for calibration purposes is large. The field program to calibrate the conversion algorithms of the ocean colour sensor CZCS on the Nimbus-7 satellite were reported by Gordon *et al.* (1983). A problem is that the results of such field programs were usually of limited value (Bukata *et al.* 1981, Fischer 1983, Mittenzwey *et al.* 1988, Doerffer *et al.* 1989, Donze *et al.* 1989, Galat and Verdin 1989, Zibordi *et al.* 1990). This problem is related to the basic advantage of the remote sensing technique: sampling of sea-truth data is too slow compared with the almost instant spatial sampling of a remote sensor. Accurate calibration is only possible for processes with limited temporal variations at stable weather conditions. In such exceptional cases accurate data at multiple stations can be collected by a single ship.

Remotely sensed spectral colour data, upward radiance is measured in absolute units, is an apparent optical property. The colour of the incident solar light varies and with it the colour of water. Reflectance, defined as the ratio of upward to downward irradiance, is used to eliminate most of the dependency on absolute intensities of the incident illumination; only

small effects owing to the angular distribution of incident light remain. Gordon and McCluney (1975b) showed by Monte Carlo simulation that the reflectance of a suspension was quite insensitive to the illumination. Diffuse sky light resulted in only a ten percent higher reflectance as light from a zenith sun. Because the reflectance is almost independent of the illumination Gordon (1989a) called this irradiance ratio a quasi-inherent optical property. In this study we focus on the interpretation of reflectance spectra.

The fundamental equations of radiative transfer are known but their application to interpret reflectance spectra is difficult because exact solutions are unavailable and detailed specification of the optical properties of the particles is essential. Simple analytical reflectance models are preferred over more complex ones, unless the increased complexity of a reflectance interpretation method is justified by an increase in its accuracy and unless its requirements for input can be met.

Three basic methods are used to interpret remotely sensed reflectance: a statistical procedure, a model optimization procedure and inverse modelling.

1. The statistical procedure is a black box method. Variations in reflectance are correlated to concentration variations of sea-truth values using linear regression or principal component analysis. Algorithms of a simple form using ratios, differences or power laws of the observed reflectance values are chosen to give a good fit with the sea-truth data. In general these algorithms have limited value because they are valid only for the original site and sensor around the time of calibration; the interpretation algorithms are site specific. They lack transferability.
2. Model optimization methods use a trial and error scheme to optimize the correspondence between model predictions and observations. A reflectance model is used to describe the optical interaction of the colour components of a volume of water. Specific spectra of absorption and backscattering are multiplied by concentration estimates and added. The ensemble spectra of the water mass are used to calculate the spectral reflectance. Concentration estimates are iterated until a good fit results. Specific spectra of inherent optical properties are based on sea-truth data or on default spectra if actual data is unavailable. Default spectra are set to global defaults, to values from literature or are determined by analysis of historical data of the region (Chapter 8). Optimization methods have the advantage that ranges can be specified with optimum sensitivity of the model to variations in concentrations. Simple interpretation algorithms for routine applications can be derived that are physically sound and have specified validity ranges for known assumptions.
3. Inverse modelling. The application of an inverse model to compute the optical properties of a water mass from the measured reflectance spectrum is strictly speaking impossible; the degrees of freedom increase going from the single reflectance spectrum via the absorption

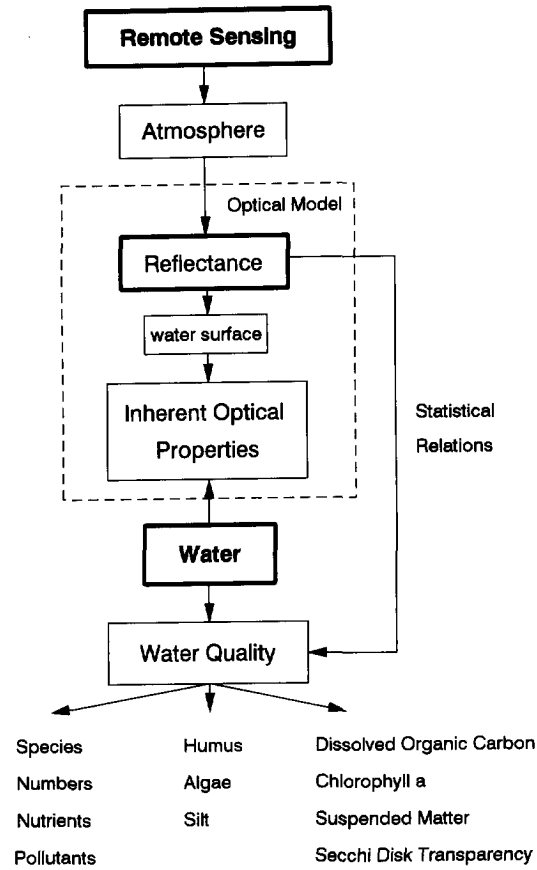

Figure 1.1 *Scheme to interpret remotely sensed reflectance. After removal of atmospheric influences the above surface reflectance is corrected for the influence of the water surface to obtain the subsurface reflectance. Statistical relations between reflectance and water quality parameters are site specific and require calibration. To improve on these relations a two step interpretation is proposed. Subsurface reflectance is related to the absorption and scattering properties of the water using an optical model. The concentrations of the water colour components are related to the water quality parameters in a separate step.*

and scattering properties of the sample volume, to the inherent optical properties of its constituents and their concentrations. In routine remote sensing, with only the remotely sensed reflectance spectrum available, inverse modelling can not be used. In research applications it can be applied to compute an unknown property if sufficient additional information is available, e.g. the backscattering spectrum can be computed if the spectra of reflectance and absorption are measured. Even in this case it is better to use the term optimization method.

Zwick *et al.* (1981) discussed modelling aspects of water quality estimation by remote sensing. They presented a scheme for the quantitative mapping of water quality parameters by interpretation of remotely sensed reflectance. Optical remotely sensed reflectance data have the best correlation with optical sea-truth data. Spectral reflectance and other optical properties of surface water are expected to show accurate and generally valid relations. The sensor calibration procedure, a regression of water quality parameters to reflectance data, is split in an optical step and a statistical step. A model is used to convert from spectral reflectance to optical component spectra (step 3). Optical components are correlated with water quality parameters in a separate step (step 4). Specific spectra of absorption and backscattering are needed to convert from inherent optical properties to water quality parameters. Or shortly:

1. Remove atmospheric influences from the upward radiance data by radiative transfer model.
2. Derive subsurface reflectance by modelling of the air-water interface.
3. Convert reflectance data to inherent optical properties, and
4. Relate inherent optical properties to water constituents concentrations by the specific optical properties of the colour components.

The topic of removal of atmospheric influences falls outside the scope of this research. Only a few aspects of step 2 will be given. In this study we focus on step 3 and 4 of this scheme. Figure 1.1 shows a scheme of the interpretation of remotely sensed reflectance. Spectra of reflectance and inherent optical properties measured with high wavelength resolution are used to compare the accuracy of simple analytical reflectance models. The optical model is used to explain the nonlinear relation between the reflectance and concentrations of the colour components. Inherent optical properties of the colour components used as input in the reflectance models are linearly related to their concentration. Remotely sensed reflectance can be interpreted by an optimization method using sea-truth data or default values. A method is given to obtain default spectra of the colour components with specified error margins.

1.1.2 Measurements of Inherent Optical Properties

Measurements of inherent optical properties on turbid suspensions are not straightforward because absorption and scattering interact and experimental errors are therefore difficult to correct for.

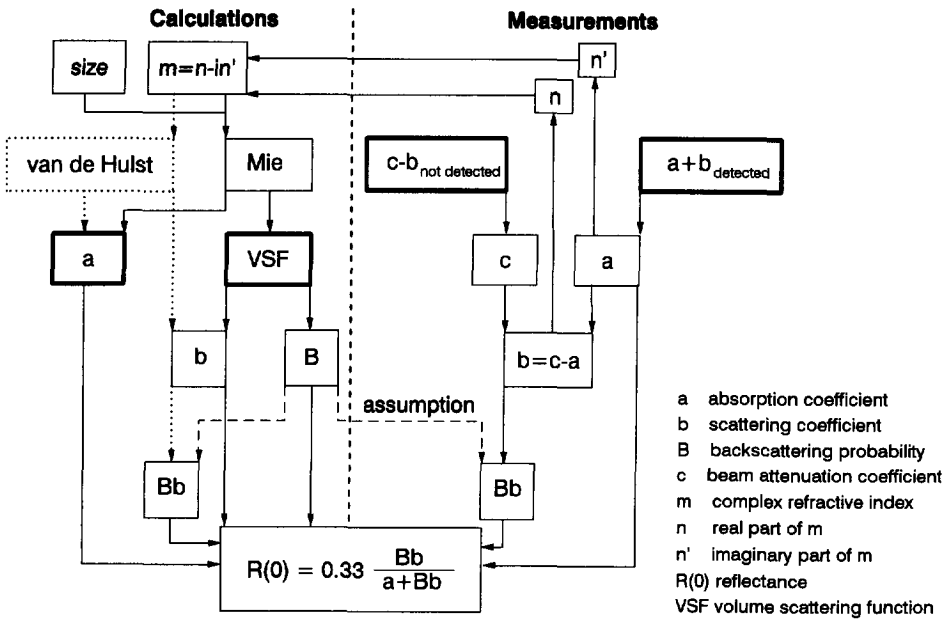

Figure 1.2 *Scheme of theoretical and empirical methods to calculate the reflectance of water. The theoretical and empirical methods are interrelated. It is concluded that the accuracy of the input parameters must be judged carefully when interpreting the results of both methods.*

Several techniques using high aperture optics have been used to measure absorption from turbid suspensions (Section 2.2.5.1). Methods to measure absorption have various experimental difficulties (Table 2.1, page 22) and need correction for scattering, for path length amplification or both. It is not clear which method will give the most accurate approximation of the inherent absorption of a suspension.

The beam attenuation of a suspension can be calculated if the size and number of particles and the efficiency factor for extinction are known. Efficiency factors for absorption and scattering can be computed by Mie-theory (1908) and by the approximation theory for anomalous diffraction of van de Hulst (1957). Light scattering calculations by Mie-theory are exact for spherical particles. Mie-calculations are complex and the formulas do not allow a comprehensive view of physical trends. If spectral data is desired Mie computations are time consuming; the approximate theory allows fast evaluation of efficiency factors. By summation of the contributions of particles from size classes of the particle size distribution the efficiencies of the ensemble can be calculated. To do this the fast and simple calculation by the approximative theory of van de Hulst is sufficient. To model the reflectance the

backscattering probability must be computed by Mie theory, known from measurements of the volume scattering function or has to be estimated by making an assumption about the shape of the volume scattering function.

For light scattering calculations the imaginary part of the refractive index associated with absorption must be known. Because this part depends in an unpredictable way on wavelength, this input parameter must be derived from the measured absorption spectrum and we return to the problem of measuring inherent optical properties on turbid suspensions. Figure 1.2 shows a scheme of theoretical and empirical methods to calculate the reflectance of water. It shows that theoretical and empirical methods are interrelated. It is concluded that the accuracy of the input parameters must be judged carefully when interpreting the results of both methods.

1.2 Summary

In Chapter 2 a survey is given of existing theories in an unified notation.

In Chapter 3 the experimental methods used are treated. Laboratory spectrophotometers measure optical properties on small sample volumes; their use alone was not sufficient for our purpose. To obtain negligible influence of bottom reflection and to preserve optical interactions at their natural level a reflectometer with a large sample volume was built for laboratory experiments. The design of this large volume reflectometer was based on analysis of a number of concepts from the literature.

In Chapter 4 laboratory investigations of reflectance spectra on suspensions with known inherent optical properties are given. The results were used as a standard to compare the performance of several published models, and a new analytical model, the backscattering albedo model, is proposed. The spectral reflectance of optical deep surface water is accurately described by this simple analytical model. Reflectance is shown to be proportional to the backscattering albedo of the mixture: the ratio of backscattering to the sum of absorption and backscattering. The analysis shows that:
1. Reflectance is backscattering reduced by absorption.
2. Reflectance spectra can be approximated by a single scattering model, inclusion of multiple scattering is not needed.
3. The accuracy of the reflectance model calculations is in practice determined by the accuracy of the input data: inherent optical properties of absorption and backscattering.

4. The results of model calculations for optical shallow suspensions did not match with the observed reflectance spectra.

In Chapter 5 the reflectance of mixtures of a green alga and inorganic suspended matter are analyzed. It was shown that the sensitivity of reflectance to concentration variations depends on the optical dominant colour components. Sensitivity to concentration variations reported vary: 1. logarithmic, 2. linear and 3. invariant. These differences can be explained by the backscattering albedo model for the observed concentration range of the component and the other colour components present. The optimum wavelengths for data interpretation show a spectral shift depending on the dominant colour components of the mixture.

The accuracy of reflectance model calculations was limited by the low accuracy of the required input of inherent optical properties. So the reflectance model itself is less important and a simple analytical model can be used.

In Chapter 6 the backscattering albedo model is applied in an extreme case of variability in the inherent optical properties of a suspension caused by physical, but not chemical changes. Three physical effects were studied using suspensions of the cyanobacterium *Microcystis aeruginosa* at a constant level of the chlorophyll *a* concentration. The effect of aggregation was investigated by pulverizing colonies to single cells, the scattering by the cells was varied by collapsing their gas vacuoles and the effect of the formation of a floating layer on reflectance was measured. Reflectance was strongly affected by the change in the scattering characteristic due to the collapse of gas vacuoles.

Variability of inherent optical properties changes the reflectance at a constant level of colour components and thus at a constant level of the water quality parameters. This natural variability induces inaccuracy in the interpretation of reflectance data. Usually this error will be smaller than observed in the extreme cases that were studied. For accurate data interpretation a field measuring program is required to calibrate the remotely sensed reflectance. An alternative method is the use of a library containing historical data to derive default estimates of the optical properties of the colour components and their variability.

In Chapter 7 a short summary of target factor analysis is given to serve as a basis in Chapter 8. The method can be used to obtain default spectra for the interpretation of reflectance data and to specify residual errors. Target factor analysis has three main advantages compared to multivariate analysis of mixtures of linear contributing components: 1. Part of the experimental error is removed from the data by decomposition of the data and using only significant component spectra, at the same time data reduction is obtained.

2. Candidate component spectra can be individually tested to be present in the data. The presence of target components can be judged independent of the other components of a complete set of real components.
3. Default component spectra can be used as initial targets and modified by projection or iteration to closely resembling spectra of the actual components present in the mixture.

In Chapter 8 we show how to improve on default values available for the absorption spectrum of aquatic humus using target factor analysis and analyze remaining errors. With three linearly independent components any spectrum of humus in the dataset was described within experimental error. Since the dataset contains much variation in the sources of humus used this is probably true in general.

Description of the absorption spectra of humus of samples of surface water by a model with the mass-specific absorption spectra of humic acid and fulvic acid of marine water was physically without meaning.

In Chapter 9 a method is given to estimate absorption *in situ* using the attenuation of upward radiance. To obtain accurate absorption measurements of particulate matter usually some method of concentrating the particles is necessary. The accuracy of absorption measurements can be improved by increasing the pathlength instead of the concentration of the sample, making sample handling unnecessary. Field measurements of upward radiance attenuation were experimentally shown to be close to laboratory measurements of absorption. It was concluded that field measurements of radiance attenuation like laboratory measurements yield an apparent absorption that still needs correction for scattering to give inherent absorption. Radiance attenuation and the apparent absorption were the same within experimental error, estimated at 10 percent.

1.3 Conclusions

1.3.1 General Conclusions

In practice model predictions of reflectance have limited accuracy because the inherent optical properties of the mixture, or its colour components, are not accurately known. The choice of the reflectance model is less important; instead of the backscattering albedo model (Chapter 4) also the quasi-single scattering model (Gordon *et al.* 1975) can be used.

Specific inherent optical properties show a natural variability (Chapter 6) in time and space. This variability is related to environmental conditions and the grouping of colour components. For instance differences in temperature, light, nutrients and water current can lead to changes in particle size distribution of an algal species and to a succession in time of algal species for the colour component associated with chlorophyll. Owing to this natural variability sea-truth data or default values together with error estimates are needed to interpret reflectance spectra.

Spectra measured with high wavelength resolution show that the use of a small number of preset wavelength bands is hazardous, because the response might be invariant to concentration variations of the mixture (Chapter 5). Preferably full spectral coverage should be used and additional sea-truth data or default values with a range of concentrations that commonly occur should be available. A solution for the interpretation of reflectance spectra can be found by an optimization procedure if a library of the colour components is available. The library should contain default spectra of the colour components of both the absorption and backscattering coefficients together with their concentration ranges.

Default spectra and residual errors can be used for sensitivity analysis to judge the gain in accuracy by executing a field program. These spectra can also be used to decompose the total *in situ* absorption in its linearly contributing component spectra.

1.3.2 Improvement of Sea-Truth

A database of sea-truth with absorption spectra of the colour components but without the spectra of backscattering coefficients or reflectance values is of limited value for the interpretation of surface water colour data.

For routine interpretation of reflectance spectra the detailed information of the volume scattering function at a single wavelength is not required. Accurate knowledge of the spectral dependence of the backscattering coefficient of absorbing particles is more important.

Spectral backscattering coefficients can be calculated from observed absorption and reflectance spectra under the assumption that the analytical reflectance model is valid. The reflectance spectra of optical deep suspensions can be measured with a large volume laboratory reflectometer. Observed subsurface reflectance spectra are accurate because in the controlled laboratory environment the disturbing effects of surface waves are absent and the sensor can be positioned just below the surface.

Calibration data for the interpretation of reflectance spectra can efficiently be obtained on a routine base. The additional logistic effort to acquire sea-truth data simultaneously with the overpass of a remote sensor is usually a waist of time and money. The attempt is expected to fail because of logistic problems, and if the attempt is successful the accurate calibration of a single pixel contributes little to the accuracy of an image with large dynamic range. It is better to put effort in an attempt to measure the total range of sea-truth data and include shipboard reflectance measurements.

Upward radiance attenuation is an *in situ* estimate of absorption. The results are comparable to laboratory measurements using an integrating sphere. Experimental errors of the methods are different. The field method does not require handling and concentration of the sample because it is possible to adjust the path length to the turbidity of the water mass. For clear water a path length of up to one meter can be used, a hundred times larger compared to laboratory measurements of absorption.

References

Dekker, A.G., 1993. *Detection of Optical Water Quality Parameters by High Resolution Remote Sensing*, Thesis, Free University, Amsterdam, 222 pp.

Doerffer, R., J. Fisher, M. Stössel and C. Brockmann, 1989. Analysis of Thematic Mapper data for studying the suspended matter distribution in the coastal area of the German Bight (North Sea), Remote Sens. Environ. **28**, 61-73.

Donze, M., R.J. Bijlsma, H. Buiteveld, J.G.P.W. Clevers, van Kasteren, Meulstee and Pellemans, 1989. CAESAR: performance and first evaluation of application possibilities, report 89-06, BCRS, The Netherlands, 101 pp.

Fischer, J., 1983. Remote sensing of suspended matter, phytoplankton and yellow substances over coastal waters, Part 1: Aircraft measurements, Mitt. Geol. Pal. Inst. **55**(12), 85-95.

Galat, D.L., and J.P. Verdin, 1989. Patchiness, collapse and succession of a cyanobacterial bloom evaluated by synoptic sampling and remote sensing, J. Plankton Res. **11**(5), 925-948.

Gordon, H.R., and W.R. McCluney, 1975a. Estimation of depth of sunlight penetration in the sea for remote sensing, Appl. Opt. **14**(2), 413-416.

Gordon, H.R., O.B. Brown and M.M. Jacobs, 1975b. Computed relationships between the inherent and apparent optical properties of a flat homogeneous ocean, Appl. Opt. **14**(2), 417-427.

Gordon, H.R., D.K. Clark, J.W. Brown, O.B. Brown, R.H. Evans and W.W. Broenkow, 1983b. Phytoplankton pigment concentrations in the Middle Atlantic Bight: comparison of ship determinations and CZCS estimates, Appl. Opt. **22**(1), 20-36.

Gordon, H.R., 1989a. Can the Lambert-Beer law be applied to the diffuse attenuation coefficient of ocean water?, Limnol. Oceanogr. **34**(8), 1389-1409.

Hulst, H.C. van de 1957. *Light scattering by small particles*, Dover Publ., New York, 450 pp.

Mie, G., 1908. Bietrage zur Optik truber Medien speziell kolloidaler Metallösungen, Ann. Physik (Leipzig), 25, 377-445.

Mittenzwey, K.H., A.A. Gitel'son, A.A. Lopatchenko, B.L. Sukhorukov and T. Voigt, 1988. In-situ monitoring of water quality on the basis of spectral reflectance. Ship-borne experiments for the development of remote sensing algorithms Especially for the estimation of algal content in natural water, Int. Revue ges. Hydrobiol. **73**(1), 61-72.

Prieur, L., and S. Sathyendranath, 1981. An optical classification of coastal and oceanic waters based on the specific spectral absorption curves of phytoplankton pigments, dissolved organic matter, and other particulate materials, Limnol. Oceanogr. **26**(4), 671-689.

Sathyendranath, S., and T. Platt, 1989a. Remote sensing of ocean chlorophyll: consequence of nonuniform pigment profile, Appl. Opt. **28**(3),490-495.

Zibordi, G., G. Maracci and P. Schlittenhardt, 1990. Ocean colour analysis in coastal waters by airborne sensors, Int. J. Remote Sensing **11**(5), 705-725.

Zwick, H.H., S.C. Jain and J.R. Miller, 1981. Modelling aspects of water quality estimation, In: *Oceanography from space*, Ed. J.F.R. Gower, Plenum Press, New York, 355-363.

CHAPTER 2
THEORY

2.1 Introduction

In this chapter models to describe the propagation of light in water are given, together with a survey of the physical principles that are needed. Also the symbols and terminology that will be used are introduced. Unified notation makes comparison of different models easier, our list of symbols is given in Appendix A. Presented are basic optical properties, light scattering by particles and reflectance models of surface water, going from basic physics via optical properties of a volume element to bulk optical properties.

Fundamental electro-magnetic properties that determine radiation transfer of visible light through an absorbing and scattering medium like water are the permeability μ_r and permittivity ϵ_r of the medium for the frequency of the radiance (Debye 1929). In optics these properties are expressed by a single term, the index of refraction m.

$$m = \sqrt{\mu_r \epsilon_r} \approx \sqrt{\epsilon_r} \qquad (2.1)$$

The refractive index m is a complex number with real part n and imaginary part n'. The real part is related to light scattering and the imaginary part to absorption of light.

If its refractive index and size are known the absorption and scattering properties of a spherical particle can be calculated by Mie-theory (Mie 1908). Scattering of light is described by the angular distribution pattern of scattered radiance intensities: the volume scattering function. For particles suspended in water the relative complex refractive indices, compared to water, and size distribution must be known. Particles found in natural waters have relative refractive indices with a real part of 1.01 to 1.07 for organic matter and of 1.15 to 1.20 for inorganic matter (Aas 1981; Bricaud *et al.* 1988). Typical values of the complex index at a wavelength of 680 nm are 1.05-0.001i for bacteria, 1.05-0.01i for phytoplankton and 1.15 for silt. Particles in marine waters have a diameter range of up to 20 μm. In turbid surface water a wider range occurs, particles of millimetre size can be abundant. Particle size distributions in marine waters can be approximated by a log-normal distribution or a Junge distribution with exponent around 4. A comprehensive review of the optics of marine particles is given by Morel (1991b).

The absorption coefficient and the volume scattering function, measured or calculated by Mie-theory, are basic optical characteristics of a volume element of water. These basic optical properties are used to describe radiative transfer. Together with the illumination they allow calculation of the underwater light field. Models of radiative transfer describe the propagation of light sufficiently accurate for most applications in optical oceanography (Jerlov 1976). Optical properties play a key role in models of primary production, monitoring of surface water quality and optical remote sensing (Kirk 1983). They can be used to estimate concentrations of water constituent indirectly and they contain information on chemical and physical components that interact with light: water itself, aquatic humus, algae and silt. Biomass of planktonic algae for example can be estimated because their spectra of absorption and reflectance show the characteristic variations associated with photosynthetic pigments. All algae contain chlorophyll *a* pigment which has a peak absorption around 675 nm.

2.2 Inherent Optical Properties

Inherent optical properties are independent of the illumination (Preisendorfer 1976), they do not depend on the angular radiance distribution of the incident light field. By contrast apparent optical properties still contain information on the light field. The two basic inherent optical properties are:

1. Absorption coefficient a
2. Volume scattering function $\beta(\theta,\phi)$

In general optical properties depend on the wavelength of the incident radiation, but the wavelength dependency is omitted in the notation unless it contributes to the clarity of the formulas.

The volume scattering function describes the angular distribution of light scattered out of the direction of an incident ray, with θ the angle of light scattered away from this direction and ϕ the azimuth angle.

$$\beta(\theta,\phi) \tag{2.2}$$

The volume scattering function becomes independent of the azimuth angle ϕ for spherical particles without internal structure and for randomly oriented particles of arbitrary shape.

$$\beta(\theta) \tag{2.3}$$

Other inherent optical properties can for convenience be derived from these basic absorption and scattering properties.

The scattering coefficient b is defined by

$$b = 2\pi \int_0^{180} \beta(\theta) \sin\theta \, d\theta \tag{2.4}$$

and the beam attenuation coefficient c or extinction coefficient is the sum of the coefficients for absorption and scattering.

$$c = a+b \tag{2.5}$$

The probability that a single photon will be scattered rather than absorbed is the single scattering albedo ω_0: the ratio of scattering to extinction.

$$\omega_0 = \frac{b}{a+b} = \frac{b}{c} \tag{2.6}$$

The scattering coefficient b can be separated in two partial integrals to be used in models of the light field.

$$b = b_f+b_b \tag{2.7}$$

with the forward scattering coefficient b_f

$$b_f = 2\pi \int_0^{90} \beta(\theta) \sin\theta \, d\theta \tag{2.8}$$

and with the backscattering coefficient b_b.

$$b_b = 2\pi \int_{90}^{180} \beta(\theta) \sin\theta \, d\theta \tag{2.9}$$

The forward scattering probability function $F(\theta)$ gives the fraction of scattered light within a cone between the forward direction and the specified half-angle. The forward scattering

probability $F(\theta)$ is computed by integration of the volume scattering function from 0° to the specified angle θ and normalized to the total scattering b.

$$F(\theta) = \frac{2\pi}{b}\int_0^{\theta}\beta(\theta)\sin\theta d\theta \qquad \textbf{(2.10)}$$

This fraction increases from 0 to 1 for angles θ from 0° to 180°. The backscattering probability function $B(\theta)$ consists of the complementary values:

$$F(\theta)+B(\theta)=1 \qquad \textbf{(2.11)}$$

For the frequently used fractions $F(90)$ and $B(90)$ the shorthand F and B is used. F is the forward scattering probability, B the backscattering probability.

$$\begin{aligned} b_f &= F(90)b = Fb \\ b_b &= B(90)b = Bb \end{aligned} \qquad \textbf{(2.12)}$$

A new term is introduced, the backscattering albedo ω_b. It is defined by the ratio of backscattering to the sum of absorption and backscattering:

$$\omega_b = \frac{b_b}{a+b_b} \qquad \textbf{(2.13)}$$

The backscattering albedo ω_b will prove to be a convenient parameter in reflectance models. The parameter ω_b is zero in the absence of scattering and equal to one in the absence of absorption. It varies between the same limits as the single scattering albedo ω_0, but in addition to this it incorporates variability in the scattering probability function.

2.2.1 Calculation of Inherent Optical Properties

The beam attenuation of a suspension can be calculated if the size and number of particles and the efficiency factor for extinction are known. Efficiency factors for absorption and scattering can be computed by Mie-theory and by the approximation theory for anomalous diffraction of van de Hulst (1957). Light scattering calculations by Mie-theory are exact for spherical particles. Mie-calculations are complex and the formulas do not allow a comprehensive view of physical trends. If spectral data is desired Mie computations are time consuming; the approximate theory allows fast evaluation of efficiency factors. By summation of the contributions of particles from size classes of the particle size distribution the

efficiencies of the ensemble can be calculated. To do this the fast and simple calculation by the approximative theory of van de Hulst is sufficient.

2.2.2 Scattering by Particles

Anomalous light scattering is shown by absorbing particles with dimensions ranging from 1 to 100 times the wavelength of the incident light, depending on their refractive index.

Interference of refracted light passing through a particle and diffracted light passing close by a particle causes spectral and angular maxima and minima of scattered light. The optical cross section C of a particle is equal to its geometrical cross section G multiplied by an optical efficiency factor Q.

$$C = GQ \tag{2.14}$$

The efficiency factor for extinction Q_e shows an oscillation around the value 2, this oscillation is damped with increasing particle size. A large particle removes twice the amount of light it can intercept owing to diffraction of light, when observed far beyond the zone where a shadow can be distinguished.

Absorption and scattering interfere: in the neighbourhood of an absorption peak the imaginary part of the refractive index causes a change in the real part of the refractive index. An anomalous effect in the beam attenuation (extinction) results. The effect on beam attenuation depends on the size and relative refractive index of the particle. The resulting beam attenuation near the absorption peak shows with increasing particle size a peak, a dip followed by a peak, a dip, or a peak followed by a dip. The dip-peak sequence is alternately repeated with decreasing amplitude until the effect becomes insignificant for particles with an efficiency factor for extinction Q_e close to the limit value 2. This anomalous behaviour of extinction around an absorption peak is typical for particles in the Mie scattering domain.

2.2.3 Mie-Theory

The efficiency factor for extinction multiplied by the particle concentration and the geometrical cross section is the beam attenuation. The efficiency factor can be computed by integration of the volume scattering function calculated by Mie-theory (Mie 1908). For uniformly sized particles, a monodisperse suspension, the volume scattering function can be computed with the algorithm for Mie computations of homogeneous spherical particles by

Bohren and Huffman (1983) if the relative refractive index m in water is known (Equation 2.17).

Efficiency factors are defined to give comparable optical data for different particle sizes. The optical effects are normalized to the geometric cross section of the particle. Efficiency factors can be calculated for extinction, Q_c, absorption, Q_a and scattering, Q_b. The efficiency factor for extinction is equal to the sum of the efficiency factors for absorption and scattering.

$$Q_c = Q_a + Q_b \tag{2.15}$$

If absorption is zero the efficiency factors for extinction and scattering are equal and the theoretical scattering spectrum will be equal to the measured beam attenuation spectrum.

The beam attenuation can be calculated by

$$c(\lambda) = \frac{\pi D^2}{4} Q_c(\lambda) N \tag{2.16}$$

if the uniform particle size, the efficiency factor for extinction and the particle concentration are known. Substitution of the diameter D in meters, the efficiency factor Q_c calculated by Mie theory and the particle concentration per cubic meter N gives the theoretical beam attenuation.

2.2.4 Van de Hulst Approximation

The approximation theory for anomalous diffraction of Van de Hulst gives insight in the way scattering is influenced by the refractive index, wavelength and size of a particle. The theory is used to evaluate the effect of such changes, especially changes in size distribution (Morel and Bricaud 1981ab; Bricaud and Morel 1986; Stramski *et al.* 1988). The approximation formulas are valid for a wide range of particle sizes, the most accurate results are obtained for particles with a relative refractive index m close to 1.

The relative refractive index of particles suspended in water is a complex number,

$$m = n - in' = \frac{n_p - in'_p}{n_w - in'_w} \tag{2.17}$$

The imaginary part of the relative refractive index n' is related to the absorption coefficient of the particle material by

$$n' = \frac{\lambda}{4\pi n_w} a_i \tag{2.18}$$

with λ the wavelength in vacuum and a_i the intracellular absorption coefficient. For spherical particles the internal absorption coefficient is related to the measured volume absorption by the number N and volume of the particles

$$a_i = \frac{a}{N\frac{\pi}{6}D^3} \tag{2.19}$$

For water the imaginary part of the refractive index is negligible in the wavelength range 350-800 nm; a_i is equal to a thus n' is of the order of 10^{-7} for the absorption peak around 760 nm. Absorbing particles like algae have n_p' values of the order of 10^{-2} (Section 2.1). So the ratio of the complex numbers can be simplified to

$$m = n - in' = \frac{n_p}{n_w} - i\frac{n_p'}{n_w} \tag{2.20}$$

The phase shift of a ray passing through the centre of a spherical particle is

$$\rho^* = 2x(m-1) = 2x(n-1) - i2xn' \tag{2.21}$$

with a size parameter x,

$$x = \frac{\pi D}{\lambda_w} = \frac{n_w \pi D}{\lambda_0} \tag{2.22}$$

By using the phase-lag factor ρ defined by

$$\rho = 2x(n-1) \tag{2.23}$$

and the parameter ρ' defined by

$$\rho' = 4xn' = Da_i \tag{2.24}$$

and the ratio

$$\tan\beta = \frac{n'}{n-1} = \frac{\rho'}{2\rho} \tag{2.25}$$

Equation 2.21 can be rewritten to

$$\rho^* = \rho(1-i\tan\beta) \tag{2.26}$$

The real part ρ of ρ^* denotes an actual phase shift of a ray passing through the centre of the particle and the imaginary part denotes the decay of its amplitude.

The efficiency factor for extinction Q_e is approximated by

$$Q_e = 2-4\exp(-\rho\tan\beta)\left[\frac{\cos\beta}{\rho}\sin(\rho-\beta)+\left[\frac{\cos\beta}{\rho}\right]^2\cos(\rho-2\beta)\right]+4\left[\frac{\cos\beta}{\rho}\right]^2\cos(2\beta) \tag{2.27}$$

The efficiency factor for extinction Q_a can be calculated by

$$Q_a = 1+\frac{2}{\rho'}\exp(-\rho')+\frac{2}{\rho'^2}(\exp(-\rho')-1) \tag{2.28}$$

For non-absorbing spheres with $n'=0$ ($\tan\beta=0$) Equation 2.27 reduces to

$$Q_c = Q_b = 2-\frac{4}{\rho}\sin(\rho)+\frac{4}{\rho^2}(1-\cos(\rho)) \tag{2.29}$$

2.2.5 Measurements of Inherent Optical Properties

Measurements of inherent optical properties on turbid suspensions are not straightforward because absorption and scattering interact and experimental errors are therefore difficult to correct for. Petzold (1977) analyzed the mutual interaction of absorption and scattering in measurements of the volume scattering function on water types with a beam attenuation coefficient c of about 1 m^{-1}. Typical errors were between 4 and 8 percent.

Several techniques with high aperture optics are in use to measure absorption from turbid suspensions (Section 2.2.5.1). It is still not clear which technique will give the most accurate approximation of the inherent absorption of a suspension. Beam attenuation is accurately measured using low aperture optics (Section 2.2.5.3).

2.2.5.1 Absorption

Various laboratory techniques are reported in the literature to measure absorption spectra of suspensions of particulate matter (Table 2.1). The methods differ with respect to the illumination of the sample, sample preparation, detection optics, the amount of scattering included, and the calibration factor between the optical and geometric path length.

1. Ulbricht (1900) presented a device to measure inherent absorption by detection of light scattered in all directions: the integrating sphere. It is the most accurate method available if the sample volume - positioned in the centre of the sphere - is small compared to the volume of the sphere and the apertures in the wall of the sphere are very small compared to its surface area. In practice calibration is needed.

2. Shibata *et al.* (1954) and Shibata (1958) invented the opal glass technique to measure absorption spectra on living micro-organisms. By placing a piece of opal glass behind the sample cuvette in a normal spectrophotometer the scattered light over half of the space angle is collected by the sensor and this way the Ulbricht sphere is approximated using routine equipment. Duysens (1956) suggested to correct the apparent absorption of algal suspensions for scattering by subtracting the measured value at 720 nm. Weidemann and Bannister (1986) measured absorption using cuvettes with opal glass backwalls. Bannister (1988) showed by Monte Carlo simulation that the inaccuracy of this method is typically between 10% and 20%.

3. Yentsch (1960, 1962) presented the filter pad method to measure absorption spectra of particles of dilute suspensions by concentrating the particles on a glass fibre filter. The method is a modification of Shibata's opal glass technique. Butler (1962) pointed out that for the filter pad method an amplification of the absorption had to be accounted for because of an increased ratio of the optical to geometrical pathlength. Kiefer and SooHoo (1982) proposed a constant amplification factor but later Mitchell and Kiefer (1988) showed that this factor is not a constant and depends mainly on the filter load also different filter types caused minor additional effects. Multiple scattering from the filter is prominent, causing absorption to be amplified by a factor β, which must be determined separately.

4. Kirk (1980) concentrated the sample by filtration and measured absorption on the resuspended material using the semi-integrating sphere technique; cuvettes are placed in front of the entrance of an integrating sphere. This method is similar to the method using opal

Table 2.1 *Methods to measure absorption of particulate matter. The methods are different with respect to the illumination of the sample, sample preparation, detection optics, the amount of scattering included, and the calibration factor between the optical and geometric path length. All methods have sources of error and need correction for scattering, for path length amplification or both. It is still not clear which method will give the most accurate approximation of the inherent absorption of a suspension.*

Method	Illumination	Scatter Correction	Calibration or Pathlength Effect	Concentration	Application Remarks	Reference(s)
Integrating Sphere	beam / isotropic	-	yes (small)	-	sample volume small compared to sphere	Ulbricht (1900) Haardt and Maske (1987)
Opal Glass	beam	$a(720)$	average cosine	-	high absorption	Shibata *et al.* (1954), Shibata (1958) Duysens (1956), Bannister (1988)
Filter Pad	beam	$a(750)$	β-factor	yes	low absorption	Yentsch (1960, 1962) Butler (1962), Kiefer and SooHoo (1982), Mitchell and Kiefer (1988)
Point Source: Irradiance Attenuation	point source	?	Monte Carlo	-	no practical use	Friedman *et al.* (1980)
Mirror Cuvette: Two Flow Method	diffuse	-	-	-	scalable design	Doerffer (1980)
Resuspension, Integrating Sphere	beam	$a(750) = B(45°)b$	-	yes	low absorption	Kirk (1980) Davies-Colley (1983)
Integrating Cavity	isotropic	-	calibration factor	-	low absorption	Fry and Kattawar (1988) Pope *et al.* (1990)
Microphotometer	beam	$a(750)$	-	-	absorption of single particle	Iturriaga *et al.* (1988)
Reflective Tube	beam	$0.11b$ $a(750)$	-	-	scalable design	Zaneveld *et al.* (1990)
Net Vector Irradiance	ambient diffuse	-	average cosine	-	*in situ* absorption, limited practical use	Gershun (1939), Voss (1989)
Inverse Two Flow Model	ambient diffuse	-	average cosine	-	*in situ* absorption	Preisendorfer and Mobley (1984)

glass. A disadvantage of the resuspension method is that about 10% of the material is lost.
5. Friedman *et al.* (1980) presented a device using a point source illumination and irradiance detectors placed at two different distances. As a consequence of the unusual design of this instrument the apparent absorption must be corrected for scattering by Monte Carlo simulation for each measurement.
6. Doerffer (1980) used a mirror cuvette and diffuse illumination to measure irradiance attenuation; absorption was calculated using the two flow model.
7. Fry and Kattawar (1988) presented a theoretical concept to measure absorption using isotropic illumination of a sample based on preliminary experiments of Elterman (1970): the integrating cavity. Pope *et al.* (1990) designed and tested an integration cavity absorption meter, the device requires calibration for the path length of a ray of light passing through the sample.
8. Iturriaga *et al.* (1988) presented a technique to measure absorption spectra on individual particles with a microscopic photometer. Spectra of algae and detritus were measured and ensemble mean spectra per sample were presented (Iturriga and Siegel 1989).
9. Zaneveld *et al.* (1990) presented a reflective tube using a beam illumination. They showed that the required correction for scattering amounted to 13% of the total scattering by comparison of the results to that of the opal glass method.

Duysens (1956) showed that the absorption spectrum of a suspension of particles is flattened compared to the absorption of the same amount of absorbing pigment in dissolved state. This flattening effect is also referred to as sieve effect, package effect or discreteness effect (Morel and Bricaud 1981a).

Absorption measurements on turbid suspensions always include a part of the scattering imbedded by the technique used. Davies-Colley (1983) gave a method to correct absorption measurements for scattering with a semi-integrating sphere. Three assumption were made: the angle of acceptance of the device was 44°, the volume scattering function was similar to that of San Diego Harbour (Petzold 1977) and scattering was inversely proportional to wavelength over the spectral range (Bricaud *et al.* 1981). The correction amounted to 8 percent.

Haardt and Maske (1987) and Maske and Haardt (1987) compared absorption measured with the filter pad method to absorption measured on filters and on sample suspensions placed inside an integrating sphere. The absorption measured on filters was amplified by a factor depending on the filter load.

All these methods have sources of error and need correction for scattering, for path length amplification or both. It is still not clear which method will give the most accurate approximation of the inherent absorption of a suspension.

2.2.5.2 Volume Scattering Function

Few volume scattering functions $\beta(\theta)$ of natural waters are known because of the experimental difficulties to measure this sharply peaked function. Intensities in the near forward scattering directions are 3 to 6 magnitudes higher compared to the backward directions. Literature values of measurements on samples of clear ocean water and turbid harbour water are available (Petzold 1977; Kullenberg 1968, 1974, 1984; Whitlock *et al.* 1981; Incropera *et al.* 1981; Sugihara *et al.* 1982). In general, the authors state that the volume scattering functions of clear and moderately turbid water are similar in shape. Normalization of the volume scattering function to the scattering coefficient b or $\beta(45)$ shows that the main difference is the relative amount of backscattering. Tanis *et al.* (1986) compiled 30 literature values of the volume scattering function and a table of backscattering probabilities. This probability B ranges from 0.012 to 0.064, if 5 extreme values are omitted this range reduces to 0.015-0.045.

Petzold's results (1977) are in common use to model scattering characteristics of turbid surface water (Kirk 1981a, 1983). By default the backscattering probability B of 0.019 in San Diego Harbor is assumed to be valid for turbid waters. This radiance distribution pattern was measured at 530 nm with 75 nm bandwidth on a suspension with scattering coefficient b of 1.583 m^{-1}. For oceanic waters B is by default assumed to be equal to 0.044, a value measured on a sample with b=0.037 m^{-1}.

2.2.5.3 Beam Attenuation

Rose (1952) showed that the acceptance angle of a spectrophotometer used to measure the beam attenuation should be a half angle of 0.5° or less. If this rule is applied the results of a concentration series are in agreement with the Lambert-Beer law. Austin and Petzold (1977) analyzed this kind of experimental error, concluding that it increases with the acceptance angle of the instrument depending on the volume scattering function of the sample; an angle of 1° may lead to 20 percent underestimation of the beam attenuation.

2.2.5.4 Backscattering

The backscattering coefficient b_b is difficult to measure. Several methods were proposed besides the measurement of the volume scattering function. Bukata *et al.* (1980) described a device to determine absorption and scattering coefficients from the difference in reflectance of a sample caused by changing the reflectance of the bottom by a known amount. The difference is interpreted using the two flow model (Section 2.8.3). Doerffer (1980) presented a method to obtain absorption and backscattering data by application of the two flow model to irradiance measurements on a sample using a mirror cuvette. Bricaud *et al.* (1983) presented a configuration to estimate backscattering from measurements with a long cuvette placed behind an integrating sphere; the 1.10 m cuvette served as light trap and contained a dilute suspension. The acceptance angles of this configuration were between 133 and 180° of the volume scattering function. Backscattering was estimated to be higher than the observed value by a factor four to five. This estimate was based on calculations using assumed as well as computed volume scattering functions. Morel and Ahn (1990) presented a modified cuvette for this measuring configuration for small samples of turbid suspensions, such as laboratory cultures of algae. The cuvette consisted of a dissymmetrical triangular light trap with black glass walls and an entrance of 15 mm diameter.

The backscattering coefficient can be computed by integration of the volume scattering function (Equation 2.9). The coefficient can be estimated from the measured absorption and beam attenuation coefficients by multiplication of the scattering coefficient $b=c-a$ with an assumed backscattering probability B (Equation 2.12 and Section 2.2.5.2).

2.3 Apparent Optical Properties

Apparent optical properties depend on both the inherent optical properties and the characteristics of the light field. Apparent optical properties include effects of the diffuse incident light.

The angular distribution of radiance of diffuse light is characterized by the average cosine of the radiance distribution $\bar{\mu}$

$$\bar{\mu} = \overline{\cos\theta} \qquad \textbf{(2.30)}$$

or by a distribution factor D, the reciprocal of the average cosine.

$$D = \bar{\mu}^{-1} = \overline{\cos\theta}^{-1} \tag{2.31}$$

The geometric path length in a diffuse light field is shorter than the actual path length traversed by an average ray of light. They are different by the reciprocal value of the average cosine of the angular distribution of radiance (Whitney 1938).

The diffuse absorption coefficient is related to the inherent absorption by a distribution factor describing the diffuseness of the light field

$$a^* = a\bar{\mu}^{-1} = aD \tag{2.32}$$

2.3.1 Irradiance

Measurements of the angular distribution of radiance are laborious and large amounts of data result. Irradiance measurements, partial integral of the angular radiance distribution, are simpler and in common use. Irradiance measurements describe the light field with sufficiently accuracy for most applications in aquatic optics. These apparent optical properties can be used to estimate the inherent optical properties of water. Two types of irradiance measurements are in use: scalar and vector irradiance. Scalar irradiance measurements are insensitive to the detection angle of the incident radiance, while vector irradiance measurements are proportional to the cosine of the detection angle of the incident radiance.

Most data available on the underwater light climate are irradiance measurements: upward and downward irradiance, E_u and E_d, their associated attenuation coefficients, K_d and K_u, and the ratio of upward to downward irradiance, the reflectance R.

Gershun (1939) showed that from the law of conservation of energy it follows that the divergence of the net irradiance vector in the direction of irradiance propagation proportional is to the absorption of the medium and the scalar irradiance.

$$div\ E(z) = -aE_0(z) \tag{2.33}$$

For the sea, where horizontal variations of the irradiance are small, the equation takes the form (Jerlov 1976):

$$\frac{d}{dz}E(z) = -a(z)E_0(z) \tag{2.34}$$

For a diffuse light field propagating in the vertical direction the net vector irradiance E is:

$$E(z) = E_d(z) - E_u(z) \tag{2.35}$$

The downward vector irradiance $E_d(z)$ is the integral over all downward directions of the radiance distribution measured with a flat cosine detector looking upward.

$$E_d(z) = \int_{\phi=0}^{2\pi}\int_{\theta=0}^{\pi/2} L(z;\theta,\phi)\cos\theta\sin\theta\, d\theta d\phi \tag{2.36}$$

using the symbols E for irradiance, L for radiance and z for depth.
The upward vector irradiance $E_u(z)$ is defined likewise except for the use of the absolute value of the cosine of the zenith angle to obtain positive values.

$$E_u(z) = \int_{\phi=0}^{2\pi}\int_{\theta=\pi/2}^{\pi} L(z;\theta,\phi)\,|\cos\theta|\sin\theta\, d\theta d\phi \tag{2.37}$$

The irradiance ratio $R(z)$ is defined by the ratio of upward irradiance to downward irradiance

$$R(z) = \frac{E_u(z)}{E_d(z)} \tag{2.38}$$

The scalar irradiance $E_0(z)$ is measured with a spherical detector

$$E_0(z) = \int_{\phi=0}^{2\pi}\int_{\theta=0}^{\pi} L(z;\theta,\phi)\sin\theta\, d\theta d\phi \tag{2.39}$$

The downward scalar irradiance $E_{0d}(z)$ is the integral over all downward directions of the radiance distribution and measured with a hemispherical detector looking upward.

$$E_{0d}(z) = \int_{\phi=0}^{2\pi}\int_{\theta=0}^{\pi/2} L(z;\theta,\phi)\sin\theta\, d\theta d\phi \tag{2.40}$$

The upward scalar irradiance $E_{0u}(z)$ is likewise defined for the upward radiance and measured with the detector looking downward.

$$E_{0u}(z) = \int_{\phi=0}^{2\pi}\int_{\theta=\pi/2}^{\pi} L(z;\theta,\phi)\sin\theta\, d\theta d\phi \qquad (2.41)$$

The ratio of the net vector irradiance $E(z)$ to the scalar irradiance $E_0(z)$ is

$$\overline{\mu} = \frac{E(z)}{E_0(z)} \qquad (2.42)$$

The average path length of the net diffuse radiance in the direction of the net vector irradiance is a factor $\overline{\mu}^{-1}$ higher than the geometric path length.

In the sea the direction of the light vector initially deviates from the vertical direction of measurement by a certain zenith angle. Because the vertical direction is used to measure geometrical distances and irradiance attenuation with depth, we suggest to denote the average cosine parameter $\overline{\mu}$ for clarity reasons in two parts: a part μ_E owing to the diffuseness of the radiance distribution and a part μ_θ owing to the angle between the direction of the light vector (usually the sun) and the direction over which the net vector is measured, usually the vertical direction.

$$\overline{\mu} = \mu_\theta \overline{\mu}_E \qquad (2.43)$$

If the net vector irradiance is perpendicular to the water surface $\mu_\theta = 1$ and only the diffuseness part remains. The separation into two factors was introduced to explicitly include this measurement angle effect.

2.3.2 Irradiance Attenuation Coefficients

Irradiance attenuation coefficients are used in primary production models to calculate the extinction of a diffuse light field with increasing depth. These coefficients can also be used to estimate the inherent optical properties of a water layer by inverse modelling (Section 2.8.3).

The scalar irradiance attenuation coefficient is

$$K_0(z) = \frac{-1}{E_0(z)}\frac{d}{dz}E_0(z) \qquad (2.44)$$

The downward irradiance attenuation coefficient is

$$K_d(z) = \frac{-1}{E_d(z)} \frac{d}{dz} E_d(z) \qquad \textbf{(2.45)}$$

The upward irradiance attenuation coefficient is

$$K_u(z) = \frac{-1}{E_u(z)} \frac{d}{dz} E_u(z) \qquad \textbf{(2.46)}$$

The attenuation coefficient of the net vector irradiance in the vertical direction is

$$K_E(z) = \frac{-1}{E(z)} \frac{d}{dz} E(z) \qquad \textbf{(2.47)}$$

Substitution of the Equations 2.47 and 2.35 in 2.34 shows that the net vector irradiance attenuation K_E is related to the absorption a by three observable quantities of the light field

$$a(z) = \frac{E_d(z) - E_u(z)}{E_0(z)} K_E(z) \qquad \textbf{(2.48)}$$

This equation and for example Equation 2.34 have limited practical value because E_d and E_0 can not be measured with sufficient accuracy because they are very sensitive to the effects of surface waves (Tyler *et al.* 1972; Zaneveld 1989).

2.4 Asymptotic Radiance Distribution

The angular distribution of radiance with increasing depth approximates asymptotically to an equilibrium distribution pattern (Poole 1945; Preisendorfer 1959). Highly directional irradiance becomes diffuse and uniform diffuse irradiance becomes more directional (Latimer and Jeong Noh 1987). In the asymptotic region the radiance distribution no longer changes with depth and the intensities decrease with increasing depth at a constant rate: the asymptotic radiance attenuation k_∞. The relation between this asymptotic radiance attenuation coefficient and the inherent optical properties was studied because potentially the relation can be used to convert near asymptotic attenuation coefficients to the inherent properties of the medium (Herman and Lenoble 1968; van de Hulst 1968; Beardsley and Zaneveld 1969; Prieur and Morel 1971; Zaneveld and Pak 1972; Timofeeva 1974; Guenther and Thomas 1984; Tanis *et al.* 1986).

Before considering this the general attenuation of radiance is treated. It is given by a simplified form of the equation for radiative transfer

$$\frac{dL(z;\theta,\phi)}{dz}\mu = -cL(z;\theta,\phi)+L_*(z;\theta,\phi) \qquad \textbf{(2.49)}$$

with the radiance $L(z;\theta,\phi)$ at depth z in the direction (θ,ϕ) of zenith angle θ and azimuth angle ϕ. The coefficient μ is the cosine of the angle θ, it is 1 for radiance in the z direction. The first term on the right gives the radiance decrease per meter due to absorption and scattering, c, the second term on the right is the path radiance L_*. The path radiance is the radiance increase per meter due to light scattered from all other directions into the beam under consideration. Details were reviewed by Jerlov (1976). In the following we use an abbreviated notation for Equation 2.49

$$\frac{dL}{dz}\mu = -cL+L_* \qquad \textbf{(2.50)}$$

When radiance is measured along the vertical and the average direction of the incident light is also perpendicular to the water surface, the cosine of the angle μ approaches one. After division by L and rearranging Equation 2.50 leads to the radiance attenuation coefficient k

$$k = \frac{-1}{L}\frac{dL}{dz} = c-\frac{L_*}{L} \qquad \textbf{(2.51)}$$

where the ratio of path radiance L_* to radiance L is the gain coefficient due to path radiance (Le Grand 1939).

The radiance attenuation k_∞ is the radiance attenuation in the asymptotic region. An equilibrium has been reached for radiance scattered in and out of the angle of acceptance. Radiance attenuation in the direction of the net light flux has become constant and the decrease in magnitude has become the same for all scattering directions of the radiance distribution. Radiance intensities decrease with depth by the same magnitude for all angles. So at great depth the radiance distribution is independent of the radiance distribution incident on the sea surface and the decay of the radiance distribution pattern with depth has become equal for all directions. This implies that in this limit all irradiance attenuations $K(z)$ have become the same, equal to the radiance attenuation k_∞.

$$k_\infty = K_d(\infty) = K_u(\infty) = K_0(\infty) = K_{0d}(\infty) = K_{0u}(\infty) \qquad \textbf{(2.52)}$$

Several functions were investigated in attempts to find a relation which would best approximate calculated ratios of K_∞/c and the single scattering albedo ω_0. The relations include that of Timofeeva (1974) for milk suspensions.

$$\frac{K_\infty}{c} = \left(\alpha_1(1-\omega_0)\right)^{\omega_0/2} \tag{2.53}$$

where the constant α_1 ranges from 0.19 to 1.8, with $\alpha_1=0.25$ for milk and $\alpha_1=0.19$ for Monte Carlo calculations by Guenther (1984).
Recently Gordon (1993) showed by Monte Carlo calculations that this relation is not a purely academic concept but may have practical applications in ocean optics. Because K_d and K_∞ were equal within a few percent at optical depths $\tau \geq 5$, measurements of K_d can be used to derive the inherent optical properties.

2.5 Optical Depth

To derive solutions of model calculations for optical equivalent cases a dimensionless parameter, the optical depth τ, is used. It is defined to convert geometric distances to a dimensionless optical equivalent. The geometric distance is multiplied by the beam attenuation of the medium to give the optical depth.

$$\tau = \int_0^z c(z)\,dz \tag{2.54}$$

If the suspension is homogeneous, its optical depth can be calculated by multiplying the constant beam attenuation by the geometric distance. The optical depth for spectrophotometric measurements on samples using a cuvette with path length l is calculated by

$$\tau = cl \tag{2.55}$$

Measurement of a tenfold diluted sample using a tenfold longer path length is an optical equivalent case, the optical depths are the same.

2.6 Optical Deep Water

Most surface waters are too deep for light to penetrate to the bottom, be reflected at the bottom, pass the water layer again and contribute significantly to surface reflectance. By

definition the reflectance spectrum of an optical deep water is not significantly influenced by light reflected at the bottom. Optical shallow waters are not optical deep, their reflectance spectrum at the water surface is significantly influenced by light reflected at the bottom.

The term optical deep describes a property of water and is not to be confused with the parameter τ called optical depth that is an optical equivalent of depth. To demonstrate the difference in use: a shallow lake with turbid water can be an optical deep water and light levels decrease with increasing optical depth.

2.7 Modelling the Volume Scattering Function

Several models have been proposed to describe the volume scattering function. According to Beardsley and Zaneveld (1969) the angular distribution of scattered radiance can be described by

$$\beta(\theta) = \frac{\beta(90)}{\left((1-e_f\cos\theta)(1+e_b\cos\theta)\right)^4} \qquad \textbf{(2.56)}$$

with fit parameters e_f and e_b. The volume scattering function is called a phase function when normalized to its integral, the scattering coefficient b. The scattering distribution pattern and its characteristic asymmetry in forward and backward directions can also be described by a Henyey-Greenstein phase function with asymmetry parameter g ($0.0 \leq g \leq 1.0$) by

$$\beta(\theta) = \frac{1-g^2}{(1+g^2-2g\cos\theta)^{2/3}} \qquad \textbf{(2.57)}$$

Y.P. Wang *et al.* (1989) gave an expression to calculate the forward scattering probability F of a normalized volume scattering function with asymmetry parameter g

$$F = \frac{1+g}{2g}\left[1-\frac{1-g}{\sqrt{1+g^2}}\right] \qquad \textbf{(2.58)}$$

2.8 Reflectance Models

Compared to the asymptotic region the angular radiance distribution pattern in the region near the surface is far more complex. Radiance and irradiance attenuation coefficients are not equal and depend on depth.

Several methods can be used to solve the radiative transfer equations. Since exact solutions are unavailable numerical methods are used to solve the equations. Among other methods Monte Carlo calculations and the method of discrete ordinates (Chandrasekhar 1960) are used. Several analytic methods exists that yield approximative solutions. These methods give insight and require less computation time. The analytical methods include the single scattering method (Jerlov 1976), the delta function scattering method (Di Toro 1981), the quasi-single scattering approximation (Gordon and Brown 1973; Gordon 1973; Gordon *et al.* 1975) and several methods with two flows (Schuster 1905; Kubelka and Munk 1931; Duntley 1942; Joseph 1950; Austin 1974; Preisendorfer 1976), three flows (Incropera and Houf 1979), or four flows (Beasley *et al.* 1967; Maheu *et al.* 1984; Maheu and Gouesbet 1986; Niklasson 1987; Maheu *et al.* 1989).

The numerical methods require that the inherent optical properties a and $\beta(\theta)$ are known. The simple analytical models do not require the full detail of the volume scattering function; the scattering coefficient b and the backscattering probability B are used. However, in most applications these properties are not known. In practice simple analytical model are used to determine the inherent optical properties by an optimization procedure using measurements on the light field.

Preisendorfer and Mobley (1984) solved the two flow vector irradiance model for direct and inverse modelling of the light field. The inverse modelling requires the input of a depth profile of irradiance measurements. Inherent optical properties of a vertically stratified medium can be calculated if measurements are available at the interfaces of each slab that can be assumed homogeneous. Aas (1987) gave a review of two flow irradiance models for (optical) deep water and concluded that the reflectance is a function of the ratio b_b/a, it is an almost linear function when the ratio is small and approaches an asymptotic value when the ratio becomes large.

The quasi-single scattering model of Gordon *et al.* (1975) can be used to calculate the reflectance of optical deep and homogeneous suspensions. In the quasi-single scattering approximation the forward part of the volume scattering function is replaced by a delta function at 0°, b_f, while the actual backward portion of $\beta(\theta)$ is used in the simulation. The model consists of a polynomial fit of simulated reflectance values to the backscattering albedo ω_b, the ratio of coefficients of backscatter to absorption plus backscatter for single scattering $b_b/(a+b_b)$. Effects of illumination conditions on the subsurface reflectance were small; compared to zenith sun illumination the reflectance for sky illumination was 10 percent higher. The validity of the approximative solution was specified by a range of single

scattering albedo's ω_0, the ratio of the scattering coefficient to the beam attenuation coefficient. The method was validated for ω_0 up to 0.85.

In two flow models up- an downward radiance distributions are described by irradiance vectors. Four flow models include additional flows to represent the non-scattered solar beam as collimated up- and downward irradiance vectors. The methods are not valid for ω_0 close to unity.

Maheu and Gouesbet (1986) presented a review of the general solution for a four flow model accounting for up- and downward flows of diffuse and collimated light. They showed that the general solution of the four flow model presented by Beasley *et al.* (1967) can be reduced to numerous other models by introducing specific assumptions. For instance the two flow model with only two diffuse flows and Kubelka-Munk's theory (1931).

2.8.1 Successive Order Scattering Model

Morel and Prieur (1977) analyzed variations in colour of ocean water. The successive order scattering method lead to the expression for reflectance

$$R_\infty(0) = 0.33\frac{Bb}{a}(1+\Delta) \approx 0.33\frac{Bb}{a} \qquad \textbf{(2.59)}$$

A similar expression was derived by Erdmann and Saint Clair (1988) with a probabilistic method to approximate Monte Carlo calculations. They used this method to speed up the simulation of satellite images with a spatial distribution of biomass.

2.8.2 Quasi-Single Scattering Model

The quasi-single scattering approximation (Gordon and Brown 1973; Gordon 1973; Gordon *et al.* 1975) was derived for homogeneous waters with a flat air-water surface. Similar expressions for sun and sky illumination resulted for the dependence of both $K_d(\tau)$ and $R(\tau)$ with optical depth.

The equation for $K_d(\tau)$ here takes the form

$$\frac{K_d(\tau)}{cD_d(\tau)} = \sum_{n=0}^{3} k_n(\tau)(\omega_0 F)^n = \sum_{n=0}^{3} k_n(\tau)\left[\frac{b_f}{c}\right]^n \qquad \textbf{(2.60)}$$

and for $R(\tau)$

$$R(\tau) = \sum_{n=0}^{3} r_n(\tau)\left[\frac{b_b}{a+b_b}\right]^n \qquad \textbf{(2.61)}$$

where $k_n(\tau)$ and $r_n(\tau)$ are parameters computed by fitting the formulas to the results of about hundred Monte Carlo simulations. Coefficients were given for illumination by collimated irradiance from the sun and for a totally diffuse irradiance from the sky. The use of a polynomial curve with three terms and negligible constant resulted in a mean error in the equations of about 3% for optical depths τ from 0 to 4 and for solar zenith angles under water $0° \leq \theta_s \leq 20°$. After substitution of the backscattering albedo in the equations the quasi-single scattering model for zenith sun illumination becomes:

$$R_\infty(0) = 0.3244\,\omega_b + 0.1425\,\omega_b^2 + 0.1308\,\omega_b^3 \qquad \textbf{(2.62)}$$

and for sky illumination:

$$R_\infty(0) = 0.3687\,\omega_b + 0.1802\,\omega_b^2 + 0.0740\,\omega_b^3 \qquad \textbf{(2.63)}$$

Jerome (1988) showed, based on Monte Carlo simulations, that compared to the reflectance with a zenith sun the reflectance with the sun at a zenith angle is proportional to the reciprocal of that angle in water. Gordon (1989b) showed that the variation of the reflectance of natural waters with sun angle depends on the volume scattering function and the sun angle. He also showed that inversely the volume scattering function can be estimated from the variation of the reflectance with the sun angle.

The effect of surface roughness on $<K>/cD_0$ of Equation 2.60 is small (<3%) for wind speeds up to 17 m s^{-1} (Gordon 1989a). The symbol $<K>$ is used for the average value of $K(\tau)$ over the depth interval of the euphotic zone, where irradiance levels drop to 1%. So measurements of three apparent optical properties K_d, D_d and R and one inherent optical property c can be used to estimate the inherent optical properties a, b_b and b_f.

2.8.3 Two Flow Model

A derivation of the two flow model is given based on the review of Aas (1987). Starting with the vector irradiance model of Gershun (1939) and the equation of radiance attenuation, the differential equations of Schuster (1905) for a two flow vector irradiance model are derived and solutions are presented for optical deep and optical shallow waters.

Gershun's equation (2.34) for a vertically stratified medium is

$$\frac{d}{dz}E = -aE_0 \tag{2.64}$$

An equivalent form using more commonly measured values is

$$\frac{d}{dz}(E_d - E_u) = -a(E_{0d} + E_{0u}) \tag{2.65}$$

Integration of Equation 2.49 for radiance attenuation over the upper hemisphere gives

$$\frac{d}{dz}E_d = -cE_{0d} + (b - b_b)E_{0d} + b_bE_{0u} = -(a + b_b)E_{0d} + b_bE_{0u} \tag{2.66}$$

Subtraction of Equation 2.66 from Equation 2.65 gives

$$-\frac{d}{dz}E_u = -(a + b_b)E_{0u} + b_bE_{0d} \tag{2.67}$$

By inserting the two distribution parameters D_u and D_d, the inverse of the average cosines of the up- and downward radiance distributions

$$\begin{aligned} D_d &= \frac{E_{0d}}{E_d} = \frac{1}{\mu_d} \\ D_u &= \frac{E_{0u}}{E_u} = \frac{1}{\mu_u} \end{aligned} \tag{2.68}$$

and with the abbreviations

$$\begin{aligned} k_d &= (a+b_b)D_d \\ k_u &= (a+b_b)D_u \\ b_{bd} &= b_b D_d \\ b_{bu} &= b_b D_u \end{aligned} \qquad \textbf{(2.69)}$$

the Equations 2.66 and 2.67 obtain the form

$$\frac{d}{dz}E_d = -k_d E_d + b_{bu} E_u \qquad \textbf{(2.70)}$$

$$-\frac{d}{dz}E_u = -k_u E_u + b_{bd} E_d \qquad \textbf{(2.71)}$$

These equations for a two flow model were first applied to an optical problem by Schuster (1905). Elimination of E_u in Equation 2.71 by means of Equation 2.70 gives

$$\frac{d^2}{dz^2}E_d = (k_u - k_d)\frac{d}{dz}E_d + (k_u k_d - b_{bu} b_{bd})E_d \qquad \textbf{(2.72)}$$

or in an equivalent form

$$\frac{d^2}{dz^2}E_d = (a+b_b)(D_u - D_d)\frac{d}{dz}E_d + (a^2+2ab_b)(D_u D_d)E_d \qquad \textbf{(2.73)}$$

The general solution for this differential equation can be found in textbooks (e.g. Weast and Astle 1981), it requires two boundary conditions and with E_d solved, E_u is determined by Equation 2.71.

The solution of this differential equation should only be applied to a depth range were the pattern of the radiance distribution can be regarded as fairly constant: either for a thin homogeneous layer or at great depths where the radiance distribution is close to its asymptotic pattern.

2.8.3.1 Solution for Optical Deep Waters

Provided that the water is so deep that no light reaches the bottom, the boundary condition for infinite depth is zero, the solution of the two flow model leads to an exponentially decreasing downward irradiance.

$$E_d(z) = E_d(0)\exp(-K_d z) \tag{2.74}$$

with

$$\begin{aligned} K_d &= \frac{(k_u - k_d)}{2} + \frac{\left((k_u+k_d)^2 - 4b_{bu}b_{bd}\right)^{1/2}}{2} \\ &= \frac{(a+b_b)(D_u - D_d)}{2} + \frac{\left((a+b_b)^2(D_u+D_d)^2 - 4b_b^2(D_uD_d)\right)^{1/2}}{2} \end{aligned} \tag{2.75}$$

Using Equation 2.70 and the definition of K_d (Equation 2.45) the irradiance reflectance of an optical deep water, $R_\infty(0)$, becomes

$$R_\infty(0) = \frac{1}{E_d}E_u = \frac{1}{E_d}\,\frac{k_d E_d + \frac{d}{dz}E_d}{b_{bu}} = \frac{k_d - K_d}{b_{bu}} \tag{2.76}$$

and after substitution of Equation 2.75

$$\begin{aligned} R_\infty(0) &= \frac{k_u + k_d - \left((k_u+k_d)^2 - 4b_{bu}b_{bd}\right)^{1/2}}{2b_{bu}} \\ &= \frac{(a+b_b)(D_u+D_d) - \left((a+b_b)^2(D_u+D_d)^2 - 4b_b^2 D_u D_d\right)^{1/2}}{2b_b D_u} \\ &= \left[\frac{a+b_b}{b_b} - \left[\frac{(a+b_b)^2}{b_b^2} - \frac{4D_uD_d}{(D_u+D_d)^2}\right]^{1/2}\right]\frac{D_u+D_d}{2D_u} \end{aligned} \tag{2.77}$$

Assuming equal distribution factors $D_u=D_d=D$ and $b_b \ll a$ Equation 2.75 reduces to

$$\begin{aligned} K_d &= \frac{\left((a+b_b)^2(2D)^2-4b_b^2D^2\right)^{1/2}}{2} \\ &= (a^2+2ab_b)^{1/2}\ D \\ &\approx aD \end{aligned} \tag{2.78}$$

and Equation 2.77 to

$$R_\infty(0) = \frac{a+b_b}{b_b} - \left[\left[\frac{a+b_b}{b_b}\right]^2 - 1\right]^{1/2} \tag{2.79}$$

or its equivalent form

$$R_\infty(0) = \frac{1}{\frac{a+b_b}{b_b} + \left[\left[\frac{a+b_b}{b_b}\right]^2 - 1\right]^{1/2}} \tag{2.80}$$

$$R_\infty(0) = \frac{b_b}{a+b_b+\left((a+b_b)^2-b_b^2\right)^{1/2}} \tag{2.81}$$

resulting in the equation derived by Duntley (1942)

$$\begin{aligned} R_\infty(0) &= \frac{b_b}{a+b_b+(a^2+2ab_b)^{1/2}} \\ &= \frac{b_b/a}{1+b_b/a+(1+2b_b/a)^{1/2}} \end{aligned} \tag{2.82}$$

Equation 2.77 can be rewritten to the form of Duntley's equation

$$R_\infty(0) = \frac{D_u+D_d}{2D_u} \frac{b_b}{(a+b_b)+\left[(a+b_b)^2-\frac{4D_uD_d}{(D_u+D_d)^2}b_b^2\right]^{1/2}} \quad \textbf{(2.83)}$$

showing how the reflectance calculated by the two flow model is affected by accounting for the distribution factors of the irradiance vectors.

2.8.3.2 Solution for Optical Shallow Water

The reflectance spectrum of an optical shallow water is significantly influenced by light reflected at the bottom.

Joseph (1950) presented a solution for the two flow model that included reflectance of light at the bottom. The solution uses the reflectance of optical deep water

$$R_\infty(0) = \frac{K_d-a}{K_d+a} = \frac{\sqrt{a(a+2ab_b)}-a}{\sqrt{a(a+2ab_b)}+a} \quad \textbf{(2.84)}$$

to calculate that of an optical shallow water:

$$R(0) = R_\infty(0)+(R_b-R_\infty(0))\frac{\left(1-R_\infty^2(0)\right)}{\left(1-R_\infty(0)R_b\right)\exp(2K_dz_b)+R_\infty(0)\left(R_b-R_\infty(0)\right)} \quad \textbf{(2.85)}$$

Spitzer and Dirks (1987) solved the two flow model for optical shallow water using the invariant imbedding method. Their solution for optical deep water can be rewritten to Equation 2.77 or by using the backscattering albedo to

$$R_\infty(0) = \left[\frac{1}{\omega_b}-\left[(\frac{1}{\omega_b})^2-\frac{4D_uD_d}{(D_u+D_d)^2}\right]^{1/2}\right]\frac{D_u+D_d}{2D_u} \quad \textbf{(2.86)}$$

The expression for optical shallow water is rather long and a new shorthand need to be introduced, R_α,

$$R_\alpha = \left[\frac{1}{\omega_b} + \left[(\frac{1}{\omega_b})^2 - \frac{4D_u D_d}{(D_u+D_d)^2} \right]^{1/2} \right] \frac{D_u+D_d}{2D_u} \qquad \textbf{(2.87)}$$

its similar to $R_\infty(0)$ except for an add sign instead of the first minus sign.
The solution for optical shallow water is given for a bottom with R_b at depth z_b by

$$R(0) = R_\infty(0) + \left[(R_\infty(0) - R_\alpha) \frac{f(R_b,z_b)}{1-f(R_b,z_b)} \right] \qquad \textbf{(2.88)}$$

with

$$f(R_b,z_b) = \left[\frac{R_b - R_\infty(0)}{R_b - R_\alpha} \right] \exp(-z_b \left[(a+b_b)^2 (D_u+D_d)^2 - 4D_u D_d b_b^2 \right]^{1/2}) \qquad \textbf{(2.89)}$$

For wavelengths where the optical deep reflectance is equal to the bottom reflectance the models predict that the reflectance becomes independent of the bottom depth (Equation 2.85 and 2.89). These typical invariant spectral points can be used to verify the validity of the two flow model. Spitzer and Dirks (1987) gave results of two flow model calculations with these typical points in the spectra without mentioning their cause. Mantovani and Cabral (1992) presented measurements of suspensions that were not optical deep and misinterpreted these invariant points in the spectrum to separate regions with insignificant and predominant bottom influences.

2.9 Inclusion of the Water-Air Interface

Austin (1974, 1980) presented an expression for the reflectance ratio for the two flow model including the effects of the water to air interface and of bottom reflectance. The reflectance $R(z)$ and irradiance transmittance $T_w(z)$ of the water depend on depth because initially the angular distribution of the light field changes with depth towards it asymptotic pattern. The changes in $R(z)$ and $T_w(z)$ are insignificant below a small optical depth; a few meters in ocean water. By assuming that these properties are constant and that the transmittance is identical for the up- and downward irradiance, the above surface reflectance $R(0+)$ was related to the subsurface reflectance $R(0)$ by

$$R(0+) = r_d + (1-r_u)\frac{(1-r_d)R(0)}{1-r_u R(0)} \tag{2.90}$$

with the Fresnel coefficients r_d and r_u and with the subsurface reflectance

$$R(0) = R_w(0) + \frac{R_b T_w^2}{1-R_b R_w(0)} \approx R_w(0) + R_b T_w^2 \tag{2.91}$$

with

$$T_w = \exp(-Kz) \tag{2.92}$$

The approximation in Equation 2.91 is allowed if $R_b\, R_w(0) \ll 1$.

The reflectance $R_w(0)$ due to water is related to the reflectance of an optical deep water by

$$R_w(0) = R_\infty(0)(1-T_w^2) \tag{2.93}$$

If $R_b\, T_w^2 \leq R_w(0)$ and the denominator approaches unity Equation 2.90 can be simplified to

$$\begin{aligned} R(0+) &\approx r_d + (1-r_u)(R_w(0) + R_b T_w^2) \\ R(0+) &\approx 0.02 + 0.52\left(R_\infty(0) + (R_b - R_\infty(0))\exp(-2Kz)\right) \end{aligned} \tag{2.94}$$

Philpot (1987) used the relation

$$R(0+) = 0.546\, R_\infty(0) \tag{2.95}$$

between the above surface reflectance and the optical deep reflectance below the surface. For optical shallow water an expression similar to Equation 2.94 was used and the different distribution factors for up- and downward irradiance were included:

$$\begin{aligned} R(0+) &= 0.546\left(R_\infty(0) + (R_b - R_\infty(0))\, T_u T_d\right) \\ &= 0.546\left(R_\infty(0) + (R_b - R_\infty(0))\exp(-az(D_u + D_d)\right) \end{aligned} \tag{2.96}$$

2.10 Radiance Reflectance Spectra

Whitlock *et al.* (1981) calculated the subsurface irradiance reflectance from radiance measurements above the water surface by

$$\frac{L_u(0+)-0.02L_{sky}(0+)}{L_{ref}(0+)} = R(0+)-R_{aw} = 0.52\,R(0) \qquad \textbf{(2.97)}$$

The reference radiance $L_{ref}(0+)$ is a measure of the incident light field, it samples downward irradiance reflected by a reference panel coated with a perfect diffusely reflecting white paint. The relation between above-surface radiance and the subsurface irradiance ratio is valid for solar zenith angles less than 60°. Dubelaar *et al.* (1992) showed that its application yielded accurate predictions of the subsurface reflectance for a clear water station at the Corfu Sea.

Bukata *et al.* (1981abc, 1988) used the water-air interface model of Austin to obtain optical water quality models of Lake Ontario and Lake St. Clair. Above surface radiance $L_u(0+)$ was related to subsurface reflectance by

$$L_u(0+) = L_{u,w}(0+)+0.02\,L_{sky}+f_s\,L_{sun} \qquad \textbf{(2.98)}$$

and

$$L_{u,w}(0+) = \frac{0.98\,R(0)}{\pi n_w^2(1-0.48\,R(0))}(0.98\,E_{sun}+0.934\,E_{sky}) \qquad \textbf{(2.99)}$$

The factor f_s owing to sun-glint is small, typically 0.003.

Carder and Steward (1985) used the following model to relate the remotely sensed ratio $R(0+)$, measured above the water surface using the upward radiance $L_u(0+)$ and a reference radiance $L_{ref}(0+)$, to its value just beneath the surface $R(0)$ and by this value to the inherent optical properties of the water under investigation.

$$R(0+) = \frac{\pi L_u(0+)}{E_d(0+)} = \frac{\pi\dfrac{(1-r_d)}{n_w^2}\dfrac{E_u(0)}{f_{E/L}}}{\dfrac{E_d(0)}{0.97}} \qquad \textbf{(2.100)}$$

the factor $f_{E/L}$ between the subsurface upward irradiance and upward radiance, $E_u(0)/L_u(0)$, is usually larger than the value π for an uniform radiance distribution, its default value is 5.

By substitution of n_w=1.341, r_d=0.021 and $f_{E/L}$=5.08 they found

$$R(0+) = 0.3264\ R(0) \qquad \textbf{(2.101)}$$

and by inserting the relation between the reflectance ratio and the inherent optical properties according to Morel and Prieur (1977) they derived an expression that is valid for waters with a negligible backscattering compared to the absorption.

$$R(0+) = 0.1076\frac{b_b}{a} \qquad \textbf{(2.102)}$$

The model was applied to spectral measurements of a bloom of the red-tide dinoflagellate *Ptychodiscus brevis*. Reflectance spectra were remotely sensed from a low-flying helicopter. The reflectance model showed good agreement for chlorophyllous pigment concentrations varying from 7 to 77 mg m^{-3}, except for a spectrally neutral offset.
Comparison of Equation 2.101 to the Equations 2.94, 2.95 and 2.97 shows that the relation between above surface and subsurface reflectance differs by a factor of 0.62 ($=\pi/f_{E/L}$). This indicates that it is not yet clear which reflectance model must be used to interpret reflectance spectra.

References

Aas, E., 1981. The refractive index of phytoplankton, Univ. Oslo, Inst. Rep. Series **46**, 61 pp.

Aas, E., 1987. Two-stream irradiance model for deep waters, Appl. Opt. **26**(11), 2095-2101.

Austin, R.W., 1974. The remote sensing of spectral radiance from below the ocean surface, In: *Optical aspects of oceanography*, Eds. N.G. Jerlov and E. Steemann Nielsen, Academic Press, London, 317-344.

Austin, R.W. and T.J. Petzold, 1977. Considerations in the design and evaluation of oceanographic transmissometer, In: *Light in the sea* (Benchmark papers in optics, V. 3), Ed. J.E. Tyler, Dowden, Hutchinson and Ross, Stroudsburg, Pennsylvania, 104-120.

Austin, R.W., 1980. Gulf of Mexico, ocean-color surface-truth measurements, Bound. Layer Meteor. **18**, 269-285.

Bannister, T.T., 1988. Estimation of absorption coefficients of scattering suspensions using opal glass, Limnol. Oceanogr. **33**(4), 607-615.

Beardsley, G.F. Jr., and J.R.V. Zaneveld, 1969. Theoretical dependence of the near-asymptotic apparent optical properties on the inherent optical properties of sea water, J. Opt. Soc. Am. **59**(4), 373-377.

Beasley, J.K., J.T. Atkins and F.W. Billmeyer Jr., 1967. Scattering and absorption of light in turbid media, In: *Electromagnetic Scattering*, Eds. R.L. Rowell and R.S. Stein, Gordon and Breach, New York, 772-785.

Bohren, C.F., Huffman, D.R., 1983. *Absorption and scattering of light by small particles*, John Wiley, New York, 500 pp.

Bricaud, A., A. Morel and L. Prieur, 1981a. Absorption by dissolved organic matter of the sea (yellow substance) in the UV and visible domains, Limnol. Oceanogr. **26**(1), 43-53.

Bricaud, A., A. Morel and L. Prieur, 1983. Optical efficiency factors of some phytoplankters, Limnol. Oceanogr. **28**(5), 816-832.

Bricaud, A., A. Morel, 1986. Light attenuation and scattering by phytoplanktonic cells: a theoretical modeling, Appl. Opt. **25**(4), 571-580.

Bricaud, A., A. Bédhomme and A. Morel, 1988. Optical properties of diverse phytoplanktonic species: experimental results and theoretical interpretation, J. Plankton Res. **10**(5), 851-873.

Bukata, R.P., J.E. Bruton and J.H. Jerome, 1980. Conceptual approach to the simultaneous determination of the backscatter and absorption coefficients of natural waters, Appl. Opt. **19**(9), 1550-1559.

Bukata, R.P., J.H. Jerome, J.E. Bruton, S.C. Jain and H.H. Zwick, 1981a. Optical water quality model of Lake Ontario. 1: Determination of the optical cross sections of organic and inorganic particulates in lake Ontario, Appl. Opt. **20**(9), 1696-1703.

Bukata, J.H., R.P. Jerome, J.E. Bruton, S.C. Jain and H.H. Zwick, 1981b. Optical water quality model of Lake Ontario. 2: Determination of chlorophyll *a* and suspended mineral concentrations of natural waters from submersible and low altitude optical sensors, Appl. Opt. **20**(9), 1704-1714.

Bukata, R.P., J.H. Jerome and J.E. Bruton, 1981c. Validation of a five-component optical model for estimating chlorophyll *a* and suspended mineral concentrations in Lake Ontario, Appl. Opt. **20**(20), 3472-3474.

Bukata, R.P., J.H. Jerome and J.E. Bruton, 1988. Particle concentrations in Lake St. Clair as recorded by a shipborne multispectral optical monitoring system, Remote Sens. Environ. **25**, 201-229.

Butler, W.L., 1962. Absorption of light by turbid materials, J. opt. Soc. Am. **52**(3), 292-299.

Carder, K.L., and R.G. Steward, 1985. A remote-sensing reflectance model of a red-tide dinoflagellate off west Florida, Limnol. Oceanogr. **30**(2), 286-298.

Chandrasekhar, S., 1960. *Radiative Transfer*, Dover, New York.

Davies-Colley, R.J., 1983. Optical properties and reflectance spectra of 3 shallow lakes obtained from a spectrophotometric study, New Zealand J. Marine Freshwater Res. **17**, 445-459.

Debye, P., 1929. *Polare Molekeln*, Verlag von S. Hirzel, Leipzig, 199 pp.

Di Toro, D.M., 1978. Optics of turbid estuarine waters: approximations and applications, Water Res. **12**, 1059-1068.

Doerffer, R., 1980. Applications of a two-flow model for remote sensing of substances in water, Boundary-Layer Meteorology **18**, 221-232.

Dubelaar, G.B.J., J.H.M. Hakvoort, J. Krijgsman, C.S. van der Reijden and M. Donze, 1992. In-situ determination of optical properties of seawater and particle characteristics in the Corfu Sea, Report on the first Joint Campaign of the Mito Project, Netherlands Remote Sensing Board, BCRS report **92-04**, 90 pp.

Duntley, S.Q., 1942. Optical properties of diffusing materials, J. Opt. Soc. Am. **32**, 61-70.

Duysens, L.N.M., 1956. The flattening of the absorption spectrum of suspension, as compared to that of solutions, Biochim. Biophys. Acta **19**, 1-12.

Elterman, P., 1970. Integrating cavity spectroscopy, Appl. Opt. **9**(9), 2140-2142.

Erdmann, J.C., and J.M. Saint Clair, 1988. Simulation of radiometric ocean images recorded from high-altitude platforms, Proc. SPIE **925** (Ocean Optics IX), 36-49.

Friedman, E., L. Poole, A. Cherdak and W. Houghton, 1980. Absorption coefficient instrument for turbid natural waters, Appl. Opt. **19**(10), 1688-1693.

Fry, E.S, and G.W. Kattawar, 1988. Measurement of the absorption coefficient of ocean water using isotropic illumination, Proc. SPIE **925** (Ocean Optics IX), 142-148.

Gershun, A. 1939. The light field, J. Math. Phys. (Cambridge Mass.) **18**, 51-151.

Gordon, H.R., and O.B. Brown, 1973. Irradiance reflectivity of a flat ocean as a function of its optical properties, Appl. Opt. **12**(7), 1549-1551.

Gordon, H.R., 1973. Simple calculations of the diffuse reflectance of the ocean, Appl. Opt. **12**(12), 2803-2804.

Gordon, H.R., O.B. Brown and M.M. Jacobs, 1975. Computed relationships between the inherent and apparent optical properties of a flat homogeneous ocean, Appl. Opt. **14**(2), 417-427.

Gordon, H.R., 1989a. Can the Lambert-Beer law be applied to the diffuse attenuation coefficient of ocean water?, Limnol. Oceanogr. **34**(8), 1389-1409.

Gordon, H.R., 1989b. Dependence of the diffuse reflectance of natural waters on the sun angle, Limnol. Oceanogr. **34**(8), 1484-1489.

Gordon, H.R., K. Ding and W. Gong, 1993. Radiative transfer in the ocean: computations relating to the asymptotic and near-asymptotic daylight field, Appl. Opt. **32**(9), 1606-1619.

Guenther, G.C., and R.W.L. Thomas, 1984. Effects of propagation induced pulse stretching in air-borne laser hydrography, Proc. SPIE **489** (Ocean Optics VII).

Haardt, H., and H. Maske, 1987. Specific in vivo absorption coefficient of chlorophyll *a* at 675 nm, Limnol. Oceanogr. **32**(3), 608-619.

Herman, M., and J. Lenoble, 1968. Asymptotic radiation in a scattering and absorbing medium, J. Quant. Spectrosc. Radiant. Transfer **8**, 355-367.

Hulst, H.C. van de, 1957. *Light scattering by small particles*, Dover Publ., New York, 450 pp.

Hulst, H.C. van de, 1968. Radiative transfer in thick atmospheres with an arbitrary scattering function, Bull. Astr. Inst. Netherlands **20**, 77-86.

Incropera, F.P., and W.G. Houf, 1979a. A three-flux method for predicting radiative transfer in aqueous suspensions, ASME J. Heat Transfer **101**, 496-501.

Incropera, F.P., T.R. Wagner and W.G. Houf, 1981. A comparison of predictions and measurements of the radiation field in a shallow water layer, Water Resources Res. **17**(1), 142-148.

Iturriaga, R., B.G. Mitchell and D.A. Kiefer, 1988. Microphotometric analysis of individual particle absorption spectra, Limnol. Oceanogr. **33**(1), 128-135.

Iturriaga, R., and D.A. Siegel, 1989. Microphotometric characterization of phytoplankton and detrital absorption properties in the Sargasso Sea, Limnol. Oceanogr. **34**(8), 1706-1726.

Jerlov, N.G., 1976. *Marine optics*, Elsevier, Amsterdam, 231 pp.

Jerome, J.H., R.P. Bukata and J.E. Bruton, 1988. Utilizing the components of vector irradiance to estimate the scalar irradiance in natural waters, Appl. Opt. **27**(19), 4012-4018.

Joseph, J., 1950. Untersuchungen über Ober- und Unterlichtmessungen im Meer und über ihren Zusammenhang mit Durchsichtigkeitsmessungen, Deutsche Hydrogr. Z. **3**(5/6), 324-335.

Kiefer, D.A., and J.B. SooHoo, 1982. Spectral absorption by marine particles of coastal waters of Baja California, Limnol. Oceanogr. **27**(3), 492-499.

Kirk, J.T.O., 1980. Spectral absorption of natural waters: contribution of the soluble and particulate fractions to light absorption in some inland waters of South-Eastern Australia, Aust. J. Mar. Freshwater Res. **31**, 287-296.

Kirk, J.T.O., 1981a. Estimation of the scattering coefficient of natural waters using underwater irradiance measurements, Aust. J. Mar. Freshwater Res. **32**, 533-539.

Kirk, J.T.O., 1983. *Light and photosynthesis in aquatic ecosystems*, Cambridge University Press, Cambridge, 401 pp.

Kubelka, P., Munk, F., 1931. Ein Beitrag zur Optik der Farbanstriche, Z. Tech. Phys. **11a**, 593-601.

Kullenberg, G., 1968. Scattering of light by Sargasso Sea water, Deep-Sea Res. **15**, 423-432.

Kullenberg, G., 1974. Observed and computed scattering functions, In: *Optical aspects of oceanography*, Eds. N.G. Jerlov and E. Steemann Nielsen, Academic Press London, 25-49.

Kullenberg, G., 1984. Observations of light scattering functions in two oceanic areas, Deep-Sea Res. **13**(3), 295-316.

Latimer, P., and S. Jeong Noh, 1987. Light propagation in moderately dense particle systems: a reexamination of the Kubelka-Munk theory, Appl. Opt. **26**(3), 514-523.

Le Grand, Y., 1939. La pénétration de la lumière dans la mer, Ann. Inst. Océanogr. **19**, 393-436.

Maheu, B., Letoulouzan, J.N., Gouesbet, G., 1984. Four-flux models to solve the scattering transfer equation in terms of Lorenz-Mie parameters, Appl. Opt. **23**(19), 3353-3362.

Maheu, B., Gouesbet, G., 1986. Four-flux models to solve the scattering transfer equation: special cases, Appl. Opt. **25**(7), 1122-1128.

Maheu, B., Briton, J.P., Gouesbet, G., 1989. Four-flux model and a Monte Carlo code: comparison between two simple, complementary tools for multiple scattering calculations, Appl. Opt. **28**(1), 22-24.

Mantovani, J.E. and A.P. Cabral, 1992. Tank depth determination for water radiometric measurements, Int. J. Remote Sensing **13**(14), 2727-2733.

Maske, H., and H. Haardt, 1987. Quantitative in vivo absorption spectra of phytoplankton: Detrital absorption and comparison with fluorescence excitation spectra, Limnol. Oceanogr. **32**(3), 620-633.

Mie, G., 1908. Beitrage zur Optik truber Medien speziell kolloidaler Metallösungen, Ann. Physik (Leipzig) **25**, 377.

Mitchell, B.G., and D.A Kiefer, 1988b. Variability in pigment specific particulate fluorescence and absorption spectra in the northeastern Pacific Ocean, Deep-Sea Res. **35**(5), 665-689.

Morel, A., Prieur, L., 1977. Analysis of variations in ocean color, Limnol. Oceanogr. **22**(4), 709-722.

Morel, A., and A. Bricaud, 1981a. Theoretical result concerning light absorption in a discrete medium, and application to specific absorption of phytoplankton, Deep-Sea Res. **28**(11), 1375-1393.

Morel, A., and A. Bricaud, 1981b. Theoretical results concerning the optics of phytoplankton, with special reference to remote sensing applications, In: *Oceanography from space*, Ed. J.F.R. Gower, Plenum Press, New York, 313-327.

Morel, A. and Y.H. Ahn, 1990. Optical efficiency factors of free-living marine bacteria: Influence of bacterioplankton upon optical properties and particulate organic carbon in oceanic waters, J. Marine Res. **48**, 145-175.

Morel, A., 1991b. Optics of marine particles and marine optics, In: *Particle analysis in oceanography*, NATO ASI Series G: Ecological Sciences Vol. 27, Ed. S. Demers, Springer-Verlag, Berlin Heidelberg New York, 141-416.

Niklasson, G.A., 1987. Comparison between four flux theory and multiple scattering theory, letter to the editor, Appl. Opt. **26**(19), 4034-4036.

Petzold, T.J., 1977. Volume scattering functions for selected ocean waters, In: *Light in the sea* (Benchmark papers in optics: V. 3), Ed. J.E. Tyler, Dowden, Hutchinson and Ross, Stroudsburg, Pennsylvania, 152-174.

Philpot, W.D., 1987. Radiative transfer in stratified waters: a single-scattering approximation for irradiance, Appl. Opt. **26**(19), 4123-4132.

Poole, H.H., 1945. The angular distribution of submarine daylight in deep water, Scient. Proc. Royal Dublin Society, **24**(4), 29-42.

Pope, R.M, E.S. Fry, R.L. Montgomery and F. Sogandares, 1990. Integrating cavity absorption meter; measurement results, Proc. SPIE **1302** (Ocean Optics X), 165-175.

Preisendorfer, R.W., 1959. Theoretical proof of the existing characteristic diffuse light in natural waters, J. Mar. Res. **18**, 1-9.

Preisendorfer, R.W., 1976. *Hydrologic optics*, Vol. I-VI, U.S. Department of Commerce.

Preisendorfer, R.W., and C.D. Mobley, 1984. Direct and inverse irradiance models in hydrologic optics, Limnol. Oceanogr. **29**(5), 903-929.

Prieur, L., Morel, A., 1971. Etude théorique du régime asymptotique: relations entre caractéristiques optiques et coefficient d'extinction relatif a la pénétration de la lumière du jour, Cah. Oceanogr. **23**, 35-48.

Rose, H.E., 1952. Breakdown of the Lambert-Beer Law, Nature **169**, 287-288.

Schuster, A., 1905. Radiation through a foggy atmosphere, Astropys. J. **21**(1), 1-22.

Shibata, K., A.A. Benson and M. Calvin, 1954. The absorption spectra of suspensions of living micro-organisms, Biochimica et Biophysica Acta **15**, 461-470.

Shibata, K., 1958. Spectrophotometry of intact biological materials, absolute and relative measurements of their transmission, reflection and absorption spectra, J. Biochem. **45**(8), 599-623.

Smith, R.C. and K.S. Baker, 1981. Optical properties of the clearest natural waters (200-800 nm), Appl. Opt. **20**, 177-184.

Spitzer, D. and R.W.J. Dirks, 1987. Bottom influence on the reflectance of the sea, Int. J. Remote Sensing, **8**(3), 279-290.

Stramski, D., A. Morel and A. Bricaud, 1988. Modelling the light attenuation and scattering by spherical phytoplanktonic cells: a retrieval of bulk refractive index, Appl. Opt. **27**(19), 3954-3956.

Sugihara, S., M. Kishino, and N. Okami, 1982. Back-scattering of light by particles suspended in water, Sci. Papers Inst. Phys. Chem. Res. **76**(1), 1-8.

Tanis, F.J., Kattawar, G.W., Hickman, G.D., 1986. Influence of scattering on the diffuse attenuation coefficient in the asymptotic region, Proc. SPIE **637** (Ocean Optics VIII), 191-202.

Timofeeva, V.A., 1974. Optics of turbid waters (results of laboratory studies), In: *Optical aspects of oceanography*, Eds. N.G. Jerlov and E. Steemann Nielsen, Academic Press, London, 177-219.

Tyler, J.E, R.C Smith and W.H. Wilson Jr., 1972. Predicted optical properties for clear natural water, J. Opt. Soc. Am. **62**(1), 83-91.

Ulbricht, R., 1900. Die Bestimmung der mittleren räumlichen Lichtintensität durch nur ein Messung, Elektrotechnische Zeitschrift **29**, 595-597.

Voss, K.J., 1989. Use of the radiance distribution to measure the optical absorption coefficient in the ocean, Limnol. Oceanogr **34**(8), 1614-1622.

Wang, Y.P., Z.S. Wu and K.F. Ren, 1989. Four-flux model with adjusted average crossing parameter to solve the scattering transfer equation, Appl. Opt. **28**(1), 24-26.

Weast, R.C., and M.J. Astle (Eds.), 1981. *CRC Handbook of Chemistry and Physics*, **61**, CRC Press, A-121.

Weidemann, A.D., and T.T. Bannister, 1986. Absorption and scattering coefficients in Irondequoit Bay, Limnol. Oceanogr. **31**(3), 567-583.

Whitlock, C.H., L.R. Poole, J.W. Ursy, W.M. Houghton, W.G. Witte, W.D. Morris and Gurganus, E.A., 1981. Comparison of reflectance with backscatter and absorption parameters for turbid waters, Appl. Opt. **20**(3), 517-522.

Whitney, L.V., 1938. Transmission of solar energy and the scattering produced by suspension in lake waters, Trans. Wisc. Acad. Sci. Arts Lett. **31**, 201-221

Yentsch, C.S., 1960. The influence of phytoplankton pigments on the colour of sea water, Deep-Sea Res. **7**, 1-9

Yentsch, C.S., 1962. Measurement of visible light absorption by particulate matter in the ocean, Limnol. Oceanogr. **7**, 207-217.

Zaneveld, J.R.V., and H. Pak, 1972. Some aspects of the axially symmetric submarine daylight field, J. Geophys. Res. **77**(15), 2677-2680.

Zaneveld, J.R.V., 1989. An asymptotic closure theory for irradiance in the sea and its inversion to obtain the inherent optical properties, Limnol. Oceanogr. **34**(8), 1442-1452.

Zaneveld, J.R.V., R. Bartz and J.C. Kitchen, 1990. A reflective-tube absorption meter, Proc. SPIE **1302** (Ocean Optics X), 124-136.

CHAPTER 3
MATERIALS AND METHODS

3.1 Design of a Large Volume Laboratory Reflectometer

Our primary aim was to experimentally test reflectance models for optical deep waters. Our secondary aim was to acquire data to analyze the reflectance of optical shallow water. To do this we had to measure reflectance spectra on optical deep suspensions with high wavelength resolution under controlled laboratory conditions. To obtain optical deep suspensions large sample volumes are required that could not be investigated with available equipment. Therefore a large volume reflectometer was designed.

3.1.1 Introduction

Theories on the distribution of light in suspensions were experimentally tested and observations were collected to compare the performance of algorithms that extract the information on the concentration of water colour components from the spectral reflectance of a suspension. Models to calculate the light field require inherent optical properties as input. By inverse modelling measurements on the light field can be related to the inherent optical properties of the colour components. The quality of laboratory measurements being superior field measurements, these were used to test theories whenever possible.

Laboratory spectrophotometers measure optical properties on small sample volumes; their use alone was not sufficient for our purpose. If small concentrated samples are used to measure optical properties light absorption by water becomes too small to realistically simulate field conditions. To obtain negligible influence of bottom reflection and to preserve optical interactions at their natural level large sample volumes must be used for laboratory experiments. Also differences in multiple scattering and the handling of samples can lead to artifacts. In the following sections the instrument we used is described. A number of investigators have for similar purposes used tanks with volumes in the range of 0.002 to 12 cubic meter. The main differences in design among these are size, the kind of illumination and the optical characteristics of the side walls. The design of our large volume reflectometer is based on analysis of these different options.

Whitlock *et al.* (1977, 1981) studied upward radiance and reflectance spectra of suspension of several types of soil. With the same instruments Witte *et al.* (1982) investigated effects

of dissolved organic materials on the optical properties of turbid water, including reflectance measurements. Reflectance spectra were measured with 16 or 32 nm wavelength resolution on samples with a volume of 11 cubic meter. The sample tank had black side walls and was illuminated by a beam of light from a 2.5 kW xenon short arc lamp. The spectrum of this light source roughly approximates the spectrum of the sun. Disturbance of the signal by specularly reflected light was avoided by illuminating a spot of 0.30 m diameter in the centre of the tank with an oblique incident beam. Upward radiance was measured above the water surface with a field of view to make the detection probe look at a spot of 0.05 m diameter in the centre of this illuminated area.

Bukata *et al.* (1980) designed an apparatus to determine absorption and backscattering coefficients of suspensions. Reflectance was measured using a white and a black bottom. The irradiance reflectance difference between these bottoms was related to the inherent optical properties by applying a two flow model for backscattering probability (or the complete volume scattering function). A photomultiplier sensor with a 20° field of view was mounted above a turnable circular bottom of 0.21 m diameter. The distance between the detector and the bottom could be varied from 0.25 m to 0.50 m and maximum sample volume was 0.017 cubic meter. A tungsten iodide filament lamp was used to illuminate a 20° source cone. The tank had black sides and the influence of reflection by the walls caused three dimensional effects not accounted for by the two-flow model. Errors due to changes in intensity or angular distribution of the light field due to artificial boundaries are sources of systematic errors called two- or three-dimensional effects. The measurements were compared with the results of Monte Carlo calculations. It was concluded that the sides of the cylindrical tank should have been highly reflective.

Incropera *et al.* (1981) investigated the angular distribution of light under water with intervals of 3.6° at 513 nm. They used a plexiglass tank of 0.293 cubic meter, 0.61 m deep and 0.56 by 0.86 on the sides and used a diffuse light field to illuminate the suspensions. The opacity of the suspension was sufficient to guarantee infinite optical depth. Since all measurements were made along the central vertical axis of the tank they assumed that two- and three dimensional effects did not occur.

Philpot (1987) measured subsurface irradiance spectra in a clear dye solution in a cubic tank with edges of 1.22 m. Its bottom was painted black and its steel side walls were coated with adhesive-backed mylar sheets acting as mirrors.

Chen *et al.* (1991) measured above surface radiance spectra to study the relationship with the concentration of suspended sediment. They used a glass-tank with internal dimensions of 0.98

× 0.98 × 0.90 m. The edges were painted matt black while base and sides were covered with black paper to minimize scatter. A beam illuminated the suspensions at 45° zenith angle. Reflectance spectra of six types of sediment were measured from 350-2500 nm (875 wavebands) for up to 30 concentrations, varying from zero to 1300 mg l^{-1}. The relation between suspended sediment concentration and above surface reflectance was found to be log-linear from 450 to 700 nm and linear from 700 to 1050 nm. Above 1050 nm no correlation was found.

Quibell (1991, 1992) used a sample container of 0.002 cubic meter, 0.30 m deep and with a diameter of 0.10 m having a back bottom and white sides. Chlorophyll concentrations were estimated from reflectance spectra of freshwater algae. Upward radiance in the zenith direction was detected with a field of view of 4° and downward irradiance with a cosine sensor. The reflectance was calculated as the ratio of upward radiance to downward irradiance. In 1991 a 45° oblique incident illumination was provided by two photoflood lamps; in 1992 the measurements were made outdoors with the sun as a light source.

3.1.2 Design Considerations

The dimensions of the tank were determined by the following arguments. Reflectance spectra would have to be measured on a sample volume large enough to obtain an optical deep suspension at a particle concentration sufficiently high to allow also measurements measurable with standard laboratory spectrophotometers; preferentially without the need to concentrate the samples. The absorption coefficient of a suspension of algae is 10 to 20 times smaller than the beam attenuation coefficient, so absorption is the critical parameter. Gordon and McCluney (1975) showed that most reflected light originates from the first optical depth, see Chapter 2. The maximum cuvette path length we could use in a spectrophotometer was 10 mm, allowing accurate measurement of particle absorption coefficients larger than 2 m^{-1}. With this value as a minimum an optical deep suspension is obtained in a tank of 1 m deep. The cross section was chosen to minimize the sample volume and unwanted optical effects of the side walls on the measurements.

If only a spot of the water surface is illuminated by a collimated beam different results are expected as compared with direct and diffuse illumination by the sun because these fields illuminate the whole surface. The field of view of the radiance detector must be small compared to the illuminated spot to assure that the incident radiance behaves like a plane field (Gupta and Ghovanlou 1978). Since reflected light originates in the first optical depth, for spot illumination the optical depth of the suspension should be less than the spot diameter

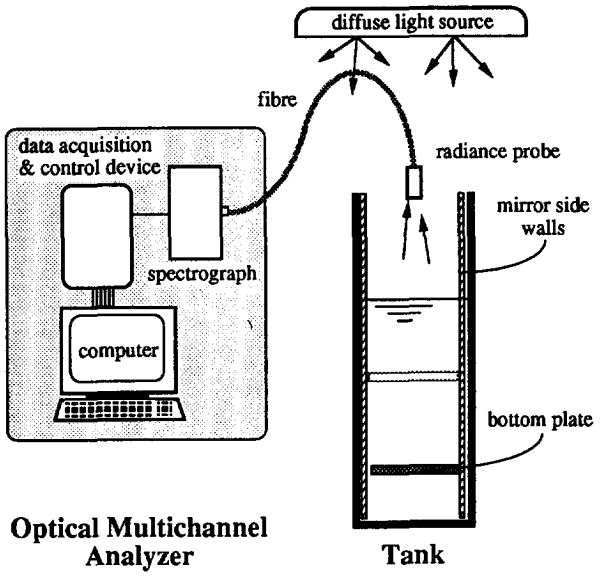

Figure 3.1 *Scheme of the large volume laboratory reflectometer. It consists of a 90 litre sample tank, optics for diffuse illumination and a radiance detection system.*

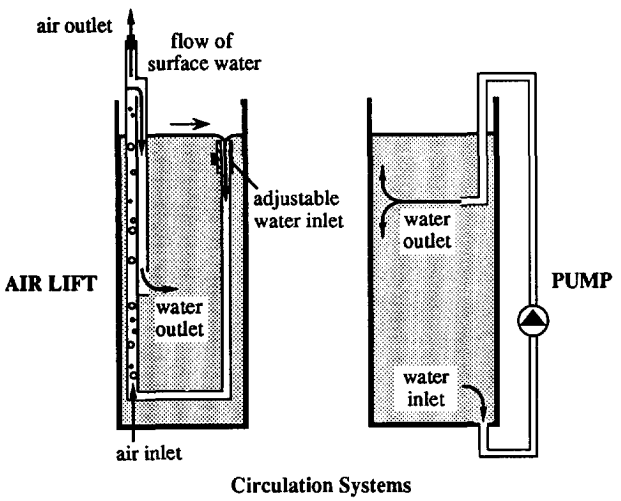

Figure 3.2 *Optional circulation systems used to keep particles in suspension and to prevent contamination of the water surface. The air-lift fluid circulation moves water from the surface to the bottom to maintain a gentle turbulence. Suspensions of particles that settle slowly or that contain fragile aggregates were gently mixed. In experiments with particles that settle significantly the air-lift circulation was replaced by the pump circulation system. The support of the bottom plates was used as a piston to mix the suspension and to make suspensions homogeneous.*

and with increasing angle of the incident beam the effective optical depth is smaller. So the effective dimensions of a tank are reduced by spot illumination, leading to a waste of sample. Therefore a diffuse illumination field was used.

Black side walls disturb the light field and its angular distribution by absorbing light, so they should be far away from the area that influences reflectance within the field of view of the detector. Diffusely reflecting white walls disturb the angular distribution of the light. Especially the ratio of upward to downward travelling light is drastically disturbed because a suspension reflects only a few percent of the incident light. We used mirrors as side walls to simulate infinite horizontal extension of the tank. Similar arguments hold for the bottom. Generally a black bottom decreases reflectance and a white bottom increases it. A bottom with the same reflectance as optically deep water does not change the reflectance of a water layer that is optical shallow. Because the reflectance of surface water is only a few percent a black bottom approximates an optical deep suspension. To test if a suspension is optical deep exchangeable black and white bottom plates were used.

The depth of the bottom plate was varied to study the reflectance of optical shallow water. At the depth where the white bottom can not be measured, or seen, the suspension is optical deep. This depth is not equal to the Secchi disc depth because the white bottom simulates infinite horizontal extension which the Secchi does not. Preisendorfer (1986) related Secchi disc visibility to the inverse of the sum of the irradiance and radiance attenuation coefficients. This was explained by the attenuation of the diffuse light field by absorption and the attenuation of the beam of light reflected from the approximately point sized white disc in the direction of the eye.

3.1.3 Design

Starting from these considerations a large volume reflectance meter was built as shown in Figure 3.1. It was designed to measure reflectance with high spectral resolution on an optical deep layer of water illuminated by a diffuse light field of approximate infinite horizontal dimension.

It consists of a 0.090 cubic meter sample tank, optics for diffuse illumination and a radiance detection system. Reflectance spectra were measured on 63 litre samples with a radiance probe coupled via a fibre bundle to an optical multichannel analyzer based detection system. The edges of the tank were 0.30 m and its total depth 1.00 m. Mirrors were placed inside to simulate a water layer and illumination field of infinite horizontal extension. A depth

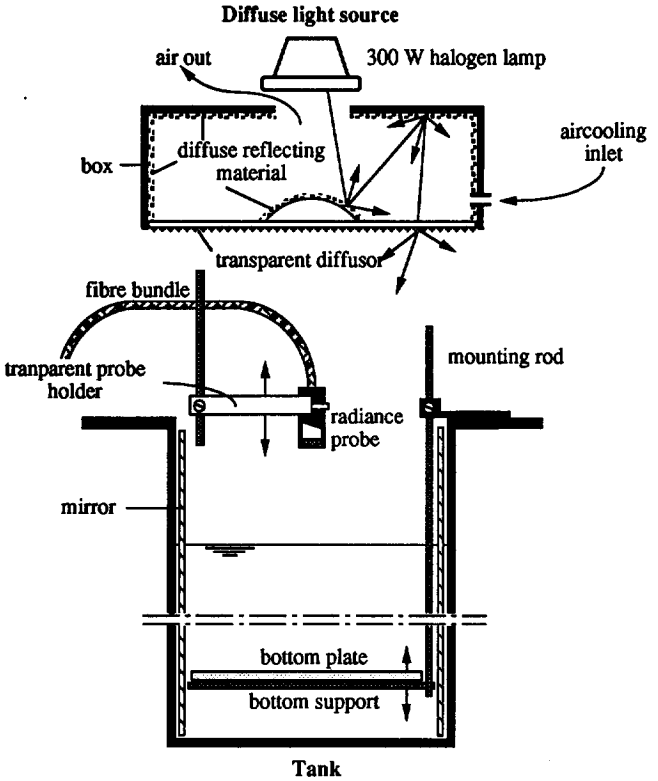

Figure 3.3 *Suspensions were illuminated by a diffuse light field from a 300 W halogen lamp and a diffusor. The diffusor consisted of a box of 0.40 × 0.40 × 0.12 m³ (l×w×h) with diffusely reflecting walls and a diffuse transparent bottom plate. The diffusor, placed on top of the tank at a distance of 0.30 m, was cooled by forced air.*

adjustable bottom support was used to hold bottom plates of 0.28 × 0.28 m². With a vertical traversing mechanism the bottom could be positioned at depth intervals of 0.100 m. Black and white plastic bottom plates were sandblasted to make their surface diffusely reflecting. The black plate had a reflectance in water of 0.004; of the white plate it was 0.90. To check if suspensions were optically deep the reflectance spectra with both bottom plates were compared. The suspension is optical deep if these spectra are equal.

In some experiments an air-lift- or pump fluid circulation system had to be used in this reflectometer, as shown in Figure 3.2. The air-lift fluid circulation prevents contamination of the water surface by floating particles, it also induces a gentle turbulence to prevent settling of suspended particles during longer experiments. The figure shows how water from

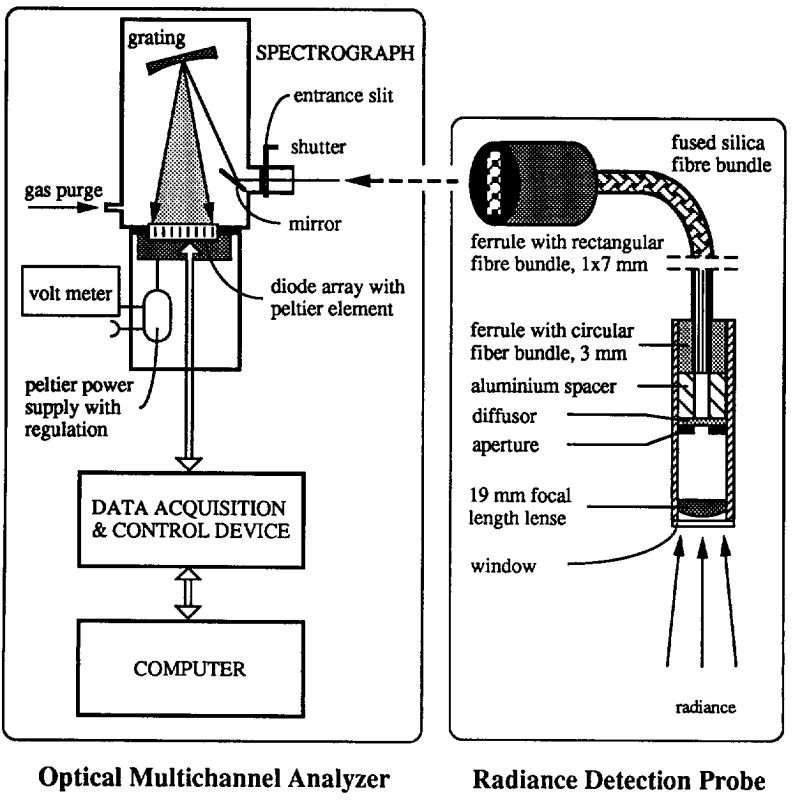

Figure 3.4 *Radiance detection probe and optical multichannel analyzer. Radiance detection probe to improve the spatial response over the field of view of a fibre bundle connected to a narrow entrance slit. The probe consist of a lens, an aperture and a transparent diffusor with spacer in front of the fibre bundle. The optical multichannel analyzer is a detection instrument that consists of a spectrograph, a linear photodiode array and a data acquisition and control unit connected to a computer.*

the surface is lead to the bottom of the tank. The bottom support could also be used as a piston to create homogeneous suspensions by mixing. If the air-lift circulation system was not sufficient to keep suspensions homogeneous in experiments with particles with a high settling rate it was replaced by a pump circulation system with a capacity of 20 litre per minute. Its inlet was at the tank bottom and its outlet 0.20 m below the water surface. The jet of the outlet along the diagonal of the horizontal plane in the tank caused vigorous mixing and a continuous renewal of the water surface.

Suspensions were illuminated by a diffuse light field from a 300 W halogen lamp and a diffusor shown in Figure 3.3. The diffusor consisted of a box with diffusely reflecting

aluminium walls and a diffuse transparent bottom plate. It was placed on top of the tank at a distance of 0.30 m and cooled by forced air. A radiance probe (Figure 3.4) was coupled via a fibre bundle to an optical multichannel analyzer based detection system. The radiance probe had a field of view of 5.0° half angle (0.024 sr.). An UV-grade fused silica fibre bundle (Querschnittswandler, Schott, Wiesbaden, BRD) of 3.2 mm diameter with a 1 × 7 mm^2 rectangularly shaped exit orifice was used to match the 250 μm × 7.5 mm entrance slit of the spectrograph. The fibre material had an acceptance angle of 22° and a numerical aperture of 0.19. The entrance slit was narrower than the fibre bundle and only part of the single fibres of the bundle were in front of this slit. This resulted in a variable response over the field of view of the detector. This disturbance also depends on the homogeneity of the light field within the field of view. At a cost of about 50% of the light intensity spatial response was improved by the detection probe as shown in Figure 3.4. It consists of a lens, an aperture and a diffusor with spacer in front of the fibre bundle. Light focused on the aperture was distributed over the single fibres of the bundle by a transparent diffusor followed by an aluminium spacer with a highly reflecting inside core.

3.1.4 Optical Multichannel Analyzer

The optical multichannel analyzer (Figure 3.4) is a detection instrument consisting of a spectrograph, a linear photodiode array and a data acquisition and control unit connected to a computer. Talmi and Simpson (1980) described the technology and its performance. In the spectrograph the incoming radiation is dispersed over the diodes of a linear photodiode array (Figure 3.5). Impinging photons generate a current in the diodes, each covering a small part of the wavelength range. This current is integrated simultaneously in all diodes during a preset illumination time. The illumination time to detect a spectrum could be varied from 0.01 to 20.00 s. The upper limit depends on the level of dark current of the photodiodes. Reflectance spectra were measured with a typical illumination time of 2.00 s.

A TN 6112 Diode Array Rapid Scan Spectrometer (Tracor Northern, Middleton, WI) was used, with a spectrograph containing an aberration corrected concave holographic grating of 70 mm diameter, 200 lines/mm and a focal length of 200 mm (Jobin Yvon UFS-200, Instruments SA, Metuchen, NJ) and a linear self-scanned photodiode array (RL 1024S, EG&G-Reticon, Sunnyvale, CA) of 1024 elements within a total length of 25 mm and a hight of 2.5 mm. The dispersion of 24 nm/mm at the plane of the photodiode array results in a wavelength range of 200-800 nm with 0.6 nm intervals. For an entrance slit width of 250 μm this yields a resolution of 6.0 nm, for 100 μm 2.4 nm and for 50 μm 1.2 nm. The effective slit hight was determined by the 2.5 mm hight of the photodiode array.

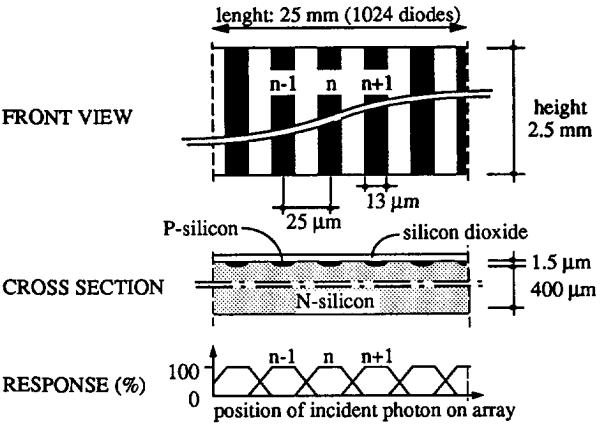

Figure 3.5 *Linear photodiode array of optical multichannel analyzer and its response function. Figure redrawn from Talmi and Simpson (1980).*

At low light intensity levels the photocurrent in the diodes is small compared to its dark current. For reproducible measurements the dark current should be smaller than the photocurrent. The photodiode array was cooled with a thermoelectric element to reduces the dark current. A temperature below -7 °C limits the dark current to 10% of the full scale, or 1% per second. Condensation of water vapour on the cooled photodiode array was prevented by purging the spectrograph with nitrogen gas. The apparent spectrum of the dark current was recorded directly before a reflectance spectrum was measured by blocking the light with a shutter, it was subtracted from the measurement before storage.

3.1.4.1 Wavelength Calibration

With an aligned system the 1024 diodes span the wavelength range from 196 nm to 810 nm. Diode number N_{diode} should yield the response at a wavelength of $195.4+0.6N_{diode}$ nm. The wavelength setting was calibrated by fitting diode numbers to the emission lines of Mercury at 404.7, 435.8 and 546.7 nm in the spectrum of a Mercury fluorescent tube lamp (Philips TLF40W/33) (Grum and Becherer 1979). A software routine fits diode numbers of measured peak response to these wavelengths. The resulting regression line should closely match the relation $195.4+0.6N_{diode}$. A typical regression line is $194.953+0.599N_{diode}$, giving wavelength values for the Hg-lines matching the known values within the maximum system resolution of 1.2 nm.

3.1.4.2 Data Handling

Control and acquisition of data was provided by a Tracor Northern TN6200 DARSS Computer Interface. The detector showed a non-linear time response of 1.5% per second. This leakage of charge becomes significant if the illumination time exceeds 1 second. Probably this effect is the same as was found by Lepla and Horlick (1990) in their investigation of the time response of a photodiode array. In all experiments this time was minimized and if it was changed during an experiment the error was corrected for. The gain was varied to extend the dynamic range within an experiment at constant illumination time. Software for acquisition and manipulation of spectral data was written for a Hewlett-Packard 310/9000 series computer.

Data of 14 bit was recorded at 0.6 nm intervals by the multichannel analyzer. Spectra in the range 400-800 nm were recalculated and stored with a spectral resolution of 2 nm with a cubic spline routine that reproduced measured data with an accuracy of 10^{-6}.

3.1.5 Reflectance

Radiance spectra were measured using the large volume reflectometer. Reflectance spectra were calculated by dividing the spectrum of the sample, $L_u(0+)$, by the spectrum of a standard reference $L_{ref}(0+)$. The reference radiance is a measure of the incident light field, it samples downward irradiance reflected by a reference panel. We used a grey panel that reflected 10% of a perfect diffusely reflecting white standard.
Reflectance spectra were calculated by Equation 2.97

$$\frac{L_u(0+)-L_{aw}}{L_{ref}(0+)} = R(0+)-R_{aw} = 0.52\,R(0) \qquad (3.1)$$

The radiance reflected at the water surface, L_{aw}, was experimentally determined. Theoretically its spectrum is 2% of the incident downward radiance. If the incident irradiance is indirectly measured using a lambertian reflecting panel the actual value of $0.02\,L_d(0+)$ is not necessarily equal to $0.02\,E_d(0+)$ as sampled using this panel. The spectrum of L_{aw} was measured by subtracting $L_u(0)$ or was estimated from a depth profile in clear water using a black bottom plate.

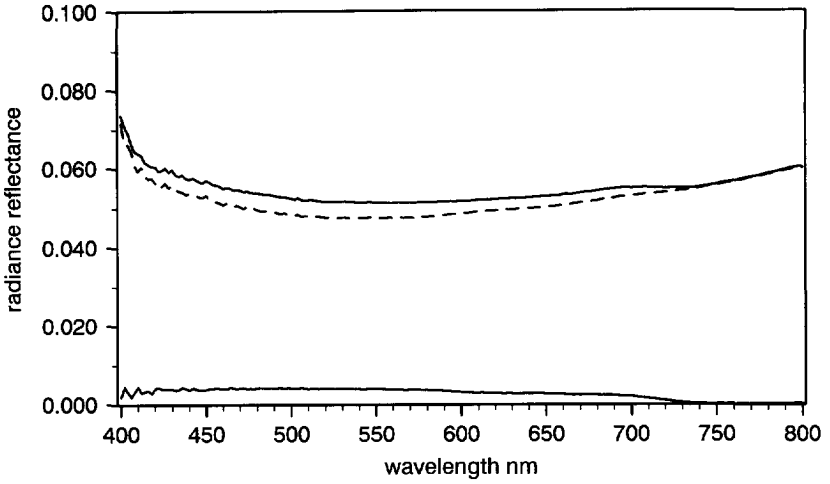

Figure 3.6a shows that subsurface reflectance from the black bottom plate is small. The specular reflectance (dashed line) was calculated as the difference between the spectra measured above and below the water surface, it was about 0.050.

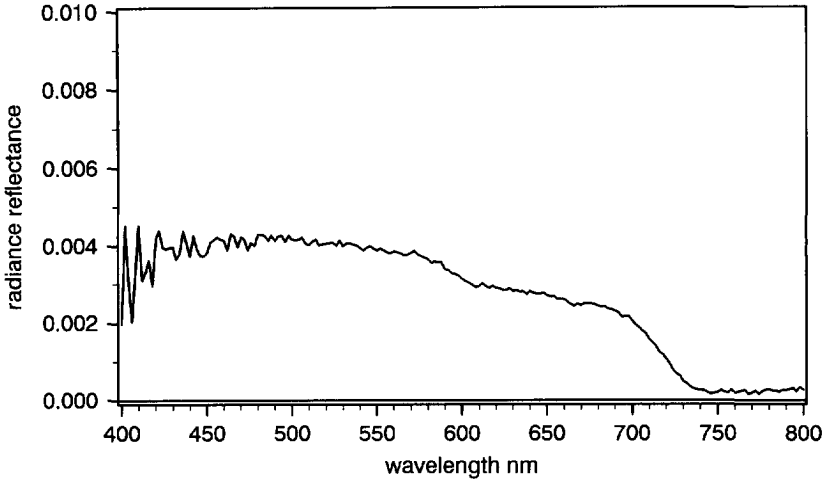

Figure 3.6b shows that the subsurface reflectance was 0.004 in the part of the spectrum where water is almost transparent, and was close to zero in the near-infrared part due to absorption by water.

Figure 3.6 *Reflectance spectra of filtered tap water measured above the water surface and just below it.*

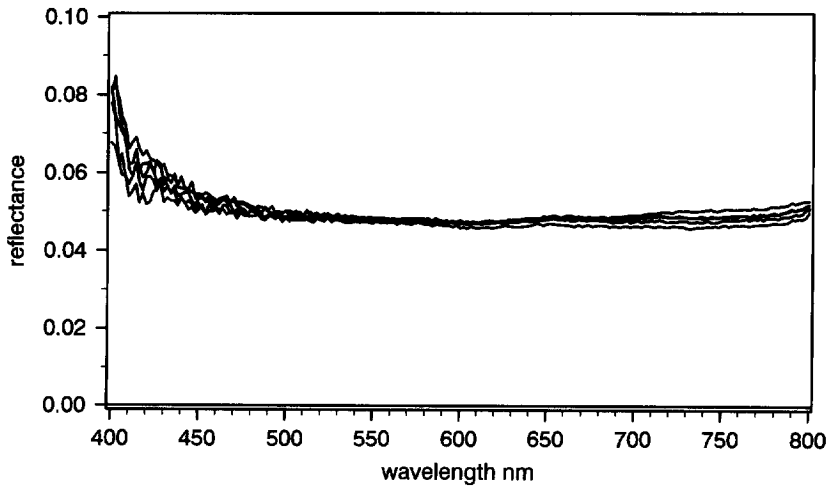

Figure 3.7 *The spectral reflectance of clear water for a series of depths with the black bottom plate. Reflectance from the black bottom is small, at short wavelengths no significant effect is seen, while above 700 nm the reflectance decreased by 0.003. Reflectance decreases with increasing bottom depth in the red to near-infrared part of the spectrum. A 0.500 m layer of water in this spectral region is almost optical deep owing to the absorption by water. The reflectance decrease of 0.003 is in reasonable agreement with the subsurface reflectance of the black bottom of 0.004. The spectral average of the specular reflectance was 0.045.*

3.1.6 Specular Reflectance

The sample tank was filled with demineralized water filtered over a 0.2 μm membrane filter. Spectra were measured on the clear water sample to determine specular reflectance at the water surface for the optical geometry of the apparatus.

Specular reflectance was calculated from measured spectra by subtracting subsurface reflectance from above surface reflectance. A typical specular reflectance of about 0.050 is given in Figure 3.6a for the experiment reported in Chapter 5. The subsurface reflectance fro the black bottom plate is small; Figure 3.6b shows that it is 0.004 in the part of the spectrum where water is almost transparent and close to zero in the near-infrared part where the absorption of water is high. During an experiment the specular reflectance was constant.

Specular reflectance can be determined indirectly from the above surface reflectance of a depth profile of clear water using the black bottom plate. Figure 3.7 shows the above surface reflectance of clear water for several depths for the experiment reported in Chapter 4. At short wavelengths no significant effect could be seen, while in the red to near-infrared part of the spectrum reflectance decreased with increasing bottom depth by 0.003 only. A 0.500 m layer of water in this spectral region is almost optical deep owing to the absorption

by water. The observed reflectance decrease of 0.003 is in reasonable agreement with the subsurface reflectance of the black bottom of 0.004. The spectral average of the specular reflectance was 0.045.

The difference in specular reflectance can not be interpreted to judge the accuracy of the method because different diffuse illumination used in the experiments. The method used in Chapter 5 is straightforward and to be preferred.

3.2 Spectrophotometric Measurements

Measurements were made with a Perkin-Elmer 551-S UV/VIS double-beam spectrophotometer connected to a HP86B computer. Data was acquired in transmission mode to obtain the maximum data resolution for samples with low attenuation. Spectra were measured against a water containing reference sample from long to short wavelengths at a scan speed of 2 nm/s with a 2 nm slit using matched quartz cuvettes.

The baseline of the instrument was flat within specification. It had a linear drift in time of about 0.002 per hour. Measured spectra were corrected by linear interpolation in time for baseline flatness and baseline drift using recorded zeroscans, reference sample against reference sample. Attenuation spectra per meter pathlength were calculated for wavelengths at 2 nm intervals using a cubic interpolation before further analysis.

3.2.1 Single Scattering Condition

The amount of light scattered within a specific acceptance angle is calculated by integration of the volume scattering function. This is valid if multiple scattering is negligible; single scattering prevails if samples are sufficiently dilute. Van de Hulst (1957) specified for beam attenuation measurements on suspension that single scattering prevails for optical depths $\tau \leq 0.1$ A correction for double scattering may be necessary if $0.1 \leq \tau \leq 0.3$. An optical depth of 0.3 corresponds with a beam attenuation c of 30 m^{-1} for a cuvette with 10 mm path length.

The single scattering condition can also be used to decide if single scattering prevails in an absorption measurement. The beam attenuation of the suspension using the same cuvette path length as the absorption measurement is used to judged its optical depth. The optical

characteristic of a sample volume can be calculated by summation of the contributions of calculated particle scattering if single scattering prevails.

3.2.2 Absorption by Aquatic Humus

Aquatic humus is defined by the following preparation procedure. Field samples were stored in polyethylene bottles at 4 °C. Within 48 hours solutions were prepared by filtration over a 1 μm Whatman GF/C glassfibre filter followed by filtration over a 0.2 μm Sartorius SM11307 membrane filter. Filters were pretreated to remove organic contamination. Glassfibre filters were kept at 500 °C for 12 hours and washed with distilled water. Membrane filters were cleaned by filtering 250 ml distilled water. Prior to use glassware was washed with filtrate.

Spectra were measured from 550 down to 350 nm at a scan speed of 2 nm/s with a 2 nm slit using 10 or 100 mm optical pathlength matched quartz cuvettes in standard geometry. Absorption spectra of humus measured with and without an integrating sphere showed no significant differences, so light scattering by humus could be neglected.

For each sample a duplicate zeroscan and a triplicate samplescan were recorded followed by a new sample or by a duplicate zeroscan at the end of a series. Measured spectra were corrected by linear interpolation in time for baseline flatness and baseline drift using the surrounding zeroscans.
The absorption per meter was calculated for wavelengths at 2 nm intervals using a cubic interpolation. For further analysis the statistical software packages SAS was used.

Absorption was measured using 10 mm cuvettes with a standard deviation of 1.5 percent. For absorption values less than 3.00 m^{-1} or a transmission mode values higher than 0.970, relative errors increased because the absolute resolution was about 0.045 m^{-1}. This threshold almost equals the factory specification of the spectrophotometer of 0.05 m^{-1} using 10 mm cuvettes.

3.2.3 Absorption by Particulate Matter

Absorption spectra were measured with high aperture optics using a semi-integrating sphere using 10 mm cuvettes placed at the entrance of an integrating sphere (79 mm diameter) to detect light scattered in the forward direction within a critical acceptance angle. The upper

limit of the critical acceptance angle is 48°, the angle of internal reflection at the exit window of the cuvette. The angle depends on the refractive index of the material of the cuvette. For the fixed aperture of the integrating sphere the effective acceptance angle reduces with an increasing path length of the cuvette. The effective acceptance angle of 38° for the method using 10 mm quartz cuvettes was determined by Dubelaar *et al.* (1989b).

The resuspension method of Kirk (1980) and Davies-Colley (1983) was used to concentrate field samples (Chapter 9). This technique was eventually abandoned because flocculation of the resuspended material occurred. Samples from the Western Scheldt estuary were tenfold concentrated by centrifugation to improved the signal to noise ratio.

3.2.4 Beam Attenuation

Beam attenuation spectra were measured directly and absorption spectra were measured on tenfold concentrated samples with a semi-integrating sphere.

3.2.5 Flow-Through Cuvette

Spectrophotometric measurements of absorption and beam attenuation of suspension that contained fast settling particles were made with a flow-through cuvette in a closed circulation system (Figure 5.1). Flow-through cuvettes of 10 mm on the sides were designed not to influence the acceptance angle of the spectrophotometer. Available flow-through cuvettes have a small funnel with black side walls that can only be used for beam attenuation measurements. An upward sample flow in the cuvette was used to flush occasional air-bubbles and to prevent settling of particles during the scan time.

3.3 Experimental Materials

3.3.1 *Chlorella* Cultures

A stock suspensions of organic particle was prepared from a set of 16 one litre batch cultures of *Chlorella pyrenoidosa*. The 1 litre batch cultures were inoculated by 75 ml of a 1.5 litre continuous culture. Algae were grown on CP100 medium in 2 litre Erlenmeyer flasks at a light level of 24 W m^{-2} using cool white fluorescence light tubes. The algae were kept in suspension by gentle rotation.

The *Chlorella pyrenoidosa* stock contained aggregates. Microscopic inspection showed single cells of about 3-4 μm and aggregates of typically 20-80 μm. A homogeneous stock of single cells was prepared by submitting the suspension to sheer-force. This was done by forcing it under 7 bar nitrogen gas pressure through an orifice of 0.7 mm diameter. This way the aggregates were pulverized into single cells as was checked by microscopy. The resulting *C. pyrenoidosa* stock contained only single cells.

3.3.2 Ferrite Particles

Suspensions of inorganic particles were prepared from powdered ferrite. This red-brown sediment was chosen because these inorganic particles do not agglomerate with the algae in mixtures and because iron is a natural colour compound. A 4 litre stock was made by suspending 40 gram ferrite in 5 litre filtered demineralized water. The suspension was stirred and allowed to settle for 10 minutes to remove fast settling particles. The supernatant was siphoned off from the sediment. Microscopic inspection showed that the supernatant contained irregularly shaped particles of 1-4 μm.

3.3.3 Microcystis Suspensions

A sample of surface water was taken at Lake Braassemermeer on August 24th, 1990, during a bloom of *Microcystis aeruginosa*. Gas vacuoles were collapsed by application of 7 bar nitrogen gas pressure to the suspension (Dubelaar *et al.* 1987). After collapse the protein walls of the gas vacuoles remain in the cytoplasm while the gas dissolves and disappears from the point of view of optical measurements. A homogeneous stock of single cells was obtained by applying shear force to the colonies. This was done by pumping a suspension of colonies through an orifice of 0.7 mm diameter. Destruction of the colonies was checked by microscope.

3.3.4 Dry Weight

Dry weight and ash free dry weight were measured according to Dutch norm NEN 6484 (1981).

3.3.5 Chlorophyll *a*

Chlorophyll *a* was measured using ethanol extraction according to Dutch norm NEN 6520 (1981).

3.3.6 Particle Concentration

Particle concentrations were measured using a flow cytometer designed to measure optical properties of particles with sizes of up to 500 μm width and 1000 μm length (Dubelaar *et al.* 1989a). This range covers most colonial plankton algae.

3.3.7 Radiance Measurements in the Field

Radiance was measured in the field in the spectral range 400-800 nm with 2 nm wavelength resolution. Field measurements were done with the same optical multichannel analyzer as used in the laboratory. Light was collected by a glass fibre of 40 m with a core diameter of 0.5 mm. The half angle of view under water was 8.5° and in air 11.3°. The fibre end was positioned 4 m away from the ship. To avoid shading of the sensor a boom was used and the ship was manoeuvred. The spectrum of incident solar radiation was measured using a grey diffusely reflecting reference panel held at a distance of 0.15 m from the sensor. The radiance reflectance above the water surface was measured followed by depth profiles of up- and downward radiance.

At Lake Wolderwijd the optical multichannel analyzer was used to measure radiance reflectance with the fibre optics used in the laboratory and a Guided Wave Model 260 glass fibre optic spectrophotometer was used to measure radiance depth profiles using a fibre light guide of 40 m long. This instrument scans a spectrum with a fixed integration time of 0.25 s per wavelength interval.

3.4 Calculation of Scattering by Polystyrene Microspheres

The scattering characteristics of a volume of monodisperse polystyrene particles (Chapter 4) are calculated by exact Mie-theory (1908) and by the approximative theory of van de Hulst (1957). The characteristics of the particles are given, details of the calculation methods were

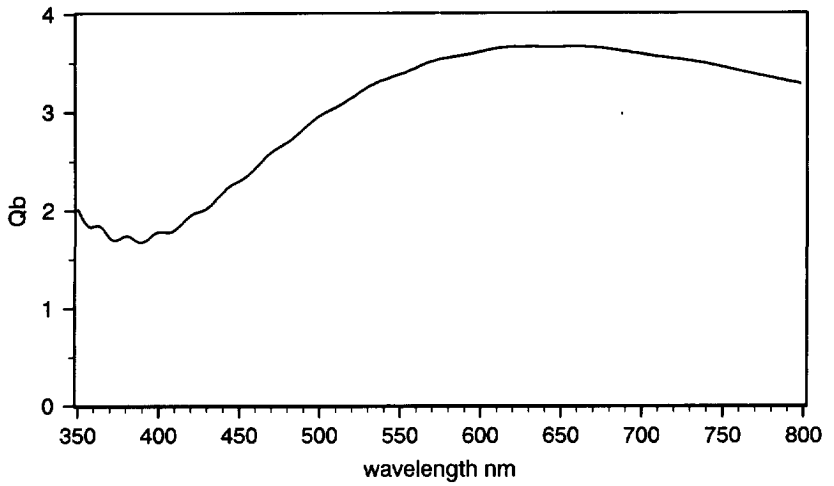

Figure 3.8 *Spectrum of efficiency factor for extinction Q_c calculated by Mie theory. For non absorbing particles the efficiency factor for scattering Q_b is equal to Q_c. The measured beam attenuation coefficient should have a similar spectral shape.*

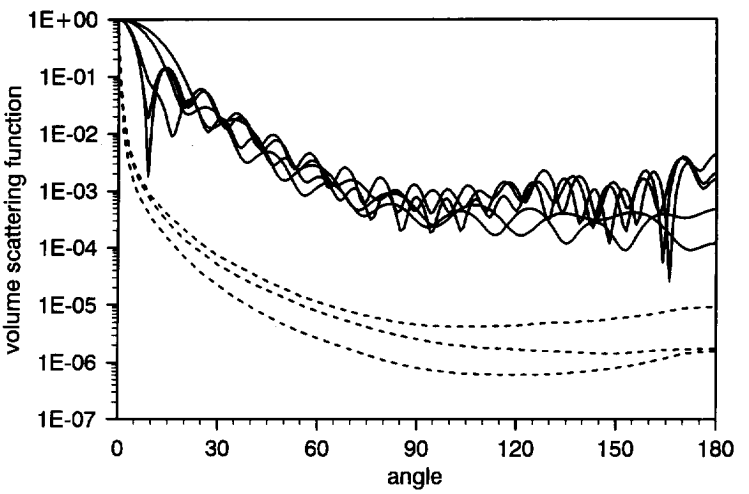

Figure 3.9a Volume scattering functions of polystyrene particles (solid lines) compared with extreme volume scattering functions of natural water from the literature (dashed lines). The latter values were measured on samples of clear ocean water and turbid harbour water.

Figure 3.9 *Comparison of volume scattering functions and scattering probability functions of polystyrene particles to those of natural water from the literature.*

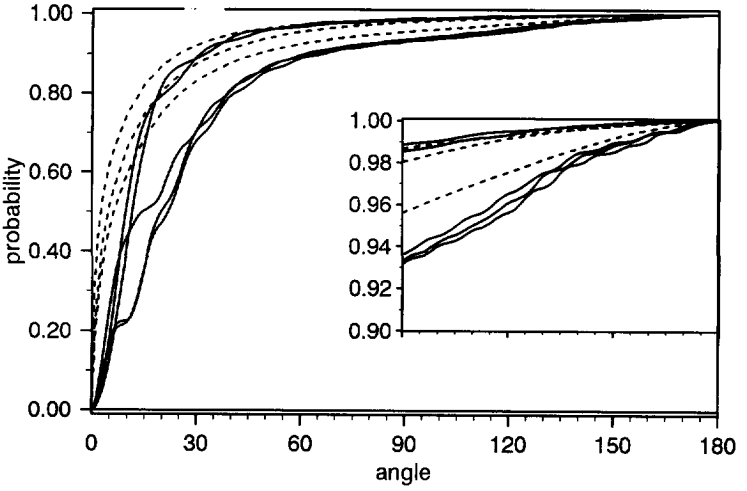

Figure 3.9b shows the forward scattering probability functions. Comparison of the scattering probability functions shows that the backscattering probabilities are in the same range.

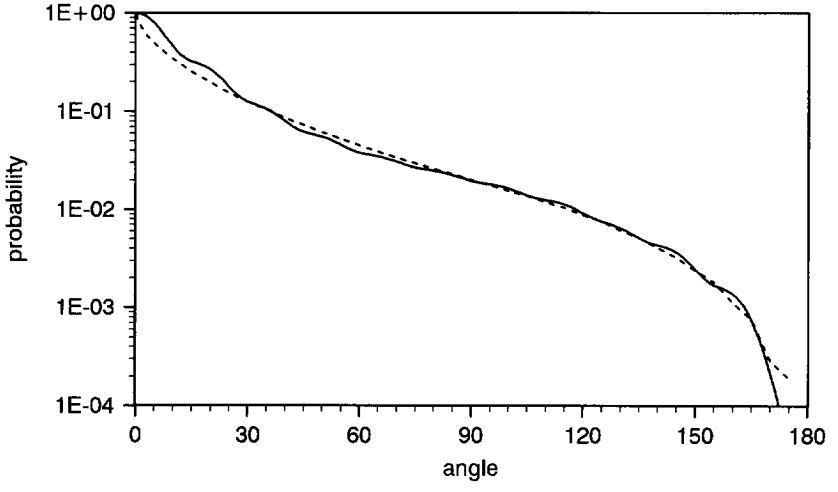

Figure 3.9c Comparison of the backscattering probability function of the polystyrene particles at 550 nm and that of San Diego Harbor (used as default in many studies).

given in Chapter 2. Mie-theory allows detailed calculation of the light scattering characteristics of spherical particles: the volume scattering function and the extinction or beam attenuation coefficient. The polarization of light is also included. If full detail of the angular distribution of scattered light intensities is not needed for model calculations the less time consuming approximation for anomalous diffraction of van de Hulst is appropriate.

3.4.1 Refractive Index and Monodisperse Size Distribution

For water and polystyrene the wavelength dependency of the real part of the refractive index was modelled by a Cauchy dispersion expression in the spectral range 350-800 nm. The refractive index of polystyrene (Bateman *et al.* 1959) is

$$n_{ps} = 1.5683 + \frac{10{,}087}{\lambda^2} \qquad (3.2)$$

and the real part of the refractive index of water (Kaye and Laby 1959) is

$$n_w = 1.3240 + \frac{3{,}046}{\lambda^2} \qquad (3.3)$$

with λ the wavelength in nm.

Monodisperse polystyrene microspheres of 1.6 μm diameter were a gift from Dr. G.B.J. de Boer, their preparation was described by de Boer (1987). The size was checked by electron microscopy, a mean diameter of 1.58 μm was measured from a photograph. The number of particles on the photograph was too small for the size difference of 1.25% to be significant. The size distribution of the particles was checked with a RELACS III flow cytometer, the coefficient of variation of the forward light scatter parameter was 0.03 for particles passing through the laser focus. From this value the coefficient of variation of the particle size was estimated at 0.045, that is 0.07 μm (Dubelaar *et al.* 1989b: Table 7 and Appendix 1).

3.4.2 Mie Calculations

Volume scattering functions and efficiency factors were computed by Mie-theory at 2 nm wavelength intervals. Figure 3.8 shows the spectrum of the efficiency factor for extinction Q_c ($=Q_b$). The spectral variation of the volume scattering function was compared to the published volume scattering functions for several characteristic wavelengths; 350, 387, 400,

636, and 800 nm. Figure 3.9a shows that these functions differ from the extreme volume scattering functions of surface water found in literature; they are less peaked in the near forward direction and less smooth. However, comparison of these scattering probability functions shows that the backscattering probabilities B are remarkably alike, and this is the more important parameter in analytical models of reflectance. The functions vary significantly with wavelength, the related backscattering probability decreases with wavelength from 0.069 to 0.012, with the commonly used value of 0.019 at 550 nm. Forward scattering probability functions are given in Figure 3.9b and the backscattering probability function of the polystyrene particles at 550 nm and that of San Diego Harbor (used as default in many studies) is shown in Figure 3.9c.

It appears that the spectral range of backscattering probabilities of the particles lies within and somewhat below the range found in surface water. Scattering probabilities of polystyrene particles are smaller than observed in nature for scattering angles less than 15 degrees.

3.4.3 Van de Hulst Approximation

Spectra of efficiency factors calculated by exact and approximative theory are shown in Figure 3.10. Figure 3.10a shows the van de Hulst approximation of the efficiency factor for extinction Q_b versus the phase-lag parameter ρ. The efficiency factor varies over the spectral range because the size parameter decreases with increasing wavelength. Figure 3.10b shows the spectrum of scattering efficiency factors Q_b computed by Mie-theory and Q_b computed by the approximation theory of van de Hulst. Approximative calculations are in reasonable agreement with exact calculations; the results were 10 to 15% lower and the secondary structure or ripple does not occur. This under estimation of the efficiency factor Q_c occurs because the assumption of a relative refractive index close to 1 is not met. Particles with higher refractive index show effects due to grazing reflection not accounted for (van de Hulst 1957; section 11.22). Substitution of the efficiency factor Q_c calculated by the approximation for anomalous diffraction of van de Hulst in Equation 2.16 to calculate the beam attenuation coefficient would yield 10 to 15% lower results for the polystyrene particles. An error of about this magnitude is consistent with the results by Moore (1968).

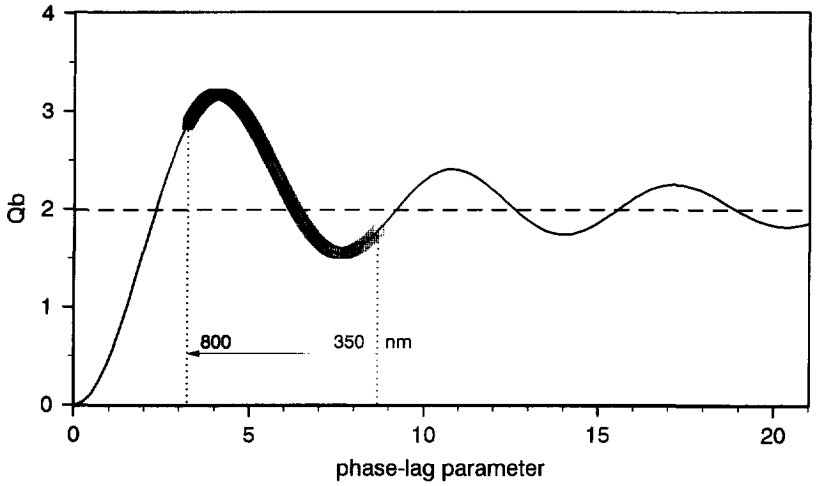

Figure 3.10a Van de Hulst approximation of the efficiency factor for extinction Q_b versus the phase-lag parameter ρ, which depends on particle size, wavelength of incident radiation and the relative refractive index of the particle.

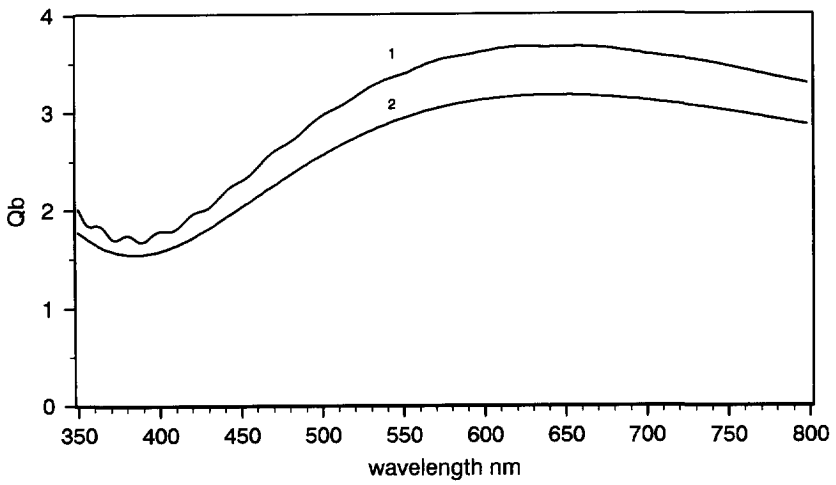

Figure 3.10b Comparison of spectra of the scattering efficiency factor Q_b computed by Mie-theory (line 1) and by the approximation of van de Hulst (line 2).

Figure 3.10 *Comparison of exact and approximate light scattering calculations of the efficiency factor for extinction. Light scattering calculations by Mie-theory are exact for spherical particles, Van de Hulst gave an approximation to anomalous light scattering.*

3.4.4 Beam Attenuation

Dubelaar *et al.* (1989b) showed that spectra of the beam attenuation of the polystyrene microspheres were linear with concentration over 4 decades. Particle concentrations of 5 10^7 -5 10^{11} l^{-1} on a log-log scale had correlations with beam attenuation of 0.992 at 636 nm and 0.988 at 387 nm. Samples with increasing particle concentration were measured in successively shorter cuvettes of path lengths 100 mm, 10 mm and 1 mm.

3.4.5 Particle Concentration

The particle concentration of the experiment reported in Chapter 4 was measured with a flow cytometer (Section 3.3.6). A sample of an intermediate polystyrene particle concentration of the series contained 2.4 10^8 particles per litre. The particle concentration of the densest suspension was 220/8 times higher resulting in a particle concentration of 6.6 10^9 l^{-1} .

References

Bateman, J.B., E.J. Weneck and D.C. Eshler, 1959. Determination of particle size and concentration from spectrophotometric transmission, J. Colloid Science **14**, 308-329.

Bukata, R.P., J.E. Bruton and J.H. Jerome, 1980. Conceptual approach to the simultaneous determination of the backscatter and absorption coefficients of natural waters, Appl. Opt. **19**(9), 1550-1559.

Boer, G.B.J. de, 1987. *Coagulation in stirred tanks*, Diss., Univ. Eindhoven, The Netherlands.

Chen, Z., J.D. Hanson and P.J. Curran, 1991. The form of the relationship between suspended sediment concentration and spectral reflectance: its implications for the use of Deadalus 1268 data, Int. J. Remote Sensing **12**(1), 215-222.

Dubelaar, G.B.J., A.C. Groenewegen, W. Stokdijk, G. van den Eng and J.W.M. Visser, 1989a. The optical plankton analyser (OPA): a flow cytometer for plankton analysis. II: Specifications, Cytometry **89**, 529-539.

Dubelaar, G.B.J., J. Krijgsman and M. Donze, 1989b. Investigation of multiple scattering in aqueous suspensions of non-absorbing polystyrene micro spheres using spectrophotometry, BCRS report 89-09, Delft, 61.

Gordon, H.R. and W.R. McCluney, 1975. Estimation of depth of sunlight penetration in the sea for remote sensing, Appl. Opt. **14**(2), 413-416.

Grum, F. and R.J. Becherer, 1979. *Optical radiation measurements: Vol. I Radiometry*, Ed. F. Grum Academic Press, New York, pp 335.

Gupta, J.N. and A.H. Ghovanlou, 1978. Radiative transfer in turbid water, Proc. SPIE **160** (Ocean Optics V), 132-147.

Incropera, F.P., T.R. Wagner and W.G. Houf, 1981. A comparison of predictions and measurements of the radiation field in a shallow water layer, Water Resources Res. **17**(1), 142-148.

Kaye, G.W.C. and T.H. Laby, 1956. *Physical and chemical constants*, 11th ed. Longman's Green, London.

Lepla, K.C. and G. Horlick, 1990. Data processing techniques for improved spectrochemical measurements with photodiode array spectrometers, Appl. Spectroscopy **44**(8), 1259-1269.

Moore, D.M., F.D. Bryant and P. Latimer, 1968. Total scattering and absorption by spheres where $m \approx 1$, J. Opt. Soc. Am. **58**, 281-283.

NEN 6484, 1982. Water - Determination of the content of not dissolved material and its ignition residue, Nederlandse Norm Instituut, Delft, 4 pp.

NEN 6520, 1981. Water - Spectrophotometric determination of Chlorophyll *a* content, Nederlandse Norm Instituut, 6 pp.

Philpot, W.D., 1987. Radiative transfer in stratified waters: a single-scattering approximation for irradiance, Appl. Opt. **26**(19), 4123-4132.

Preisendorfer, R.W., 1986. Secchi disk science: Visual optics of natural waters, Limnol. Oceanogr., **31**(5), 909-926.

Quibell, G., 1991. The effect of suspended sediment on reflectance of freshwater algae, Int. J. Remote Sensing, **12**(1), 177-182.

Quibell, G., 1992. Estimating chlorophyll concentrations using upwelling radiance from different freshwater algal genera, Int. J. Remote Sensing, **13**(14), 2611-2621.

Talmi, Y. and R.W. Simpson, 1980. Self-scanned photodiode array: a multichannel spectrometric detector, Appl. Opt., **19**(9), 1401-1414.

Whitlock, C.H., L.R. Poole, J.W. Ursy, W.M. Houghton, W.G. Witte, W.D. Morris and E.A. Gurganus, 1981. Comparison of reflectance with backscatter and absorption parameters for turbid waters, Appl. Opt. **20**(3), 517-522.

Whitlock, C.H., 1982. Marine sediment tolerances for remote sensing of atmospheric aerosols over water, Appl. Opt. **21**(23), 4196-4198.

Witte, W.G., C.H. Whitlock, R.C. Harris, J.W. Ursly, L.R Poole, W.M. Houghton, W.D. Morris and E.A. Gurganus, 1982. Influence of dissolved organic materials on turbid water optical properties and remote-sensing reflectance, J. Geophysical Research, **87**(C1), 441-446.

CHAPTER 4
MODELLING REFLECTANCE OF SURFACE WATER

4.1 Introduction

Models of reflectance have not often been tested against experimental data, in most studies Monte Carlo simulations of the light field are used as the best approximation of reality. To develop analytical solution methods to predict the reflectance spectra of surface water the results of such methods, together with their requirements for experimental input data, is compared with measurements in an experimental model system. Laboratory investigations of reflectance spectra on suspensions with known inherent optical properties were done and the results are used as a standard to compare the performance of several published models, and a new analytical model, the backscattering albedo model, is proposed.

The underwater light field and its change with depth are usually described by a two flow model. The solutions of Preisendorfer and Mobley (1984) for both direct and inverse modelling of the light field by the two flow model suggest that this model is sufficiently accurate. However, Daniel *et al.* (1979) found that predictions by the two flow model were the least accurate of a set of four models, primarily because the effects of the change in refractive index at the water surface are not accounted for in this model. The models included the method of discrete ordinates (Hottel *et al.* 1968) for which Incropera *et al.* (1981) experimentally showed that it accurately predicts the light field. So there is indirect evidence that the reflectance predicted by the two flow model might be inaccurate.

Jain and Miller (1977) compared results of the two flux model and the quasi-single scattering model with the results of Monte Carlo simulations. They found that predictions by both models were accurate within 7% for single scattering albedo ω_0 less than 0.8.

Whitlock *et al.* (1981) compared field measurements of above surface reflectance measurements at 8 wavelengths for 3 river waters with predictions by the models of Gordon *et al.* (1975) and Morel and Prieur (1977). Experimental data of beam attenuation, absorption and backscattering coefficients as well as the measured volume scattering functions at these wavelengths were used as input. Absorption was measured with 10 nm bandwidth using the instrument of Friedman *et al.* (1980). As a consequence of the unusual design of this instrument the apparent absorption must be corrected for scattering by Monte Carlo simulation for each measurement. This leads to much additional work and may lead to errors

when not sufficient input data are available. Whitlock *et al.* found poor agreement between the experimental data and predictions of both models; measured reflectance values were up to 40% lower. One of the considerations given by the authors was that the data for these turbid waters did not fit to the single scattering model because the single scattering albedo's ω_0 were high, larger than 0.8 at all wavelengths, and outside the range for which the model was validated. Aas (1987) argued that the two flow model would give better results than the two models applied by Whitlock *et al.* because these models underpredict reflectance values for b_b/a ratios in the range 0.05-0.5. We found that this argument is not correct because the model calculations yielded overpredicted values as compared to the observed reflectance and the two flow model would increase the residuals.

Concentration series of suspensions of scattering non-absorbing polystyrene particles with additions of a water soluble dye were investigated. Reflectance spectra were measured with the large volume reflectometer described in Chapter 3. The volume scattering function of the particles was calculated by Mie theory and absorption by the non-scattering dye (Ecoline 236) was known by spectrophotometry. The accuracy of model predictions is analyzed by comparing several analytical reflectance models and the best model is chosen to interpret the reflectance spectra.

4.2 Measurements of Reflectance in an Experimental Model System

The results of laboratory measurements of reflectance spectra on suspensions with known inherent optical properties are described in this section. Radiance was measured with a detector placed above the water surface to simulate remotely sensed reflectance of surface water. These spectra simulate a set of sea-truth colour data with an accuracy that can not be obtained in the field. The spectra were measured with high wavelength resolution on homogeneous suspensions without effects due to sun glint, surface waves or atmospheric influences.

Reflectance spectra were measured with the large volume reflectometer described in Chapter 3. A sample tank with mirror side walls was used to simulate infinite horizontal extensions of the light field and of the layer of water. Suspensions in the tank were illuminated by a diffuse light field and reflectance was measured with an optical multichannel analyzer. The optical multichannel analyzer was set to a spectral resolution of 6 nm by a 250 μm slit and an illumination time of 2.00 s. Upward radiance was detected 0.37 m above the water surface. Reflectance spectra of the suspensions were measured for a series of different bottom depths with a black and with a white diffusely reflecting bottom to analyze the influence of

the bottom on reflectance. The reflectance spectra of optical deep suspensions are discussed and interpreted in detail, while some remarks are made on the interpretation of data on optical shallow water.

The sample tank was filled with a 63 litre sample of demineralized water filtered over a 0.2 μm membrane filter. Spectra need to be corrected for specular reflection as discussed in Chapter 3. Figure 3.7 shows the spectral reflectance of clear water for several depths with a black bottom. This correction amounted to 4.5% on average.

4.2.1 Adding Scattering Particles

Suspensions with an increasing amount of scattering were prepared by adding monodisperse polystyrene microspheres of 1.6 μm diameter to the filtered demineralized water. The particles were described in Chapter 3. They were added until an optical deep suspension resulted for a water layer of 0.500 m depth. Figure 4.1 shows the increase of reflectance with increasing particle concentration. Reflectance spectra of the suspensions show a near linear increase with particle concentration in the blue part of the spectrum. Absorption by water here is low and particle scattering dominates in the blue part of the spectrum.

Figure 4.2 shows the reflectance spectra of the depth profiles measured on the suspension with the highest particle concentration of 6.6 10^9 l^{-1} (Section 3.4.5). The suspension was checked to be optical deep. With increasing depth of the water layer the difference between the reflectance spectra using a black and a white bottom decreases. Reflectance spectra for the black and the white bottom plate converged with increasing depth, for a depth of 0.500 m these spectra were close to equal and for wavelengths above 730 nm the suspension was optical deep.

The reflectance values using the white bottom are probably too high (Section 3.1.2). In the following the suspension is assumed to be optical deep over the whole spectral range for reflectance values measured with a black bottom.

An alternative method to check if a suspension is optical deep is by comparing reflectance spectra with a black bottom at increasing depths. As shown in Figure 4.3 these reflectance spectra converge to a limiting shape. This is less sensitive than the previous method if the depth interval is small compared to total depth.

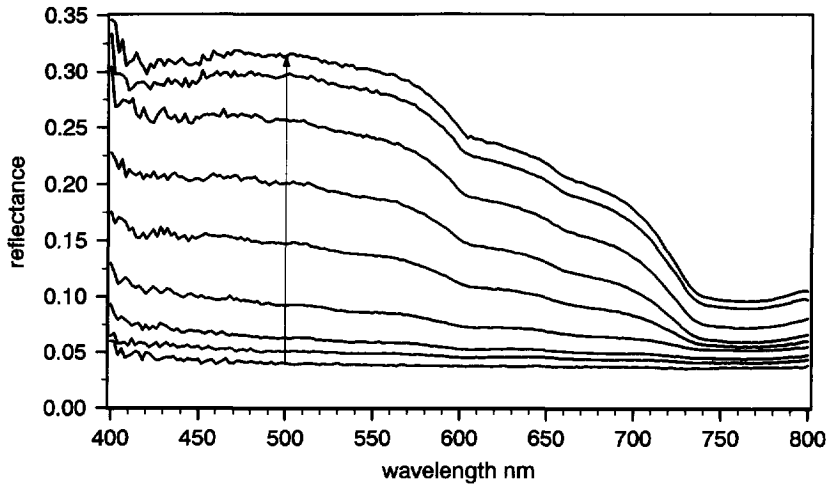

Figure 4.1 *Reflectance spectra of a concentration series of non-absorbing polystyrene spherical particles of 1.6 μm diameter. Particles were added until the additional scattering resulted in an optical deep suspension for a water layer of 0.500 m depth. The reflectance spectra show a linear increase with particle concentration (or number of particles) in the blue part of the spectrum. Absorption by water is low and particle scattering is dominant in the blue part of the spectrum.*

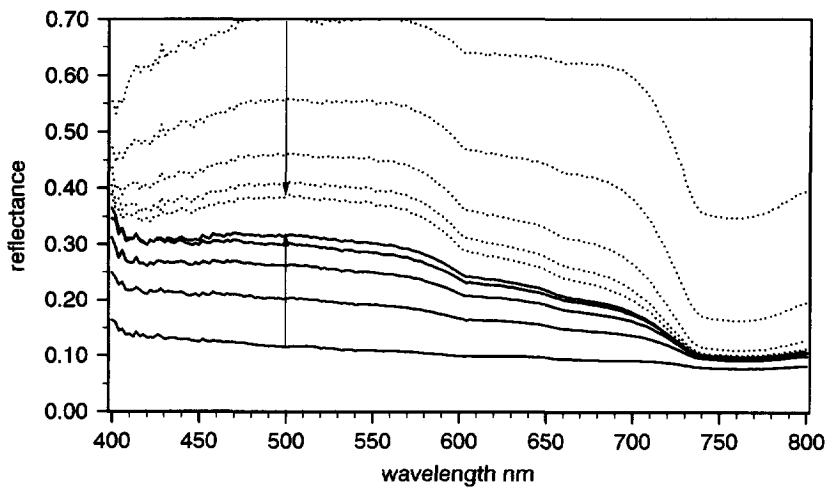

Figure 4.2 *Bottom depth profiles of the suspension with the highest particle concentration of 6.6 10^9 l^{-1}, the arrows indicate an increasing depth. The suspension was checked to be optical deep by comparing the reflectance spectra of a black bottom plate to that of a white one. With increasing depth the difference between the reflectance spectra using a black (solid lines) and a white bottom plate (dotted lines) decreases. The two spectra were equal for wavelengths longer than 730 nm. The suspension using the black bottom plate is approximately optical deep.*

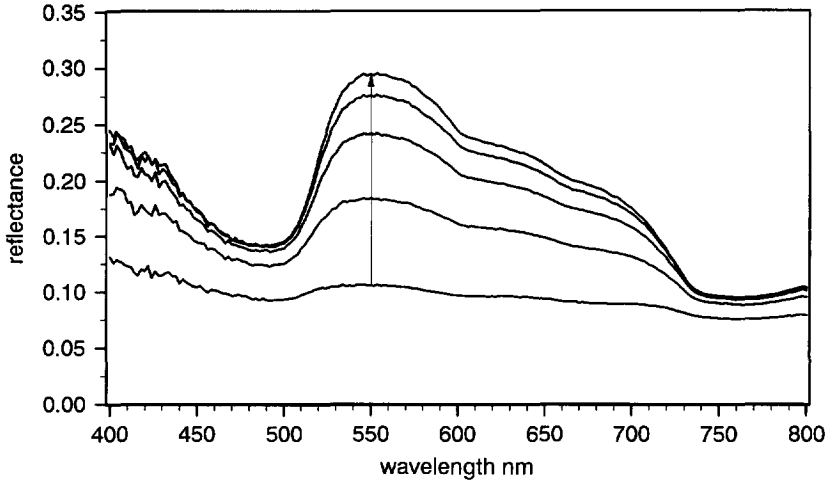

Figure 4.3 *A less sensitive method to check if a suspension was optical deep is to compare spectra with increasing depth (indicated by the arrow). For the black bottom plate successive spectra became equal. The solid lines in Figure 4.2 show the results for the optical deep suspension of polystyrene particles, this figure shows the results for the highest concentration of the dye concentration series.*

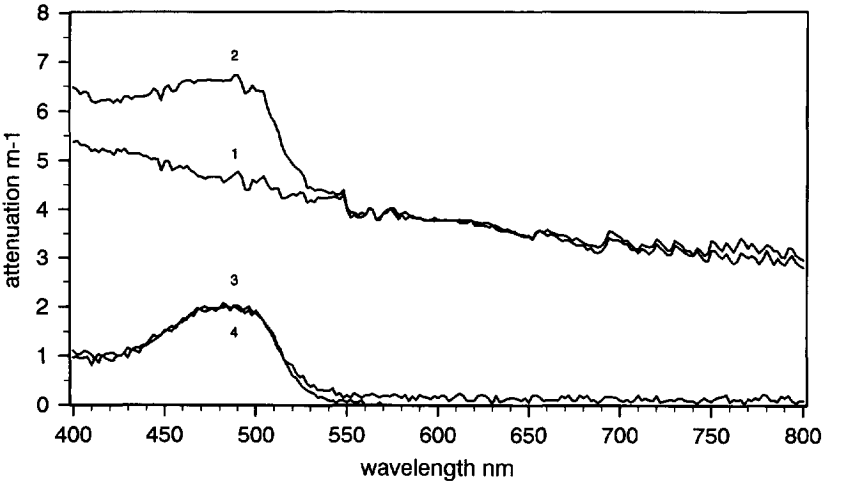

Figure 4.4 *Absorption spectrum of the suspension before (line 1) and after (line 2) adding the dye and the difference (line 3) owing to the absorption of the dye. The absorption spectra of the dye (line 3) was retrieved after the particles settled from the suspension (line 4).*

4.2.2 Adding a Water Soluble Dye

The absorption of the medium of the optical deep suspension was increased by adding a water soluble dye. An orange dye was used because it changes absorption of the medium only in the wavelength range where absorption by water is low. Figure 4.4 shows the absorption spectrum of the suspension before and after adding the dye and the difference owing to light absorption by the dye. The reflectance in the red part of the spectrum did not change during the experiment. This should be so and reflectance values at wavelengths in the red and blue part with equal amounts of absorption by the medium can be compared. Figure 4.5 shows the reflectance spectra of the dye concentration series.

The dye did not adsorb on the polystyrene particles as was checked on a sample of the suspension with the highest dye concentration. Colourless polystyrene particles settled out in a few days and a clear dye suspension was retrieved. Figure 4.4 shows that absorption by the dye had not decreased after removal of the particles.

4.2.3 Optical Deep Suspensions

Model calculations of the reflectance of optical deep waters were for ocean water based on an approximative model (Section 2.8.1 and Equation 2.101) for the optical deep reflectance $R_\infty(0)$ assuming that the backscattering b_b is small compared to the absorption a. The subsurface reflectance $R(0)$ of homogeneous waters is the optical deep reflectance $R_\infty(0)$ for waters for which the bottom depth can assumed to be infinite, and is a function of $R_\infty(0)$ and the bottom reflectance R_b for waters that are optical shallow.

Simple analytical models of the reflectance $R_\infty(0)$ of optical deep surface water assume that some terms of the solution can be neglected because backscattering is small compared to absorption. This assumption can be acceptable for clear ocean waters but not for turbid coastal- and inland waters. For example, if backscattering becomes larger than absorption, the models not incorporating account significant backscattering lead to reflectance values larger than one. This is obviously impossible. This kind of error is not hypothetical because water absorption at wavelengths from 400 to 500 nm is low (less than 0.02 m^{-1}). Even for clear seawater with a=0.0171 and b_b=0.0076 m^{-1} at 400 nm (Smith and Baker 1981) the assumption that $b_b \ll a$ is not true.

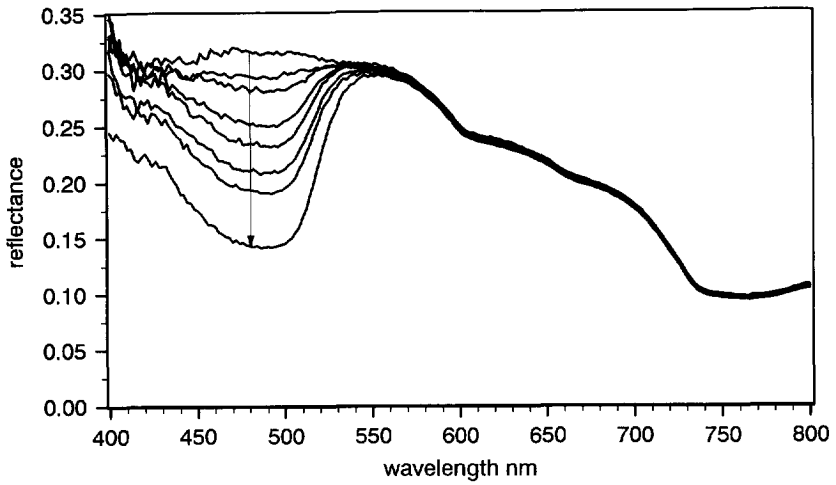

Figure 4.5 *Reflectance spectra of a dye concentration series. In the optical deep suspension the absorption of the medium was increased (the arrow indicates the direction) by adding a concentration series of an orange dye.*

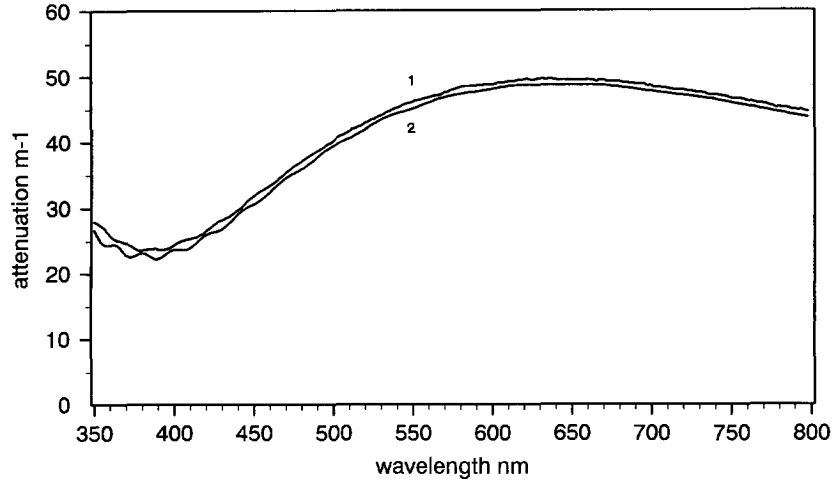

Figure 4.6 *Measured and calculated beam attenuation spectra of a suspension of 6.6 10^9 l^{-1} polystyrene spheres of 1.6 μm diameter. The uniformly sized spherical particles show a beam attenuation spectrum with a shape typical for anomalous scattering. Polystyrene does not absorb visible light, the effect is purely due to scattering. The beam attenuation maximum at 630 nm is two times the minimum at 380 nm. Measured scattering coefficients are within 3 percent of the theoretical values calculated with Mie-theory.*

There is no good reason to neglect the backscattering coefficient compared to the absorption coefficient; the coefficient b_b needs to be known in any case and model calculations do not become simpler.

4.3 Spectrophotometry and Inherent Optical Properties of Suspensions

The scattering characteristics of a volume of monodisperse polystyrene microspheres of 1.6 μm diameter were calculated by exact Mie-theory (1908) and by the approximative theory of van de Hulst (1957). The characteristics of the particles were given in Chapter 3, details of the calculations in Chapter 2. Mie-theory allows detailed calculation of the light scattering characteristics of spherical particles: the volume scattering function and the extinction or beam attenuation coefficient. It also includes the polarization of light. If the full detail of the angular distribution of scattered light intensities is not needed for model calculations the less time consuming approximation for anomalous diffraction of van de Hulst is appropriate.

4.3.1 Beam Attenuation of Polystyrene Microspheres

The beam attenuation spectrum of the polystyrene particles has a shape typical for anomalous diffraction, shown in Figure 4.6. The maximum at 630 nm is twice the minimum at 380 nm. The attenuation coefficient varied over the spectral range owing to the wavelength dependency of the efficiency factor for extinction. The phase-lag parameter ρ is proportional to the reciprocal value of wavelength (Equation 2.23), causing a twofold decrease of this parameter over the spectral range from 400 to 800 nm.

According to the single scattering condition (Section 3.2.1) the maximum particle concentration for the cuvettes were calculated by Equation 2.16 to be respectively 7.5 10^8, 7.5 10^9, 7.5 10^{10} l^{-1}. This experiment showed that the condition for single scattering, requiring an optical depth less than 0.3, is a safe restriction to ensure a linear response of beam attenuation of the polystyrene particles.

4.3.2 Calculated Beam Attenuation

The beam attenuation can be calculated by Equation 2.16 if the uniform particle size, the efficiency factor for extinction and particle concentration are known. Substitution of the diameter D in meters, the efficiency factor Q_e calculated by Mie theory (Section 3.4.2) and

the particle concentration per cubic meter N (Section 3.4.5) shows close agreement with the measured beam attenuation. Figure 4.6 shows that the observed scattering coefficient was within 3 percent of the theoretical values.

Estimation of the particle concentration from the measured beam attenuation is possible if D and Q_c are known. To show this the particle concentrations was calculated from the beam attenuation for the two extreme efficiency factors in the spectral range. With Equation 2.16 a value of 6.7 10^9 l^{-1} was found at the maximum by substituting $c(634)=49.42$ m^{-1} and $Q_c(634)=3.668$. At the minimum the same concentration resulted with $c(380)=23.64$ m^{-1} and $Q_c(380)=1.745$. This result from theory was in close agreement with the result of flow cytometric particle counting giving a concentration of 6.6 10^9 l^{-1}. Light scattering calculations proved to be accurate with respect to this test.

4.3.3 Apparent Absorption

Spectra of apparent absorption were measured to study the effect of scattering on absorption measurements. Since the particles do not absorb visible light the absorption spectrum should have a shape similar to that of the scattered light not detected.

The apparent absorption of a suspension of the non-absorbing particles should be proportional to the backscattering probability incorporated in the measuring technique. Figure 4.7 shows the apparent absorption together with calculated spectra of $B(38)$ and $B(90)$. The backscattering probabilities $B(38)$ and $B(90)$ were computed by integration of the volume scattering function assuming single scattering. Theoretical spectra were calculated by multiplication with the beam attenuation coefficient. The spectrum calculated with an effective acceptance angle θ_{am} of 38° shows good agreement with the absorption measurements using the semi-integrating sphere technique in 10 mm quartz cuvettes.

$$a_m = a+B(\theta_{am})b = a+B(38)b \qquad (4.1)$$

For samples with an unknown volume scattering function the backscattering coefficient must be estimated to interpret reflectance spectra. The volume scattering function can be estimated from measurements of absorption and beam attenuation at a wavelength where absorption is negligible together with an assumption about the backscattering probability, see Sections 2.2.5.2 and 2.2.5.4. Another method would be to use only the apparent absorption measured with an integrating sphere together with an assumption about the ratio $B(38)/B(90)$. The ratio $B(38)/B(90)$ was about four to five for the volume scattering function of San Diego Harbor as well as for the polystyrene particles at 550 nm (Table 4.1); this value of the ratio might

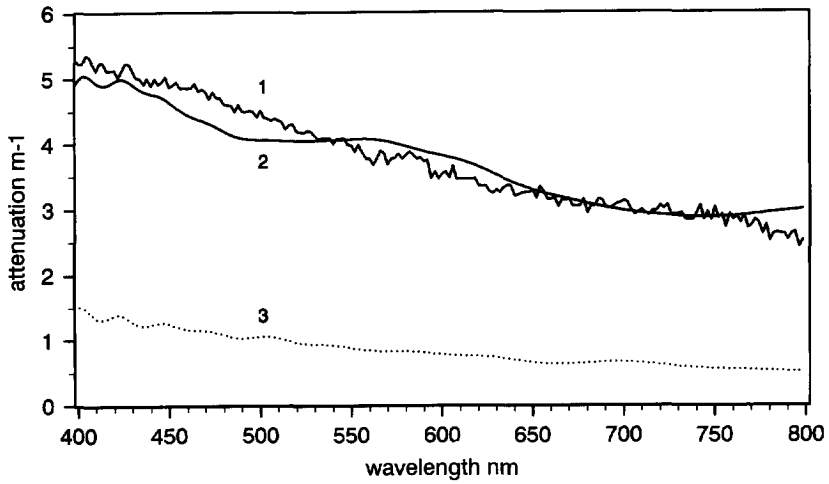

Figure 4.7 *The measured apparent absorption spectrum of a suspension of non-absorbing polystyrene particles compared with theoretical radiance attenuation spectra. Apparent absorption (line 1) was measured with the semi-integrating sphere technique using 10 mm quartz cuvettes. The effective acceptance angle was 38°. Spectra of the backscattering coefficients of B(38)b (line 2) and B(90)b (line 3) were calculated from the volume scattering function assuming single scattering. Measurements with an integrating sphere overestimate backscattering for the polystyrene particles by a factor three to five (see Table 4.1). Significant errors are made if the apparent absorption is used as a direct measurement of $a+b_b$ or b_b.*

be used as a default. This problem will be discussed in more detail in Section 4.6 and in Chapter 7.

4.3.4 Inherent Optical Properties of the Suspensions

Absorption and beam attenuation spectra of the suspensions were measured with a double-beam spectrophotometer against a water containing reference.

The total absorption coefficient of the suspension is the sum of the absorption coefficients of water and the added dye. Literature values were used for the absorption coefficient of water (Smith and Baker 1981 as modified by Buiteveld and Donze, unpublished). The absorption coefficient of the stock solution of the dye was measured.

The beam attenuation spectrum of these suspensions of purely scattering particles was equal to the spectrum of the theoretical scattering coefficient (Section 2.2.3). The theoretical coefficient was computed by integration of the volume scattering function calculated by Mie theory.

Table 4.1 *Spectral variation of optical properties of spherical polystyrene particles. The particles of 1.6 μm diameter do not absorb visible light, they are pure scatterers. The efficiency factor for extinction Q_c is given together with two backscattering probabilities, B(90) and B(38), and their ratio B(90)/B(38). Note that the backscattering probability at 550 nm is 0.019. The same value is in common use to model reflectance spectra of turbid surface water.*

wavelength nm	$Q_c=Q_b$	$B(38)$	$B(90)$	$B(90)/B(38)$
350	2.012	0.209	0.069	0.328
400	1.787	0.210	0.064	0.304
450	2.307	0.152	0.041	0.270
500	2.974	0.103	0.027	0.260
550	3.397	0.090	0.019	0.216
600	3.622	0.079	0.016	0.205
650	3.666	0.068	0.013	0.199
700	3.594	0.062	0.014	0.222
750	3.464	0.063	0.012	0.192
800	3.285	0.069	0.012	0.168

Table 4.2 *The absorption and backscattering coefficients are equal at three wavelengths for the highest concentration of the dye concentration series (compare Figure 4.8).*

wavelength nm	$a=b_b$	ω_0	ω_b	$R(0+)$-R_{aw}
438	1.12	0.96	0.50	0.146
516	0.50	0.98	0.51	0.150
702	0.66	0.98	0.50	0.123

The backscattering coefficient needed in the reflectance model was computed by multiplying the measured attenuation coefficient c with the theoretical backscattering probability $B(\theta)$. The backscattering coefficient $b_b = B(90)b$ is a fraction of the total scattering coefficient b. For non-absorbing particles b_b is a fraction of the beam attenuation c. The backscattering probability function at 2 nm interval was obtained by integrating the volume scattering functions calculated by Mie theory. The backscattering coefficient b_b was calculated by multiplying the backscattering probability $B(90)$ with the measured beam attenuation c.

$$b_b = B(90)b = Bc \qquad \textbf{(4.2)}$$

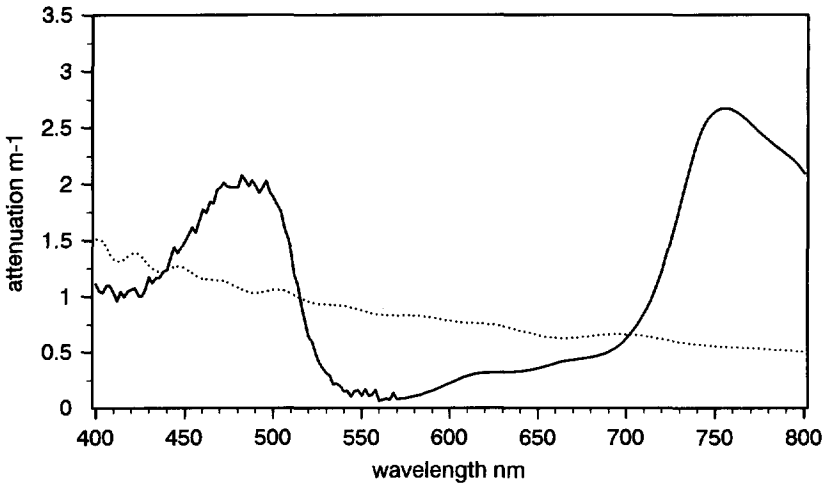

Figure 4.8 *Spectra of absorption coefficient of the medium (solid line), the sum of water and dye absorption, and the backscattering coefficient of the polystyrene particles (dotted line) for highest concentration of the dye concentration series. The absorption and backscattering are equal at three wavelengths (Table 4.2).*

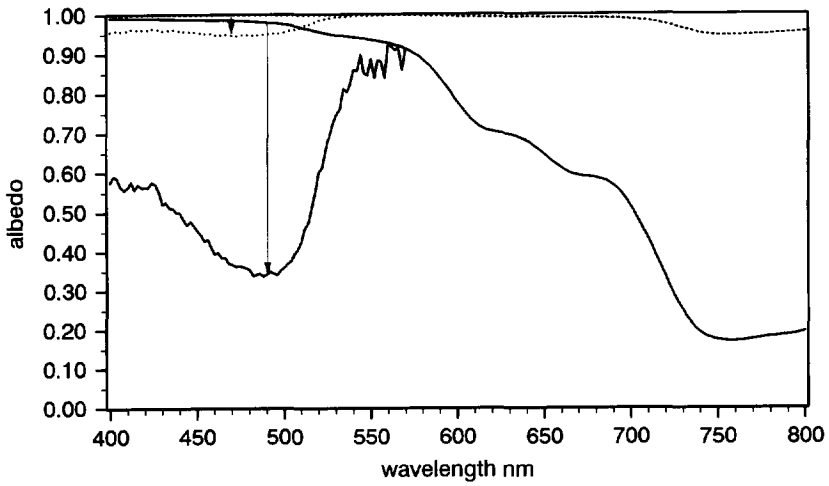

Figure 4.9 *Spectra of the single scattering albedo ω_0 (dotted lines) and backscattering albedo ω_b (solid lines) for zero and maximum concentration of the dye series. The lines for the two suspensions overlap for wavelengths above 550 nm where the dye does not absorb. Single scattering albedo's were high for all wavelength for both suspensions; larger than 0.95 and close to one. Backscattering albedo's ranged from 0.15 to close to one.*

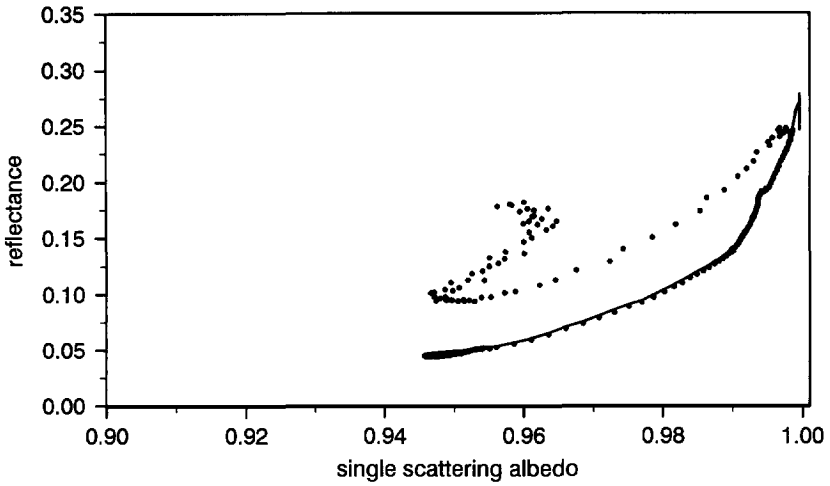

Figure 4.10 *The relation between the albedo ω_0 and the measured reflectance corrected for the specular reflectance for the begin (solid line) and end (•) concentration of the series. The single scattering albedo ω_0 was not related to reflectance in a simple way.*

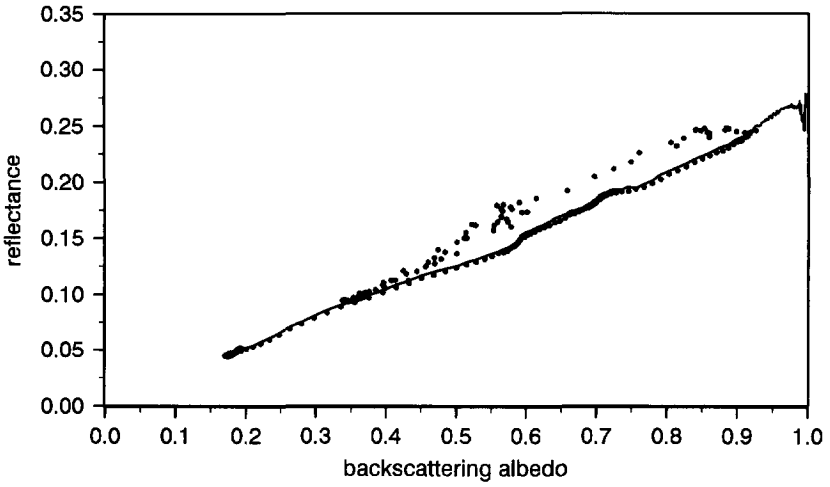

Figure 4.11 *The relation between the backscattering albedo ω_b and the measured reflectance corrected for the specular reflectance for the begin (solid line) and end (•) concentration of the series. The reflectance was almost linearly related to the backscattering albedo ω_b.*

Figure 4.8 shows the spectra of the absorption coefficient of the medium (the sum of water and dye absorption) and the backscattering coefficient of the polystyrene particles for the highest concentration of the dye concentration series. The absorption and backscattering are equal at three wavelengths (Table 4.2).

4.3.5 Albedo Spectra

The single scattering albedo ω_0 is an inherent optical property in general use, the backscattering albedo ω_b defined before is a more useful inherent property when analyzing reflectance. Figure 4.9 shows the spectra of ω_0 and ω_b for zero and maximum concentrations of the dye series. The lines for the two suspensions overlap for wavelengths above 550 nm. Single scattering albedo's were high for all wavelengths in both suspensions: larger than 0.95 and close to one. Backscattering albedo's ranged from 0.15 to nearly one.

The spectral shape is similar to that of the measured reflectance spectra (Figure 4.5). The relation between albedo and reflectance, corrected for the specular reflectance, is given in Figure 4.10 for ω_0 and Figure 4.11 for ω_b. A relation between the single scattering albedo ω_0 and reflectance is not easily seen in Figure 4.10. The backscattering albedo ω_b increased almost linearly with reflectance. Reflectance is mainly determined by the backscattering albedo ω_b.

Figures 4.11 and 4.8 show that reflectance values were different for equal absorption values in the blue and the red part of the spectrum. It appears that equal amounts of absorption in the presence of different amounts of backscattering yield different reflectance values. At wavelengths with twofold different absorption coefficients equal reflectance values were measured if the backscattering varied proportionally (Table 4.2).

4.4 Comparison of Reflectance Models

The experimental results were compared with reflectance model calculations. Model predictions of reflectance were analyzed in two steps. The reflectance $R_\infty(0)$ of an homogenously optical deep water was analyzed followed by the analysis of reflectance of optical shallow water.

Reflectance spectra were measured on suspensions with known inherent optical properties to judge the accuracy of model calculations. The data was also used to judge the propagation of errors of experimentally derived inherent optical properties.

4.4.1 Remotely Sensed Reflectance

The reflectance spectra measured on optical deep suspensions of an absorbing medium containing purely scattering particles were shown to be related to the inherent optical properties a and b_b.

The remotely sensed reflectance $R(0+)$, measured above the water surface, was compared with the sum of measured specular reflectance R_{aw} and modelled subsurface irradiance reflectance $R(0)$ at depth $z=0$. This value is equal to $R_\infty(0)$ for optical deep waters, corrected by a factor f_{wa} for the transmittance of subsurface irradiance through the water surface.

$$R(0+) = R_{aw}+R_\infty(0)f_{wa} = R_{aw}+R(0)f_{wa} \qquad \textbf{(4.3)}$$

Literature values for the transmittance factor of the water to air interface for irradiance f_{wa} vary from 0.52 to 0.5625 for an undisturbed water surface.

$$f_{aw} = \frac{(1-0.022)}{n_w^2} \approx 0.55 \qquad \textbf{(4.4)}$$

4.4.2 Optical Deep Suspensions

The accuracy of model predictions was determined for the successive order scattering model (Morel and Prieur 1977), the two flow model (Joseph 1950; Spitzer and Dirks 1987) and the quasi-single scattering model (Gordon *et al.* 1975). In the two flow model the propagation of light is described by two diffuse light fluxes. A series of single scattering events is assumed in the quasi-single scattering model. These models are treated in detail in Chapter 2.

4.4.2.1 Successive Order Scattering Model

For the turbid suspensions of polystyrene particles backscattering is not negligible compared to absorption and for wavelengths where absorption is less than backscattering, the model

obviously predicts incorrect reflectance values larger than one. This occurs at short wavelengths for the optical deep suspension of clear water containing only non absorbing particles (Figure 4.8). The model of Morel and Prieur (1977) is not valid for turbid suspensions and can only be used for clear ocean water, for which it was intended.

4.4.2.2 Quasi-Single Scattering Model

Reflectance spectra of optical deep suspensions, corrected for specular reflectance at the water surface, were calculated with the quasi-single scattering approximation by Gordon *et al.* (1975). The reflectance $R(0)$ was proportional to the backscattering albedo as defined before in Section 2.8.2:

$$R_{\infty}(0) = \sum_{n=1}^{3} k_n(0)\, \omega_b^n \qquad \textbf{(4.5)}$$

The polynomial expansion coefficients $k_n(0)$ for zero optical depth were applied (Equations 2.62 and 2.63). Modelled reflectance spectra $R(0+)$-R_{aw} of the dye concentration series are given in Figure 4.12a for zenith sun illumination and in Figure 4.12b for sky illumination together with the measured reflectance spectra (Figure 4.5). The modelled spectra of these turbid suspensions show a reasonable fit to the experimental spectra. The modelled reflectance $R(0+)$ was systematically too high for large ω_b and too low for small ω_b. When ω_b is small de deviancy occurs in spectral regions where the suspensions were optical deep, as seen by comparing Figure 4.2 for wavelengths above 730 nm with Figure 4.9. For sky illumination this approximation gives better results than for a directed beam, except when the backscattering albedo is high.

4.4.2.3 Two Flow Model

The two flow model for radiative transfer assumes an upward and a downward diffuse light flux. Figure 4.13 shows that the reflectance values were overestimated by the model of Joseph (1950) using Equation 2.84. In the solution of the two flow model by Spitzer and Dirks (1987) also the distribution factors of irradiance were included.
The irradiance in the up- and downward direction are represented by vectors and their distribution factors to describe the radiance distribution pattern. The distribution factors D_d and D_u give the relative increase in path length of the vector irradiance owing to the diffuseness of the irradiance. In Section 2.8.3 a solution for the optical deep reflectance $R_{\infty}(0)$ was derived (Equation 2.77) that can be rewritten to Equation 2.86:

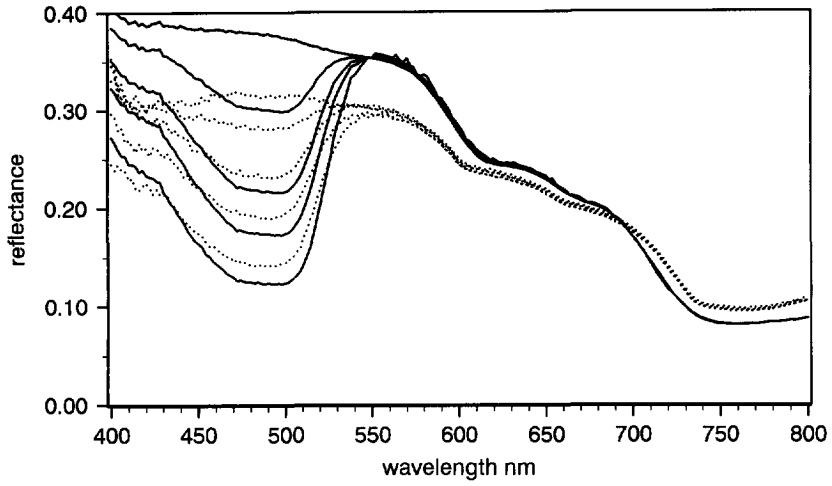

Figure 4.12a.

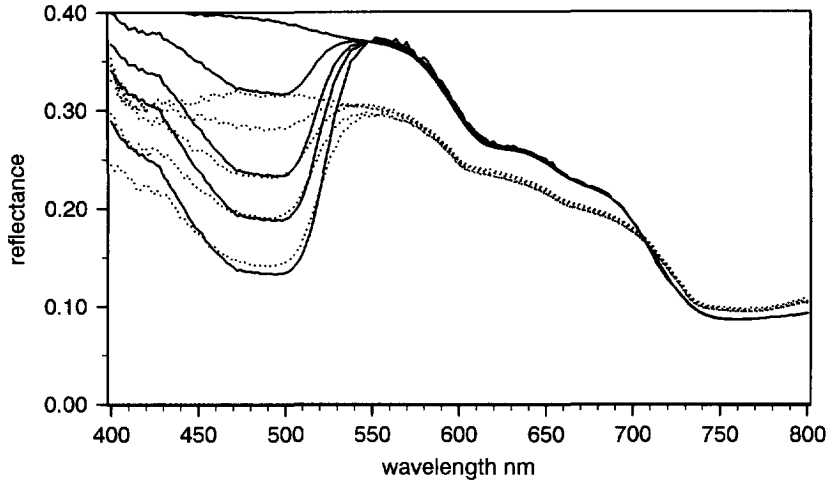

Figure 4.12b.

Figure 4.12 *Predicted reflectance spectra (solid lines) of the dye concentration series using the quasi-single scattering model of Gordon et al. (1975) with coefficients for zenith sun illumination (Figure 4.12a) and for sky illumination (Figure 4.12b). The observed reflectance spectra (dotted lines) are given as a reference.*

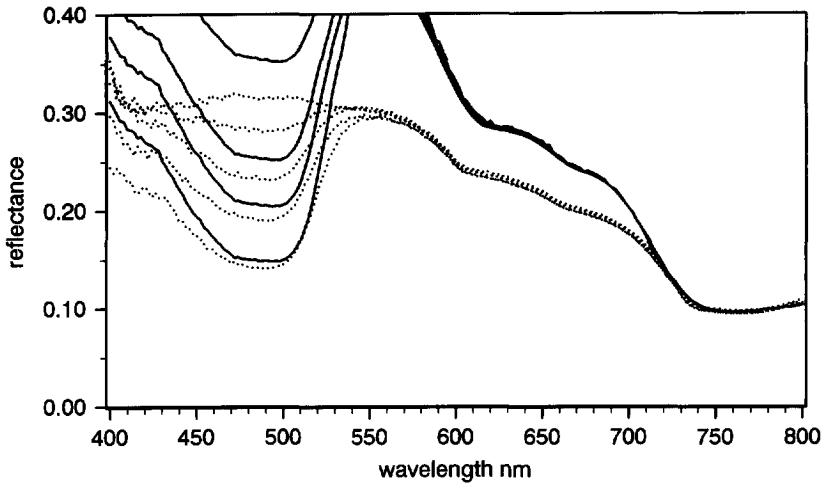

Figure 4.13 *Reflectance values (dotted lines) were overestimated by the model of Joseph (1950) for optical deep water (solid lines) except for ω_b less than 0.40, compare Figure 4.9.*

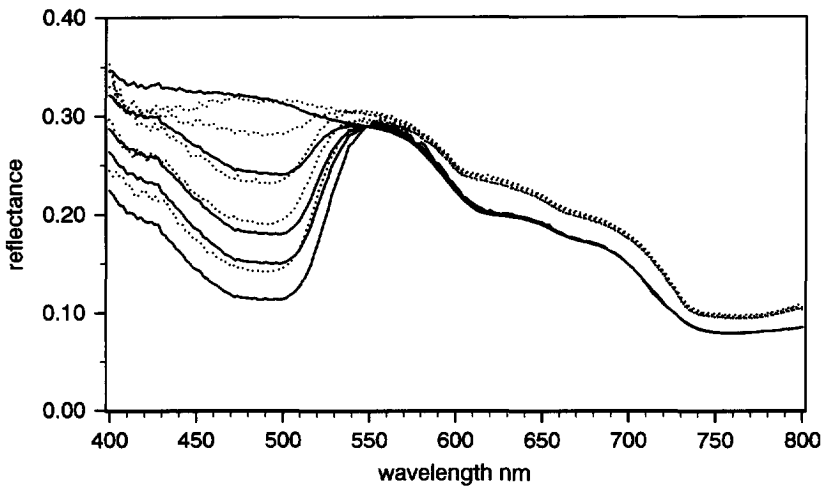

Figure 4.14 *Reflectance of the dye concentration series (dotted lines) predicted by the two flow model of Spitzer and Dirks (1987) for optical deep water (solid lines). The reflectance was calculated assuming commonly used values for the distribution factors; $D_d=1.2$ and $D_u=2.4$. The model underpredicts the reflectance except for ω_b close to one.*

$$R_\infty(0) = \left[\frac{1}{\omega_b} - \left[\left(\frac{1}{\omega_b}\right)^2 - \frac{4D_u D_d}{(D_u+D_d)^2}\right]^{1/2}\right]\frac{D_u+D_d}{2D_u} \qquad \textbf{(4.6)}$$

Figure 4.14 shows the results of the two flow model calculations for the reflectance of the dye concentration series using distribution factors in common use of $D_d=1.2$ and $D_u=2.4$. This leads to predicted reflectance values that are too low. Compared to the model of Joseph the use of distribution factors leads to lower model predictions.

4.4.2.4 Backscattering Albedo Model

A simple analytical reflectance model was derived from the reflectance measurements. Figure 4.11 shows an almost linear relation between reflectance and backscattering albedo. The regression line through the observations over an extended range of ω_b values was $R(0+)\text{-}R_{aw}=0.000+0.269\omega_b$ with $r^2=0.9944$. The reflectance at $\omega_b=1$ is close to its upper limit of 0.275 calculated from the limiting value for $R(0)$ of 0.5 (Bukata *et al.* 1980) multiplied by the water-to-air factor f_{wa} of 0.55.

$$R(0+)-R_{aw} = f_{wa}R_\infty(0) = f_{wa}0.5\,\omega_b = 0.275\frac{Bb}{a+Bb} \qquad \textbf{(4.7)}$$

Figure 4.15 shows that this model fits the measured reflectance spectra accurately. We call this single scattering model the backscattering albedo model. The backscattering albedo model describes the measured spectra more accurately than the other models do.

4.4.3 Optical Shallow Suspensions

The reflectance of optical shallow suspensions is affected by light reflectance at the bottom. The spectra were modelled by the optical deep reflectance $R_\infty(0)$ and the optical depth of the suspension according to the two flow model. Predictions using the expressions for optical deep and for optical shallow water were compared to reflectance measurements of the dye concentration series. Figure 4.16a shows results for the model of Joseph (1950), Equation 2.85. Observed reflectance values are correctly predicted in the spectral range 750-800 nm for low ω_b, but are too low in the range 400-750 nm. Figure 4.16b shows that the measured reflectance values are systematically underpredicted by the model of Spitzer and Dirks (1987), Equations 2.86 to 2.89.

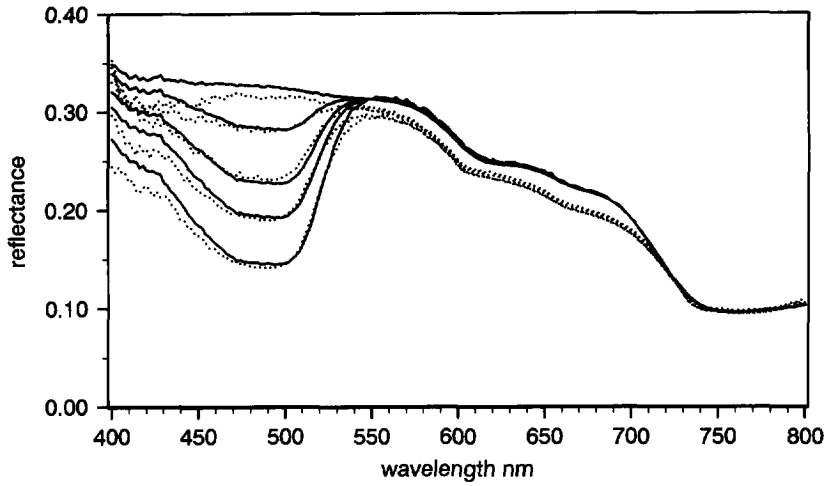

Figure 4.15 *The backscattering albedo model (solid lines) fits the measured reflectance (dotted lines) accurately. In the spectral range between 550 and 700 nm the model overpredicts the observations without an obvious relation to the value of* ω_b. *An explanation was not found for this error. However, compared to the other models this model is the most accurate to predict the observed reflectance spectra.*

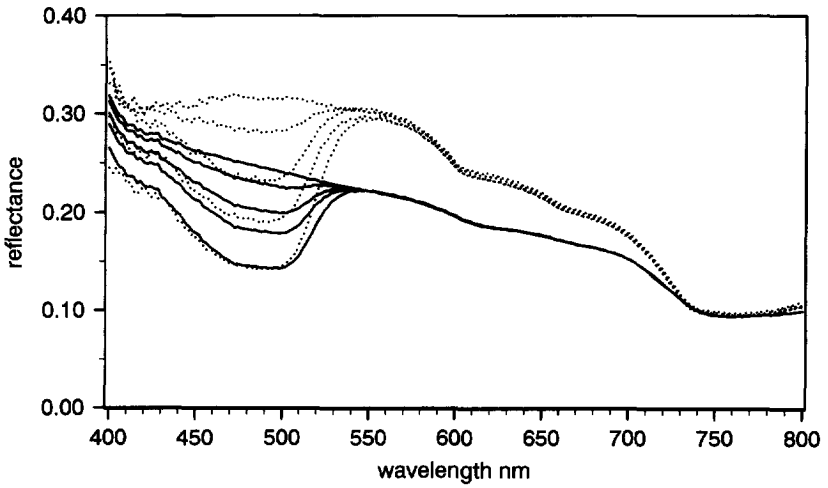

Figure 4.16 *Comparison of measured and calculated spectra of the dye concentration series using the two flow model for optical shallow suspensions.*
Figure 4.16a Measured (dotted lines) and calculated (solid lines) spectra using the two flow model of Joseph (1950) for optical shallow suspensions.

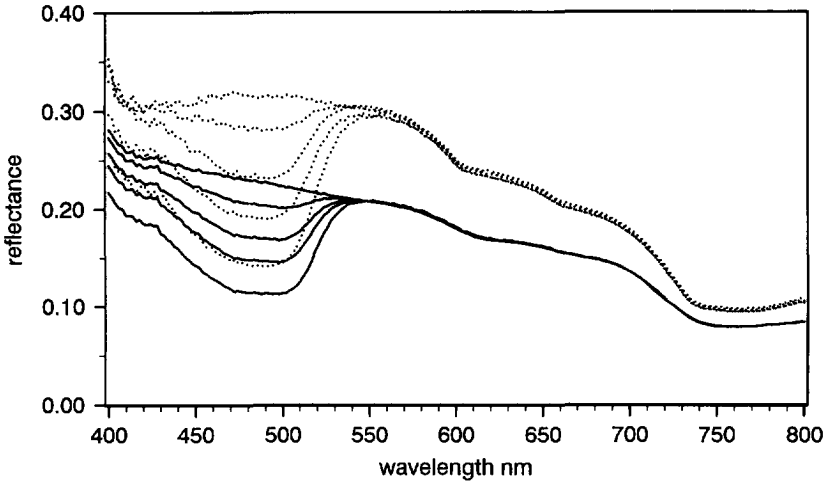

Figure 4.16b Measured (dotted lines) and calculated (solid lines) spectra using the two flow model of Spitzer and Dirks (1987) for optical shallow suspensions with diffuseness factors D_u=2.4 and D_d=1.2 for up- and downward irradiance.

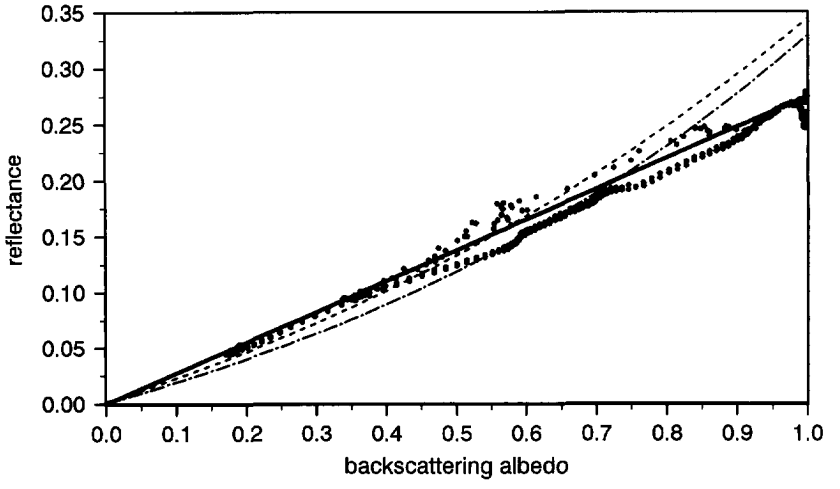

Figure 4.17 *Observed and predicted reflectance values of $R(0+)$-R_{aw} as a function of the backscattering albedo. Reflectance values measured on the begin and end concentration of the dye concentration series (•) are given together with the results of model calculations using the quasi-single scattering model for sky (dashed line) and sun illumination (dash-dotted line), and the backscattering model (solid line).*

Approximate solutions of the two flow model exist, e.g. Austin (1974) (Equation 2.94) and Philpot (1987) (Equation 2.96), that account for the influence of bottom reflectance by the difference between the reflectance of the bottom and the optical deep reflectance of the suspension multiplied by an exponential function of the bottom depth:

$$\begin{aligned} R(0) &= R_\infty(0)+(R_b-R_\infty(0))\exp(-(K_d+K_u)z) \\ R(0) &= R_\infty(0)+(R_b-R_\infty(0))\exp\left(-(a+b_b)(D_u+D_d)z\right) \end{aligned} \qquad \textbf{(4.8)}$$

with diffuseness factors D_u=2.4 and D_d=1.2 for up- and downward irradiance.

Optical equivalent solutions for this expression are related to the attenuation coefficient for irradiance; the geometric depth can be scaled by the diffuse attenuation coefficient to a diffuse optical depth. In a similar way as the optical depth is related to the beam attenuation coefficient (Equation 2.54) the diffuse optical depth can be related to the irradiance attenuation coefficient multiplied by the geometric depth:

$$\tau^* = \int_0^z K_{u,d}(z)dz \qquad \textbf{(4.9)}$$

with the irradiance attenuation equal to the sum of absorption and backscattering multiplied by a diffuseness factor. This expression for the reflectance of optical shallow water can be used to find better solution by substitution of the optical deep reflectance calculated by other models, e.g. the quasi-single scattering model. For small optical depths, either dilute suspensions or shallow bottom depths, large deviations from the experimental results occurred. By adjusting the distribution factors D_u and D_d to values of 1.2 or 1.0 the fit could be improved.

However, the almost perfect linear relation with particle concentration for optical shallow suspensions shown in Figure 4.1 can not be explained by an exponential term using the difference in reflectance between the optical deep suspension and the bottom ($R_\infty(0)$-R_b). With a backscattering coefficient large compared to the absorption coefficient of water, for the first particle concentration shown $b_b(500)$ is 0.195 m^{-1}, the optical deep reflectance $R_\infty(0)$ is constant and thus independent of the particle concentration. For a water body with constant depth and linearly increasing particle concentration the increase of reflectance is expected to diminish exponentially to the optical deep reflectance of the suspension because the linear change in the irradiance attenuation coefficient that is proportional to the particle concentration.

The measured reflectance of optical shallow waters could not be described by the models given for optical shallow water. Further research is needed to explain the observed spectra and to decide on the best model to use for optical shallow water.

4.5 Conclusions

The backscattering albedo model predicts the spectral reflectance of optical deep suspensions measured with the large volume reflectometer. Figure 4.17 shows that observed and modelled reflectance values are a function of the backscattering albedo ω_b. The model is expected to be generally valid since the observed reflectance values cover a wide range of backscattering albedo's, from 0.15 to almost one, partially overlapping the range of ω_b values from 0.00 to 0.35 for turbid natural waters, as estimated based on data of turbid river water presented by Whitlock *et al.* (1981).

The required input of inherent optical properties to compute the spectral reflectance consists of the properties of water from literature, of the measured absorption of the dye, while the scattering properties of the polystyrene particles were calculated by theory and experimentally verified. Scattering calculations of the polystyrene particles with monodisperse size distribution by Mie-theory were within 5% of measured values. Compared to exact Mie-theory the van de Hulst approximation results in 10% lower values because the relative refractive index of polystyrene particle is not close to one. An error of about this magnitude is consistent with the results by Moore (1968).

The backscattering albedo reflectance model was the most accurate model. A summary of the comparison of reflectance models is given in Table 4.3. The second best model was the quasi-single scattering approximation using the coefficients for sky illumination. The two flow model predicted reflectance values for optical deep suspensions that were too high while for optical shallow water the results were too low. The successive order scattering model is not valid for turbid suspensions nor for weakly absorbing suspensions, it results in incorrect reflectance values larger than one.

Table 4.3 *Comparison of predictions by analytical reflectance models with experimental results. Listed are the model, the required input parameters, the predicted parameter(s) and an indication of the prediction accuracy. Predictions using the expressions for optical deep and for optical shallow water were compared to reflectance measurements of the dye concentration series. It is concluded that the backscattering albedo model is as yet the best model to interpret reflectance spectra.*

Model	Input	Output	Prediction of $R(0)$
OPTICAL DEEP WATER			$R(0+)$-R_{aw}=0.55 $R_\infty(0)$
Successive Order Scattering Model Morel and Prieur (1977)	a, Bb	$R_\infty(0)$	not valid too high
Quasi-Single Scattering Model Gordon *et al.* (1975)	a, Bb	$R_\infty(0)$	too low for low ω_b too high for high ω_b sky case results are better
Two Flow Model Joseph (1950)	a, Bb	$R_\infty(0)$, $R(z)$	accurate for low ω_b, too high for high ω_b
Two Flow Model Spitzer and Dirks (1987)	a, Bb, D_d, D_u	$R_\infty(0)$, $R(z)$	too high
Backscattering Albedo Model present study	a, Bb	$R_\infty(0)$	accurate too high for 550-700 nm
OPTICAL SHALLOW WATER			$R(0)=f(R_\infty(0),R_b)$
Two Flow Model Joseph (1950)	a, Bb, R_b	$R(0)$, $R(z)$	accurate for low ω_b, too low for high ω_b
Two Flow Model Spitzer and Dirks (1987)	a, Bb, D_d, D_u, R_b	$R(0)$, $R(z)$	too low

4.6 Discussion: How to Estimate the Backscattering Coefficient

The volume scattering function of the polystyrene particles was calculated by Mie-theory. This function varies significantly with wavelength, the related backscattering probability B decreases with wavelength from 0.069 to 0.012, at 550 nm it was 0.019, a value commonly used for marine waters.

For samples with an unknown volume scattering function the backscattering coefficient must be estimated to interpret reflectance spectra. An estimate of the volume scattering function can be derived from measurement of absorption and attenuation at a wavelength where absorption is negligible, or from absorption alone at such a wavelength as shown in Section 4.3.3. Usually the backscattering coefficient is estimated by making an assumption about the backscattering probability and measuring the beam attenuation.

4.6.1 Estimation from the Apparent Absorption

The apparent absorption spectrum measured with the semi-integrating sphere technique on a scattering suspension is partly caused by scattering. For samples with an unknown volume scattering function forward - and backscattering must be estimated to interpret reflectance spectra. To do this we suggest to use the average ratio between the backscattering probabilities at 38° and 90°. An estimate of the main characteristics of the volume scattering function can be derived from the combined measurements of absorption and beam attenuation at a wavelength where absorption is negligible.

The apparent absorption measured using a semi-integrating sphere at a wavelength without inherent absorption can be used to estimate the backscattering coefficient b_b (Section 4.3.3). Figure 4.7 shows that $B(90)b$ can be estimated from the apparent absorption $B(38)b$ using the ratio between the backscattering probabilities. The ratio $B(38)/B(90)$ was about four to five for the volume scattering function of the polystyrene particles at 550 nm (Table 4.1). At 550 nm the polystyrene particles have a volume scattering function with a backscattering probability of 0.019. The volume scattering function of San Diego Harbor (Petzold 1977) with the same backscattering probability is in common use to model the optical characteristics of turbid surface water. So division of the apparent absorption at a wavelength without inherent absorption by a factor of four to five gives an estimate of the backscattering coefficient b_b.

4.6.2 Estimation from a_m and c_m

To calculate a reflection spectrum with the single scattering approximation a and b_b must be known or estimated. Measured absorption values must be corrected for scattering to derive the inherent absorption a.

The backscattering coefficient at 550 nm is overestimated by a factor four; instead of the correct value of $0.019b$ the measured value was $0.078b$. A simple method to make an approximation of the inherent absorption and backscattering coefficients is to interpret the integrating sphere measurement of turbid water as $a_m=a+0.078b$.

Combination of the apparent absorption with the beam attenuation measurements $c=a+b$ leads to a straightforward estimate if beam attenuation measurements are assumed to be ideal, with an acceptance angle indistinguishable from 0°. The error in the beam attenuation

measurement depends on the acceptance angle of the device, θ_{cm} estimated at 3° for our Perkin Elmer spectrophotometer in the diffraction peak of the volume scattering function. For the polystyrene particles the error in c is insignificant (about 8%) but for water with the volume scattering function of San Diego Harbor the fraction of scattering in c would have been underestimated by 58%.

$$\begin{aligned} a_m &= a+B(\theta_{am})b = a+0.08b \\ c_m &= a+B(\theta_{cm})b = a+0.92b \\ c_m-a_m &= (B(\theta_{cm})-B(\theta_{am}))b = 0.84b \end{aligned} \tag{4.10}$$

For an assumed volume scattering function, the two equations can be solved to give the two unknown inherent optical properties a and b.

Estimates for the scattering probabilities can be found by solving the two equations in a part of the spectrum where absorption can be neglected. For the remaining parts of the spectrum the equations can be solved by assuming that $B(90)b$ is constant or proportional to λ^{-1} (Bricaud *et al.* 1981, Section 2.2.5.1).

4.6.3 Estimation from a and c Using an Equivalent Spherical Particle

A method to analyze absorption and beam attenuation spectra of a suspension is given by Bricaud *et al.* (1983), Bricaud and Morel (1986) and Stramski *et al.* (1988). The method accounts for anomalous particle scattering and absorption by the approximation theory of van de Hulst. They presented a method to decompose attenuation and absorption spectra for a given size distribution into a single equivalent spherical particle with spectral variations in the imaginary part of the refractive index. The size distribution of the particles in the suspension is determined relative to the numbers of cells per unit volume. The absorption efficiency factor Q_a spectrum was decomposed in gaussian oscillators (spectral variations in the imaginary part of the refractive index) and together with a central value for the real part of refractive index, Q_b, the attenuation Q_c (scatter and absorption) spectrum is recomposed using the approximation theory for anomalous diffraction by van de Hulst (1957). The backscattering efficiency is calculated from the volume scattering function of the equivalent spherical particle.

The method was not applied because the particles do not absorb and the results for non-absorbing spheres are already given in this chapter. The method will be used in Chapter 5 to estimate the backscattering coefficient of a *Chlorella pyrenoidosa* suspension.

4.6.4 Estimation from a_m and $R_\infty(0)$

The spectrum of backscattering coefficients can be calculated from the apparent absorption and the reflectance of an optical deep suspension by application of the backscattering albedo model. The inherent absorption is estimated by correcting the apparent absorption for scattering (Section 4.6.5). With Equation 4.7 rewritten to

$$Bb = \frac{R_\infty(0)}{0.5 - R_\infty(0)}\, a \qquad (4.11)$$

the total backscattering is found by substitution of the observed reflectance and the estimated inherent absorption. If the scatter correction is assumed to have a certain relation to the backscattering coefficient the results can be verified or a solution can be computed iteratively. The accuracy of the results depends mainly on the accuracy of the scattering correction procedure.

4.6.5 Scattering Correction of Apparent Absorption: Propagation of Errors

To obtain the inherent absorption of a suspension the observed apparent absorption must be corrected for scattering. To asses the propagation of errors in the calculation of reflectance spectra we applied these methods to the apparent absorption of the polystyrene microspheres. The following three correction procedures are considered:

1. a is a_m, assuming perfect absorption measurements
2. a is $a_m(\lambda)$-$a_m(720)$ according to the common correction procedure for measurements on suspensions of algae
3. b_b is $a_m/4$ assuming that at all wavelengths with negligible absorption the apparent absorption is close to a fourth of the backscattering.

The backscattering coefficient b_b was calculated as $0.019b$ with $b=c_m-a$ in the procedures 1 and 2. Reflectance was calculated by the backscattering albedo model. Application of the correction procedures to the suspensions of non-absorbing particles result are an extreme case for the propagation of errors because the true inherent absorption is zero. To judge the effect of the assumption of a constant backscattering coefficient b_b equal to $0.019b$ the reflectance

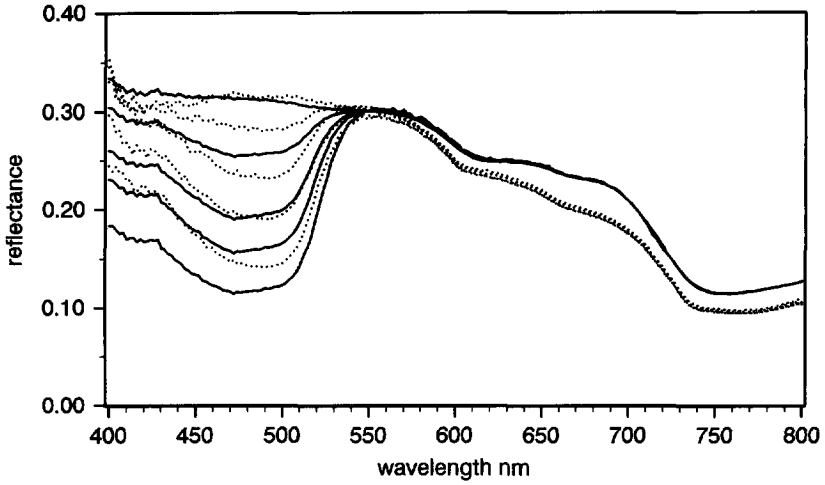

Figure 4.18 *Comparison of three simple methods to interpret the apparent absorption measured with an semi-integrating sphere. It is shown how the errors of these methods affect model predictions of the reflectance (solid lines).*
Figure 4.18a To judge the effect of the assumption of a constant backscattering coefficient b_b equal to 0.019b the reflectance was calculated assuming non absorbing polystyrene particles, only a minor effect resulted.

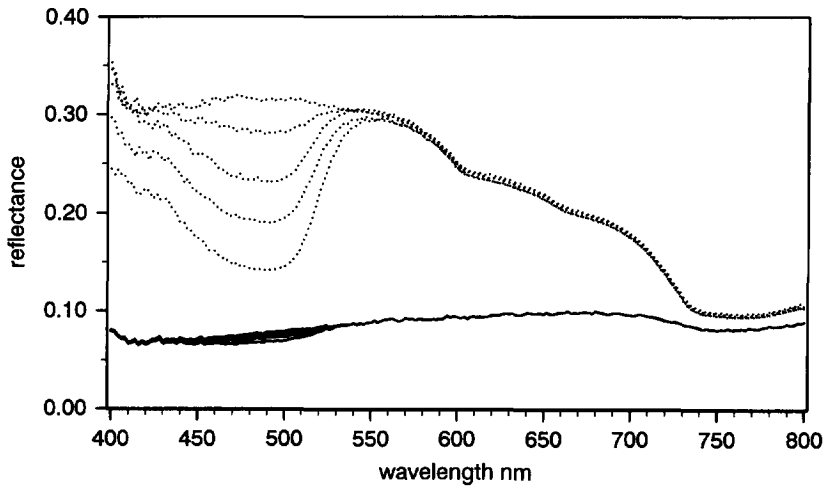

Figure 4.18b Using the measured absorption without correction for scattering as an estimate of the inherent absorption ($a=a_m$) leads to reflectance values that are systematically too low.

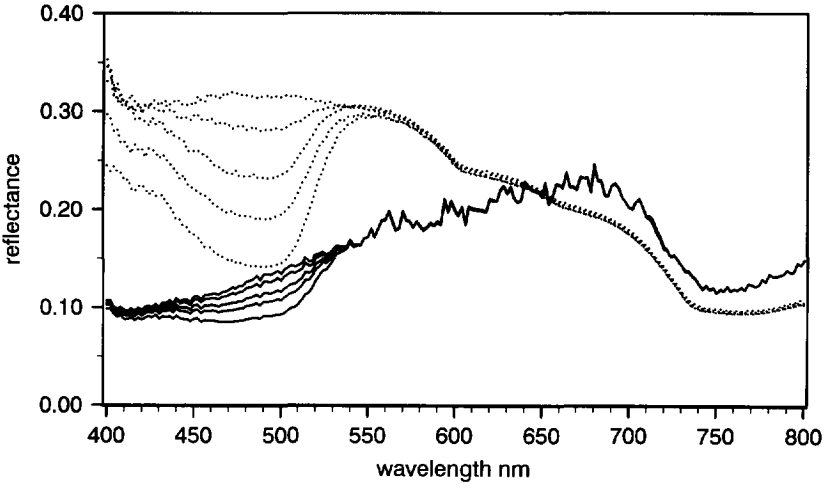

Figure 4.18c Correction for scattering by $a=a_m(\lambda)-a(720)$ leads to reflectance values that are systematically too low, except for wavelengths close to 720 nm.

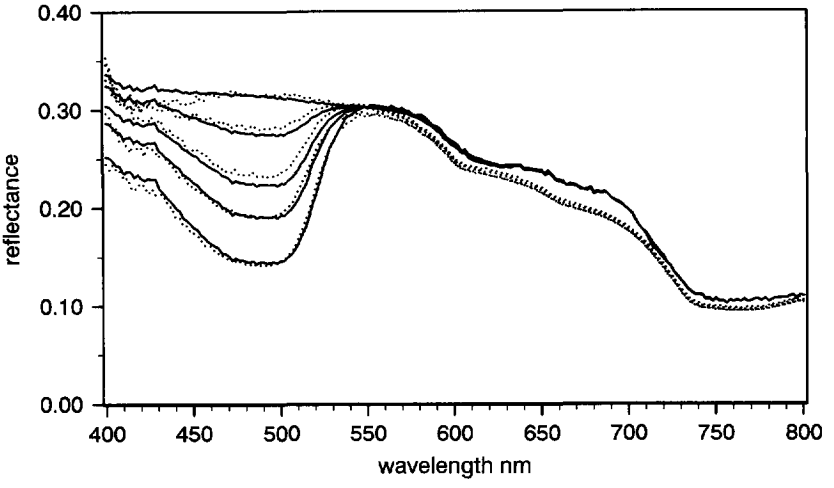

Figure 4.18d Estimation of the backscattering coefficient by $b_b=a_m/4$ leads only to minor deviations compared to observed reflectance spectra. Because the relation was derived for these particles this figure shows only the differences that arise using a constant factor instead of the calculated factors (Figure 4.7 and Table 4.1)

was calculated assuming non absorbing polystyrene particles. Figure 4.18a shows that compared to only a minor effect results.

1. If integrating sphere absorption measurements are used to calculate the reflectance without the correction for scattering to obtain the inherent absorption significant errors are made. Figure 4.18b shows that reflectance values are systematically too low.

2. If integrating sphere absorption measurements are used to calculate reflectance by the correction method for scattering subtracting the measured apparent absorption at 720 nm to obtain the inherent absorption significant errors are made. Figure 4.18c shows that reflectance values are systematically too low, except for wavelengths close to 720 nm.

3. If semi-integrating sphere absorption measurements are used to calculate the reflectance with a fourth of the detected apparent absorption to obtain inherent coefficients of b_b, only minor errors are made. Figure 4.18d shows that reflectance values are close. Because the relation was derived for these particles this figure shows only the difference that arise by using a constant factor instead of the calculated factors (Figure 4.7 and Table 4.1)

The results indicate that the choice of the procedure to correct apparent absorption for scattering can have a larger effect on the predictions of reflectance than the choice of the model. The accuracy of reflectance model calculations is apparently determined by the accuracy of the inherent optical properties and less by the accuracy of the reflectance model.

References

Austin, R.W., 1974. The remote sensing of spectral radiance from below the ocean surface, In: *Optical aspects of oceanography*, Eds. N.G. Jerlov and E. Steemann Nielsen, Academic Press, London, 317-344.

Aas, E., 1987. Two-stream irradiance model for deep waters, Appl. Opt. **26**(11), 2095-2101.

Bricaud, A., A. Morel and L. Prieur, 1983. Optical efficiency factors of some phytoplankters, Limnol. Oceanogr. **28**(5), 816-832.

Bricaud, A., A. Morel, 1986. Light attenuation and scattering by phytoplanktonic cells: a theoretical modeling, Appl. Opt. **25**(4), 571-580.

Bukata, R.P., J.E. Bruton and J.H. Jerome, 1980. Conceptual approach to the simultaneous determination of the backscatter and absorption coefficients of natural waters, Appl. Opt. **19**(9), 1550-1559.

Daniel, K.J., N.M. Laurendreau and F.P. Incropera, 1979. Prediction of radiation absorption and scattering in turbid water bodies, ASME J. Heat Transfer **101**, 63-67.

Friedman, E., L. Poole, A. Cherdak and W. Houghton, 1980. Absorption coefficient instrument for turbid natural waters, Appl. Opt. **19**(10), 1688-1693.

Gordon, H.R., O.B. Brown and M.M. Jacobs, 1975. Computed relationships between the inherent and apparent optical properties of a flat homogeneous ocean, Appl. Opt. **14**(2), 417-427.

Hottel, H.C., A.F. Sarofim, L.B. Evans and I.A. Vasalos, 1968. Radiative transfer in anisotropically scattering media: allowance for Fresnel reflection at the boundaries, ASME J. Heat Transfer, 56-62.

Hulst, H.C. van de, 1957. *Light scattering by small particles*, Dover Publ., New York, 450 pp.

Incropera, F.P., T.R. Wagner and W.G. Houf, 1981. A comparison of predictions and measurements of the radiation field in a shallow water layer, Water Resources Res. **17**(1), 142-148.

Joseph, J., 1950. Untersuchungen über Ober- und Unterlichtmessungen im Meer und über ihren Zusammenhang mit Durchsichtigkeitsmessungen, Deutsche Hydrogr. Z. **3**(5/6), 324-335.

Mie, G., 1908. Beitrage zur Optik truber Medien speziell kolloidaler Metallösungen, Ann. Physik (Leipzig) **25**, 377.

Moore, D.M., F.D. Bryant and P. Latimer, 1968. Total scattering and absorption by spheres where $m \approx 1$, J. Opt. Soc. Am. **58**, 281-283.

Morel, A., Prieur, L., 1977. Analysis of variations in ocean color, Limnol. Oceanogr. **22**(4), 709-722.

Petzold, T.J., 1977. Volume scattering functions for selected ocean waters, In: *Light in the sea* (Benchmark papers in optics: V. 3), Ed. J.E. Tyler, Dowden, Hutchinson and Ross, Stroudsburg, Pennsylvania, 152-174.

Philpot, W.D., 1987. Radiative transfer in stratified waters: a single-scattering approximation for irradiance, Appl. Opt. **26**(19), 4123-4132.

Preisendorfer, R.W., and C.D. Mobley, 1984. Direct and inverse irradiance models in hydrologic optics, Limnol. Oceanogr. **29**(5), 903-929.

Smith, R.C. and K.S. Baker, 1981. Optical properties of the clearest natural waters (200-800 nm), Appl. Opt. **20**, 177-184.

Spitzer, D. and R.W.J. Dirks, 1987. Bottom influence on the reflectance of the sea, Int. J. Remote Sensing, **8**(3), 279-290.

Stramski, D., A. Morel and A. Bricaud, 1988. Modelling the light attenuation and scattering by spherical phytoplanktonic cells: a retrieval of bulk refractive index, Appl. Opt. **27**(19), 3954-3956.

Whitlock, C.H., L.R. Poole, J.W. Ursy, W.M. Houghton, W.G. Witte, W.D. Morris and Gurganus, E.A., 1981. Comparison of reflectance with backscatter and absorption parameters for turbid waters, Appl. Opt. **20**(3), 517-522.

CHAPTER 5
MIXTURES OF SUSPENDED MATTER

5.1 Introduction

Turbid surface water contains particulate matter consisting of a mixture of algae, detritus and suspended sediment. The organic and inorganic fractions of suspended particulate matter can, to a certain extent, be discriminated as separate water colour components. The photosynthetic pigments in plankton algae have characteristic absorption spectra with specific peaks while the absorption by detritus and inorganic particles is much less characteristic. Usefulness of passive optical remote sensing of turbid waters will improve considerably if these fractions can be estimated from spectral reflectance data. In this chapter measured reflectance spectra of known mixtures of algae and silt are analyzed and the applicability of a simple reflectance model is tested. This model was chosen based on the analysis of a series of mixtures of purely scattering particles and a purely absorbing water soluble dye as described in Chapter 4.

Reflectance properties of coloured organic and inorganic particles were studied on mixtures of *Chlorella pyrenoidosa* and ferrite. The green alga *Chlorella pyrenoidosa* was chosen as organic particle because its optical properties have been well investigated. Latimer (1959) found good agreement between measured values and theoretical predictions of extinction for different refractive indices of the medium. Das *et al.* (1967) studied the discreteness effect in suspensions of *Chlorella pyrenoidosa*. Privoznik *et al.* (1978) measured the specific inherent optical properties of this species. Powdered ferrite, a red-brown sediment, was chosen because these inorganic particles did not agglomerate with the algae and because iron is a natural colour compound. Several other inorganic materials: Illite, Ball clay and Western Walder clay were tested but found unsuitable since agglomerates were formed in mixtures with algae. Optical effects associated with the formation of agglomerates like the flattening of absorption spectra due to the discreteness effect had to be avoided in this experiment. The effects of such changes are discussed in Chapter 6.

5.2 Materials and Methods

Reflectance Spectra

Reflectance spectra were measured with the large volume laboratory reflectometer (Section 3.1). Suspensions were illuminated by a diffuse light field. This was created by illuminating a diffusely reflecting white panel with two 300 W halogen lamps. The sample tank had mirror side walls to simulate infinite horizontal dimensions of the light field and the layer of water.

Spectra were measured with the optical multichannel analyzer set to a spectral resolution of 2.4 nm by a 100 μm slit and the illumination time of the photodiode array was 15.00 s. Radiance spectra were measured to simulate remotely sensed reflectance data. Upward radiance was detected just below the water surface and 0.40 m above the water surface. The radiance probe was positioned using a vertical mounting rod with prefixed intervals of 50.0 mm. This rod was aligned so that at its zero position the window of the radiance probe touched the water surface. The incident light intensity was measured using a grey reference panel with 10% diffuse reflectance held just above the water surface. Reflectance spectra of suspensions were measured with a black bottom plate positioned 0.60 m below the water surface. Particles were kept in suspension with the pump circulation system. The support of the bottom plate could be used as a piston to homogenize suspensions after addition of particles. Characteristic mixtures of the concentration series were checked to be optical deep by measuring a depth profile with a white bottom plate positioned at depths from 0.100 m to 0.600 m with 0.100 m increments.

Spectrophotometric measurements of absorption and beam attenuation were made simultaneously (Figure 5.1) with a flow-through cuvette in a closed circulation system. Flow-through cuvettes of 10 mm on the sides were designed not to influence the acceptance angle of the spectrophotometer (Section 3.2.5). An upward sample flow in the cuvette was used to flush occasional air-bubbles and to prevent settling of particles during the scan time.

Inorganic Particle Suspensions

Two stock suspensions of inorganic particles were prepared from powdered ferrite. A 4 litre stock, ferrite stock I, was made by suspending 40 gram ferrite in 5 litre filtered demineralized water. The suspension was stirred and allowed to settle for 10 minutes to remove fast settling particles. The supernatant was siphoned off from the sediment.

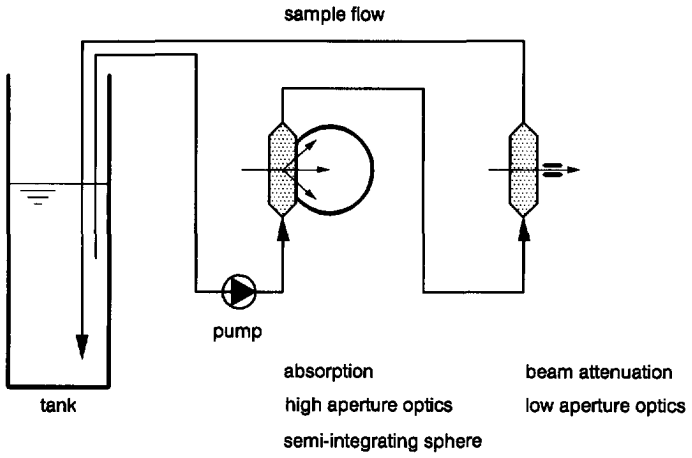

Figure 5.1 *Spectrophotometric sample circuit to measure absorption and beam attenuation spectra on line. The sample stream was pumped through flow-through cuvettes to prevent settling of the particle during the scan time. The cuvettes were designed not to influence the acceptance angle of the absorption measurement.*

Microscopic inspection showed that the supernatant contained irregularly shaped particles of 1-4 μm. A second stock with a higher sediment load of 3 litre, ferrite stock II, was made by suspending 400 gram ferrite in 5 litre water. This suspension still showed significant settling after 10 minutes and the settling procedure was repeated twice for 5 minutes. The ferrite stock suspensions were prepared just before use. During measurements the suspensions were kept homogeneous by stirring.

The dry weight and ash free dry weight (Section 3.3.4) of the concentrations series was calculated and some intermediate concentrations were checked.

Organic Particle Suspension

A stock of organic particle was prepared from a set of 16 one litre batch cultures of *Chlorella pyrenoidosa*. The 1 litre batch cultures were inoculated by 75 ml of a 1.5 litre continuous culture. Algae were grown on CP100 medium in 2 litre Erlenmeyer flasks at a light level of 24 W m^{-2} using cool white fluorescence light tubes. The algae were kept in suspension by gentle rotation.

The *Chlorella pyrenoidosa* stock contained aggregates. Microscopic inspection showed single cells of about 3-4 μm and aggregates of typically 20-80 μm. A homogeneous stock of single cells was prepared by submitting the suspension to sheer-force. This was done by forcing it under 7 bar nitrogen gas pressure through an orifice of 0.7 mm diameter. This way the aggregates were pulverized into single cells as was checked by microscopy. The resulting *C. pyrenoidosa* stock contained only single cells.

5.3 Specular Reflectance

The sample tank was filled with 52 litre of tap water filtered over a 0.2 μm membrane filter. Spectra of the clear tap water were measured to determine specular reflectance at the water surface under conditions of diffuse illumination (see Figure 3.6). Specular reflectance calculated by subtracting subsurface reflectance from above surface reflectance was about 0.050. During the experiments the specular reflectance was constant.

5.4 Reflectance Spectra of Mixtures

Starting from the clear tap water three concentration series were prepared of mixtures of organic and inorganic particles.

1. Ferrite particles were added to increase the inorganic particle concentration until an optical deep suspension resulted. Figure 5.2 shows the subsurface reflectance spectra of the concentration series of ferrite in tap water labelled by the code FExx, indicating that x.x litre of the ferrite stock I was added.

2. Algal particles were added to the optical deep suspension to study changes in reflectance with increasing organic particle concentration at a constant level of inorganic particles. The suspensions were labelled by the code FCxx indicating that x.x litre of the *C. pyrenoidosa* stock was added. Figure 5.3 shows subsurface reflectance spectra of a concentration series of *Chlorella pyrenoidosa* at a level of ferrite that was constant except for a small dilution error. Arrows indicate the change in reflectance with increasing algal concentration. The spectra show invariant reflectance at three wavelengths. These stable reflectance values occur where the reflectance of an added colour component is equal to the reflectance of the suspension. The ratios of the inherent optical properties of the dominant colour components in the mixture are the same at these wavelengths. This effect is similar to the occurrence of isosbestic points in absorption spectroscopy of reacting mixtures in chemical kinetics.

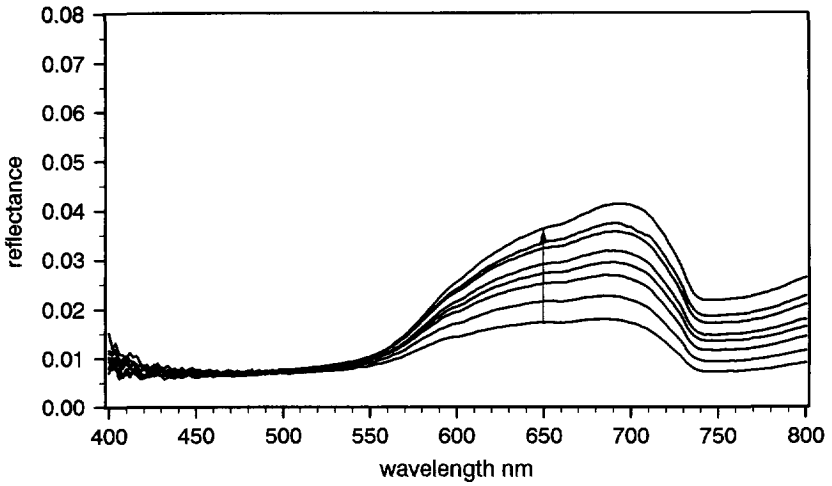

Figure 5.2a Spectra measured on the first day with concentrations up to FE18.

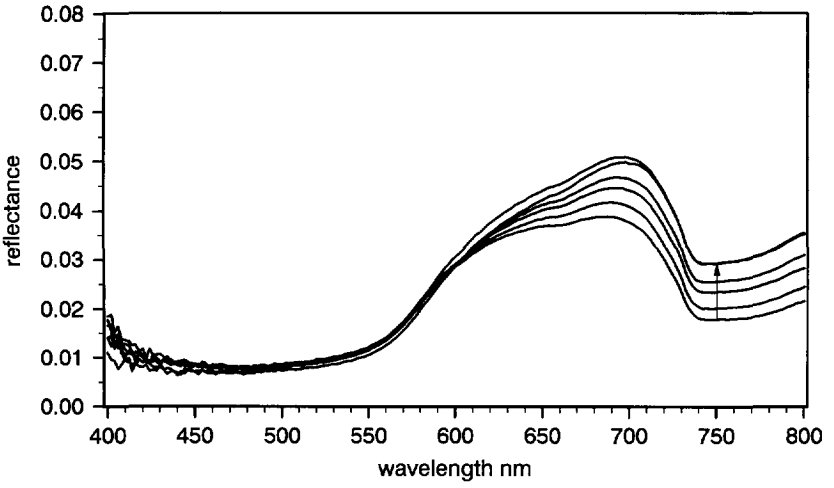

Figure 5.2b Spectra measured on the second day starting from the recovered suspension FE18R. The shape of the recovered spectrum was flattened probably because approximately 10 percent of the particles were settled from the suspension.

Figure 5.2 *Subsurface reflectance spectra of a concentration series of ferrite stock I in filtered tap water. Ferrite particles were added to increase the inorganic particle concentration until an optical deep suspension resulted.*

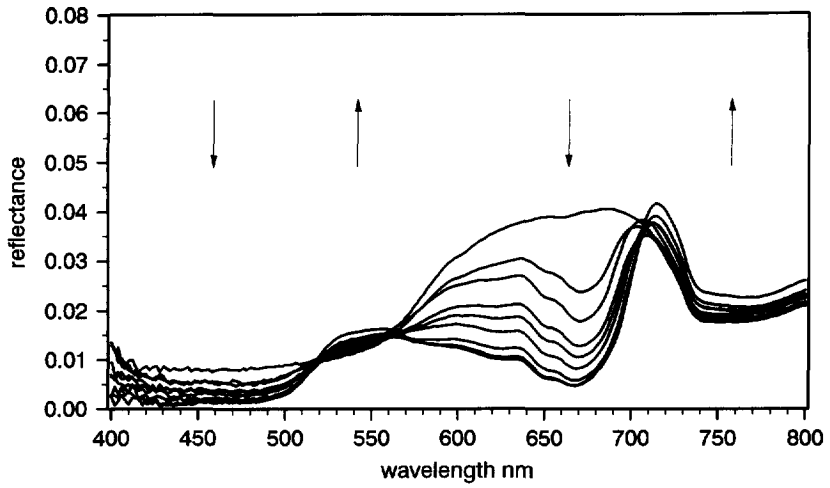

Figure 5.3 *Subsurface reflectance spectra of the concentration series of Chlorella pyrenoidosa at a level of ferrite that was constant except for a small dilution error. Arrows indicate the change in reflectance with increasing algal concentration. The spectra show invariant reflectance at three wavelengths. These stable reflectance values occur where the reflectance of an added colour component is equal to the reflectance of the suspension. The ratios of the inherent optical properties of the dominant colour components in the mixture are the same at these wavelengths.*

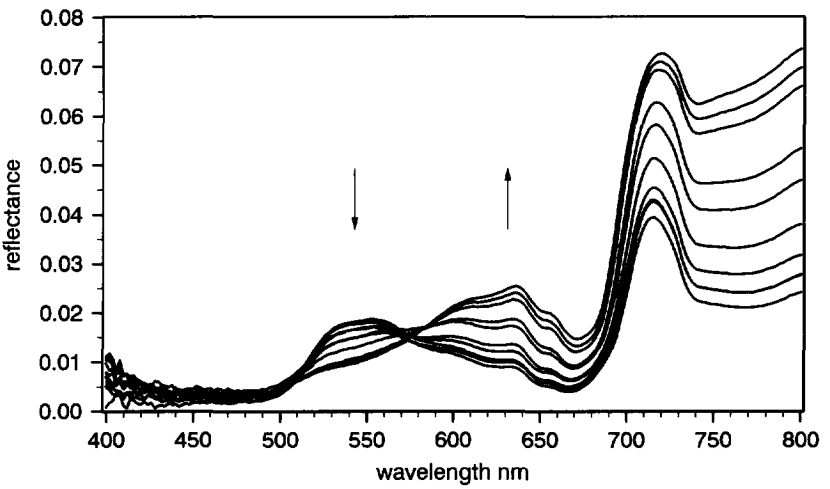

Figure 5.4 *Subsurface reflectance spectra of a concentration series of ferrite stock II at an almost constant level of Chlorella pyrenoidosa. Arrows indicate the change in reflectance with increasing ferrite concentration. The spectra show invariant reflectance at two wavelengths. The third invariant reflectance vanishes because with increasing particle concentration water becomes a less dominant colour component: the contribution of water absorption relative to the total absorption diminishes as the geometric depth of an optical deep suspension decreases with increasing particle concentration.*

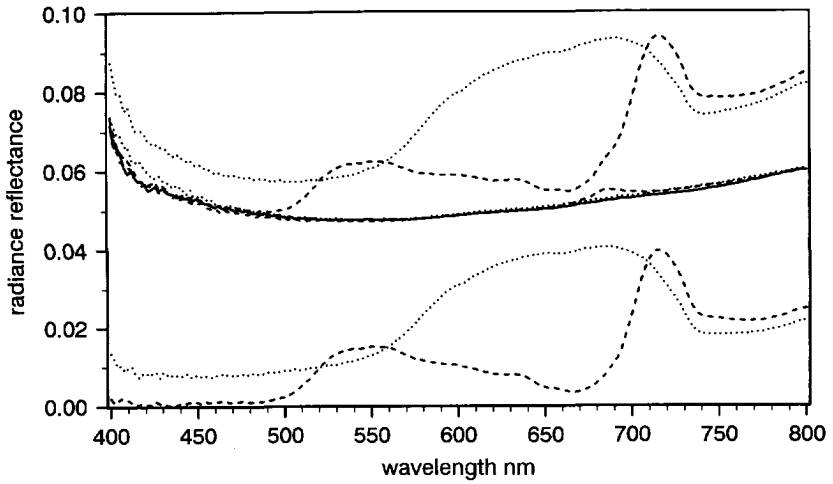

Figure 5.5 *Spectra of above surface, subsurface and specular reflectance for the suspensions FE38 (dotted lines) and FC70 (dashed lines) together with the specular reflectance of the clear tap water (solid line). The spectra are the same except for the offset due to the specular reflectance at the water surface. The small local increase in the specular reflectance around 690 nm for the algal containing suspension is not explained.*

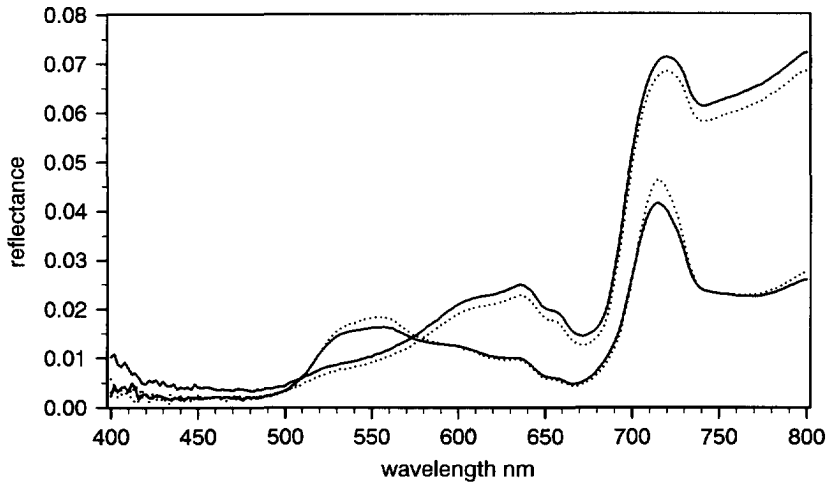

Figure 5.6 *Reflectance spectra of the suspensions CF0000 and CF3000 were optical deep. The spectra measured using the black bottom plate (solid lines) were almost equal to those measured using the white bottom plate (dotted lines).*

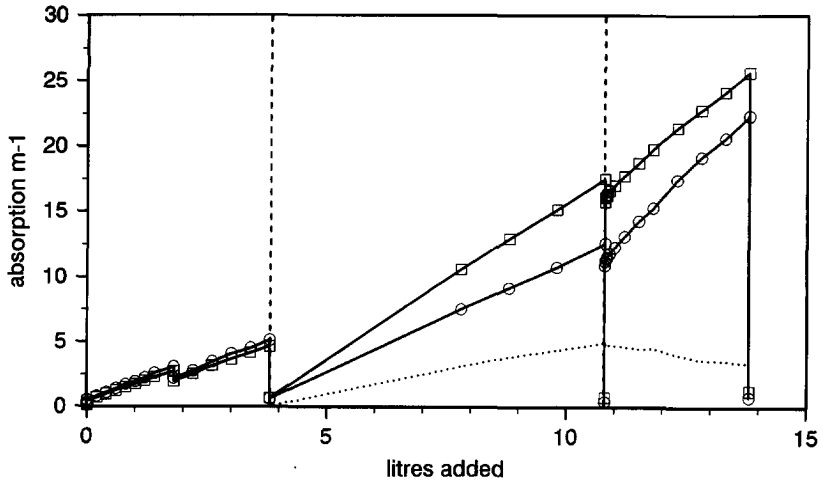

Figure 5.7a Absorption coefficients.

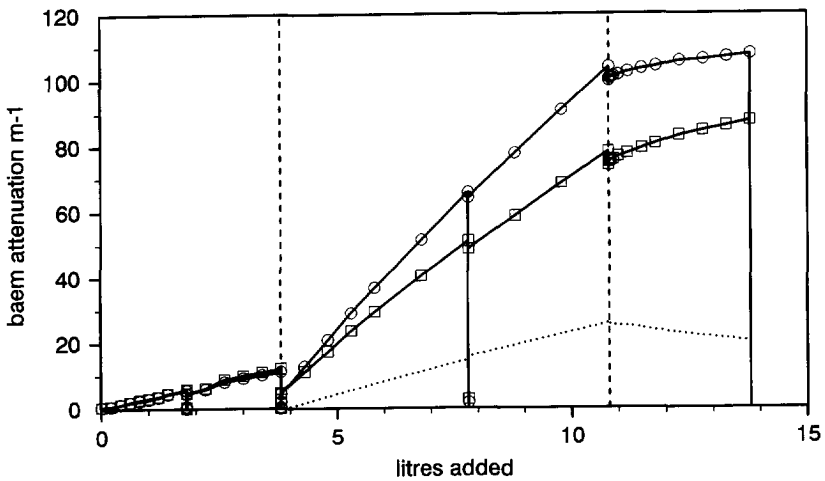

Figure 5.7b Beam attenuation coefficients.

Figure 5.7 *The coefficients of absorption and beam attenuation at 500 (○) and 676 nm (□) during the experiment as a function of the total volume of added stock suspension. The absolute difference between the two values (dotted line) is proportional to the concentration of algae. First 3.8 litre of ferrite stock I, then 7.0 litres of C. pyrenoidosa stock and then 3.0 litre of ferrite stock II. A total of 13.8 litre was added, dashed vertical lines separate the three concentration series.*

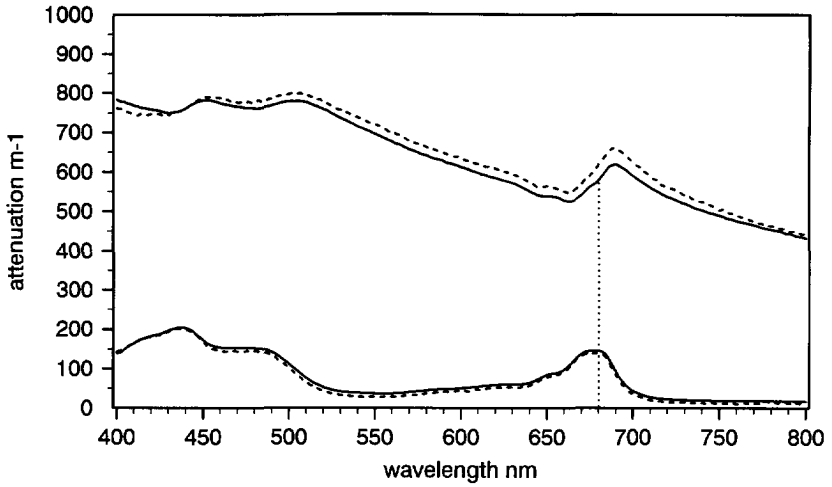

Figure 5.8 *The spectra of the algal stock recalculated from spectra of suspensions FC40 and FC70 (dashed line) and those measured on the algal stock suspension (solid line) were identical. The beam attenuation of this stock was measured on a tenfold diluted sample. The dotted line marks the anomalous scattering around the absorption peak at 680 nm.*

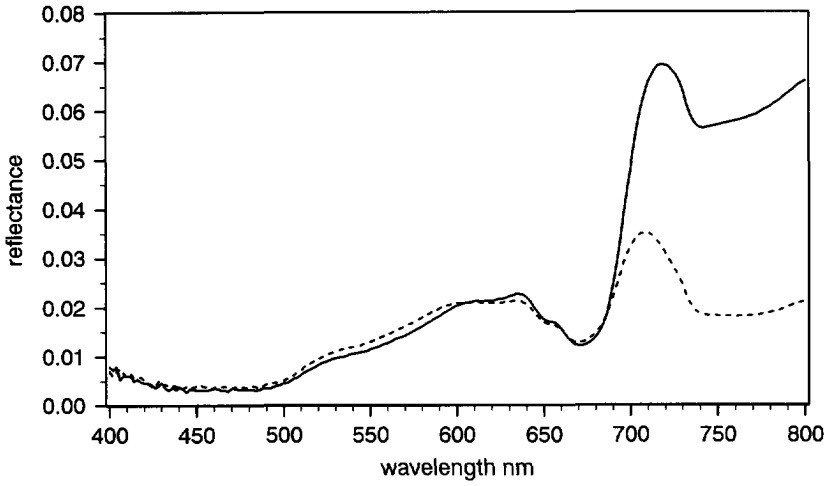

Figure 5.9 *Subsurface reflectance spectra measured on the suspensions FC15 (dashed line) and CF2000 (solid line). The spectra are very similar in the visible part of the spectrum but for wavelengths above 690 nm the spectrum of suspension CF2000 is significantly higher. The suspension CF2000 contains a fourfold higher concentration of both the organic and the inorganic fraction. The third colour component, water, is constant and at these wavelengths becomes less important and the increased ratio of the two other colour components becomes detectable.*

Table 5.1 *Characteristic properties of the stock suspensions.*

stock suspension	dry weight mg l^{-1}	$a(676)$ m^{-1}	$c(676)$ m^{-1}
ferrite stock I	225	44	84
ferrite stock II	566	145	322
C. pyrenoidosa stock	262	145	563

3. The organic particle concentration was kept constant and the concentration of inorganic particles was increased by adding ferrite. Suspensions were labelled by the code CFxxxx, indicating that x.xxx litre of ferrite stock II was added. Figure 5.4 shows the subsurface reflectance spectra of a concentration series of ferrite at an almost constant level of *Chlorella pyrenoidosa*. The spectra show invariant reflectance at two wavelengths. The third invariant reflectance vanishes because with increasing particle concentration water becomes a less dominant colour component: the contribution of water absorption relative to the total absorption diminishes as the geometric depth of an optical deep suspension decreases with increasing particle concentration.

Figure 5.5 shows the spectra of above surface, subsurface and specular reflectance for suspensions FE38 and FC70 together with the specular reflectance of filtered tap water. The spectra are identical except for an offset due to specular reflectance at the water surface. The small local increase in the specular reflectance around 690 nm seen in the suspension with algae FC70 is not explained, it might be due to fluorescence of chlorophyll *a*.

Figure 5.6 shows that the suspensions were optical deep. Reflectance spectra measured using the black bottom plate were almost equal to those measured using the white bottom plate for the first and last suspensions of the ferrite stock II concentrations series.

The actual concentration in the mixture was slightly different because the volume of the sample in the tank was kept constant and addition caused a small dilution effect. In Table 5.1 some characteristic properties of the stock suspensions are given. Calculated and measured values for the concentration series are given in Table 5.2 (page 126). Figures 5.7 and 5.8 show the absorption and beam attenuation coefficients of the mixtures. Figure 5.7 shows the increase of the coefficients at 500 and 676 nm during the experiment as a function of the total volume of added stock suspension. First 3.8 litre of ferrite stock I, then 7.0 litres of *C. pyrenoidosa* stock and then 3.0 litre of ferrite stock II. A total of 13.8 litre was added, dashed vertical lines separate the three concentration series. Figure 5.8 shows that the spectra of absorption and beam attenuation of the algal stock recalculated from spectra of suspensions

FC40 and FC70 and those directly measured on the algal stock suspension are identical. The beam attenuation of this stock was measured using a tenfold diluted sample.

Mixtures with a fourfold different concentration of both the organic and the inorganic fraction are shown in Figure 5.9. In the backscattering albedo model equal ratios of dominant colour components give equal spectral reflectance values. Figure 5.9 illustrates this confirming the model.

5.5 Modelling Reflectance Spectra

The inherent optical properties of the colour components must be known to model the reflectance spectra of the mixtures. The absorption and backscattering coefficient of the green algal *Chlorella pyrenoidosa* can be derived from the absorption and beam attenuation spectra measured on the stock suspension. The optical properties of the ferrite stock suspensions cannot be obtained from the spectrophotometric measurements.

5.5.1 Estimation of Backscattering by *Chlorella*

The backscattering coefficient b_b of *Chlorella* was calculated by a method comparable to that of Bricaud and Morel (1986b).

1. For the real part n of the refractive index in the absence of absorption the value of 1.40 was taken (Latimer 1959), average diameter of the cells was 3.2 μm.
2. The imaginary part n' of the refractive index was calculated from the measured absorption spectrum using Equations 2.18 and 2.19.

$$n' = \frac{\lambda}{4\pi n_w} a_i = \frac{\lambda}{4\pi n_w} \frac{a}{N\frac{\pi}{6}D^3} \qquad (5.1)$$

The measured absorption was converted to that of the intracellular material by multiplication with a factor of 2.10^3, equal to the reciprocal of the volume fraction of the particles multiplied by the refractive index of water.

3. The interaction between absorption and scattering was accounted for using the Ketteler-Helmholtz formula that describes the anomalous change in the real part n of the refractive index induced by the imaginary part n' for particles with a relative refractive index close to one.

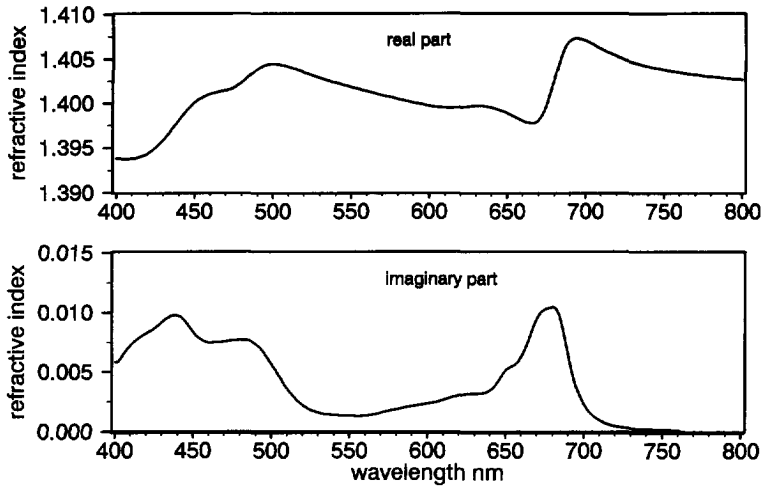

Figure 5.10 *Spectra of the real and imaginary part of the refractive index of Chlorella pyrenoidosa. The spectra were used as input data for Mie-calculations to obtain the spectrum of the backscattering probability B(90).*

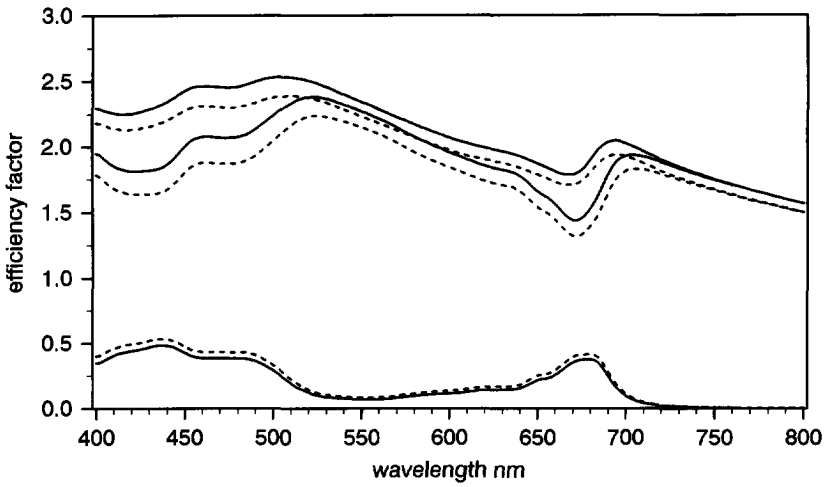

Figure 5.11 *Efficiency factors calculated with the approximation theory of van de Hulst (dashed lines) are in close agreement with that of the exact Mie theory (solid lines); Q_c was underestimated by 5%, Q_a was overestimated by 10-20% and Q_b by 5-10%. Accurate results are expected because the particles have a relative refractive index close to one.*

Mixtures

$$
\begin{aligned}
m &= n - in' \\
n &= 1 + \epsilon - \epsilon \sum_j v_j \frac{K_j}{1+v_j^2} \\
n' &= \epsilon \sum_j \frac{K_j}{1+v_j^2} \\
\text{with } v_j &= 4\pi \frac{(\lambda^{-1} - \lambda_{0j}^{-1})}{\gamma_j}
\end{aligned}
\qquad \textbf{(5.2)}
$$

The absorption spectrum was modelled by a number of j absorption bands with amplitude ϵK_j and damping constant γ_j.

4. The effective particle diameter of the algal suspension was iterated by comparing calculated and measured efficiency factors. Efficiency factors for absorption Q_a and extinction Q_c were calculated by the approximation for anomalous diffraction of van de Hulst. Normalization of the measured spectra by a factor GN (the geometrical cross section G multiplied by the particle concentration N) should yield the same spectral results.

5. The particle concentration N was checked by comparing the measured Chlorophyll *a* contents of 3300 mg l^{-1} with an estimated value of 0.729 10^{-10} N. This estimate is based on the cell pigment concentration of mature cultures given by Privoznik *et al.* (1978).

Iteration of steps 2 to 5 resulted in a good fit for an effective diameter of the size distribution of 3.3 μm. Correlations between measured and modelled spectra were 0.9943 for the absorption spectra and 0.9624 for the beam attenuation spectra.

6. The spectra of the real and imaginary part of the refractive index of *Chlorella pyrenoidosa* shown in Figure 5.10 were used as input data for Mie-calculations to obtain spectral values for the backscattering probabilities $B(90)$ and $B(38)$. Figure 5.11 shows that the efficiency factors of these particles with m around $1.05\text{-}0.005i$ calculated with the approximation of van de Hulst are in close agreement with that of exact Mie theory: Q_c was underestimated by 5%, Q_a was overestimated by 10-20% and Q_b was overestimated by 5-10%. Accurate results are expected for particles with a relative refractive index close to one. The spectral shape of the efficiency factor for extinction Q_c is typical for an absorbing particle with phase-lag parameter ρ around 2. At short wavelengths with ρ larger than 2 absorption causes a decreased anomalous extinction, at longer wavelengths with ρ smaller than 2 absorption causes an increased anomalous extinction. Figure 5.12 shows the backscattering probabilities $B(38)$ and $B(90)$ of a *Chlorella pyrenoidosa* particle with a diameter of 3.3 μm. The probability $B(90)$ is low, on average 5 10^{-4}, increases with wavelength from 1-9 10^{-4} and is affected by absorption. The decrease of $B(90)$ at shorter wavelengths is unusual but in

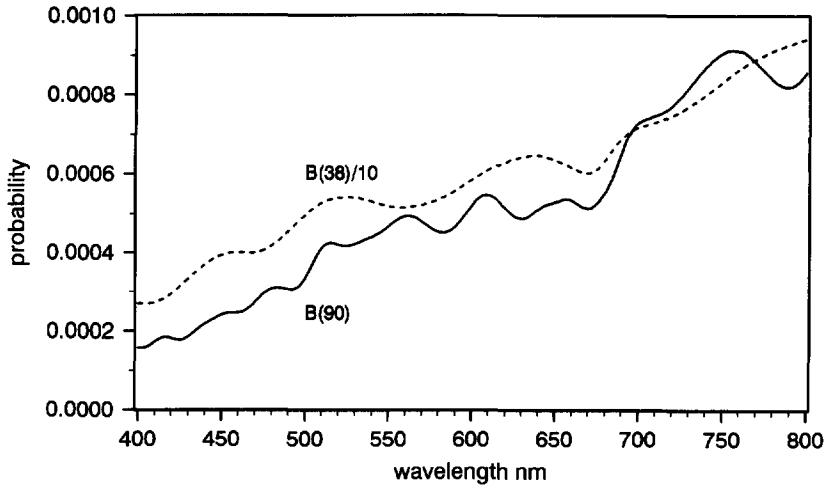

Figure 5.12 *Backscattering probabilities B(38) (dashed line) and B(90) (solid line) of the Chlorella pyrenoidosa particles using an effective diameter of 3.3 μm. The probability B(90) is low, on average 5 10^{-4} and close to its limiting value for large phase-lag values of 5.9 10^{-4}. It is affected by absorption and decreases towards shorter wavelengths. The probability B(38) related to the integrating sphere absorption measurement is tenfold larger than the probability B(90).*

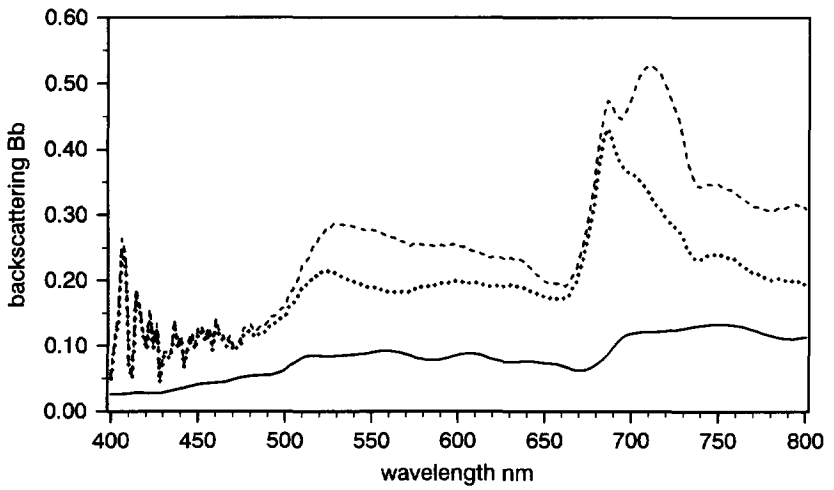

Figure 5.13 *Comparison of estimated backscattering coefficients of Chlorella pyrenoidosa. The estimation method using the backscattering albedo model is compared to the theoretical method to compute B(90)b (solid line). Two different methods were used to correct the apparent absorption for scattering assuming zero inherent absorption at 800 nm: a spectral neutral correction (dotted line) and a wavelength dependent correction using the shape of B(38)b (dashed line). These spectra show roughly the same shape but are threefold higher compared to the theoretical results of B(90)b assuming particles without internal structure.*

agreement with Morel and Bricaud (1981), see Figure 1ab; line 3 for size parameter alpha $\approx 10\rho$ around 20. The limit value of $B(90)$ for large phase-lag values ρ is proportional to the Fresnel factor, for $n=1.05$

$$\left[\frac{n-1}{n+1}\right]^2 = 5.9\ 10^{-5} \qquad \textbf{(5.3)}$$

Estimation of the backscattering coefficient by the methods described in Section 4.6 using the default backscattering probability or the default ratio of $B(38)/B(90)$ would overestimate Bb by a factor of 2.5 or more. The probability $B(90)$ of 5 10^{-4} is factor of 38 smaller, the probability $B(38)$ related to the integrating sphere absorption measurement is tenfold larger than the probability $B(90)$ instead of fourfold. Larger errors can be made using default values (Sections 2.2.5.2 and 4.6.1).

The estimation method using the backscattering albedo model (Section 4.6.4) is compared to the theoretical method that assumes spherical particles of an equivalent uniform size without internal structure to compute $B(90)b$. Two different method were used to correct the apparent absorption for scattering: a spectral neutral correction and a wavelength dependent correction using the shape of $B(38)b$. The inherent absorption at 800 nm was assumed to be zero, the ratio $B(38)/B(90)$ was set to ten. Figure 5.13 shows the resulting backscattering coefficients of *Chlorella pyrenoidosa*. The spectra show roughly the same shape, the theoretical spectrum of $B(90)b$ is threefold smaller. Because the reflectance model was proven to be accurate (Chapter 4) while the theoretical method may lead to large errors (Sections 6.4 and 6.5), probably the best estimate of the backscattering spectrum is obtained using the absorption and reflectance spectra of an optical deep suspension.

5.5.2 Estimation of Backscattering by Ferrite

The inherent optical properties of the ferrite stock suspensions cannot be obtained from the spectrophotometric measurements. The particles approximate opaque bodies with a ratio between beam attenuation and absorption coefficient close to the limiting value of 2 for ordinary diffraction. No light passes through the particle and interference between transmitted and diffracted light does not occur. The absorption and beam attenuation of the ferrite stock suspensions (Figure 5.14) showed no clear spectral characteristics. The suspensions had a red-brown colour indicating that absorption or backscattering or both are wavelength dependent. If opaque particles are present in a mixture they hamper the estimation of backscattering by the theoretical method using van de Hulst and Mie calculations as was

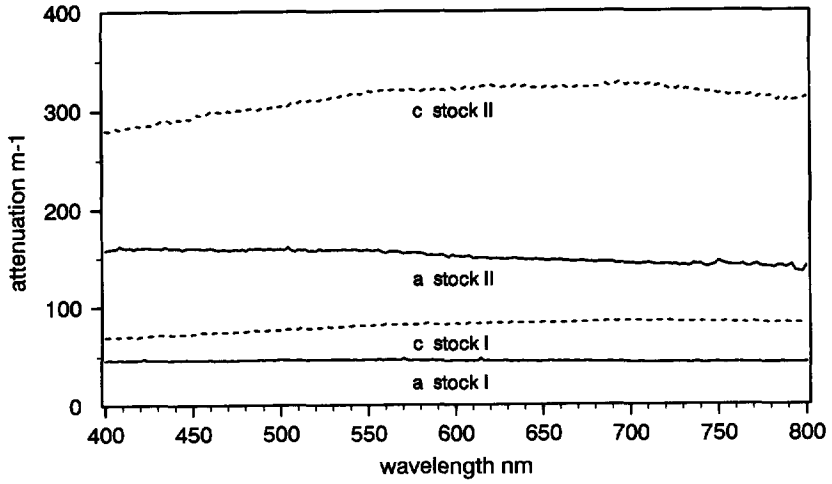

Figure 5.14 *Spectra of absorption (solid lines) and beam attenuation (dashed lines) of the ferrite stock suspensions showed no clear spectral characteristics. The suspensions had a red-brown colour indicating that absorption or backscattering or both depend on wavelength. The particles approximate opaque bodies with a ratio of beam attenuation to absorption close to the limiting value of 2 for ordinary diffraction because no light passes through the particle and interference between transmitted and diffracted light does not occur.*

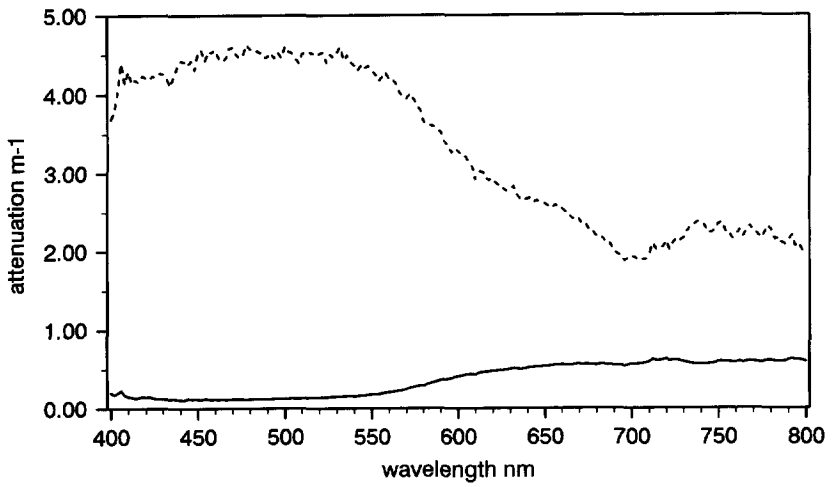

Figure 5.15 *Spectra of inherent absorption and backscattering of ferrite suspension FE38 calculated by iteration with the method of Section 4.6.4. The apparent absorption was corrected for scattering assuming a ratio B(38)/B(90) of four and an initial guess of $a=a_m$.*

applied to the *C. pyrenoidosa* stock. With the method of Section 4.6.4 the spectra of inherent absorption and backscattering shown in Figure 5.15 were calculated by iteration using the spectra of suspension FE38. The apparent absorption was corrected for scattering assuming a ratio $B(38)/B(90)$ of four and an initial guess of $a=a_m$.

A method is given that potentially can be used to derive both the absorption and backscattering spectra of an unknown optical component. The reflectance spectrum of an optical deep suspension is according to the backscattering albedo model proportional to ω_b of the suspension. Because the optical properties of water are known from literature the ratio between a and Bb can be calculated. By increasing the known concentration of ferrite by a known amount (absolutely or relatively) and measuring the reflectance spectrum of this second optical deep suspension a system of two equations with two variables is created that can be solved to give a_x and B_xb_x of the colour component.

$$R_1(0) = 0.5\,\frac{C_1(B_xb_x)+B_wb_w}{C_1(a_x+B_xb_x)+a_w+B_wb_w}$$
$$R_2(0) = 0.5\,\frac{C_2(B_xb_x)+B_wb_w}{C_2(a_x+B_xb_x)+a_w+B_wb_w} \qquad \textbf{(5.4)}$$

The equations can not be solved at wavelengths with invariant reflectance. The solution matrix is ill- conditioned at wavelengths for which the value of the reflectance or its change is of the same order as the experimental noise. Inspection of the reflectance spectra shows that for the analysis only the spectral region 520-680 nm of the *Chlorella* concentration series (Figure 5.3) can be used and the region 600-800 nm for the ferrite concentration series (Figure 5.4).

A solution for mixtures of two (or more) unknown components using the reflectance spectra of four optical deep suspensions is not possible because the determinant of the matrix to solve the equations becomes zero. It is concluded that a general inverse calculation to interpret reflectance spectra with the backscattering albedo model does not exist. An optimization method has to be used to decompose reflectance spectra of mixtures with known (or default) components and determine their concentration.

5.6 Interpretation of Reflectance Spectra

The interpretation of reflectance spectra is not straightforward. The volume scattering function is not usually measured and accurate values for the backscattering coefficient are not available. This coefficient varies tenfold in natural waters. It is sensitive to variations in particle size and in internal structures of cells (Meyer 1979). So the coefficient must be obtained in another way. Perhaps the simplest way to do this is to measure the reflectance spectrum of an optical deep suspension of the sample, because observed spectra can be accurately predicted by a simple analytical reflectance model. So the backscattering probability is the critical parameter in the interpretation of reflectance data and not the reflectance model; the model is better than its input.

A problem that arises in the interpretation of reflectance values in remote sensing is illustrated when the two series of mixtures of algae and ferrite measurements described before are considered together. Figure 5.9 shows the subsurface reflectance spectra measured on the suspensions FC15 and CF2000. The spectra are very similar in the visible part of the spectrum only for wavelengths above 690 nm reflectance of suspension CF2000 is significantly higher. The suspension CF2000 contains a fourfold higher concentration of both the organic and the inorganic fraction. The third colour component, water, is constant and at these wavelengths becomes less important and the increased ratio of the two other colour components becomes detectable.

Spectra measured with high wavelength resolution also show that the use of a small number of preset wavelength bands is hazardous because the response might be invariant to concentration variations of the mixture. Preferably full spectral coverage should be used and additional sea-truth data should be available or default values with a range of concentrations that commonly occur. An optimum solution can be found by an optimization procedure if a library of the colour components is available. The library should contain default absorption and backscattering spectra of the colour components together with boundary conditions for their concentration ranges.

5.7 Conclusions

1. The accuracy of reflectance model calculations is limited because of the low accuracy of the required input of inherent optical properties. The volume scattering function of a mixture or of the colour components is unknown. If estimates of the backscattering probability can

be made, their accuracy will still limit the accuracy of model predictions. The reflectance model itself is less important, so a simple analytical model can be used.

2. The experiments support the backscattering albedo model (Section 5.4).

3. Preferably data with full spectral coverage should be analyzed. In Section 5.5 it was shown how to estimate the backscattering coefficient by an iterative fitting procedure; model calculations were fitted to the measured reflectance values to estimate the unknown backscattering probability for known concentrations of the colour components.

4. If opaque particles are present in a mixture they will hamper the estimation of backscattering from apparent absorption.

References

Bricaud, A., Morel, A., 1986. Light attenuation and scattering by phytoplanktonic cells: a theoretical modeling, Appl. Opt. **25**(4), 571-580.

Das, M., Rabinowitch, E., Szalay, L., Papageorgiou, G., 1967. The "sieve effect" in Chlorella suspensions, J. Phys. Chem. **71**(11), 3543-3549.

Hulst, H.C. van de 1957. *Light scattering by small particles*, Dover Publ., New York, 450 pp.

Latimer, P., 1959. Influence of selective light scattering on measurements of absorption spectra of Chlorella, Plant Physiology **34**, 193-199.

Meyer, R.A., 1979. Light scattering from biological cells: dependence of backscatter radiation on membrane thickness and refractive index, Appl. Opt. **18**(5), 585-588.

Morel, A., Bricaud, A., 1981b. Theoretical results concerning the optics of phytoplankton, with special reference to remote sensing applications, In: *Oceanography from space*, Ed. J.F.R. Gower, Plenum Press, New York, 313-327.

Privoznik, K.G., Daniel, K.J., Incropera, F.P., 1978. Absorption, extinction and phase function measurements for algal suspensions of Chlorella pyrenoidosa, J. Quant. Spectrosc. Radiat. Transfer **20**, 345-352.

Table 5.2 *The dry weight of the organic and inorganic fractions of the concentrations series. Starting with filtered tap water 3.8 litre of ferrite stock I, 7.0 litres of C. pyrenoidosa stock, and 3.0 litre of ferrite stock II were added. The lower case code of the labels xx or xxxx indicate that a total of x.x or x.xxx litre stock suspension was added. Concentrations were calculated from the dry weight of the stock suspensions. Some intermediate concentrations were checked. The total dry weight is given as the sum of the inorganic and organic fractions.*

sample	volume	inorganic		organic		measured
name	ml	mg	mg l^{-1}	mg	mg l^{-1}	mg l^{-1}
FE00	52000	0				
FE02	52275	62	1.2			
FE04	52475	107	2.0			
FE06	52675	152	2.9			
FE08	52275	195	3.7			
FE10	52475	240	4.6			
FE12	52275	283	5.4			
FE14	52475	328	6.3			
FE18	52875	418	7.9			
FE18R	52075	412	7.9			
FE22	52475	502	9.6			
FE26	52875	592	11.2			<10
FE30	52475	673	12.8			
FE34	52875	763	14.4			
FE38	52475	841	16.0			10+2=12
FC00	52000			0		
FC10	52000			249	4.8	
FC15	52000			371	7.1	
FC20	52000			493	9.5	
FC30	52000			733	14.1	
FC40	52000			969	18.6	4+18=22
FC50	52000			1201	23.1	
FC60	52000			1428	27.5	4+20=23
FC70	52000			1650	31.7	
CF0000	52000	238	4.6			
CF0010	52010	244	4.7			
CF0030	52030	255	4.9			
CF0050	52050	266	5.1			
CF0100	52100	295	5.7			
CF0200	52000	350	6.7			
CF0400	52000	461	8.9			
CF0700	52000	628	12.1			
CF1000	52000	794	15.3			
CF1500	52000	1069	20.6			
CF2000	52000	1341	25.8			
CF2500	52000	1611	31.0			
CF3000	52000	1878	36.1			30+28=58

CHAPTER 6
VARIABILITY OF REFLECTANCE BY PHYSICAL CHANGES IN ALGAE

6.1 Introduction

In this chapter the backscattering albedo model will be applied in an extreme case of variability in the inherent optical properties of a suspension caused by physical, but not chemical changes. Four physical effects were studied using suspensions of the cyanobacterium *Microcystis aeruginosa* at a constant level of chlorophyll *a* concentration. The effect of aggregation was investigated by pulverizing colonies to single cells, scattering by the cells was varied by collapsing their gas vacuoles and the effect of the formation of a floating layer on reflectance was measured.

Microcystis aeruginosa appears an ideal object to investigate the physical difficulties in the interpretation of remotely sensed reflectance spectra. Blooms and surface blooms of the cyanobacterium *Microcystis aeruginosa* frequently occur in eutrophic inland waters. It is potentially toxic (Reynolds 1973). The spherical cells of about 4 micron form colonies ranging up to several millimetres. Like most planktonic cyanobacteria the cells contain gas vacuoles that can keep the colonies floating. Several regulation mechanisms play a role in vertical migration of the species. Extensive literature is available on conditions that trigger nuisance blooms (Paerl 1988) and on the role of cell buoyancy on the maximum growth rate (Humphries and Lyne 1988). The cyanobacteria float or sink dependent on physical and physiological conditions. Scums can form quickly under calm weather conditions. At low turbulence a floating layer or surface bloom can be formed. Winddrift causes a horizontal concentration mechanism leading to severe local nuisance problems, e.g. in harbours and at the intake sites of drinking water plants. These phenomena were illustrated by areal photography and satellite images by Donze *et al.*, (1990).

Microcystis and some similar species present one of the most difficult problems in quantitative sampling in plankton biology because the spatial distribution can be extremely inhomogeneous on all scales from single cell to a whole lake. And this distribution can vary within hours. On the smallest scale flow cytometry would be the method of choice to approach this. On a large scale remote sensing would be necessary, but not sufficient since it can not measure concentrations at greater depth. To do this a fast submersible optical

detection system could be used from one or more ships, together with several fixed profiling stations. This chapter is based on some preliminary investigations in this direction.

The accuracy of a reflectance model and its conversion factors to water quality parameters determine how useful remote sensing is in water quality management. In remote sensing the measured reflectance values are usually converted to estimates of water quality parameters in a single statistical step (Gordon and Morel 1983; Bukata *et al.* 1988; Mittenzwey *et al.* 1992; Quibell 1992). These conversion algorithms use a ratio of observed reflectance values, they are simple in use but they become inaccurate when applied to turbid surface water and in situations where more than one colour component must be determined.

Two sources of variability contribute to this inaccuracy. The reflectance of a mixture depends on the optical characteristics of all the dominant colour components (Chapter 5). Since the contributions to reflectance by more than one component interact in a non-linear way, calibration of such a model for one component varies with the concentrations of the other ones. Also variation of the inherent optical properties of a component changes the reflectance at constant concentration of this component. In nature the inherent optical properties of phytoplankton at a constant level of chlorophyll *a* is variable because other pigments vary in concentration and because of physical effects. Physical effects include variation in aggregation state and in scattering properties of cells caused by variation in shape, internal structure and biomass. Variability in absorption spectra of algae at a constant level of chlorophyll *a* (chlorophyll *a* specific absorption spectra) were presented, among others, by Prieur and Satheyendranath (1981), Mitchell and Kiefer (1988), Bricaud *et al.* (1988), and Augustí and Phlips (1992). The two sources of variability cause inaccurate estimates of concentrations because the non-linear behaviour of reflectance, an apparent optical property, is not taken account of in statistical algorithms.

A two step interpretation of reflectance spectra makes the non-linear behaviour of reflectance explicit and it may be expected to yield more accurate results. Progress in this direction was made by Zwick *et al.* (1981), Carder and Steward (1985) and Gallie and Murtha (1992). In Chapter 4 the backscattering albedo model was introduced, it was shown to be better than previous models. In the two step interpretation errors due to non-linearity are largely removed; natural variability as a second source of errors remains.

The physical effects in planktonic algae that induce these errors vary in time and over space. This makes recalibration of the conversion factors necessary on the relevant scales of time and space. Not much is yet known about the quantitative nature of this scaling. If such changes occur within hours the amount of work involved would be cumbersome and the two

step interpretation would no longer add much in accuracy and the statistical approach might be the only practical one.

Three physical effects were investigated on suspensions of *Microcystis aeruginosa* with constant chlorophyll *a* concentration.

1. The effect of size distribution was studied by comparing spectra measured on suspensions of colonies to that of single cells. By disintegration of colonies into single cells an example of the packaging effect (Duysens 1956) is obtained. This effect describes changes in absorption due to the aggregation of pigment as compared to the same amount of pigment dissolved state. In this special two size distributions are compared: single cells and colonies that consist of a hundred to several thousand cells.
2. The effect of a variable volume scattering function is illustrated by changing the internal structure. Scattering was decreased by collapsing the gas vacuoles without affecting pigment content. (Walsby, 1980, Dubelaar *et al.* 1987).
3. The spectral reflectance of a homogeneous suspension is compared to the reflectance after the colonies had formed a floating layer. This illustrates the most extreme case of vertical inhomogeneity.

Measurements of the reflectance spectra on two different concentrations of colonies also confirmed the conclusion from Chapter 5 that these spectra become invariant to concentration in spectral ranges where the ratio of dominant colour components is constant.

6.2 Materials and Methods

Reflectance spectra were measured using the large volume laboratory reflectometer described in Chapter 3. A sample of surface water was taken at Lake Braassemermeer on August 24th, 1990, during a bloom of *Microcystis aeruginosa*. Gas vacuoles were collapsed by application of 7 bar nitrogen gas pressure to the suspension (Dubelaar *et al.* 1987). After collapse the protein walls of the gas vacuoles remain in the cytoplasm while the gas dissolves and disappears from the point of view of optical measurements. A homogeneous stock of single cells was made by suction of a suspension of colonies through an orifice of 0.7 mm diameter. This way colonies disintegrated into single cells by shear force as was checked by microscope.

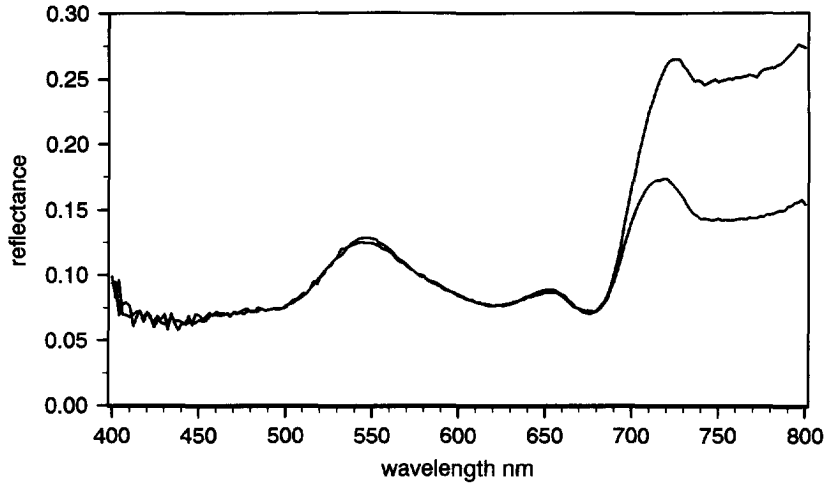

Figure 6.1 *Reflectance spectra of a sample of surface water from Lake Braassemermeer during a bloom of Microcystis aeruginosa (upper curve) and a three-fold dilution of this sample (lower curve). The spectra are indistinguishable in the visible part of the spectrum. The constant reflectance in this wavelength region is consistent with the backscattering albedo model. The algae are the dominant colour component and cause a constant backscattering albedo.*

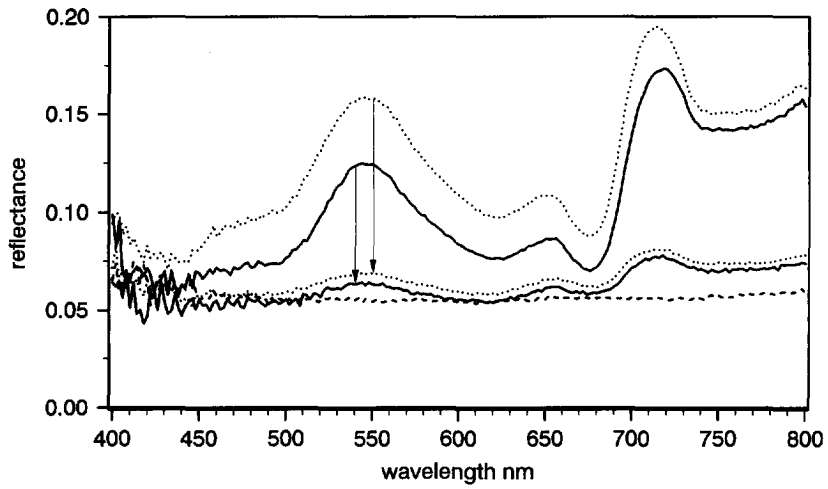

Figure 6.2 *Variability of reflectance spectra of a suspension of Microcystis aeruginosa induced by changing the optical properties but not the concentration of cyanobacteria. Internal structure was changed by collapsing gas vacuoles and aggregation was changed by disintegrating colonies into single cells. At a constant chlorophyll a and biomass contents reflectance is strongly affected by these physical variables. The specular surface reflectance given as a reference was measured on filtered tap water (dashed line). Removal of gas vacuoles strongly decreased reflectance of a suspension of colonies (solid lines) and of a suspension of single cells (dotted lines). Suspensions of single cells showed higher reflectance over the whole spectral range compared to suspensions of colonies.*

Beam attenuation spectra were measured directly and absorption spectra were measured on concentrated samples with a semi-integrating sphere. By the resuspension method of Kirk (1980) and Davies-Colley (1983) tenfold concentrated samples were made.

Particle concentrations were counted with a flow cytometer designed to measure optical properties of particles with sizes of up to 0.5 mm width and 1 mm length (Dubelaar *et al.* 1989a). This range covers most colonial plankton algae.

6.3 Experimental Results

The field sample was diluted threefold and the effects of size distribution and internal structure were measured. Figure 6.1 shows the reflectance spectra measured on the initial concentration of the sample and a three-fold diluted concentration. The spectra were indistinguishable in the visible part of the spectrum where absorption by water is low. The constant reflectance at these wavelength is consistent with the backscattering albedo model of reflectance. The algae are the dominant colour component and this leads to a constant backscattering albedo in the model. At wavelengths longer than 690 nm the absorption of water significantly decreases reflectance and this effect becomes more pronounced at lower concentration of the algae.

Figure 6.2 shows reflectance spectra measured on a suspension *Microcystis aeruginosa* with variable optical properties owing to internal structure and aggregation of cells. At a constant level of the chlorophyll *a* content a wide range of reflectance values is found. The specular reflectance shown as reference was measured on filtered tap water. Collapse of gas vacuoles caused a strong decrease of the reflectance spectrum for both the suspension of colonies and that of single cell. Disintegration of colonies leads to lower reflectance values. The suspension of colonies also contained many single cells; flow cytometric particle counting showed an increase of particle concentration after disintegration by a factor of 20 (Table 6.1).

Figure 6.3 shows that apparent absorption decreases strongly after removal of the gas vacuoles. At 750 nm it was more that fourfold reduced. Because at this wavelength the inherent absorption of algae is zero and the acceptance angle of the integrating sphere is fixed, the change must be due to decrease of the volume scattering function. The beam attenuation (Figure 6.4) increased after collapse of the gas vacuoles. This anomalous behaviour was described by Dubelaar *et al.* (1987) for a culture of *Microcystis aeruginosa*.

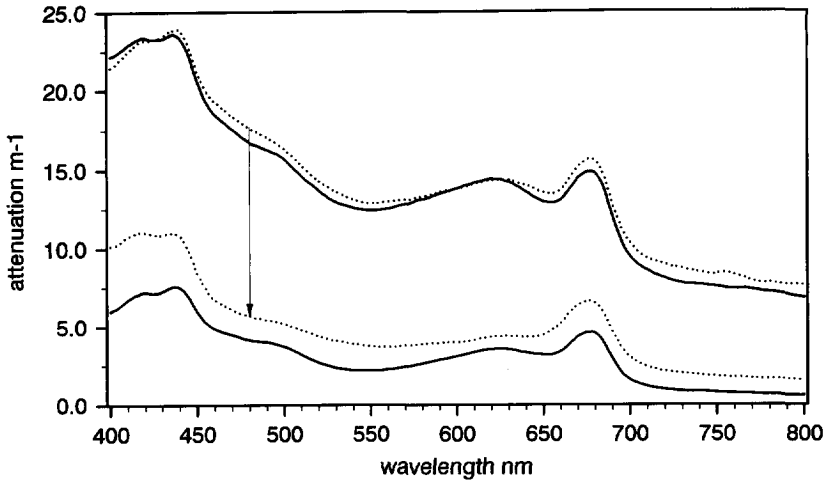

Figure 6.3 *Decrease of apparent absorption after collapse of gas vacuoles for colonies (solid lines) and single cells (dotted lines). Apparent absorption at 750 nm was reduced by more than a factor of 4. Assuming that the ratio between the backscattering probabilities B(38) and B(90) does not change, the backscattering coefficient b_b should proportionally decrease. The decrease of b_b is in agreement with the observed decrease of the reflectance spectra.*

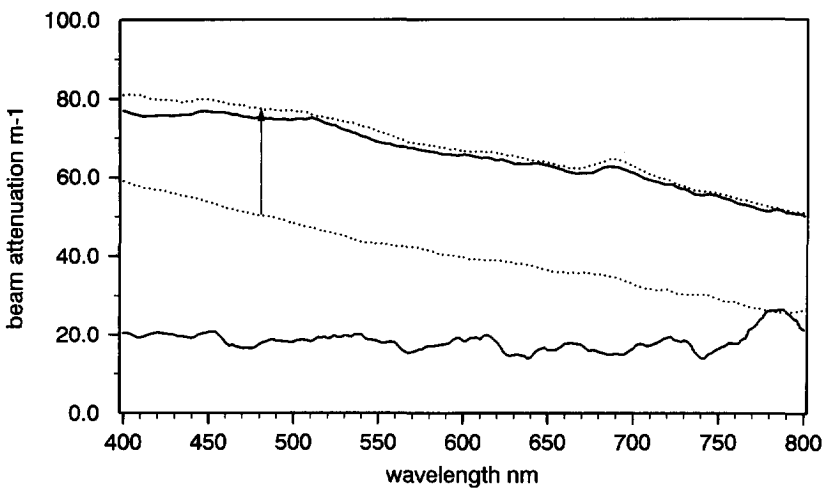

Figure 6.4 *Increase of beam attenuation after collapse of gas vacuoles for colonies (solid lines) and single cells (dotted lines). This anomalous behaviour was described by Dubelaar et al. (1987) for a culture of Microcystis aeruginosa.*

Table 6.1 *Particle concentration measured using the Optical Plankton Analyzer flow cytometer.*

Lake Braassemermeer, sample August 24, 1990 suspension	particle concentration ml^{-1}
colonies	$1.7\ 10^5$
colonies, collapsed gas vacuoles	$2.0\ 10^5$
single cells	$3.8\ 10^6$
single cells, collapsed gas vacuoles	$3.3\ 10^6$

The measured spectra of suspensions of single cells could be accurately modelled using the approximative formulas of van de Hulst. The same method was applied to *Chlorella pyrenoidosa* in Section 5.5. Good results were obtained for particles of 4.5 μm diameter at a concentration of $3.1\ 10^6$ ml^{-1} with a refractive index in the absence of absorption of 1.37 for the suspension with collapsed gas vacuoles and of 1.36 for the suspension with intact gas vacuoles. The refractive index was lowered by the presence of gas vacuoles, the phase-lag factor decreases at 800 nm from 1.5 to 1.0 by their presence. This leads to a decrease of the efficiency factor for extinction Q_c. So the presence of gas vacuoles increases backscattering and, in apparent contrast, decreases beam attenuation.

6.4 Calculation of the Backscattering Coefficient b_b

Validation of backscattering albedo model is hampered by lack of accurate knowledge of the backscattering coefficient or, more specifically, of the complete volume scattering function. Cells with intact gas vacuoles would require a Mie calculation algorithm accounting for the unknown internal structure. If the volume scattering function is computed by the Mie calculation algorithm for homogeneous spherical particles the backscattering probability can not be expected to give valid results. Estimation of $B(90)$ using Figure 1[a] of Morel and Bricaud (1981) with size parameter x between 43-68 and relative refractive indices of 1.02 and 1.03 for intact and collapsed gas vacuoles respectively, gave a lower estimate of $B(90)$ for the cells with intact gas vacuoles, in contrast with the observed apparent absorption and reflectance spectra. Apparently no progress can be expected in this direction.

6.5 Use of Reflectance Spectra to Estimate b_b

Instead of Mie computations measured spectra can be used to obtain the backscattering coefficient b_b, see also Chapter 5. If we assume that the reflectance model is valid, the observed spectral reflectance is an indirect measure of b_b. Model calculations using the spectra of absorption and beam attenuation should yield predictions close to the observed reflectance values. If the inherent absorption is known the backscattering coefficient can be calculated by solving the model equation. In practical applications the measured apparent absorption has to be corrected for scattering to obtain the inherent absorption. An estimate of the backscattering probability can be obtained by an trial and error method comparing model predictions to the observed reflectance. Model predictions were calculated using the measured spectra of absorption of the particulate matter and aquatic humus and beam attenuation. The procedure to estimate the backscattering coefficient consist of five steps. This procedure can be used if a wavelength exist where particulate matter does not absorb light.

Assume that particulate matter does not absorb light at 800 nm. The first approximation consists in:

1) Calculate $b=c-a_h-a_p-a_p(800)$.
2) Estimate $B(90)$ and calculate $B(90)b$; use a probability based on an assumed volume scattering function or a backscattering probability measured on a comparable particle.
3) Calculate $B(38)$ from the apparent absorption by $a_p(800)/B(90)b$.
4) Calculate the reflectance spectrum using $ap=a_p-B(38)b$ and $b_b=B(90)b$.
5) For a second approximation: compare predicted and observed spectra and return to step 1 or 2.

After a number of iterations a good fit resulted for the suspension of single cells with intact gas vacuoles with the values $B(90)=0.05$ and $B(38)=0.29$ and a ratio of 5.8. Values of $B(90)=0.003$ and $B(38)=0.03$ (ratio 10) yielded a reasonable approximation of the observed reflectance spectrum for the suspension of single cells with collapsed gas vacuoles as show in Figure 6.5. Using the spectral shape of the backscattering probability of *Chlorella pyrenoidosa* with 3.3 μm diameter to estimate the backscattering coefficient of *Microcystis aeruginosa* resulted in an improved fit.

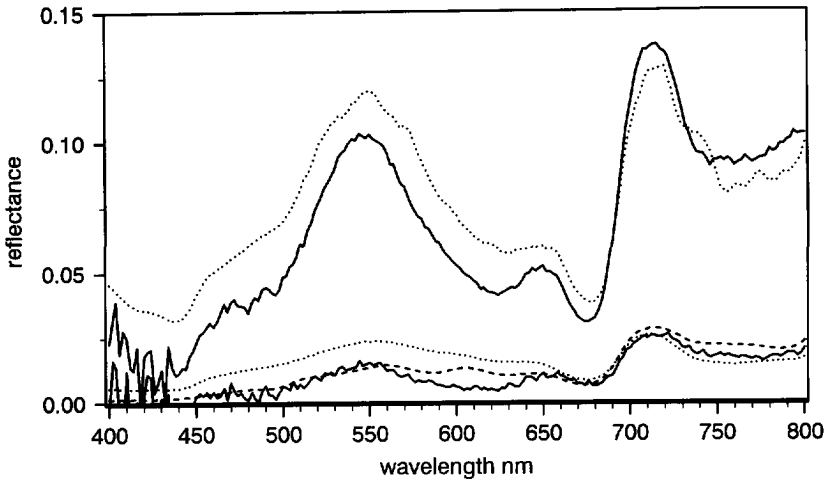

Figure 6.5 *Modelled (dotted lines) and observed (solid lines) reflectance spectra of suspensions of single cells. Mie calculations assuming that particles have no internal structure give good results for the suspension with collapsed gas vacuoles (lower curve). Use of the computed backscattering probability of Chlorella pyrenoidosa with 3.3 μm diameter to estimate the spectral shape resulted in an improved fit (dashed line).*

6.6 Floating Layers of *Microcystis aeruginosa*

Formation of a floating layer of algae at the water surface is an extreme of vertical stratification. The presence of floating layers is most easily detected by optical remote sensing by their very high reflectance in the near-infrared. Among others observations have been reported with Landsat imagery (Galat and Verdin 1989) and with the daily images of NOAA (Prangsma and Roozekrans 1989). Quantification of the amount of algae in a scum has not yet been attempted. To find relations between biomass and spectral reflectance a preliminary experiment was carried out. Reflectance spectra of a concentration series of homogeneous suspensions and of the same suspensions after floating up of the algae were measured.

A field sample of *Microcystis aeruginosa* was taken from the river Andelse Meuse September 1, 1988 with a 30 μm net. A concentration series was prepared by repeated twofold dilution of the stock suspension of 11,400 mg Chl-a m^{-3} (Table 6.2). Suspensions were stirred, split into two equal parts and diluted with tap water. One part was allowed to form a floating layer and the other part was used for further dilution after measuring its reflectance spectrum. The reflectance spectra of suspensions are given in Figure 6.6. In the visible part of the spectrum reflectance values were almost identical except for the lowest concentration

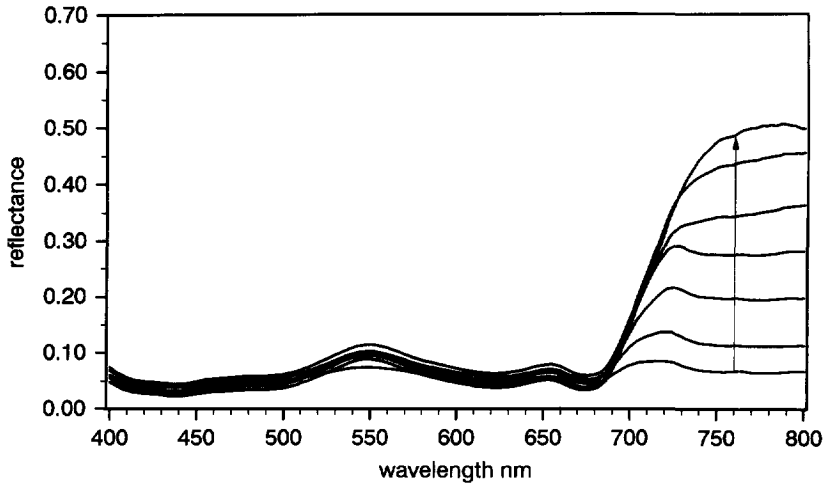

Figure 6.6 *Reflectance spectra of a concentration series of suspensions. In the visible part of the spectrum reflectance is almost independent of concentration. Only the lowest concentration of the series deviates; it was not optical deep and a contribution of the bottom of the tank is included in the spectrum (see 550 nm). In the near-infrared reflectance increased with concentration and the shape of the spectrum changed. At concentrations larger than 1,450 mg Chl-a m^3 the decreasing effect of water absorption on reflectance vanishes.*

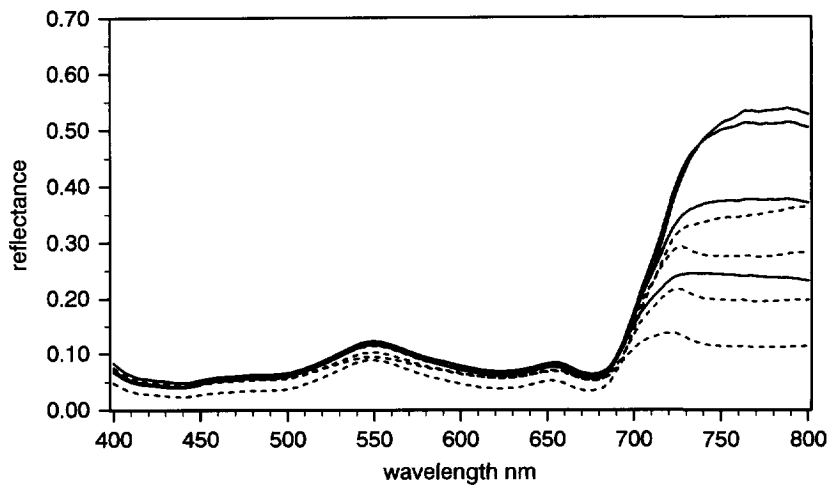

Figure 6.7 *Reflectance spectra of floating layers (solid lines) and their corresponding suspensions (dashed lines). The subtle difference in the near-infrared of the spectra of a suspension and of a floating layer formed from a four fold lower concentration can only be detected using high wavelength resolution spectra, compare floating layer no. 5 to suspension no. 3 and no. 6 to no. 4.*

of the series, this was optical shallow and reflection by the bottom of the tank is included in the spectrum. In the near-infrared reflectance increased with concentration and the shape of the spectrum changed. With increasing concentration the spectra show invariant reflectance for increasing wavelengths. At concentrations higher than 1,450 mg Chl-a m^{-3} the lowering of reflection by the absorption of water on reflectance becomes negligible. Figure 6.7 shows the spectra of floating layers and of the corresponding suspensions. It appears difficult to distinguish a floating layer from a suspension with a fourfold higher concentration. The small difference in the near-infrared of spectra in this case can only be detected using spectra with high wavelength resolution.

Table 6.2 *Dilution series of a field sample of Microcystis aeruginosa taken from the river Andelse Meuse on September 1, 1988 to measure the spectral reflectance of suspensions and floating layers. Chlorophyll a concentrations between brackets were calculated. Suspensions with a total depth of 0.17 m were checked to be optical deep for a depth of 0.10 m. Assuming that algae in the upper 3 m layer of surface water contribute to the formation of a floating layer the corresponding natural concentration of the suspension can be calculated by multiplication with a factor of 0.057; floating layer no. 4 would be formed at a concentration of 83 mg Chl-a m^{-3}.*

sample no.	concen-tration	Chlorophyll *a* mg m^{-3}	optical deep suspension	floating layer
1	1	11,400	yes	-
2	1/2	5,800	yes	-
3	1/4	(2,900)	yes	full coverage
4	1/8	(1,450)	yes	full coverage
5	1/16	(725)	almost	full coverage
6	1/32	(363)	partly	large patches
7	1/64	(181)	no	small patches

6.7 Discussion

Application of remote sensing to the quantification of floating layers of algae will solve some, but by no means all problems. In thick layers reflectance will soon saturate and become independent of further growth in thickness, when in dense suspensions water absorption becomes undetectable these can not be distinguished from scums. Also patchiness below pixel size will remain a problem in quantifying floating algae.

Variability of inherent optical properties changes the reflectance at a constant level of colour components and thus at a constant level of the water quality parameters. This natural variability induces inaccuracy in the interpretation of reflectance data. Usually this error will be smaller than observed in the extreme cases that were studied here. For accurate data interpretation a field measuring program is required to calibrate the remotely sensed reflectance. An alternative method is the use of a library containing historical data to derive default estimates of the optical properties of the colour components and their variability.

Assuming the chosen reflectance model to be valid, the observed reflectance spectrum is an indirect measure of the spectrum of b_b. The proposed method to estimate b_b can be used to build a library of backscattering probabilities for the colour components of surface water. Measurements with a large volume laboratory reflectometer yield complete spectra of b_b. The accuracy in the interpretation of reflectance data will improve by including measurements of the variable backscattering coefficient in a sea-truth program.

The method proposed in Chapter 5 to estimate b_b can be used to build a library of backscattering probabilities for the colour components of surface water. The use of a large volume laboratory reflectometer requires less sample and less sensitive instrumentation compared to volume scattering function meters. Full spectral coverage is obtained at the cost of details on the angular distribution. Interpretation of reflectance data will gain accuracy if more accurate defaults are available for the colour components of water, or if the backscattering coefficient is included in the calibration (sea-truth) data.

References

Augustí, S. and E.J. Phlips, 1992. Light absorption by cyanobacteria: implications of colonial growth form, Limnol. Oceanogr. **37**(2), 434-441.

Bricaud, A., A. Bédhomme and A. Morel, 1988. Optical properties of diverse phytoplanktonic species: experimental results and theoretical interpretation, J. Plankton Res. **10**(5), 851-873.

Bukata, R.P., J.H. Jerome and J.E. Bruton, 1988. Particle concentrations in Lake St. Clair as recorded by a shipborne multispectral optical monitoring system, Remote Sens. Environ. **25**, 201-229.

Carder, K.L., and R.G. Steward, 1985. A remote-sensing reflectance model of a red-tide dinoflagellate off west Florida, Limnol. Oceanogr. **30**(2), 286-298.

Davies-Colley, R.J., 1983. Optical properties and reflectance spectra of 3 shallow lakes obtained from a spectrophotometric study, New Zealand J. Marine Freshwater Res. **17**, 445-459.

Donze, M., C. Nieuwendijk, A. van Boxtel and M. Quaak, 1990. *Aquatic pollution and dredging in the European Community*. Delwel, The Hague, 184 pp.

Dubelaar, G.B.J., J.W.M. Visser and M. Donze, 1987. Anomalous behaviour of forward and perpendicular light scattering of a cyanobacterium owing to intracellular gas vacuoles, Cytometry **8**, 405-412.

Dubelaar, G.B.J., A.C. Groenewegen, W. Stokdijk, G. van den Eng and J.W.M. Visser, 1989a. The optical plankton analyser (OPA): a flow cytometer for plankton analysis. II: Specifications, Cytometry **89**, 529-539.

Duysens, L.N.M., 1956. The flattening of the absorption spectrum of suspension, as compared to that of solutions, Biochim. Biophys. Acta **19**, 1-12.

Galat, D.L., and J.P. Verdin, 1989. Patchiness, collapse and succession of a cyanobacterial bloom evaluated by synoptic sampling and remote sensing, J. Plankton Res. **11**(5), 925-948.

Gallie, E.A., and P.A. Murtha, 1992. Specific absorption and backscattering spectra for suspended minerals and chlorophyll-a in Chilko Lake, British Columbia, Remote Sens. Environ. **39**, 103-118.

Gordon, H.R., and A.Y. Morel, 1983. *Remote assessment of ocean reweighs for interpretation of satellite visible imagery*, a review, Springer-Verlag, New York, 114.

Humphries, S.E., and V.D. Lyne, 1988. Cyanophyte blooms: The role of cell buoyancy, Limnol. Oceanogr. **33**(1), 79-91.

Kirk, J.T.O., 1980. Spectral absorption of natural waters: contribution of the soluble and particulate fractions to light absorption in some inland waters of South-Eastern Australia, Aust. J. Mar. Freshwater Res. **31**, 287-296.

Mitchell, B.G., and D.A. Kiefer, 1988. Variability in pigment specific particulate fluorescence and absorption spectra in the northeastern Pacific Ocean, Deep-Sea Res. **35**(5), 665-689.

Mittenzwey, K.H., S. Ullrich, A.A. Gitelson and K.Y. Kondratiev, 1992. Determination of chlorophyll *a* of inland waters on the basis of spectral reflectance, Limnol. Oceanogr. **37**(1), 147-149.

Morel, A., and A. Bricaud, 1981. Theoretical results concerning the optics of phytoplankton, with special reference to remote sensing applications, In: *Oceanography from space*, Ed. J.F.R. Gower Plenum Press, New York, 313-327.

Paerl, H.W., 1988. Nuisance phytoplankton blooms in coastal, estuarine, and inland waters, Limnol. Oceanogr. **33**(4), 823-847.

Prangsma, G.J., and J.N. Roozekrans, 1989. Using NOAA RHUS imagery in assessing water quality parameters, Int. J. Remote Sensing **10**, 811-818.

Prieur, L., and S. Sathyendranath, 1981. An optical classification of coastal and oceanic waters based on the specific spectral absorption curves of phytoplankton pigments, dissolved organic matter, and other particulate materials, Limnol. Oceanogr. **26**(4), 671-689.

Quibell, G., 1992. Estimating chlorophyll concentrations using upwelling radiance from different freshwater algal genera, Int. J. Remote Sensing, **13**(14), 2611-2621.

Reynolds, C.S., 1973. Growth and buoyancy of *Microcystis aeruginosa* in a shallow eutrophic lake, Proc. R. Soc. Lond. B. **184**, 29-50.

Walsby, A.E., 1980. The water relations of gas-vacuolate prokaryotes, Proc. R. Soc. Lond. B. **208**, 73-102.

Zwick, H.H., S.C. Jain and J.R. Miller, 1981. Modelling aspects of water quality estimation, In: *Oceanography from space*, Ed. J.F.R. Gower, Plenum Press, New York, 355-363.

CHAPTER 7
TARGET FACTOR ANALYSIS

7.1 Introduction

In this chapter a mathematical outline of the target factor analysis method is given. The theory of target factor analysis is shortly reviewed with emphasis on techniques that in our opinion are most useful in aquatic optics. In Chapter 8 the method is applied to improve on the default absorption spectrum of aquatic humus.

Target factor analysis (Malinowski and Howery 1980) is a method to handle spectral data of mixtures of components. The method is based on the method of Lawton and Sylvestre (1971) to decompose the spectra of a mixture of two components without *a priori* knowledge of the component spectra and of the concentrations. One application of target factor analysis is to analyze time resolved spectral data in high performance liquid chromatography (Vandeginste *et al.* 1985; Strasters 1989). It uses linear algebra techniques to study large data matrices. Results from of a number of experiments are analyzed for the existence of linear dependencies without the need for assumptions concerning the presence of specific compounds. Such assumptions are introduced later in the analysis.

The method consists of two steps. The first step called abstract factor analysis is also known as principal component analysis or empirical orthogonal function analysis. Variability in spectral shape is supposed to be caused by varying linear contributions of constituent components. This assumption is met if the components behave conform Lambert-Beer's law. The data can be reproduced at various levels of allowable residual errors, or variance not explained. When the data can be reproduced within experimental error using a small number of abstract vectors with corresponding vector scores, substantial data reduction is achieved. At the same time noise is removed because the data is reproduced without the vectors that contain only noise. So data reproduction by abstract factor analysis results in reduction of noise and in reduction of the amount of data.

In the second step the matrix of abstract vectors is rotated to real components. This way a reduced set of components best fitting the data is extracted from a set of components hypothetically present. It is possible to test for the presence of a single component with known spectrum in the mixtures. It is tested whether a candidate component or target is present in the data. A target can be tested without the need to know the other components present in the data set. If the component spectra are unknown an iterative procedure of target

testing (Vandeginste *et al.* 1985) can be applied to find suggestions for the spectra of possible components by imposing restrictions on the spectral shapes or on the concentrations. In target testing the linear combination of abstract vectors best fitting the target spectrum is calculated and compared with the target. If the target is present in the data the residuals between the target and the best fitting component are zero or minimal; the target is compared with its projection onto the reduced data space.

The data reproduction using rotated abstract vectors is identical to that using the same number of abstract vectors. With target factor analysis maximum reduction of noise is achieved for the number of components used. Candidate components are modified to their projections to achieve this. If in data reproduction it is desired to use the candidate components without modification, they can be fitted to the measured data or to the data after reduction of noise. Residual errors increase if the targets are not exact linear combination of the abstract vectors.

In target factor analysis part of the experimental error is removed before the least sum of squares fit procedure by analyzing the data using only significant abstract components. For mixtures of components that show a natural variability factor analysis can be used find the actual shape of the spectrum of the component present. A presumed shape of the default spectrum can be relaxed to its modified shape using the spectrum of its projection in the data space. The effect of a target factor analysis is that not all natural variability of the components is incorporated in the concentration estimates. Target factor analysis has three main advantages compared to multivariate analysis of mixtures of linear contribution components:

1. Part of the experimental error is removed from the data by decomposition of the data and using only significant component spectra, at the same time data reduction is obtained.
2. Candidate component spectra can be individually tested to be present in the data. The presence of target components can be judged independent of the other components of a complete set of real components.
3. Default component spectra can be used as initial targets and modified by projection or iteration to closely resembling spectra of the actual components present in the mixture.

7.2 Target Factor Analysis

The method uses the result of an abstract analysis of spectral data. The original data matrix [*D*] of *ns* mixture spectra measured over *nw* wavelengths can be written as a product of the

spectral characteristics of the *nc* components and their linear contributions to the mixture spectra.

ns	number of spectra
nw	number of wavelengths
nc	number of components $\leq n$
n	dimension of the data space, $nc \leq n \leq$ minimum of *ns* and *nw*

[*D*]	*nw*×*ns*	data matrix
[*Conc*]	*n*×*ns*	concentration matrix
[*S*]	*nw*×*n*	component spectra matrix

$$[D]=[S][Conc] \tag{7.1}$$

Before analysis the data can be normalized or log-transformed to reduce differences in variance. Pretreatment of a single type of spectral data is not needed because all values are in the same units and differences in variance are significant.

7.2.1 Principal Component Analysis

Calculate principal components from the covariance matrix about the origin

[*COV*]	*ns*×*ns* or *nw*×*nw*	covariance matrix

$$[COV]=[D]^T[D] \text{ or } [D][D]^T \tag{7.2}$$

The eigenvectors and eigenvalues that emerge from the factor analysis are exactly the same if the covariance matrix is calculated of the data matrix or of its transpose (Malinowski and Howery 1980).

Make an abstract decomposition of the matrix using principal component analysis

[*R*]	*n*×*ns*	row matrix
[*C*]	*nw*×*n*	column matrix

$$[D]=[C][R] \tag{7.3}$$

The matrix [*C*] contains the principal components or eigenvectors derived from the covariance matrix.

7.2.2 Number of Significant Components

Determine the optimum number, *nc*, of significant component spectra: the dimension of the data space. Use the minimum number of components to describe the data sufficiently accurate, that is, within experimental error. In Section 7.3 theory of errors in given to determine the number of *nc* components.

$[D_{red}]$	$nw \times ns$	reproduced data matrix
$[R_{red}]$	$nc \times ns$	reduced row matrix
$[C_{red}]$	$nw \times nc$	reduced column matrix

$$[D] \approx [D_{red}] = [C_{red}][R_{red}] \tag{7.4}$$

7.2.3 Transformation to Target Spectra

The reduced number of abstract vectors may be transformed to real component spectra. Transformations include orthogonal and oblique rotations and scaling.

$[T]$	$nc \times nc$	transformation matrix
$[S]$	$nw \times nc$	matrix of real or actual spectra
$[CON]$	$nc \times ns$	contribution matrix, sometimes concentration matrix

$$[D_{red}] = [C_{red}][T][T]^{-1}[R_{red}]$$
$$[D_{red}] = [S][CON] \tag{7.5}$$

Factor analysis is a general name for different methods to derive a transformation matrix, either $[T]$ or $[T]^{-1}$, depending on the available information on the system or by imposing a number of boundary conditions.

7.2.4 Target Testing

Target factor analysis allows individual examination of spectral characteristics of candidate spectra. Every candidate spectrum is approximated in a least squares sense by means of the

columns of $[C_{red}]$, i.e. a target spectrum $[S_{targ\ (i)}]$ is projected onto the data space defined by $[C_{red}]$ and is compared with its projection $[S_{pro\ (i)}]$.

The projection can be found by a transformation of the eigenvectors.

$[S_{pro}]$ $nw \times nc$ projection spectra matrix

$[S_{targ}]$ $nw \times nc$ target spectra matrix

$$[S_{pro}] = [C_{red}][T] \tag{7.6}$$

$$[T] = [C_{red}]^{-1}[S_{pro}] = [C_{red}]^{T}[S_{pro}] \tag{7.7}$$

If the target spectrum is within the data space, the spectrum closely resembles its projection.

$$[S_{pro}] \approx [S_{targ}] \tag{7.8}$$

By minimizing the differences of

$$[C_{red}][T] = [S_{targ}] \tag{7.9}$$

in a least sum of squares sense an optimum transformation matrix results.

$$[T] = ([C_{red}]^{T}[C_{red}])^{-1}[C_{red}]^{T}\ [S_{targ}] \tag{7.10}$$

$$[S_{pro}] = [C_{red}]\ ([C_{red}]^{T}[C_{red}])^{-1}[C_{red}]^{T}\ [S_{targ}] \tag{7.11}$$

The transformation of the significant abstract component spectra to the projection of an individual target spectrum gives one of the columns of the transformation matrix $[T]$.

$$[S_{pro(i)}] = [C_{red}][T_{(i)}] \tag{7.12}$$

$$[S_{pro(i)}] = [C_{red}]\ ([C_{red}]^{T}[C_{red}])^{-1}[C_{red}]\ [S_{targ(i)}] \tag{7.13}$$

$$[T_{(i)}] = [C_{red}]^{T}[S_{pro(i)}] \tag{7.14}$$

7.2.5 Choosing a Valid Set of Target Spectra

Once all candidate spectra from a library are tested, a set of *nc* component spectra must be chosen that spans the data space completely. Verify that the data reproduction is equally good for the set of target spectra as for the abstract spectra:

$$[D] \approx [D_{targ}] = [S_{targ}][T]^{-1}[R_{red}] \tag{7.15}$$

$$[D] \approx [D_{red}] = [C_{red}][R_{red}] \tag{7.16}$$

If the matrix $[D_{targ}]$ matches the original data matrix $[D]$ within experimental error, a valid set of real components has been found.

7.3 Theory of Experimental Error

Theory of experimental error is given on which the determination of the number of significant components and the extraction of experimental error are based. Experimental error or real error, *RE*, can be separated in a part that is extractable from the data, *XE*, and a part that is imbedded in the data, *IE*. The relation between these errors and how they are calculated from the data is the subject of this section.

Malinowski (1977) showed that these three errors were related by the expression

$$RE^2 = XE^2 + IE^2 \tag{7.17}$$

and that the real error is equal to residual standard deviation, $RE=RSD$, and the extracted error is equal to root mean square error, $XE=RMS$, for data reproduced with the right number of significant components. The residual standard error *RSD* measures the difference between the raw data and the data without experimental error. The root mean square error *RMS* measures the difference between the raw data and the data reproduced.

The sum of squares of the values of the raw data matrix is equal to the trace of its covariance matrix and is equal to the sum of the eigenvalues of this factor analyzed covariance matrix. The eigenvalues as well as the eigenvectors are separated in two parts: a primary part

containing the first *nc* eigenvalues related to the significant components and a secondary part related to noise vectors. The errors depend on these secondary eigenvalues λ_{sec}:

$$RE^2 = \frac{1}{nw(ns-nc)} \sum_{i=ns-nc}^{ns} \lambda_{(i)} \tag{7.18}$$

$$XE^2 = \frac{1}{nw\,ns} \sum_{i=ns-nc}^{ns} \lambda_{(i)} = \frac{(ns-nc)}{ns} RE^2 \tag{7.19}$$

$$IE^2 = \frac{nc}{ns\,nw(ns-nc)} \sum_{i=ns-nc}^{ns} \lambda_{(i)} = \frac{nc}{ns} RE^2 \tag{7.20}$$

by rewriting the equations for *XE* and *IE* to *RE* it is seen that the Equation 7.17 holds.

Assuming that the data without experimental error is known the three errors can be calculated and the number of spectra is less than the number of wavelengths, $ns < nw$. The root mean square error *RMS*, calculated from the observed data and reproduced data, is equal to the extracted error *XE*.

$$RMS^2 = \frac{1}{nw\,ns} \sum_{iw=1}^{nw} \sum_{is=1}^{ns} (D_{(iw,is)} - D_{red\,(iw,is)})^2 \tag{7.21}$$

For the right number of significant components the sum of squared residuals is equal to the sum of the difference of squared values because the residuals are random noise.

$$RMS^2 = \frac{1}{nw\,ns} \sum_{iw=1}^{nw} \sum_{is=1}^{ns} (D^2_{(iw,is)} - D^2_{red\,(iw,is)}) \tag{7.22}$$

The sum of squares of the values of the raw data matrix is equal to the trace of its covariance matrix and equal to the sum of the eigenvalues of this covariance matrix. The eigenvalues and the eigenvectors are separated in two parts, a primary part containing the first *nc* eigenvalues related to the significant components and a secondary part related to noise vectors.

$$RMS^2 = \frac{1}{nw\,ns}\left(\sum_{i=1}^{ns}\lambda_{(i)} - \sum_{i=1}^{nc}\lambda_{red\,(i)}\right) \qquad (7.23)$$

The sum of the residuals between the squares of the raw data and the reproduced data equals the sum of the secondary eigenvalues.

$$RMS^2 = \frac{1}{nw\,ns}\sum_{i=ns-nc}^{ns}\lambda_{(i)} = XE^2 \qquad (7.24)$$

A similar expression was derived for the *RSD*:

$$RSD^2 = \frac{1}{nw(ns-nc)}\sum_{i=ns-nc}^{ns}\lambda_{(i)} = RE^2 \qquad (7.25)$$

Once these two errors are known the imbedded error *IE* can be calculated.

So the three types of error can be calculated using the eigenvalues of the eigenvectors. The error variables *RE*, *XE* and *IE* can be used to judge the accuracy of data reproduction and to find the right number of components present in the data by constructing a table of error variables for an increasing number of supposed significant components. The right number of significant components *nc* is derived by comparing the error variables to the known or estimated experimental error.

7.4 Comparison of Component Analysis Methods

Target factor analysis is compared to multiple component analysis. Both methods can be used to fit experimental data to a model with components that contribute linearly to the signal measured. A brief indication of the use of some other techniques is given.

7.4.1 Multiple Component Analysis

The data can be forced to fit a presumed model by a least sum of square procedure. A problem is that systematic errors are implicitly introduced if the component spectra differ

from the actual components. Multiple component analysis gives the least sum of squares solution to the equation:

$$[D] = [S][CON] \tag{7.26}$$

For a set of *nc* candidate spectra the contributions are calculated by

$$[CON] = ([S]^T[S])^{-1}[S]^T [D] \tag{7.27}$$

If a library of candidate spectra contains more spectra than those present in the data, the component spectra present in the data must be selected. To do this the root mean square error (Equation 7.21) is used to quantify the average residual between the data and the data reproduced by the model.

7.4.2 Target Factor Analysis

With target factor analysis Equation 7.15 is solved

$$\begin{aligned} [D] \approx [D_{targ}] &= [S_{targ}][T]^{-1}[R_{red}] \\ [D] &= [S_{targ}][CON] \end{aligned} \tag{7.28}$$

The least sum of squares solution is given by

$$[CON] = ([S_{targ}]^T[S_{targ}])^{-1}[S_{targ}]^T [D] \tag{7.29}$$

The extracted error *XE* calculated using the secondary eigenvalues by Equation 7.24 was shown to be equal to the *RMS* for data reproduced within experimental error.

Targets are modified to their projection in the reduced data space if they do not completely span the data space of the reduced data matrix.

$$[D] \approx [D_{red}] = [C_{red}][R_{red}] \tag{7.30}$$

After transformation

$$[D_{red}] = [C_{red}][T][T]^{-1}[R_{red}] \tag{7.31}$$

$$[D_{red}] = [S_{pro}][CON_{pro}] \tag{7.32}$$

targets are modified to their projections by Equation 7.11 leading to a contribution matrix of

$$[CON_{pro}] = [S_{pro}]^{-1}[D_{red}] \tag{7.33}$$

or by comparison of the Equations 7.31 and 7.32 to its equivalent form:

$$[CON_{pro}] = [T]^{-1}[R_{red}] \tag{7.34}$$

These modified targets are linear combinations of the abstract vectors. So data reproduced using modified targets is equivalent to data reproduction using abstract vectors. The residuals before ($[D]$-$[D_{red}]$) and after the transformation ($[D]$-$[C_{red}][T]$ $[T]^{-1}[R_{red}]$) are equal.

7.4.3 Other Methods

Several methods were presented in the literature to derive solutions for the decomposition problem for unknown components. The self modelling curve resolution of Lawton and Sylvestre (1971) is a two component method. The iterative target transformation factor analysis of Vandeginste *et al.* (1985) is a multi-component method. These two methods do not require presumed component spectra. The problem is solved by imposing a number of restrictions on valid solutions, e.g. spectral values and concentration values are non-negative. The iterative scheme of target transformation is used to derive a valid solution; per spectrum a set of candidate spectra is iterated to a valid spectrum. The projection of the target is calculated and compared to the restrictions. If the target is not a valid spectrum, the projection is, after some modification according to the imposed restrictions, used as an improved target. The solution is tested to span the data space, that is no iterations occurred that produced linear combinations of the other valid spectra.

The iterative procedure of Vandeginste *et al.* (1985) generates initial target spectra from the eigenvectors to start an iterative procedure of target testing. After an orthogonal Varimax

rotation the spectra form a set of projection spectra that are modified in an attempt to find a valid solution given the restrictions for actual components.

If pure component spectra are supposed to be present in the observed mixture spectra, a set of basic spectra can be constructed from the observed spectra that spans the data space. This involves the testing of a large number of sets of *nc* measured spectra to span the data space within experimental error.

The method to analyze a data set of spectra of mixtures will depend on available knowledge of the system. If we know the actual components in the mixture there is no need to use target factor analysis. Or, in other words, except for reduction in noise, its results would not be better than those of multivariate analysis. But if the number or the shape of the actual components are not accurately known, target factor analysis will prove to be an useful tool.

References

Lawton, W.H., and E.A. Sylvestre, 1971. Self modeling curve resolution, Technometrics **13**, 617-633.

Malinowski, E.R., 1977. Anal. Chem. **49**, 606 and 617.

Malinowski, E.R., and D.G. Howery, 1980. *Factor analysis in chemistry*, Wiley, New York, 251.

Strasters, J.K., 1989. *Multivariate analysis of UV-spectral data for solute tracking in HPLC*, Thesis, Delft Univ. Press, 144.

Vandeginste, B.G.M., W. Derks and G. Kateman, 1985. Multicomponent self-modelling curve resolution in high-performance liquid chromatography by iterative target transformation analysis, Anal. Chim. Acta **173**, 253-264.

CHAPTER 8
DEFAULT ABSORPTION SPECTRUM OF AQUATIC HUMUS

8.1 Introduction

In this chapter we show how to improve on default values available for the absorption spectrum of aquatic humus and we analyze remaining errors. A method is sketched by which the accuracy gained by carrying out a field measuring program to support a remote sensing investigation can be estimated.

In passive remote sensing of surface water using visible light the aim is to derive concentrations of aquatic humus, algae and silt from spectral reflectance measurements. Usually algorithms to do this are postulated on a common sense basis and calibrated by a statistical technique with a small number of chemical and optical measurements on water samples. The synoptic nature of pictures obtained has made important contributions to knowledge of processes in surface water. A problem is that accuracy and repeatability of the quantitative relations obtained is low (Gordon and Morel 1983). Going from the open ocean via coastal seas to estuaries and freshwater this problem increases and becomes more complex (Bukata *et al.* 1981; Fischer 1983). In the same direction the concentration of humus increases which is part of the problem.

For the interpretation of satellite observations field data can vary from nonexistent to a considerable amount. Sea-truth is always inadequate compared to the spatial resolution of the images. So a strategy is needed to incorporate field data into the calibration procedure. The amount and kind of field measurements that would form an optimal contribution at a reasonable price to enhance the value of satellite or airborne measurements is not obvious.

In the absence of field data default values are needed for the optical properties of the constituents of water together with error estimates of these values for sensitivity analysis (Prieur and Sathyendranath 1981). Since the optical properties of dissolved and suspended matter vary over place and in time the purpose of field measurements in a specific investigation is to improve on the default values and their error margins.

Water and aquatic humus determine the optical background in which the contribution from particulate material is studied. Pure water has constant optical properties. These were reviewed by Smith and Baker (1981) and by Buiteveld and Donze (unpublished results). The error margins are due to the difficulty of obtaining pure water and by the measuring

technique. No accurate formula to describe the shape of the water attenuation spectrum is available. The table of data is numerically described by a vector.

The default absorption spectrum of aquatic humus was determined for inland waters and compared to the literature spectrum of the global default derived for marine waters by Bricaud *et al.* (1981). The default spectrum and its accuracy was determined by a target factor analysis of measurements of field samples. The shape and variability of the absorption spectrum of aquatic humus of inland waters of the Netherlands was analyzed. Since the dataset contains much variation in the sources of humus used the default can be used as a default for inland waters.

8.2 Aquatic Humus

Humus is a general name for organic compounds of large molecular weight. Aquatic humus or dissolved organic matter is also called yellow substance or Gelbstoff because of its colour. Aquatic humus is defined by the sample preparation technique (Kirk 1976). Usually a water sample is filtered over a membrane filter, type and pore size of the filter define aquatic humus in a particular investigation. The concentration of humus is defined by the method of measurement. At high concentrations chemical analysis of total carbon can be used. Measurement of light absorption at a single wavelength, usually 380 nm, is more sensitive. It is in general use as are fluorescence measurements, which are still more sensitive. Since humus is not well defined in a chemical sense intercalibration of the results of these different methods is a statistical affair: conversion factors vary in time and space.

Kalle (1966) showed that the shape of the absorption spectrum of humus from different sites is not constant. This was confirmed in a number of investigations (Zepp and Schlotzhauer 1981; Bricaud *et al.* 1981; Buiteveld *et al.* 1986; Davies-Colley and Vant 1987; Højerslev 1988; Carder *et al.* 1989; Roesler *et al.* 1989). The effect is usually described by the ratio of extinctions at 365 and 665 nm or at 420 and 665 nm. These ratios have been used to distinguish different water masses in hydrological investigations.

De Haan (1983) showed that the ratio of extinctions at 250 nm and 365 nm can be used as a parameter to describe annual variations in the extent of internal humus formation in a lake. Low ratios correspond with increasing molecular weight and aromaticity of fulvic acids. Humus can be fractionated chemically into a humic acid and a fulvic acid part. Carder *et al.* (1989) demonstrated that for Gulf of Mexico samples the variations in the shape of the humus spectrum are in first approximation proportional to the ratio of these fractions.

8.3 Experimental Results

Samples of surface water were collected at 40 locations in the Netherlands. These were selected *a priori* using a soil map aiming at a large variability in the properties of the humus. Absorption spectra of aquatic humus were measured by the method described in chapter 3. Strictly speaking aquatic humus is defined by the way it is isolated, in this work by filtration over a 0.2 μm membrane filter.

Absorption spectra from 40 locations in the Netherlands are shown in Figure 8.1a. Absorption at 380 nm was on average 21.0 m^{-1}, ranging from 3 to 63 m^{-1}. These values are ten to hundred times higher than in marine waters. After normalization of the spectra to one at 380 nm (Figure 8.1b) the variability in shape of the spectra is seen.

8.4 Modelling the Shape of the Spectrum

8.4.1 Exponential Model

The shape of the absorption spectrum of humus is, from short to long wavelengths, a monotonously decreasing function (Kalle 1966). In first approximation it can be described by an exponential function

$$f_{norm}\, a(\lambda) = a_h^*(\lambda_0) \exp(-s(\lambda-\lambda_0)) \qquad \textbf{(8.1)}$$

$a(\lambda)$ measured absorption coefficient m^{-1} at wavelength λ

λ wavelength nm

λ_0 chosen reference wavelength nm

$a^*(\lambda_0)$ specific absorption coefficient at a chosen reference wavelength λ_0 nm, calculated by a least square fit on the measured spectrum.

f_{norm} normalization factor, dependent on the type of investigation. Values used, other than 1, include

- $f_{norm}=1/DOC$ used in an investigation of conversion factors by Zepp and Schlotzhauer (1981). DOC is the concentration of dissolved organic carbon.
- $f_{norm}=1/a(\lambda_0)$ this normalization removes information on concentrations, it can be used to study the shape of the spectrum

s slope coefficient calculated by a least square fit nm^{-1}

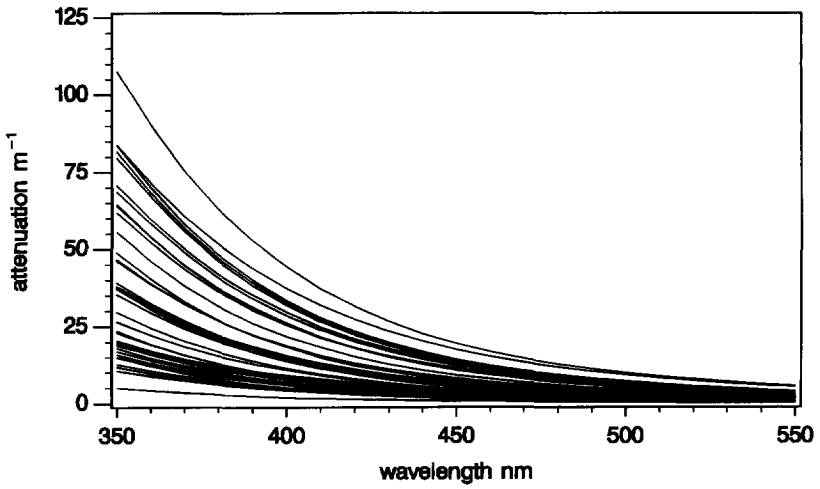

Figure 8.1a Measured humus absorption spectra from 40 different locations in the Netherlands after filtration over a 0.2 μm filter.

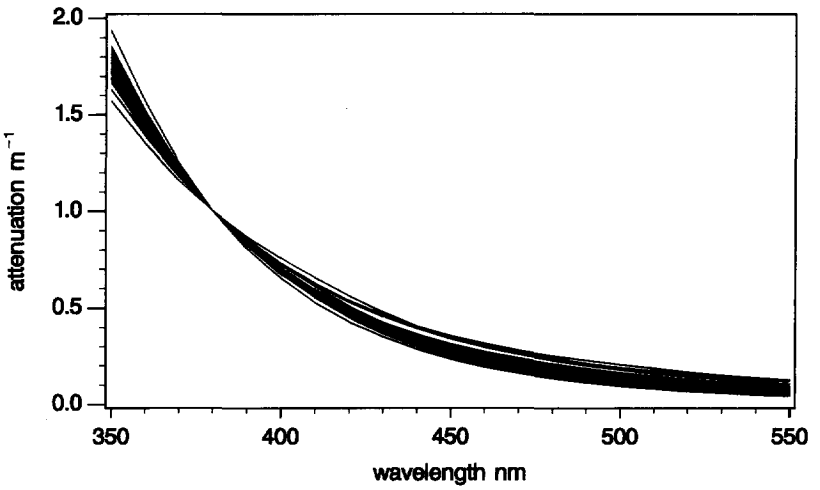

Figure 8.1b Variability in the shape of the spectra after normalization of the spectra to one at 380 nm. The absorption measured at this single wavelength is often extrapolated to a full spectrum with an exponential model.

Figure 8.1 *Variability in the shape of the absorption spectrum of aquatic humus.*

Default Absorption Spectrum of Aquatic Humus

In this model $a^*(\lambda_0)$ contains most of the information on the concentration of humus to be derived from absorption measurements and s describes the shape of the spectrum. The accuracy obtained this way was studied by several authors, references are given in Table 8.1. Individual spectra can be fitted with high overall precision, r^2 values of 0.99 are usual. The wavelength range used in these regressions was about 200 nm. Among spectra of samples from different locations s varied between 0.010 and 0.021 nm^{-1}. In these investigations the mean value of s varied. Bricaud *et al.* (1981) measured almost the entire s range, they found a mean value of 0.014 m^{-1} with a standard deviation of 0.0032 nm^{-1}. Investigations of freshwater lakes tend to have higher mean slope values (Davies-Colley and Vant 1987; Carder *et al.* 1989).

In aquatic optics and in remote sensing applications an exponential description of the humus spectrum using this average of 0.014 nm^{-1} is often used as a default value for the slope. Bricaud specified that application of this default value to calculate humus absorption at 440 nm from measured values at 375 nm resulted in data reproduction with fractional errors up to 0.25. This may lead to significant errors in the calculation of chlorophyll concentrations. At high aquatic humus concentrations field measurements or a more accurate model must be used.

The 40 spectra were normalized at 380 nm using f_{norm} is $1/a(380)$ and fitted to the exponential model without intercept. Variation in shape of the spectrum is witnessed by the range of shape coefficient values found, 0.013-0.020 (Table 8.1), almost covering the range found in literature.

To compare the accuracy of data reproduction by different models two indicators of goodness of fit are used: the root mean square error and the mean residual fraction specified at two wavelengths. In Table 8.2 these indicators are given for the models treated in this paper. At this place two exponential models are considered, one with the default value for the slope s of 0.014 and one with the value of 0.016 best fitting the data. The root mean square error, rms, represents the difference between the data and the reproduced data. Errors in data reproduction at 440 and 550 nm are expressed by the mean residual fraction, reproduced values are subtracted from the measured values and specified as fractional part of the measured values. Positive residuals are misfits underestimating the data, mean residuals indicate systematic errors.

The *rms* shows good overall fit, but reproduction of the high absorption values at short wavelengths dominates in its calculation. Since the humus absorption values decrease by two

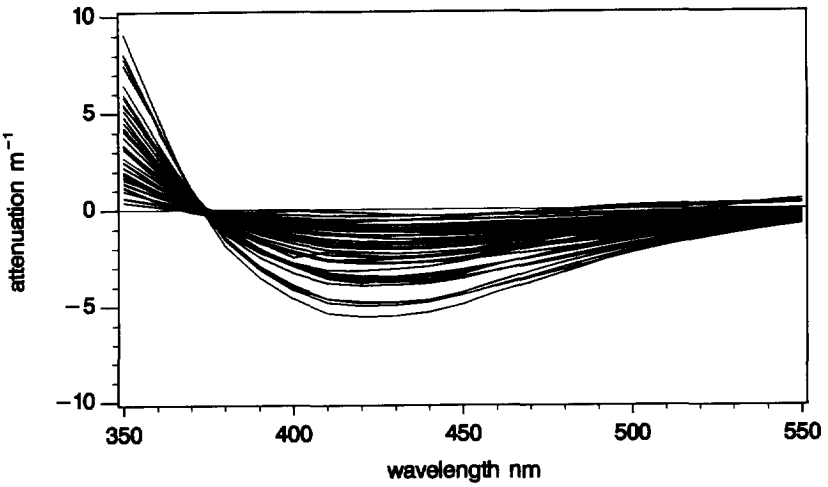

Figure 8.2a

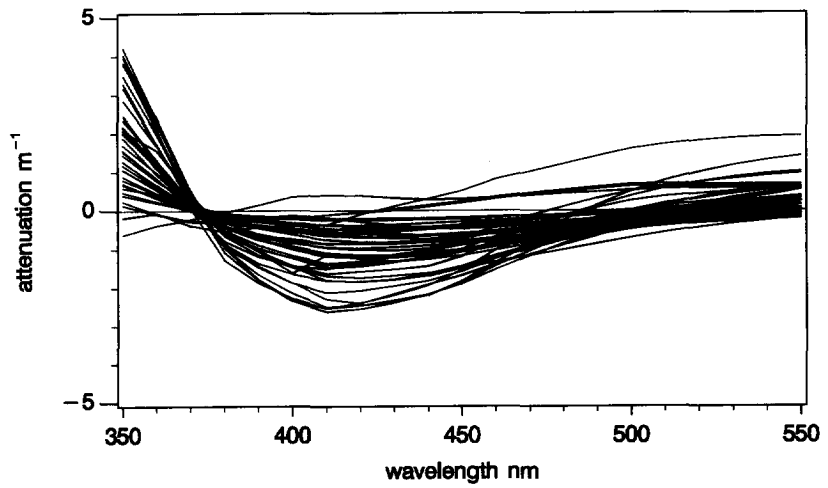

Figure 8.2b

Figure 8.2 *Spectra of residuals for two exponential models to describe the shape of the absorption spectrum of aquatic humus. The spectra show systematic errors in data reproduction. In Figure 8.2a the default slope $s=0.014$ is used and in Figure 8.2b the slope $s=0.016$, best fitting the data.*

Table 8.1 *Values for the slope of the absorption spectrum of aquatic humus as described by an exponential curve. The preparation method used to define aquatic humus is indicated. Listed are the wavelength range used in the regression, the reference wavelength, the number of different sampling locations, the range and the mean value of the slope s of the exponential model.*

reference within ref.	preparation method	range nm	λ_0 nm	range s nm^{-1}	number of loc.	mean s nm^{-1}
Zepp (1981)	ultra-centrifugation	300-500	450	0.012-0.018	12	0.0145
	fulvic acid				3	0.0138
	humic acid				3	0.0102
Bricaud (1981)	GF/C glassfibre filtration	375-500	375	0.010-0.020	105	0.014
Davies-Colley (1987)	0.2 μm membrane filtration	280-460	450	0.015-0.021	12	0.0187
Kirk					22	0.0161
Højerslev (1988)	GF/C glassfibre filtration		450	0.012-0.017		0.014
Carder (1989)	concentration, extraction		450			
	fulvic acid				2	0.0189
	humic acid				1	0.0111
Harvey (1983)		370,440		0.012-0.017	4	0.0141
Roesler (1989)	GF/C glassfibre filtration	400-750	400		21	0.017
present study	0.2 μm membrane filtration	350-550	380	0.013-0.020	40	0.016

orders of magnitude over the wavelength range large relative errors occur at higher wavelengths. These errors also depend on the reference wavelength chosen for normalization. So it is difficult to determine at which value of the *rms* the data description is sufficiently accurate. To describe the low variance values also within experimental error the *rms* should be equal to 0.05, the accuracy of the measurements.

If the best choice for the exponential slope is used the overall fit improves twofold and the mean misfit decreases strongly. Spectra of the residuals for both models are given in Figure 8.2. The deviations of the measured absorption spectra from a fixed exponential shape lead to systematic, wavelength dependent errors in data reproduction. If the default slope is used significantly higher errors occur.

Table 8.2 *Accuracy of data reproduction applying different candidate component spectra to the 40 absorption spectra of aquatic humus. The results of a least sum of squares fit and target factor analysis are given. With target factor analysis minimum residual errors are made. The root mean square error, rms, represents the difference between the measured data and the reproduced data. Relative errors in data reproduction at 440 and 550 nm are specified by the mean residual fraction, residuals were calculated as fractional part of the measured values. Negative values correspond with overestimation in data reproduction. Exponential models are; EXP14 with the default slope of 0.014, EXP16 with a slope of 0.016 best fitting the data and EXPMHA+EXPMFA for the mass-specific absorption spectra for marine humic and fulvic acid of Carder et al. (1989), see Table 8.6. Models with abstract vectors are F_1 for one component, F_1+F_2 for two components and $F_1+F_2+F_3$ for three components.*

Model	*RMS* 350-550	Mean Residual Fraction at 440 nm	Mean Residual Fraction at 550 nm
Least Sum of Square			
EXP14	1.942	-0.293	-0.347
EXP16	0.956	-0.149	0.039
EXPMHA+EXPMFA	0.377	-0.025	0.254
Abstract Factor Analysis			
F_1	0.469	-0.036	-0.184
F_1+F_2	0.107	0.002	-0.044
$F_1+F_2+F_3$	0.050	0.002	-0.001
Target Factor Analysis			
one component	0.469	-0.036	-0.184
two components	0.107	0.002	-0.044
three components	0.050	0.002	-0.001

8.4.2 Improved Model

In models of light distribution in water the effects of particulate material are superposed on a background of the optical properties of pure water and humus. The spectrum of humus, weighed by its concentration, is added to the spectrum of water. The water spectrum is only available as a table of data values, a vector. A description of the humus spectrum as a function of wavelength would not simplify mathematical formulation and calculation of compound spectra in surface water. So we can drop the assumptions about the shape of the spectrum of humus and avoid systematic errors imposed by the presumed shape.

8.4.2.1 Target Factor Analysis

Target factor analysis (Malinowski and Howery 1980) is a method to handle spectral data of mixtures of components. The method is used to determine a set of components best fitting the data, details are given in Chapter 7. Target factor analysis can be used to analyze spectra of absorption and beam attenuation by a principal component analysis followed by a transformation of significant abstract components to a set of real components, the targets. Candidate spectra of real components can be tested to be actually present in the mixture. This is done by comparison of the spectra to their projection in the data space of the significant components. Candidate components can be tested individually. For a model with one component the first abstract vector is the best candidate component to be used in data reproduction because equivalent rotated solutions do not exist.

Several authors applied principal component analysis to remotely sensed reflectance spectra (Mueller 1976; Doerffer 1981; Lin *et al.* 1984; Fischer *et al.* 1986). Its use is limited to a first approximation since in general reflectance spectra will depend in a non-linear way on the combined effects of absorption and scattering in surface water. A successful transformation of the resulting abstract decomposition to real components can not be expected.

8.4.2.2 Results

In our set of aquatic humus absorption spectra the number of components and their abstract shape were determined by abstract factor analysis. From the data the covariance matrix about the origin was calculated, it was decomposed into eigenvectors with corresponding vector scores. The covariance matrix about the origin is used because all spectral absorption values are expressed in the same units and differences in the amount of variance are significant. Eigenvectors are chosen to represent wavelength dependency: the shape of abstract spectra. Vector scores represent the contribution of the abstract vectors to the measured spectra. The first abstract vector explains most of the variance, it is close to the mean spectral shape.

Several criteria with corresponding variables can be used to determine the optimum number of components used in data reproduction. Preferably criteria incorporating knowledge about experimental errors are used. In Table 8.3 the increase in accuracy of data reproduction with the number of components is shown. The number of components in the absorption spectrum of humus was derived using the known experimental errors of 1.5 percent with a minimum of 0.045 m^{-1}. Interpretation of the cumulative fraction of variance explained is not

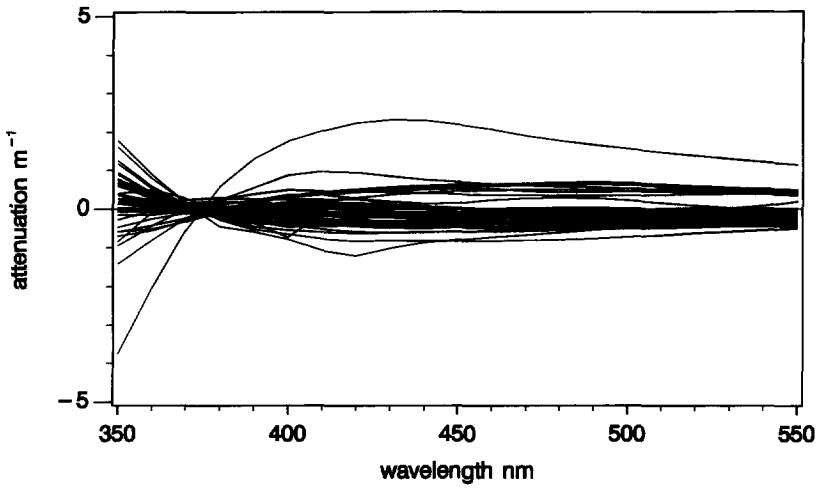

Figure 8.3a Most of the variance in the dataset is described by the first vector. This represents the relatively constant shape of the humus spectrum without assumptions.

Figure 8.3 *Spectra of residuals reproducing the data with one, two and three abstract vectors.*

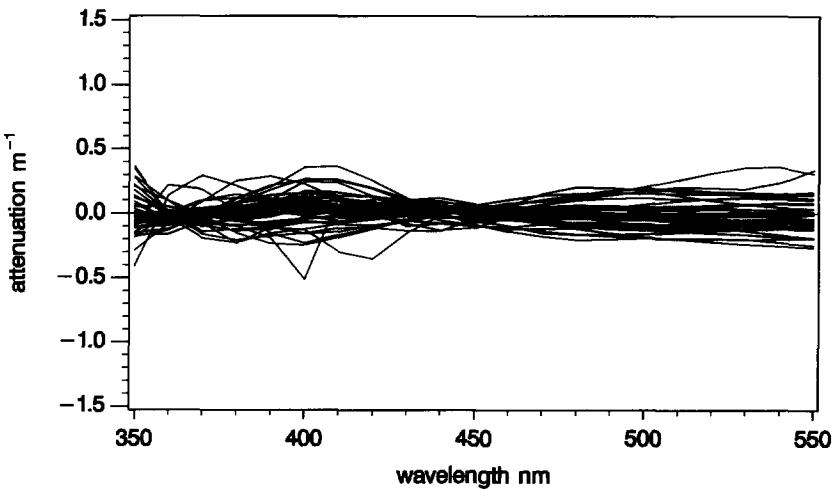

Figure 8.3b: With 2 components data reproduction is improved; systematic errors are reduced.

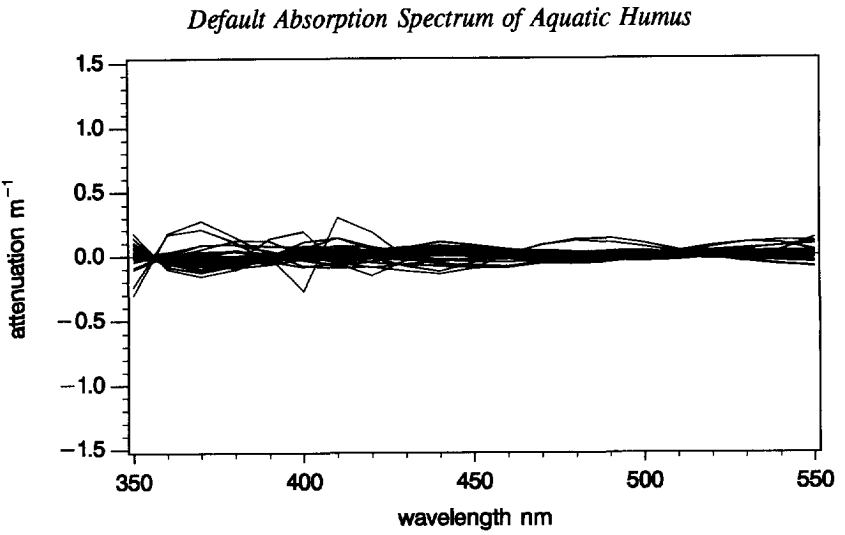

Figure 8.3c: With 3 components the data is described within experimental error. Target factor analysis for a models with an equal number of components results in identical residual spectra.

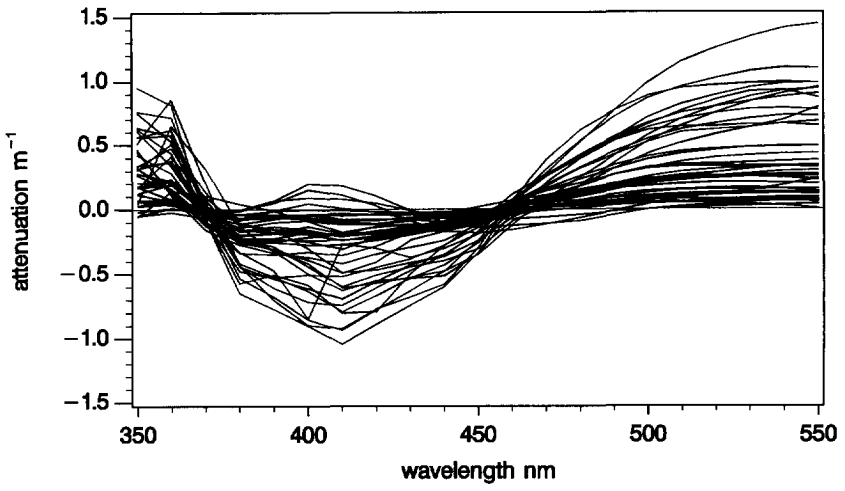

Figure 8.4 *Spectra of residuals if the mass-specific absorption spectra of marine humic acid and marine fulvic acid with exponential shape are fitted to the data. The absorption spectrum of aquatic humus is decomposed into the spectra of its primary chemical estimates. Residuals are increased compared to a target factor analysis for a two component model with the same residuals as in Figure 8.3b.*

Table 8.3 *Variables calculated to determine the number of components present in the humus absorption spectra with abstract factor analysis. Analysis of 40 spectra of aquatic humus in the UV/Visible range 350 - 550 nm. Values at 10 nm intervals were analyzed. The total number of values is 840. The number of components in the absorption spectrum of humus was derived using experimental errors of 1.5 percent with a minimum of 0.045 m^{-1}. With three components the root mean square error is 0.0497 m^{-1} (XE=RMS), the chi-squared sums are almost equal and the number of misfits is zero. According to these criteria three components must be used for data reproduction within experimental error.*

Number of Components	*CFV*	*XE*	χ_{exp}	χ_{cal}	misfits $\geq 3 \cdot \sigma_{(i,j)}$
1	0.99935	0.4692	780	24047	357
2	0.99997	0.1068	722	2014	59
3	0.99999	0.0497	666	170	0
4	1.00000	0.0336	612	148	0
5	1.00000	0.0254	560	53	0
Criteria	≈ 1	*XE=RMS*	$\chi_{exp} \approx \chi_{cal}$		≈ 0

CFV *Cumulative fraction of variance explained. The variance explained by an abstract vector is equal to the eigenvalue of the corresponding eigenvector of the covariance matrix calculated about the origin.*

XE *Extracted error, equal to the root mean square error. In case of an uniform distributed error this value should be less than or equal to the experimental error.*

χ_{exp} *Expected chi-squared sum, based on the assumption that random error due to noise is equally distributed over the superfluous abstract vectors. Noise introduces additional non zero eigenvalues of eigenvectors.*

χ_{cal} *Calculated chi-squared sum; the sum of the squared values of the weighed difference between measured and reproduced data relative to the standard deviation.*

$$(D_{(i,j)} - D_{red(i,j)})^2 / \sigma_{(i,j)}^2$$

In case of a non uniform error χ_{cal} should be equal to χ_{exp}. In practice the number of components closest to the crossover point, where $\chi_{cal}=\chi_{exp}$, is chosen.

misfits *The number of misfits; the number of residuals, the difference between the measured data $D_{(i,j)}$ and the reproduced data $D_{red(i,j)}$, larger than 3 times the standard deviation $\sigma_{(i,j)}$.*

$$| D_{(i,j)} - D_{red(i,j)} | \geq 3 \cdot \sigma_{(i,j)}$$

straightforward. If three components are postulated the root mean square error is 0.0497 m^{-1}, the chi-squared sums are almost equal and the number of misfits is zero. According to these criteria three components suffice for maximum accuracy of data reproduction in the 350-550 nm range. In Figure 8.3 the spectra of residuals are given for data reproduced with one, two and three abstract vectors (Table 8.4). Most of the variance in the dataset is described by the first component, representing the relatively constant shape of the humus spectrum. The second and third components each yield a gain in accuracy, small in terms of variance but significant in terms of residual errors, the number of misfits is reduced by one order of magnitude. Beyond this not much progress can be obtained.

Table 8.4 *Abstract vectors and vector scores resulting from factor analysis of 40 absorption spectra of aquatic humus. With three components the data was reproduced within experimental error. Abstract vectors correspond with the wavelength dependency of the components, vector scores with their relative contribution. The transposed matrix of the score matrix is given. Data reproduction using nc components is done by matrix multiplication of the 21×nc abstract vector matrix with the nc×40 score matrix.*

Wavelength	Abstract Vectors		
nm	F_1	F_2	F_3
350	0.5462	-0.4376	0.3066
360	0.4589	-0.2324	0.1188
370	0.3816	-0.0630	-0.0542
380	0.3174	0.0647	-0.1989
390	0.2657	0.1426	-0.2575
400	0.2221	0.1967	-0.3323
410	0.1857	0.2316	-0.2537
420	0.1564	0.2545	-0.2103
430	0.1330	0.2590	-0.1220
440	0.1117	0.2564	-0.0348
450	0.0953	0.2492	0.0381
460	0.0823	0.2415	0.1023
470	0.0712	0.2285	0.1541
480	0.0619	0.2175	0.1948
490	0.0542	0.2073	0.2233
500	0.0478	0.1965	0.2439
510	0.0421	0.1844	0.2580
520	0.0372	0.1728	0.2643
530	0.0331	0.1621	0.2699
540	0.0295	0.1527	0.2771
550	0.0263	0.1452	0.2811

In Table 8.2 the data reproduction using the first and subsequent abstract factors are given in the same terms as used before to discriminate between the exponential models. The fixed shape model F_1, the first abstract factor, is the least square fit on the measured spectra. The overall fit to the measured spectra is better than obtained with the exponential models, as seen by comparing Figure 8.3a with Figure 8.2ab. Already model F_1 results in a reduction of the *rms* by a factor of two. Compared to the default exponential shape fourfold better accuracy is found. Mean residual fractions are reduced except for the values with low

Table 8.4 *Continued*

Sample	Vector Score			Sample	Vector Score		
Number	1	2	3	Number	1	2	3
1	25.227	-2.5176	0.1592	21	37.464	0.2208	-0.2922
2	65.038	-3.4931	-0.0675	22	66.824	-2.0722	-0.3505
3	35.849	2.1418	0.6124	23	63.331	-1.7548	-0.5406
4	37.247	2.3759	0.6612	24	151.920	-1.2193	0.4303
5	20.864	-0.8381	-0.0473	25	148.226	-1.4336	-0.0941
6	19.205	-0.0881	-0.1465	26	84.142	-0.3378	-0.0657
7	114.176	1.5268	0.6637	27	131.130	1.8474	-0.1212
8	116.886	-1.5687	0.1787	28	27.115	-0.1337	-0.1828
9	145.097	-1.1426	0.4359	29	31.500	-1.7770	-0.3810
10	40.934	-2.4269	-0.0140	30	22.869	-0.7576	-0.3442
11	20.571	-1.5233	-0.1951	31	69.520	-0.0102	-0.4207
12	27.959	-1.2959	-0.1020	32	68.548	0.0069	-0.4327
13	70.135	-1.1083	0.7202	33	99.861	-1.7276	0.2239
14	86.157	-3.3548	0.9494	34	84.620	-0.8567	-0.0970
15	52.774	-1.8882	-0.2676	35	34.344	-0.9631	-0.7819
16	160.277	8.4817	-0.3254	36	48.276	-0.6533	-0.7683
17	30.304	-0.4989	0.2324	37	37.678	-0.0086	-0.8870
18	36.830	3.1042	-0.3992	38	197.901	1.8473	0.3868
19	116.930	-0.9293	-0.6486	39	127.175	0.9921	-0.3437
20	40.662	-1.8046	-0.1159	40	8.954	-0.3615	0.0046

variance at high wavelengths. Using more components in data reproduction reduces the mean misfits and the spread in misfits, Figure 8.3, especially at wavelengths with low variance values.

Our dataset contains absorption values one magnitude higher than reported before, extending the concentration range of humus spectra that have been analyzed. With three linearly independent components any spectrum of humus in the dataset can be described within experimental error. Since the dataset contains much variation in the sources of humus used, witnessed in terms of the exponential model by the large range of values for the slope, this is probably true in general.

8.5 Target Testing

8.5.1 Accuracy of Default Specific Spectra

Aquatic humus is not well defined in a chemical sense. Methods of isolation and measurement define its nature and its concentration. If absorption spectroscopy is used for its determination the variability in shape of the spectrum leads to the notion that representing its concentration by a single value is only a first approximation. It was shown that three values are needed not to lose information contained in a number of measured absorption spectra. This complicates intercalibration with measuring techniques that yield a single value, like total carbon. In this case the conversion factor is a vector of three elements going from the absorption spectra to carbon and a scalar with loss of information going the other way. If fluorescence emission- and excitation spectra are measured, the data on a single sample consist of a matrix. Factor analysis would yield information on the number of fluorescent species present (Weber 1961). And interconversion would consist of a matrix going from fluorescence to absorption and a vector with loss of information going the other way.

Carder *et al.* (1989) used a two component description in chemical terms and the exponential model to describe absorption spectra of humus. They explained the variations in the slope of the spectra in terms of fulvic acid and humic acid, the primary fractions of aquatic humus. In samples from the Gulf of Mexico marine fulvic acid had a slope value of 0.01890 nm^{-1} and marine humic acid a value of 0.01105 nm^{-1}. The slope would therefore be a measure of the ratio of these two primary subdivisions of aquatic humus. This leads to a model for the humus spectrum consisting of a weighed sum of two exponential functions with fixed slopes. This model would, for numerical reasons, give a better description of our dataset than a single exponential model with gain in chemical knowledge. However, this approach will lead to significant systematic errors since both component spectra deviate from an exponential shape while they also vary in nature. In Table 8.5 exponential slope values are given for humic acid and fulvic acid spectra from several sources. In a single sample the fulvic acid spectrum is steeper than the spectrum of the humic acid fraction. But the slope of fulvic acid from one sample may be lower than that of humic acid in another.

Carder *et al.* (1989) showed that in a restricted area it is possible to build a detailed concentration map of both components from absorption spectra alone, after intercalibration of the expensive chemical estimates and the cheaper optical estimates. But this calibration has to be repeated in every application of this technique, since the relationships involved are not fixed, as appears from Table 8.5 and the following discussion.

Table 8.5 *Natural variability of the shape of the absorption spectra of humic acid and fulvic acid. Exponential slope values are calculated from extinction ratios specified in the references.*

Reference	Extinction Ratio	Fraction	Ratio	Exponential slope s
Kalle (1966)	E365/E420		5.5-32	0.007-0.014
		Humic Acid	5.5-8.0	0.007-0.009
		Fulvic Acid	23-32	0.013-0.014
Schnitzer (1973)	E465/E665	Humic Acid	3.0-5.0	0.005-0.008
		Fulvic Acid	6.0-8.5	0.009-0.011
Zepp (1981)	E366/E465	Humic Acid	2.4-3.4	0.009-0.012
		Fulvic Acid	4.1	0.014
de Haan (1983)	E250/E365	Humic Acid	4.0	0.012
		Fulvic Acid	5.3-7.6	0.014-0.018

Target factor analysis (Malinowski and Howery 1980) can be illustrated using our dataset of humus spectra and the exponential models of the spectra of the two fractions found by Carder *et al.* (1989). The first two abstract factors were rotated to the mass-specific absorption spectra for marine humic acid and marine fulvic acid. Table 8.6a gives the target spectra and the best fitting components present in the data. Table 8.6b gives the concentrations of humic and fulvic acid calculated using these modified target vectors. Some negative humic acid concentrations result and the fulvic acid concentrations are too high, probably by a factor ten. Spectra of the residuals fitting the mass-specific spectra without modification to the data are shown in Figure 8.4 (page 163). Comparing this model to the ones specified in Table 8.2, data reproduction appears better than with the models with one component having fixed shape; EXP14, EXP16 and F_1, but a target factor analysis with two components is better. This also follows from the residual spectra by comparing Figure 8.4 with Figure 8.2 and Figure 8.3a for the models with fixed shape and by comparing Figure 8.4 with Figure 8.3b for the two component model.

The absorption spectra of humus of samples of surface water were not successfully described by the model with the mass-specific absorption spectra of humic acid and fulvic acid of marine water. The specified target spectra are close to component spectra present in the data but the concentrations are in error. This result confirms that an intercalibration of chemical and optical estimates must be repeated in every application and that the spectral shape of humic acid and fulvic acid varies in nature.

Table 8.6 *Concentrations of humic and fulvic acid derived using target factor analysis. Targets used are the mass-specific absorption spectra for marine humic and fulvic acid of Carder (1989). The targets are exponentials with reference wavelength $\lambda_0=450$ nm. The specific absorption and exponential slope are for marine humic acid $a(450)=0.1304\ m^2g^{-1}$ and $s=0.01105\ nm^{-1}$, and for marine fulvic acid $a(450)=0.00728\ m^2g^{-1}$ and $s=0.01890\ nm^{-1}$.*

Table 8.6a

Wavelength	Marine Fulvic Acid		Marine Humic Acid	
nm	target	component present	target	component present
350	0.04819	0.04857	0.39371	0.39180
360	0.03989	0.04027	0.35252	0.35343
370	0.03302	0.03298	0.31564	0.31734
380	0.02733	0.02697	0.28262	0.28498
390	0.02263	0.02222	0.25306	0.25444
400	0.01873	0.01828	0.22658	0.22669
410	0.01551	0.01502	0.20288	0.20161
420	0.01284	0.01242	0.18166	0.18051
430	0.01063	0.01031	0.16265	0.16033
440	0.00880	0.00857	0.14564	0.14231
450	0.00728	0.00720	0.13040	0.12689
460	0.00603	0.00611	0.11676	0.1143
470	0.00499	0.00521	0.10454	0.10243
480	0.00413	0.00446	0.09361	0.09247
490	0.00342	0.00384	0.08382	0.08399
500	0.00283	0.00332	0.07505	0.07648
510	0.00234	0.00289	0.06720	0.06944
520	0.00194	0.00251	0.06017	0.06311
530	0.00161	0.00220	0.05387	0.0576
540	0.00133	0.00193	0.04824	0.05282
550	0.00110	0.00168	0.04319	0.04872

8.5.2 Improvement on Accuracy of Default Spectra

With target factor analysis the variability of the optical properties of humus can be included in algorithms for the interpretation of airborne optical measurements of surface water. This inclusion requires execution of a field measuring program if improvement on the default

Table 8.6b

Sample Number	Marine Fulvic Acid g m^{-3}	Marine Humic Acid g m^{-3}	Sample Number	Marine Fulvic Acid g m^{-3}	Marine Humic Acid g m^{-3}
1	356.49	-6.21	21	348.07	8.84
2	781.79	-2.34	22	733.79	4.52
3	244.63	17.26	23	685.85	5.24
4	247.28	18.62	24	1508.29	26.20
5	237.86	0.54	25	1482.78	24.45
6	187.64	3.61	26	819.91	16.05
7	1021.66	30.83	27	1169.06	35.84
8	1189.34	17.28	28	265.35	5.06
9	1439.54	25.12	29	382.55	-1.52
10	502.50	-2.51	30	253.34	1.33
11	266.44	-2.65	31	665.12	14.49
12	326.66	-0.07	32	655.04	14.36
13	721.29	9.61	33	1033.85	12.00
14	977.36	2.71	34	848.25	13.78
15	591.03	2.42	35	372.46	2.79
16	1143.86	72.19	36	491.47	7.11
17	312.57	4.06	37	360.61	7.84
18	209.94	21.86	38	1807.43	49.80
19	1160.47	20.20	39	1170.42	31.11
20	471.39	0.27	40	102.17	0.22

spectrum is desired. The accuracy gained can be estimated by target factor analysis.

To do this Table 8.2 can be used or, preferentially, a similar table is calculated from an existing data set of the region under consideration. The available default spectra are used as targets in the analysis giving the base line against which improvement can be judged. Maximum improvement is obtained with a number of abstract factors. The result is judged by inspecting the residual spectra as in Figure 8.3 and the criteria as listed in Tables 8.2 and 8.3.

If in an application a model with one component is not sufficiently accurate for data reproduction, the shape of the spectrum is not fixed and variability in shape must be

accounted for. Variability in shape of the absorption spectrum of humus can be described in three ways:

1. Use the measured spectra, which are exact for the time and location of the samples.
2. Use the exponential model with a range of fitted slope values. Systematic errors are made because of the assumed exponential shape.
3. Use target factor analysis and test data reproduction for models with arbitrary shape.

According to the target factor analysis a decomposition of the absorption spectra of aquatic humus into three component spectra results in data reproduction within experimental error. In most applications the use of two components will be sufficiently accurate.

8.5.3 Colour Component Spectra of Surface Water

A similar analysis can be made of the spectra of absorption and scattering of silt and algae. This would lead to a better founded decomposition of optical sea-truth for one pixel. The kind of algorithm developed this way would have to be implemented in an image analysis system, that would include spatial interpolation techniques to cover the variability of the optical properties of the constituents of surface water.

References

Bricaud, A., A. Morel and L. Prieur, 1981. Absorption by dissolved organic matter of the sea (yellow substance) in the UV and visible domains, Limnol. Oceanogr. **26**, 43-53.

Buiteveld, H., F. de Jong, R. Spanhoff and M. Donze, 1986. Shape and variability of the absorption spectrum of aquatic humus, Symposium on remote sensing for resources development and environmental management, Enschede, 703-705.

Bukata, R.P., J.H. Jerome, J.E. Bruton, S.C. Jain and H.H. Zwick, 1981. Optical water quality model of Lake Ontario. 1: Determination of the optical cross sections of organic and inorganic particulates in Lake Ontario, Appl. Opt. **20**(9), 1696-1703.

Carder, K.L., R.G. Steward, G.R. Harvey and P.B. Ortner, 1989. Marine humic and fulvic acids: Their effects on remote sensing of ocean chlorophyll, Limnol. Oceanogr. **34**, 68-81.

Davies-Colley, R.J., and W.N. Vant, 1987. Absorption of light by yellow substance in freshwater lakes, Limnol. Oceanogr. **32**, 416-425.

Doerffer, R., 1981, Factor analysis in ocean color interpretation, In *Oceanography from space*, Ed. J.F.R. Gower, Plenum Press, New York, 339-345.

Fischer, J., 1983. Remote sensing of suspended matter, phytoplankton and yellow substances over coastal waters, Part 1: Aircraft measurements, Mitt. Geol. Pal. Inst. **55**, 85-95.

Fischer, J., R. Doerffer and H. Grassl, 1986. Factor analysis of multispectral radiances over coastal and ocean water based on radiative transfer calculations," Appl. Opt. **25**(3), 448-456.

Gordon, H.R and A.Y. Morel, 1983. *Remote assessment of ocean color for interpretation of satellite visible imagery*, Springer-Verlag, New York, 114

Haan, H. de, 1983. Use of ultraviolet spectroscopy, gel filtration, pyrolysis/mass spectroscopy and numbers of benzoate-metabolizing bacteria in the study of humification and degradation of aquatic organic matter, In *Aquatic and terrestrial humic materials*, Eds. R.F. Christman and E.T. Gjessing, Ann Arbor Sci. Publ., Ann Arbor, Michigan, 165-182.

Harvey, G.R., D.A. Boran, L.A. Chesal and J.M. Tokar, 1983. The structure of marine fulvic and humic acids, Marine Chemistry **12**, 119.

Højerslev, N.K., 1988. Natural occurrences and optical effects of Gelbstoff, Univ. Copenhagen, Report 50, 30 pp.

Kalle, K., 1966. The problem of Gelbstoff in the sea, Oceanogr. Mar. Biol. Ann. Rev. **4**, 91-104.

Kirk, J.T.O., 1976. Yellow substance (Gelbstoff) and its contribution to the attenuation of photosynthetically active radiation in some inland and coastal South-Eastern Australian Waters, Aust. J. Freshwater Res. **27**, 61-71.

Lin, S., G.A. Borstad and J.F.R. Gower, 1984. Remote sensing of chlorophyll in the red spectral region, In *Remote sensing of shelf sea hydrodynamics*, Oceanography series 38, Ed. J.C.J. Nihoul, Elsevier, Amsterdam, 317.

Malinowski, E.R. and D.G. Howery, 1980. *Factor analysis in chemistry*, Wiley, New York, 251.

Morel, A., and R.C. Smith, 1982. Terminology and units in optical oceanography, Marine Geodesy **5**, 335-349.

Mueller, J.L., 1976. Ocean color spectra measured off the Oregon coast: characteristic vectors, Appl. Opt. **15**(2), 394-402.

Prieur, L. and S. Sathyendranath, 1981. An optical classification of coastal and oceanic waters based on the specific spectral absorption curves of phytoplankton pigments, dissolved organic matter, and other particulate materials, Limnol. Oceanogr. **26**(4), 671-689.

Roesler, C.S., M.J. Perry and K.L. Carder, 1989. Modeling *in situ* phytoplankton absorption from total absorption spectra in productive inland marine waters," Limnol. Oceanogr. **34**(8), 1510-1523.

Schnitzer, M., and S.U. Khan, 1972. *Humic substances in the environment*, Marcel Dekker, New York, 55-67.

Smith, R.C. and K.S. Baker, 1981. Optical properties of the clearest natural waters (200-800 nm), Appl. Opt. **20**, 177-184.

Weber, G., 1961. Nature **190**, 27.

Zepp, R.G. and P.F. Schlotzhauer, 1981. Comparison of photochemical behavior of various humic substances in water: III Spectroscopic properties of humic substances," Chemosphere **10**, 479-486.

CHAPTER 9

UPWARD RADIANCE ATTENUATION IS AN *IN SITU* ESTIMATE OF ABSORPTION; A COMPARISON WITH LABORATORY MEASUREMENTS

J.H.M. Hakvoort, J. Krijgsman and M. Donze.

9.1 Introduction

The optical properties of natural waters can be described by the absorption coefficient and the volume scattering function. These inherent optical properties (Preisendorfer 1976) contain information on chemical and physical components that interact with light: water itself, aquatic humus, algae and silt. Together with the incident radiation field the inherent optical properties describe the underwater light field with sufficient accuracy for most applications in optical oceanography (Jerlov 1976). The inherent properties have a basic role in models of primary production, monitoring of surface water quality and inverse calculations in optical remote sensing (Kirk 1983). Routine measurements of absorption spectra in monitoring programs are labour-intensive and therefore expensive. Development of *in situ* measuring techniques of absorption may offer a faster and cheaper alternative.

Field measurements of irradiance are related to the *in situ* absorption by theory. Gershun (1939) showed using a two flow model for radiative transfer that the divergence of the net vector irradiance E is equal to the inherent absorption (Equations 2.33 to 2.35). The theoretical relation has limited practical value because the irradiance parameters E_d and E_0 are very sensitive to the effects of surface waves and experimental errors (Tyler *et al.* 1972; Zaneveld 1989) and must be measured over an infinitesimal distance. Voss (1989) analyzed instrumental errors and found that these amount to 21% for his instrument. When investigating the accuracy of absorption measurements of suspensions a basic problem arises: which absorption technique must be taken as a reference to compare the results to.

Several techniques using high aperture optics have been used to measure absorption from turbid suspensions (Section 2.2.5.1). Methods to measure absorption have various experimental difficulties (Table 2.1, page 22) and need correction for scattering, for path length amplification or both. It is not clear which method will give the most accurate approximation of the inherent absorption of a suspension.

To obtain accurate absorption measurements of particulate matter usually some method of concentrating the particles is necessary. Yentsch (1962) measured absorption of particles concentrated on filter paper. Multiple scattering from the filter is prominent, causing absorption to be amplified by a factor β, which must be determined separately. Kirk (1980) concentrated the sample by filtration and measured absorption on the resuspended material using the semi-integrating sphere technique. A disadvantage of the resuspension method is that about 10% of the material was lost. Artifacts may be introduced during resuspension like particle loss or formation and breaking up of flocs during sampling and further handling. The accuracy of absorption measurements can be improved by increasing the pathlength instead of the concentration of the sample, making sample handling unnecessary.

It is shown how measurements of radiance can be used to obtain apparent absorption. Radiance attenuation measured in the field is compared to apparent absorption measured in the laboratory. Field measurements of upward radiance attenuation as well as laboratory measurements yield an apparent absorption that still needs correction for scattering to give inherent absorption. The section on theory explains the relation between field measurements of radiance attenuation and laboratory measurements of apparent absorption.

9.2 Theory

The equation for radiative transfer (Equation 2.49) is

$$\frac{dL(z;\theta,\phi)}{dz}\mu = -cL(z;\theta,\phi)+L_*(z;\theta,\phi) \qquad (9.1)$$

with $L(z;\theta,\phi)$ the radiance at depth z in the direction (θ,ϕ) of zenith angle θ and azimuth angle ϕ. The coefficient μ is the cosine of the angle θ, it is 1 for radiance in the z direction and c is the beam attenuation coefficient. The first term on the right gives the radiance decrease per meter due to absorption and scattering, the second term on the right is the path radiance L_*. The path radiance is the radiance increase per meter due to light scattered from all other directions into the beam considered. Details were reviewed by Jerlov (1976). In the following we use an abbreviated notation for Equation 9.1:

$$\frac{dL}{dz}\mu = -cL+L_* \qquad (9.2)$$

Estimation of In Situ Absorption

When radiance is measured along the vertical and the average direction of the incident light is also perpendicular to the water surface, the cosine of the angle μ approaches one. After division by L and rearranging Equation 9.2 leads to the radiance attenuation coefficient k

$$k = \frac{-1}{L}\frac{dL}{dz} = c - \frac{L_*}{L} \tag{9.3}$$

where the ratio of path radiance L_* to radiance L is the gain coefficient due to path radiance (Le Grand 1939).

Absorption by turbid suspensions is investigated with high aperture optics, often a semi-integrating sphere. The absorption or radiance attenuation measured this way is an apparent absorption. For clarity we denote this apparent absorption as α. If single scattering is assumed the apparent absorption consists of inherent absorption a and part of the scattering coefficient. This part is defined by the amount of scattered light not detected $(1\text{-}F(\theta_\alpha))b$, where $F(\theta)$ is the forward scattering probability and θ_{am} is the detection angle of the integrating device. As the beam attenuation is the sum of absorption and scattering the apparent absorption can also be written as part of the beam attenuation:

$$\alpha = a + (1 - F(\theta_\alpha))b \tag{9.4}$$

$$\alpha = c - F(\theta_\alpha)b \tag{9.5}$$

Theoretical proof for this equivalence can not be given, however the relation can be of practical use. If the forward scattering coefficient $F(\theta_\alpha)b$ is close to the ratio of path radiance L_* to radiance L, then the apparent absorption is close to k and *in situ* absorption can be estimated from radiance measurements in the field. The forward scattering coefficient (Petzold 1977) and the gain coefficient due to path radiance can be measured directly, but take additional efforts.

In the experimental part we deduce the close correspondence between these parameters from correspondence between apparent absorption and radiance attenuation. For waters encompassing the range from clear ocean water to very turbid inland water it is shown that results of the two approaches match. This indicates that in practice the forward scattering coefficient for the collection angle of our detector $F(38)b$, is almost equal to the gain coefficient due to path radiance.

9.3 Materials and Methods

9.3.1 Study Areas

Optical measurements were carried out in three waters with different optical properties. Lake Wolderwijd is part of a chain of shallow eutrophic lakes near Harderwijk in the Netherlands that was created in the reclaiming of the Southern Flevopolder in 1969. In summer phytoplankton is dense and dominated by the cyanobacterium *Oscillatoria aggardhii*. The Corfu Sea near Greece is an oligotrophic clear water in the Mediterranean Sea which was classified as a "case I" water (Morel and Prieur 1977). The Western Scheldt is an estuary in the south-west of the Netherlands with a high concentration of suspended silt. Background information on these waters and on conditions during the measurements is given in Table 9.1.

9.3.2 Field Measurements

Radiance was measured in the field in the spectral range 400-800 nm with 2 nm wavelength resolution (Section 3.3.7). In Lake Wolderwijd a Guided Wave Model 260 glass fibre optic spectrophotometer was used. It scans a spectrum in about 20 s and has a 0.025 s integration time per wavelength interval. In the Corfu Sea and the Western Scheldt estuary a Tracor Northern 6112 photodiode array spectrometer was used. It detects a spectrum at all wavelengths simultaneously, integration time was 2 s at Corfu Sea and 10 s at the Western Scheldt estuary. Light was collected by a glass fibre of 40 m with a core diameter of 0.5 mm. The half angle of view under water was 8.5° and in air 11.3°. To avoid shading of the sensor a boom was used and the ship was appropriately manoeuvred. The fibre end was positioned 4 m away from ship. Five spectra were measured and averaged at Lake Wolderwijd, two spectra were averaged at the Corfu Sea and at the Western Scheldt estuary.

In Lake Wolderwijd depth profiles of upward radiance L were measured at 0.10 m intervals from the surface to 0.50 m deep at eight stations. Below this depth the intensity upward light was too low for accurate measurements. The amplitude of surface waves was approximately 0.025 m causing an inaccuracy of about 0.01 m in the depth estimate and variations of about 10 percent in the downwelling spectra as seen in Figure 9.2a. The waves had a negligible effect on the spectral shape of upwelling radiation. In the Corfu Sea upward radiance was measured from just below the surface to 5.0 m depth at 1.0 m depth intervals. The water surface was flat during measurements in the Corfu Sea. At two stations in the Western Scheldt estuary upward radiance measurements were made at 0.10 m and 0.75 m depth and

Table 9.1 *Descriptive parameters for the three sites of the field experiments. In the Western Scheldt two stations were investigated.*

STUDY SITE	Lake Wolderwijd	Corfu Sea	Western Scheldt estuary	Units
Surface Area	2.7	950	250	km^2
Average Depth	1.6	75	9	m
Dominant Particulate Matter	*Oscillatoria agardhii*	none	silt	-
CONDITIONS				
Date	14-sept-1990	5-sept-1991	13-oct-1992	-
Greenwich Mean Time	10:30-12:45	13:20	10:50 / 12:00	hour
Solar Zenith Angle	48°	35°	58°	-
Sky Condition	bright/hazy	bright	bright	-
Average Wind Speed	2	2	6	$m\ s^{-1}$
Surface Wave Amplitude	<0.025	0	0.1	m
Secchi Disk Transparency	0.35	25	0.7 / 0.8	m
Chlorophyll *a*	81.8	0.18	4.46 / 3.81	$\mu g\ l^{-1}$
Phaeopigments	13.1	-	-	$\mu g\ l^{-1}$
Total Particulate Matter	26.2	-	42.0 / 18.5	$mg\ l^{-1}$
Inorganic Particulate Matter	10.4	-	38.2 / 16.1	$mg\ l^{-1}$

at 0.10 m and 0.55 m depth respectively. In the Western Scheldt estuary the surface waves of about 0.3 m amplitude were occasionally reflected by the ship reducing amplitudes below 0.1 m. Measurements were made at these moments.

In Lake Wolderwijd downward radiance was measured at 0.10 m intervals from a depth of 0.10 m to 0.50 m at two stations. In the Corfu Sea downward radiance was measured at 0.1 m intervals from a depth of 2.0 m to 5.0 m depth. Downward radiance was not measured in the Western Scheldt estuary.

Attenuation spectra of radiance were calculated for upward and downward radiance depth profiles with the Lambert-Beer equation:

$$k = \frac{-1}{\Delta z} \ln \frac{L_{z2}}{L_{z1}} \qquad \textbf{(9.6)}$$

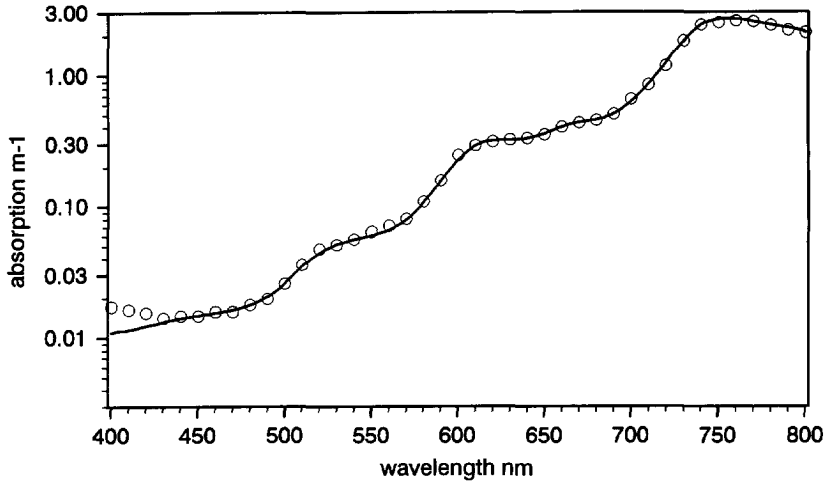

Figure 9.1 *Absorption of pure water according to Smith and Baker (1981) (symbols) and the modified absorption according to Buiteveld and Donze (unpublished data) (line).*

The attenuation spectra of downward and upward radiance at Lake Wolderwijd were also analyzed as a function of depth and were calculated for 0.1 m depth intervals.

9.3.3 Laboratory Measurement

Spectra of beam attenuation were measured (Section 3.2) on the water samples to compare the water types. The field samples from Lake Wolderwijd and the Western Scheldt estuary were separated into a dissolved aquatic humus part and a particulate matter part. Aquatic humus was obtained by filtration over a 0.2 μm Sartorius membrane filter and absorption spectra were measured. Absorption spectra of particulate matter for Lake Wolderwijd were measured on the resuspended filter cake as described by Davies-Colley (1983). About 10 percent of the particulate matter was lost in this procedure, as was also found by Kirk (1980). The measured absorption spectra were corrected for this loss. This technique was eventually abandoned because flocculation of the resuspended material occurred. No absorption spectra were available from the Corfu Sea, since the filtration technique failed to provide sufficient particulate matter due to rapid filter clogging. The samples from the Western Scheldt estuary were concentrated by centrifugation. A flow-through cuvette was used for these samples to prevent settling of particles (Section 3.2.5). Tenfold concentration of particulate matter improved the signal to noise ratio sufficiently to allow accurate measurements.

Estimation of In Situ Absorption

The beam attenuation c was measured using 10 mm cuvettes and low aperture optics. Absorption spectra of aquatic humus a_h were measured with low aperture optics using 100 mm cuvettes. The apparent absorption spectrum of turbid suspensions α_p was measured using 10 mm cuvettes and high aperture optics to collect radiation transmitted and scattered within a 38° half angle of view (Section 3.2.3).

The total apparent absorption α was calculated as the sum of the absorption of water, the aquatic humus and particulate matter:

$$\alpha = a_w + a_h + \alpha_p \tag{9.7}$$

Figure 9.1 shows the absorption spectrum of pure water of Smith and Baker (1981) as modified by Buiteveld and Donze (unpublished results) used in the calculations.

9.4 Results

Spectra of downward radiance and upward radiance were measured at a series of depth and radiance attenuation was calculated using Equation 9.6. Samples of surface water were collected and absorption spectra of aquatic humus and particulate matter were measured. Spectra of total apparent absorption were calculated using Equation 9.7.

Spectra of total apparent absorption α calculated from laboratory measurements on fractions of the samples and spectra of radiance attenuation calculated from field measurements are almost equal as shown in Figure 9.2. From these results, together with Equations 9.3 and 9.5, we can deduce that the scattering coefficient $F(38)b$ did not deviate significantly from the gain coefficient. Close correspondence between the two experimental methods was found for waters with widely different optical characteristics. The beam attenuation spectra (Figure 9.3) show the wide range in concentrations of absorbing and scattering matter in the studied waters. We conclude that the spectra of total apparent absorption can be calculated from radiance spectra measured at two depths and that correction terms for multiple scattering in the field measurements and in the laboratory measurements are small enough to be insignificant as assumed or sufficiently close to cancel.

In Lake Wolderwijd a difference occurred between the absorption spectra and radiance attenuation spectra measured. The difference was most pronounced in spectral region of low absorption (Figure 9.4), either radiance attenuation underestimated the apparent absorption or apparent absorption was overestimated. This difference was not seen for the spectra measured in the Western Scheldt. The origin of this difference is not obvious. The gain

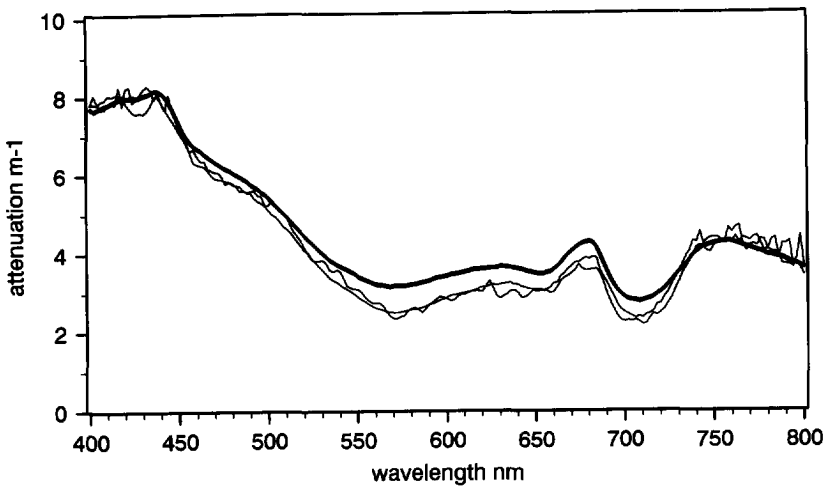

Figure 9.2a: Lake Wolderwijd, SD of 0.35 m. The attenuation spectra of upward k_u and downward radiance k_d were almost equal, the spectrum of k_u was smoother than that of k_d.

Figure 9.2 *Correspondence between the total apparent absorption (bold lines) and radiance attenuation (thin lines) for waters with different Secchi Disk transparencies SD.*

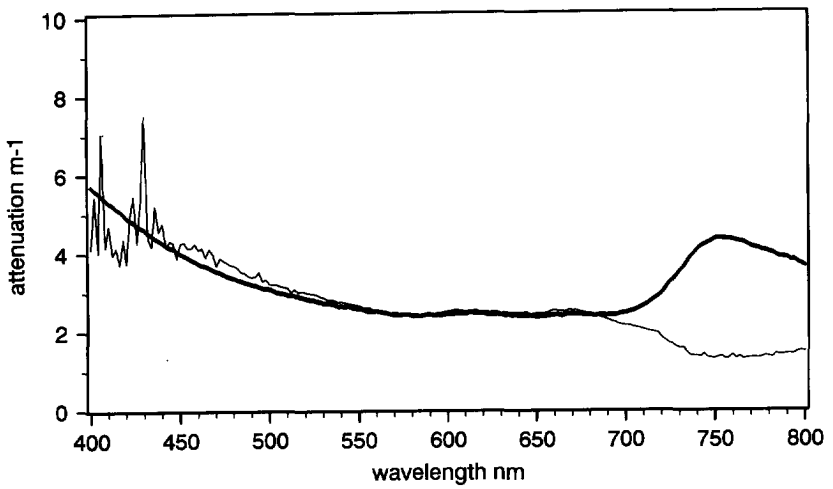

Figure 9.2b: Western Scheldt, SD of 0.7 m. Red and near-infrared light intensities decreases quickly as a function of depth. Low light intensities can lead to a systematic underestimation of radiance attenuation.

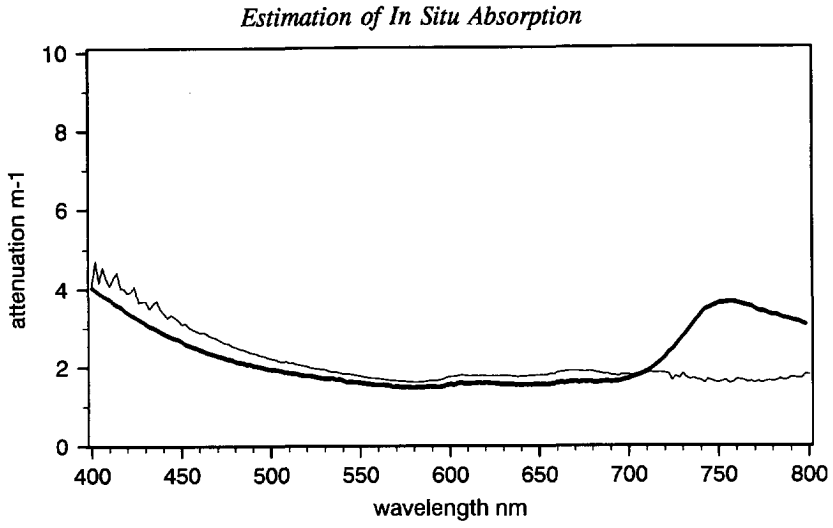

Figure 9.2c: Western Scheldt, SD of 0.8 m.

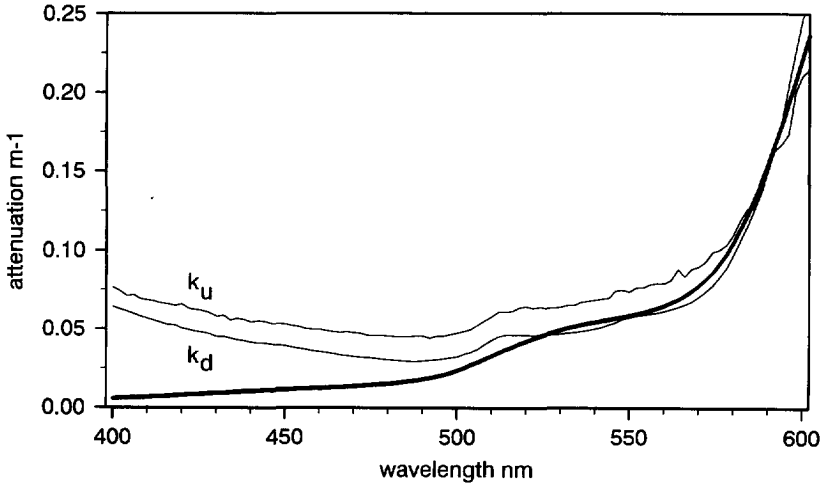

Figure 9.2d: Corfu Sea, SD of 25 m. Please, note the change in scale used for both axis. A measured absorption spectra is not available. In the spectral range from 550 to 600 nm the radiance attenuation k_u was close to the absorption of pure water (bold line), k_d is too low. The redistribution of light from the direction of the sun causes a high gain coefficient in the downward direction.

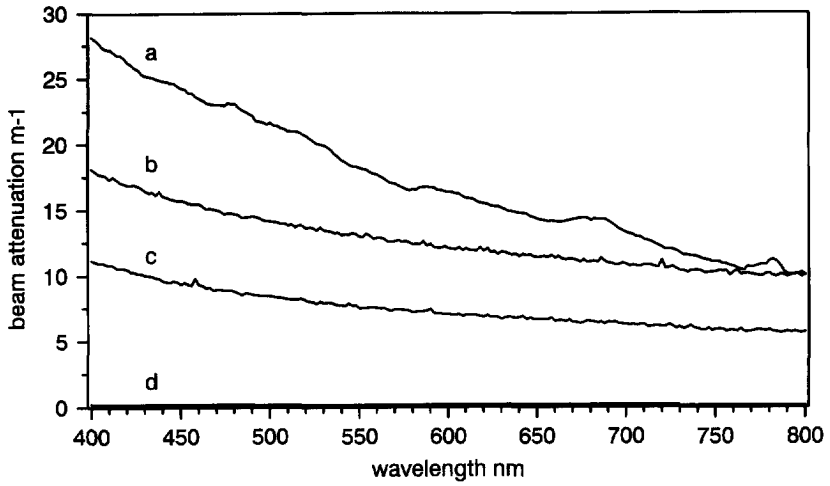

Figure 9.3 *The range of beam attenuation spectra wherein correspondence between the measured absorption and radiance attenuation was found. Lake Wolderwijd with SD of 0.35 m (line a), Western Scheldt estuary with SD of 0.70 m (line b) and of 0.80 m (line c), and Corfu Sea with SD of 25 m (line d).*

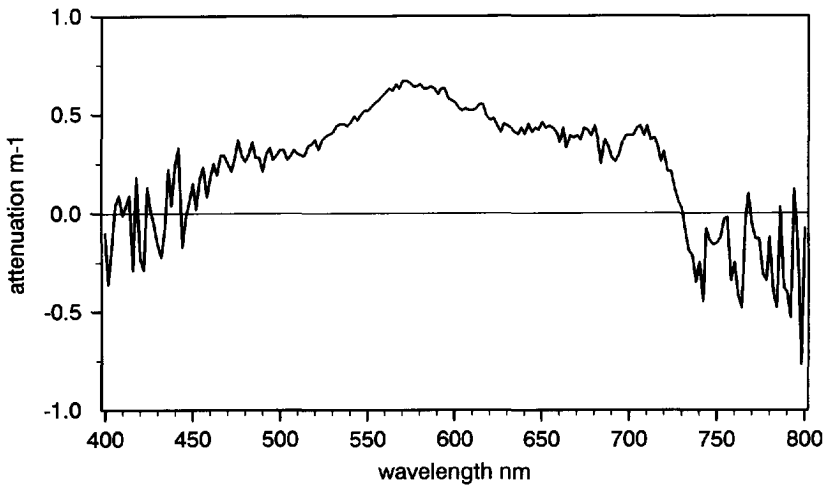

Figure 9.4 *Spectral difference (α-k_w) between the apparent absorption measured in laboratory and the radiance attenuation measured in Lake Wolderwijd. The origin of this difference is not obvious. The gain coefficient can be high if absorption is low or artifacts are introduced in the apparent absorption by sample handling.*

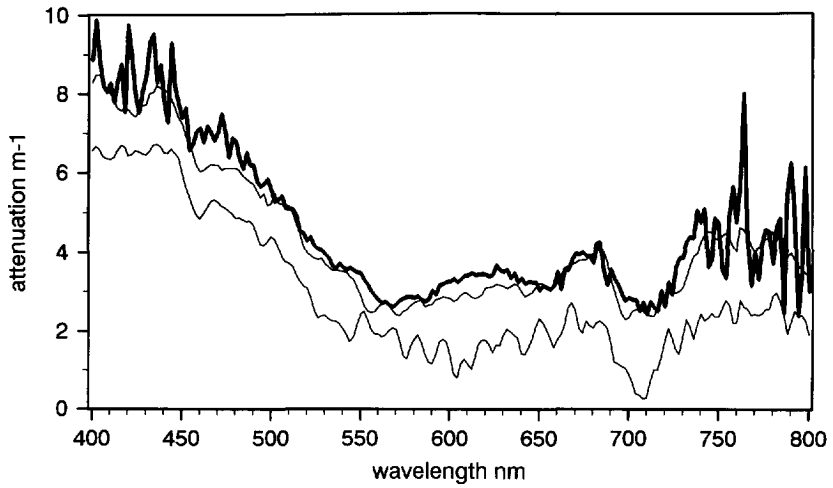

Figure 9.5 *Attenuation spectra measured over 0.10 m depth intervals in Lake Wolderwijd. Shown are k_u over 0.40-0.50 m (bold line) and k_d at two depths (thin lines). Upward radiance attenuation was independent of depth and no systematic change was found in its spectrum. The spectrum of k_d at greater depth corresponds closely to that of k_u. The value of k_d at shallow depth (0.10-0.20 m) is about 2 m^{-1} lower than k_d at greater depth (0.40-0.50 m).*

coefficient can be high if absorption is low or artifacts are introduced by sample handling. A reduction of the attenuation coefficient by solar-stimulated fluorescence of humus can be excluded because the attenuation of upward radiance was independent of depth (see Figure 9.5).

Laboratory measurements on concentrated particles contain artifacts from formation and breaking up of flocs during sampling and further handling or amplified absorption due to multiple scattering when particles are concentrated and measured on filter paper (Butler 1962; Mitchell and Kiefer 1988). Such errors do not affect the direct field measurements nor the laboratory estimation of humus. By an inverse calculation the apparent absorption of particulate matter k_p was obtained from field measurements. The measured absorption spectra of aquatic humus and the known absorption of pure water were subtracted from the field spectrum of radiance attenuation. This inverse calculation to obtain absorption spectra of particulate matter can save experimental work and increase the reliability of results. Absorption spectra of concentrated samples need not be measured, only the spectrum of aquatic humus must be measured in the laboratory or be known by other methods.

The apparent absorption spectrum of particulate matter can be used to obtain information on physical and chemical characteristics of the particles. First the inherent absorption must be

estimated from the apparent absorption. The apparent absorption comprises the total absorption by algae and silt and deviates from the inherent absorption by two correction terms. The first is multiple scattering, which is not considered in the context of this work. The second is light loss in the laboratory spectrometer since not all scattered light is collected by the aperture. Light loss also enters in the interpretation of field spectra when the scattering coefficient is not compensated by the gain coefficient.

The effect of light loss is usually corrected for by the technique suggested by Duysens (1956) to correct the apparent absorption measured by the opal glass method of Shibata *et al.* (1954). The absorption peak of chlorophyll at 680 nm and a wavelength close by where chlorophyll does not absorb are used to estimate chlorophyll concentrations in suspensions. The following assumptions are made:

1. No real absorption by algae occurs in the 720-800 nm wavelength range.
2. The fraction of light scattered away from the aperture of the semi-integrating sphere is constant over the spectral range 650-750 nm.
3. The absorption spectrum of silt is constant over the spectral range 650-750 nm.

Under these assumptions, absorption by chlorophyll in its red absorption maximum is calculated by subtracting the value at 720 nm from the apparent absorption $\alpha_p(680)$ and $k_p(680)$. This corrected absorption value, a_{chl}, is often used in correlation analysis with the results of chemical methods.

The variance of the optical and chemical parameters to determine the biomass concentration are compared. In Lake Wolderwijd measurements were made at eight stations. Coefficients of variation in the optical methods at 680 nm and coefficients of variation in the chemical methods are given in Table 9.2. The standard deviation was between 7 and 9 percent for the apparent absorption and between 8 and 10 percent for the radiance attenuation. The optical parameters a_{chl} and k_{chl} were on average equal, the variations were not correlated within the small range of observations. The standard deviation of the chemical parameter for the chlorophyll *a* plus phaeopigment extraction was 5 percent. We conclude that the two optical methods yield equally accurate estimates of this chemical parameter.

9.5 Applications and Limitations

The spectral shape and angular distribution of radiance change as a function of water depth. The light field under water near the surface under clear sky conditions is highly directional: most of the radiance flux enters from the approximate direction of the sun. The downward part is changed by refraction at the water surface and gradually by scattering with increasing

Table 9.2 *Variation of the chlorophyll a concentration in Lake Wolderwijd determined by chemical analysis and by two optical techniques. Measurements of apparent absorption α and radiance attenuation k were corrected for residual scatter to calculate absorption by chlorophyll at 680 nm, a_{chl} and k_{chl}. The optical parameters a_{chl} and k_{chl} were on average equal, the variations were not correlated within the small range of observations. We conclude that the two optical methods yield equally accurate estimates of the chemical parameter.*

OPTICAL	680 nm	
	mean m^{-1}	std %
α	4.31	7.0
k	3.73	8.0
a_{chl}	1.78	8.7
k_{chl}	1.78	9.3
CHEMICAL	mean mg m^{-3}	std %
Chlorophyll *a*	80.3	3.6
Phaeopigment	13.4	21.4
Total pigment	93.7	4.9

depth. At greater depths the angular distribution of radiance in homogeneous water reaches an equilibrium called the asymptotic angular distribution of radiance (Poole 1945; Preisendorfer 1959; Tanis *et al.* 1986). This means that at greater depth the angular distribution of light from the sky is not seen: the equilibrium distribution depends only on the inherent optical properties of the water. Theoretical prediction of the asymptotic radiance attenuation given in Section 2.4. shows that this limit is not equal to the inherent absorption and that correction for scattering is required.

Near the water surface, as long as the angular distribution of light has not reached its equilibrium, downward radiance attenuation changes with depth. In the upper layer the direct solar light becomes diffuse (Jerlov 1976). With the sun at zenith the probability of downward light being scattered into the zenith direction is relatively low and leads a to high downward radiance attenuation. When the sun is not in the zenith direction the contribution of scattered light from the direction of the sun into the vertical, downward radiance direction is relatively high and leads to low downward radiance attenuation. Upward radiance consists of light at least once scattered and has lost most information on the original angular distribution of downward light. The angular distribution of upward light therefore changes more gradually

towards its final form. This was well illustrated by Voss (1989) who measured the angular distribution of downward and upward radiance as a function of depth simultaneously for all zenith and azimuth angles. As a consequence of the gradual change with the depth the attenuation of upward radiance can be measured near the surface.

The radiance attenuation as a function of depth was analyzed using the data from Lake Wolderwijd. Attenuation spectra were calculated from the measured radiance spectra for each interval of 0.1 m depth. In the downward direction attenuation about doubled in the red part of the spectrum in the upper 0.2 m and was constant at greater depth (Figure 9.5). At depths below 0.2 m the attenuation spectrum of downward radiance was equal to the attenuation spectrum of upward radiance. The attenuation of upward radiance was independent of depth and no systematic change was found in its spectrum. So apparent absorption spectra are measured more accurately from the upward radiance than from the downward radiance. Field measurements are easier to do and are qualitatively better than laboratory measurements on the particulate fraction.

The upward radiance attenuation corresponds with the apparent absorption when two boundary conditions are met:
1. The angular distribution of radiance must be stable or slowly changing. In general this is true for upward radiance in homogeneous water. If stratification causes a slow change in angular distribution of radiance the radiance attenuation can still be measured accurately.
2. Light conditions must be stable or the spectra must be measured fast and preferably simultaneously.

Accurate spectral measurements of upward radiance attenuation in the visible light region using ambient light can only be carried out in the upper water layer. In deeper layers light levels are too low. The accuracy of a measurement of radiance attenuation is mainly determined by two parameters that act in an opposite way. With increasing depth the light intensity becomes limiting, while with decreasing depth the effect of surface waves disturbs the measurements. The ratio of the amplitude of waves to the depth interval between measurements must be low. Weather conditions set a limit to the accuracy with which radiance attenuation can be measured.

Field measurements of upward radiance attenuation were experimentally shown to be close to laboratory measurements of apparent absorption. This was found for turbid estuary water and lake water during an algal bloom. Data indicated that this is also true for clear ocean water. The results indicates that in practice the forward scattering coefficient for the collection angle of our detector $F(38)b$, is almost equal to the gain coefficient due to path

radiance. It is concluded that the field measurements of radiance attenuation like laboratory measurements yield an apparent absorption that still needs correction for scattering to give inherent absorption. Radiance attenuation and total apparent absorption were the same within experimental error, estimated at 10 percent.

9.6 Discussion

The promising results justify further investigation of the empirical relations between the upward radiance attenuation, the apparent absorption and the inherent absorption. Comparable results and a simpler determination of *in situ* absorption might result from this method because the pathlength can be increased pathlength and sample handling is omitted.

Limitations of passive radiance attenuation measurements using the ambient light field can be circumvented doing active measurements using an artificial light field. An active method may lead to a device for routine shipboard monitoring of *in situ* absorption without sample handling.

We suggest to aim future investigations on the merits of active measurements using an artificial diffuse light field and low aperture optics. With an active method the optical properties of a volume of water are investigated, the properties of the natural light field are excluded and have to be measured separately. The empirical relation can be theoretically better founded by a sensitivity analysis using literature values of the volume scattering function. The match between the radiance attenuation and the apparent absorption depends on the diffuse light field, the volume scattering function of the particles, the acceptance angle of the detector and the pathlength.

References

Butler, W.L., 1962. Absorption of light by turbid materials, J. Opt. Soc. Am. **52**, 292-299.

Duysens, L.N.M., 1956. The flattening of the absorption spectrum of suspension, as compared to that of solutions, Biochim. Biophys. Acta **19**, 1-12.

Davies-Colley, R.J. 1983. Optical properties and reflectance spectra of 3 shallow lakes obtained from a spectrophotometric study, New Zealand J. Mar. Freshwater Res. **17**, 445-459.

Gershun, A., 1939. The light-field. J. Math. Phys. **18**, 51-151.

Jerlov, N.G., 1976. *Marine optics*, Elsevier, Amsterdam, 231 pp.

Kirk, J.T.O., 1980. Spectral absorption of natural waters: contribution of the soluble and particulate fractions to light absorption in some inland waters of South-Eastern Australia, Aust. J. Mar. Freshwater Res. **31**, 287-296.

Kirk, J.T.O., 1983. *Light and photosynthesis in aquatic ecosystems*, Cambridge University Press, Cambridge, 401 pp.

Le Grand, Y., 1939. La pénétration de la lumière dans la mer, Ann. Inst. Océanogr. **19**, 393-436.

Mitchell, B.G., and D.A. Kiefer, 1988a. Chlorophyll *a* specific absorption and fluorescence excitation spectra for light-limited phytoplankton, Deep-Sea Res. **35**(5), 639-663.

Morel, A., and L. Prieur, 1977. Analysis of variations in ocean color, Limnol. Oceanogr. **22**(4), 709-722.

Petzold, T.J., 1977. Volume scattering functions for selected ocean waters, In: *Light in the sea* (Benchmark papers in optics: V. 3), Ed. J.E. Tyler, Dowden, Hutchinson and Ross, Stroudsburg, Pennsylvania, 152-174.

Poole, H.H., 1945. The angular distribution of submarine daylight in deep water, Scient. Proc. Royal Dublin Society, **24**(4), 29-42.

Preisendorfer, R.W., 1959. Theoretical proof of the existing characteristic diffuse light in natural waters, J. Mar. Res. **18**, 1-9.

Preisendorfer, R.W., 1976. *Hydrologic optics*: Vol. I-IV, U.S. Department of Commerce.

Shibata, K., A.A. Benson and M. Calvin, 1954. The absorption spectra of suspensions of living micro-organisms, Biochimica et Biophysica Acta **15**, 461-470.

Smith, R.C., and K.S. Baker, 1981. Optical properties of the clearest natural waters (200-800 nm), Appl. Opt. **20**(2), 177-184.

Tanis, F.J., G.W. Kattawar and G.D. Hickman, 1986. Influence of scattering on the diffuse attenuation coefficient in the asymptotic region, Proc. SPIE **637** (Ocean Optics VIII), 191-202.

Tyler, J.E, R.C Smith and W.H. Wilson Jr., 1972. Predicted optical properties for clear natural water, J. Opt. Soc. Am. **62**(1), 83-91.

Ulbricht, R., 1900. Die Bestimmung der mittleren räumlichen Lichtintensität durch nur ein Messung, Elektrotechnische Zeitschrift **29**, 595-597.

Voss, K.J., 1989. Use of the radiance distribution to measure the optical absorption coefficient in the ocean, Limnol. Oceanogr. **34**(8), 1614-1622.

Yentsch, C.S., 1962. Measurement of visible light absorption by particulate matter in the ocean, Limnol. Oceanogr. **7**, 207-217.

Zaneveld, J.R.V., 1989. An asymptotic closure theory for irradiance in the sea and its inversion to obtain the inherent optical properties, Limnol. Oceanogr. **34**(8), 1442-1452.

ACKNOWLEDGEMENTS

The writer wishes to express his gratitude to all persons and organisations who contributed to the completion of this thesis. In particular I like to thank:

Professor M. Donze, my promotor, for his support during the project. His comments, criticism and editorial remarks were of great help in writing this thesis.

H. Buiteveld of the Institute for Inland Water Management and Wastewater Treatment, RIZA, for his comments on preliminary chapters of the manuscript and for setting up part of the Optical Multichannel Analyzer.

George Dubelaar for helping to build and test the large volume reflectometer, for the discussions about anomalous effects in light scattering by particles, for contributing the flow cytometric data given in the Chapters 4 and 6, and for providing the Figures 3.1 to 3.5.

Hans Hakvoort for his contribution to Chapter 9, for assisting in the laboratory reflectance measurements and for providing the slides used for the cover. I look forward to your thesis on the merits of radiance attenuation measurements using an artificial diffuse light field and low aperture optics to obtain *in situ* absorption as suggested in Chapter 9.

Nout Beeker for making equipment modifications and solving all kinds of practical problems. Thanks to you the optical multichannel analyzer could be used in field experiments; fragile optical fibres were not damaged and remote moveable parts could be pneumatically controlled.

George, Hans and Nout, it was a pleasure working together. All these years I enjoyed sharing the room with good friends. Carrying out laboratory experiments was exciting. However, the time we spent together carrying out field measurements I enjoyed the most.

I also like to express my sincere thanks to J.J. Gerritsen, Ch. Breit and A.C. van der Toorn, who assisted in the experimental part of the aquatic humus analysis, and to O. Gotsis-Skretas of The Greek National Centre for Marine Research and J.C. Kromkamp of the Netherlands Institute of Ecology for the facilities provided during the cruises reported in Chapter 9.

Bart, Hans, Jaap, Jos, Rob, Tonny and many other co-workers of the Sanitary Engineering Laboratory it was fun playing cards while having lunch together.

Special thanks I owe to my wife Benedicte van Hooft. Her support, care and patience enabled me to complete this thesis. Benedicte, I dedicate this work to you.

Part of this work was funded by the Netherlands Remote Sensing Board, BCRS, as a part of the project "Interpretation of Imaging Spectroscopy Data of Inland and Coastal Waters". It was instructive to exchange information with the other participants. Arnold Dekker of the Free University of Amsterdam, now we both have completed our thesis on this subject we really should find time to write a joint publication.

CURRICULUM VITAE

Johan Krijgsman was born in Rotterdam on May 20, 1960. After completing his secondary education (VWO) in 1978 he studied civil engineering at the Delft University of Technology. During the last three and a half years of his study he was part-time employed by the university to assist in a computer programming course. In 1986 he graduated with a specialization in sanitary engineering. Until he was employed as a conscientious objector from 1987 to 1988 he developed multi-user software for a trailer rental company. Thereafter he returned to the Faculty of Civil Engineering of the Delft University of Technology to do research on the subject of optical remote sensing in the group of prof. dr. M. Donze. The results of the investigations are described in this thesis. In 1993 he joined the consulting engineering company DHV Water BV in Amersfoort.

SAMENVATTING

Inhoud

De inleiding in hoofdstuk 1 geeft een globaal overzicht over de mogelijkheden van optische remote sensing van oppervlakte water, een techniek waarbij de kleur van water op (grote) afstand wordt gemeten. Het waargenomen kleurenspectrum is onder meer afhankelijk van de samenstelling van het water. Door interpretatie van de reflectiespectra kunnen concentraties worden geschat voor een aantal aan kleur gerelateerde kenmerken van de waterkwaliteit. Met optische remote sensing kunnen concentraties van humus, chlorofyl *a* en zwevendstof van afgelegen of uitgestrekte gebieden worden bepaald tegen aanvaardbare kosten. De patronen die zichtbaar zijn op de beelden hebben een belangrijke bijdrage geleverd aan de kennis over de primaire produktie op mondiale schaal.

Een probleem bij de interpretatie van gemeten reflectiewaarden is dat de relaties niet algemeen geldig zijn en kalibratie telkens weer noodzakelijk is. Dit probleem wordt onder meer veroorzaakt doordat de relaties tussen de reflectie en de waterkwaliteitskenmerken niet lineair zijn en doordat de huidige satelliet-sensoren de reflectie meten in enkele brede golflengtebanden. De gegevens worden met behulp van de verkregen statistische relaties geïnterpreteerd. Het is nog niet duidelijk hoe een veldmeetprogramma er moet ziet dat een optimale verbetering van de nauwkeurigheid geeft ten opzichte van beschikbare statistische relaties tegen redelijke kosten.

Om algemeen geldige relaties af te leiden zijn spectrale metingen verricht met hoge golflengteresolutie en wordt de data geïnterpreteerd met behulp van een reflectiemodel. Met het model wordt de reflectie geconverteerd naar de absorptie- en verstrooiingseigenschappen van de in het water aanwezige kleurcomponenten. Deze inherente optische eigenschappen hebben een lineaire relatie met de concentratie van de componenten. Verwacht mag worden dat statistische relaties tussen inherente optische eigenschappen en een aantal waterkwaliteits-kenmerken algemeen geldig zijn.

Het meten van de inherente optische eigenschappen aan troebel water wordt bemoeilijkt doordat verstrooiing de meting van absorptie beïnvloed, en omgekeerd. Er zijn diverse methoden om de absorptie aan suspensies te meten die allemaal een correctie behoeven voor verstrooiing, een weglengte-effect of beide. Het is nog niet duidelijk welke methode in een gegeven situatie moet worden toegepast om de inherente absorptie zo nauwkeurig mogelijk te benaderen. De nauwkeurigheid van modelberekeningen van de reflectie wordt mede

bepaald door de nauwkeurigheid van de invoergegevens: de inherente optische eigenschappen absorptie en terugverstrooiing.

In hoofdstuk 2 wordt een overzicht gegeven van definities en bestaande theorieën in een consequent doorgevoerde notatie.

In hoofdstuk 3 worden de gebruikte beproevingsmethoden behandeld. Laboratorium spectrofotometers meten optische eigenschappen aan kleine volumes; het gebruik hiervan was voor ons doel niet voldoende. Om een verwaarloosbare invloed van de reflectie aan de bodem te krijgen en om optische interacties op hun natuurlijke niveau te handhaven is voor laboratoriumproeven een reflectiemeter met een groot monstervolume gebouwd. Het ontwerp van deze 'large volume reflectometer' is een verbetering ten opzichte van ontwerpen uit de literatuur.

Hoofdstuk 4 handeld over laboratoriumonderzoek van reflectiespectra van suspensies met bekende inherente optische eigenschappen. De resultaten zijn gebruikt als een maat om de prestaties van enkele gepubliceerde modellen te vergelijken, en er wordt een nieuw analytisch model voorgesteld: het backscattering albedo model. De spectrale reflectie van optisch diep oppervlaktewater wordt nauwkeurig beschreven door dit eenvoudige analytische model. Aangetoond wordt dat reflectie evenredig is met de backscattering albedo van het mengsel: de verhouding van terugverstrooiing tot de som van absorptie en terugverstrooiing. De analyse laat zien dat:
1. Reflectie is terugverstrooiing verminderd door absorptie.
2. Reflectiespectra kunnen worden benaderd met behulp van een enkelvoudig verstrooiingsmodel, het verdisconteren van meervoudige verstrooiing is niet nodig.
3. De nauwkeurigheid van modelberekeningen van de reflectie wordt in de praktijk bepaald door de nauwkeurigheid van de invoergegevens: de inherente optische eigenschappen absorptie en terugverstrooiing.
4. De resultaten van modelberekeningen voor optische ondiepe suspensies kwamen niet overeen met de waargenomen spectra.

In hoofdstuk 5 worden de reflectiespectra van mengsels van een groenwier en anorganisch zwevendstof geanalyseerd. Er werd aangetoond dat de gevoeligheid van de reflectie voor concentratie veranderingen afhankelijk is van de optisch dominante kleurcomponenten. Gerapporteerde gevoeligheden voor concentratieveranderingen variëren: 1. logaritmisch, 2. lineair en 3. invariant. Deze verschillen worden verklaard door het model voor het waargenomen concentratiebereik van de component en de overige kleurcomponenten. De

optimale golflengten voor interpretatie van de data vertonen spectrale verschuivingen die afhankelijk zijn van de dominante kleurcomponenten in het mengsel.

De nauwkeurigheid van modelberekeningen van de reflectie werd beperkt door de geringe nauwkeurigheid van de benodigde invoer van inherente optische eigenschappen. Dus het reflectiemodel zelf is minder belangrijk; het toepassen van een eenvoudig analytisch model is voldoende nauwkeurig.

In hoofdstuk 6 is het backscattering albedo model toegepast op een extreem geval van variabiliteit in de inherente optische eigenschappen van een suspensie veroorzaakt door fysische, maar niet chemische veranderingen. Drie fysische effecten werden bestudeerd gebruikmakend van suspensies van de cyanobacterium *Microcystis aeruginosa* met een constante concentratie chlorofyl *a*. Het effect van aggregatie werd onderzocht door kolonies te desintegreren tot losse cellen, de verstrooiing door de cellen werd gevarieerd door de gasvacuolen te laten bezwijken en het effect van het vormen van een drijflaag op de reflectie werd gemeten. De reflectie werd sterk beïnvloed door de veranderingen in de verstrooiingseigenschappen tengevolge van het bezwijken van de gasvacuolen.

Variabiliteit van inherente optische eigenschappen verandert de reflectie bij een constant niveau van de kleurcomponenten en dus bij een constant niveau van de waterkwaliteitskenmerken. Deze natuurlijke variabiliteit veroorzaakt onnauwkeurigheden in de interpretatie van reflectiemetingen. Gewoonlijk zal deze fout kleiner zijn dan waargenomen in de extreme gevallen die zijn bestudeerd. Voor nauwkeurige data-interpretatie is een veldmeetprogramma nodig voor het kalibreren van de (op afstand) waargenomen reflectiespectra. Een alternatieve methode is gebruik te maken van een bibliotheek met historisch data om defaults (verstekwaarden) voor de optische eigenschappen van de kleurcomponenten en hun variabiliteit af te leiden.

In hoofdstuk 7 word een korte samenvatting van target factor analysis gegeven om te dienen als basis voor hoofdstuk 8. De methode kan worden gebruikt om defaultspectra te verkrijgen voor de interpretatie van reflectiemetingen en om onnauwkeurigheden te specificeren. Target factor analysis heeft drie belangrijke voordelen ten opzichte van multivariantie analyse bij het analyseren van mengsels van lineair bijdragende componenten:
1. Een gedeelte van de ruis wordt verwijderd van de data door het in componenten ontbinden van de data en alleen gebruik te maken van significante componentspectra, gelijktijdig wordt hiermee een datareductie bereikt.

2. Spectra van kandidaatcomponenten kunnen individueel worden getest op hun aanwezigheid in de data. De aanwezigheid van een component kan onafhankelijk van de andere componenten van een volledige set componenten worden beoordeeld.
3. Spectra van defaultcomponenten kunnen worden gebruikt als initiële targets en door projectie of iteratie worden gemodificeerd tot spectra met sterke overeenkomsten met in het mengsel aanwezige componentspectra.

In hoofdstuk 8 laten we zien hoe met target factor analysis ten opzichte van de beschikbare default voor het absorptiespectrum van humus een verbetering kan worden bereikt. Met drie lineair onafhankelijke componenten werd elk humusspectrum in de dataset beschreven binnen de meetnauwkeurigheid. Omdat de dataset veel variatie in de oorsprong van het humus bevat is dit waarschijnlijk in het algemeen waar.

De beschrijving van de humus-absorptiespectra van monsters oppervlaktewater door een model met de massa-specifieke absorptiespectra van humine-zuur en fulvine-zuur van zeewater was fysisch zonder betekenis.

In hoofdstuk 9 wordt een methode gegeven om de *in situ* absorptie te schatten aan de hand van de verzwakking met de diepte van het omhoog gerichte licht. Om nauwkeurige absorptiemetingen van zwevendstof te verkrijgen is meestal een methode nodig om de deeltjes te concentreren. De nauwkeurigheid van de absorptiemetingen kan worden verbeterd door de weglengte van de meting te vergroten in plaats van de concentratie van het monster, waardoor de monsterbehandeling overbodig wordt. Proefondervindelijk werd aangetoond dat de opwaartse lichtverzwakking gemeten met een kleine acceptatiehoek vrijwel gelijk is aan de laboratoriummeting van de absorptie gemeten met een grote acceptatiehoek. Geconcludeerd werd dat veldmetingen van de opwaartse lichtverzwakking net zo als de laboratoriummetingen resulteren in een schijnbare absorptie die nog gecorrigeerd moet worden voor verstrooiing om de inherente absorptie te krijgen. De lichtverzwakking en de schijnbare absorptie waren gelijk binnen de meetnauwkeurigheid van ongeveer 10 procent.

Conclusies

Algemene conclusies

In de praktijk hebben modelberekeningen van de reflectie een beperkte nauwkeurigheid omdat de inherente optische eigenschappen van het mengsel, of de kleurcomponenten, niet nauwkeurig bekend zijn. De keuze van het reflectiemodel is minder belangrijk; in plaats van

het backscattering albedo model (hoofdstuk 4) zou ook het quasi-single scattering model (Gordon *et al.* 1975) kunnen worden gebruikt.

Specifieke inherente optische eigenschappen laten een natuurlijke variabiliteit (hoofdstuk 6) zien in ruimte en tijd. Deze variabiliteit is gerelateerd aan de milieu-omstandigheden en het groeperen van de kleurcomponenten. Bijvoorbeeld verschillen in temperatuur, licht, nutriënten of waterstroming kunnen leiden tot verschillen in deeltjesgrootte-verdeling van een algensoort en tot een successie in de tijd van algensoorten voor de aan chlorofyl gerelateerde kleurcomponent. Als gevolg van deze natuurlijke variabiliteit zijn veldmetingen of default-waarden met foutenmarges nodig om reflectiespectra te kunnen interpreteren.

Spectra gemeten met een hoge golflengteresolutie laten zien dat het gebruik van een klein aantal van tevoren ingestelde golflengten gewaagd is, omdat de reflectie gelijk kan blijven bij concentratieveranderingen in het mengsel (hoofdstuk 5). Bij voorkeur zouden volledige spectra gebruikt moeten worden en zouden er aanvullende veldmetingen of defaultwaarden met het gebruikelijke concentratiebereik beschikbaar moeten zijn. Er kan een oplossing voor de interpretatie van reflectiespectra worden gevonden met behulp van een optimalisatie procedure als een er een bibliotheek beschikbaar is van de kleurcomponenten. Deze bibliotheek zou de defaultspectra van de kleurcomponenten moet bevatten van zowel de absorptie- als de terugverstrooiings-coëfficiënten samen met hun concentratiebereik.

Deze defaultspectra en foutenmarges kunnen worden gebruikt voor een gevoeligheidsanalyse om de winst in nauwkeurigheid te beoordelen bij het uitvoeren van een veldmeetprogramma. Ook kunnen de defaultspectra worden gebruikt om gemeten *in situ* absorptiespectra te ontbinden in de lineaire bijdragen van de kleurcomponenten.

Verbetering veldmeetprogramma

Een gegevensbestand van veldmetingen met de absorptiespectra van de kleurcomponenten maar zonder spectra van de terugverstrooiingscoëfficiënten of reflectiespectra is van beperkte waarde voor de interpretatie van de kleur van oppervlaktewater.

Voor routinematige interpretatie van reflectiespectra is de gedetailleerde informatie van de volumeverstrooiingsfunctie bij een enkele golflengte niet vereist. Het is belangrijker om de spectrale afhankelijkheid van de terugverstrooiingscoëfficiënt van absorberende deeltjes nauwkeurig te kennen.

Spectrale terugverstrooiingscoëfficiënten kunnen worden berekend uit de waargenomen absorptie- en reflectiespectra onder de aanname dat het analytische reflectiemodel geldig is. De reflectiespectra van optisch diepe suspensies kunnen worden gemeten met een large volume reflectometer (hoofdstuk 3). De beneden het wateroppervlak waargenomen reflectiespectra zijn nauwkeurig omdat onder de gecontroleerde laboratorium omstandigheden de storende invloed van golven niet aanwezig is en de sensor vlak onder het wateroppervlak gepositioneerd kan worden.

Kalibratie data voor de interpretatie van reflectiespectra kan op een efficiënte manier worden verkregen op basis van routine veldmetingen. De extra logistieke inspanning om veldmetingen gelijktijdig met de overkomst van de remote sensor te verzamelen is meestal een verspilling van tijd en geld. De poging zal waarschijnlijk mislukken door logistieke problemen, en als de poging succesvol is draagt de nauwkeurige kalibratie van een enkel beeldpunt weinig bij aan de nauwkeurigheid van een beeld met een groot dynamisch bereik. Het is beter om zich in te zetten voor een poging het gehele bereik van de kalibratie data te meten en om reflectiemetingen vanaf het schip op te nemen in het veldmeetprogramma.

De verzwakking van omhoog gericht licht is een *in situ* schatting van de absorptie. De resultaten zijn vergelijkbaar met laboratorium metingen met een integrerende bol. De meetfouten van de bepalingen zijn verschillend. De veldmethode vereist geen behandeling en concentratie van het monster omdat het mogelijk is om de weglengte van de meting aan te passen aan de troebelheid van de watermassa. Voor helder water kan een weglengte tot een meter worden toegepast, vergeleken met de laboratorium absorptiemetingen een factor honderd groter.

APPENDIX A: LIST OF SYMBOLS

Symbol	Description	Unit
a	absorption coefficient	m^{-1}
a^*	specific absorption coefficient	
a_{chl}	absorption coefficient of algae	m^{-1}
a_h	absorption coefficient of aquatic humus	m^{-1}
a_i	absorption coefficient of internal particle material	m^{-1}
a_m	measured absorption coefficient or apparent absorption α	m^{-1}
a_p	absorption coefficient of particulate matter	m^{-1}
a_w	absorption coefficient of pure water	m^{-1}
b	scattering coefficient	m^{-1}
b_b	backscattering coefficient $b_b = B\,b$	m^{-1}
b_f	forward scattering coefficient $b_f = F\,b$	m^{-1}
B	backscattering probability $B(90)$	-
$B(\theta)$	backscattering probability function	-
c	beam attenuation coefficient $c = a + b$	m^{-1}
c_m	measured beam attenuation coefficient	m^{-1}
C	optical cross section	m^2
D	diameter or distribution factor for irradiance	m -
D_d	distribution factor for E_d	-
D_u	distribution factor for E_u	-
E	net vector irradiance	$W\,m^{-2}$
E_d	downward vector irradiance	$W\,m^{-2}$
E_u	upward vector irradiance	$W\,m^{-2}$
E_0	scalar irradiance	$W\,m^{-2}$
f_{aw}	transmittance factor from air to water	-
f_{norm}	normalization factor	
f_{wa}	transmittance factor from water to air	-
$f_{E/L}$	factor between irradiance and radiance $E_u(0)/L_u(0)$	-
F	forward scattering probability $F(90)$	-
$F(\theta)$	forward scattering probability function	-
G	geometrical cross section	m^2
k	radiance attenuation	m^{-1}

Appendix A

Symbol	Description	Unit
k_d	downward radiance attenuation	m^{-1}
k_u	upward radiance attenuation	m^{-1}
k_∞	asymptotic radiance attenuation	m^{-1}
K	irradiance attenuation	m^{-1}
K_d	downward irradiance attenuation	m^{-1}
K_u	upward irradiance attenuation	m^{-1}
K_E	net irradiance attenuation	m^{-1}
$L(\theta)$	radiance	W m^{-2} sr^{-1}
$L_*(\theta)$	path radiance	W m^{-3} sr^{-1}
L_d	downward radiance	W m^{-2} sr^{-1}
$L_{ref}(0+)$	reference radiance of a perfect diffusely reflecting white reference panel	W m^{-2} sr^{-1}
L_u	upward radiance	W m^{-2} sr^{-1}
m	refractive index $m = n - i\,n'$	-
n	real part of refractive index	-
n'	imaginary part of refractive index	-
N	number of particles	-
N_{diode}	number of photodiode	-
Q_a	efficiency factor for absorption	-
Q_b	efficiency factor for scattering	-
Q_c	efficiency factor for extinction	-
r_d	Fresnel coefficient for downward irradiance	-
r_u	Fresnel coefficient for upward irradiance	-
$R(z)$	reflectance or irradiance ratio $R = E_u/E_d$	-
$R(0+)$	remotely sensed reflectance	-
R_{aw}	specular reflectance at the water surface	-
R_b	reflectance of bottom	-
$R_\infty(0)$	subsurface reflectance of optical deep water	-
T_w	transmittance for irradiance in water	-
T_d	transmittance for downward irradiance	-
T_u	transmittance for upward irradiance	-
x	size parameter	-
z	depth	m
α	apparent absorption coefficient	m^{-1}

List of Symbols

Symbol	Description	Unit
β	arctan($n'/(n-1)$)	
$\beta(\theta)$	volume scattering function	$m^{-1}\ sr^{-1}$
θ	scattering angle or zenith angle	°
$\theta_{am}, \theta_{\alpha}$	acceptance angle of absorption measurement	°
θ_{cm}	acceptance angle of beam attenuation measurement	°
λ	wavelength	nm
λ_0	reference wavelength	nm
ϕ	azimuth angle	°
μ	cosine of angle θ	-
$\overline{\mu}$	average cosine of angular distribution	-
$\overline{\mu}_E$	average cosine of the angular distribution of the net vector irradiance in its direction of propagation	-
μ_θ	cosine of zenith angle of the net vector irradiance	-
ρ	real part of the phase-lag factor	-
ρ'	two times the imaginary part of the phase-lag factor	-
ρ^*	complex phase-lag factor	-
τ	optical depth	-
ω_0	single scattering albedo $\omega_0 = b/(a + b)$	-
ω_b	backscattering albedo $\omega_b = Bb/(a + Bb)$	-

Symbol	Description
	MATRIX NOTATION
[ ]	matrix
$[\ ]^T$	transposed matrix
$[\ ]^{-1}$	inverse data matrix
$[\ _{(i)}]$	column i of the matrix
$[\ _{(iw,is)}]$	element (iw,is) of the matrix
	MATRICES
$[C]$	$nw \times n$ column matrix
$[Conc]$	$n \times ns$ concentration matrix
$[CON]$	$nc \times ns$ contribution matrix
$[COV]$	$ns \times ns$ or $nw \times nw$ covariance matrix

Appendix A

Symbol	Description
$[D]$	$nw \times ns$ data matrix
$[R]$	$n \times ns$ row matrix
$[S]$	$nw \times n$ matrix of real or actual spectra
$[T]$	$nc \times nc$ transformation matrix
λ	eigenvalue
n	dimension of the data space, $nc \leq n \leq$ minimum of ns and nw
nc	number of components, $\leq n$
ns	number of spectra
nw	number of wavelengths
	SUBSCRIPTS
i	column index
is	index of spectrum number ns
iw	index of wavelength number nw
pro	projection matrix
red	reduced matrix
sec	secondary
targ	target matrix
	STATISTICAL SYMBOLS
CFV	Cumulative Fraction of Variance explained
IE	Imbedded Error
RE	Real Error
RMS	Root Mean Square error
RSD	Residual Standard Deviation
XE	eXtracted Error
χ_{cal}	calculated chi-squared sum
χ_{exp}	expected chi-squared sum
	OTHER SYMBOLS
DOC	Dissolved Organic Carbon
s	slope coefficient of exponential function